RHODES UNIVERSITY

Thermoluminescence and Phototransferred Thermoluminescence of Synthetic Quartz

by

Robert Rangmou Dawam

Submitted in fulfillment of the
academic requirements for the degree of
Doctor of Philosophy
in
Physics
Rhodes University, Grahamstown

Supervised by **Prof. Makaiko L. Chithambo**

April 2020

This work is dedicated to my late father who passed away while I was on the journey of this degree and to my mother whose constant love made this work possible…

Declaration of Authorship

I, **Robert Rangmou Dawam**, declare that this thesis titled, **Thermoluminescence and photo-transferred thermoluminescence of synthetic quartz** and the work presented in it are my own. All information in this document has been obtained and presented in accordance with academic rules and conduct. I also declare that, as required by these rules and conduct, I have fully cited and referenced all materials and results that are not original to this work.

Signed:

Date:

Abstract

The main aim of this investigation is on thermoluminescence and phototransferred thermoluminescence of synthetic quartz. Thermoluminescence was one of the tools used in characterising the electron traps parameters. The samples of quartz annealed at various temperatures up to 900 °C and the unannealed were used. The thermoluminescence glow curve was measured at 1 °C s^{-1} following beta irradiation to 40 Gy from the samples annealed at 500 °C and the unannealed consist of main peak at 70 °C and secondary peaks at 110, 180 and 310 °C. In comparison, the thermoluminescence glow curve for the sample annealed at 900 °C have main peak at 86 °C and the secondary ones at 170 and 310 °C. The kinetic analysis was carried out only on the main peak in each case. The activation energy was found to be decreasing with increase in annealing temperatures. The samples annealed at 500 °C and the unannealed were found to be affected by thermal quenching while sample annealed at 900 °C shows an inverse quenching for irradiation dose of 40 Gy. However, when the dose was reduce to 3 Gy the effects of thermal quenching was manifested. The activation energy of thermal quenching was also found to decrease with increase in annealing temperature. Thermally assisted optically stimulated luminescence measurement was carried out using continuous wave optical stimulated luminescence (CW-OSL). The samples studied were those annealed at 500 °C for 10 minutes, 900 °C for 10, 30, 60 minutes and 1000 °C for 10 minutes prior to use. The CW-OSL is stimulated using 470 nm blue

LEDs at sample temperatures between 30 and 200 °C. It is measured after preheating to either 300 and 500 °C. When the integrated OSL intensity is plotted as a function of measurement temperature, the intensity goes through a peak. The increase in OSL intensity as a function of temperature is associated to thermal assistance and the decrease to thermal quenching. The kinetic parameters were evaluated by fitting the experimental data. The values of activation energies of thermal quenching are the same within experimental uncertainties for all the experimental conditions. This shows that annealing temperature, duration of annealing and irradiation dose have a negligible influence on the recombination site of luminescence using OSL. Phototransferred thermoluminescence (PTTL) induced from annealed samples using 470 nm blue light was also investigated. The quartz were annealed at 500 °C for 10 minutes, 900 °C for 10, 30, 60 minutes and 1000 °C for 10 minutes prior to use. The glow curves of conventional TL measured at 1 °C s^{-1} following irradiation to 200 Gy shows six peaks in each case labelled I-VI for ease of reference whereas peaks observed under PTTL are referred to as A1 onwards. Only the first three peaks were reproduced under phototransfer for the sample annealed at 900 °C for 60 minutes and 1000 °C for 10 minutes. Interestingly, for the intermediate duration of annealing of 30 minutes, the only peak that appears under phototransfer is the A1. For quartz annealed at 900 °C for 10 minutes, the PTTL appears as long as the preheating temperature does not exceed 560 °C. All other annealing temperatures, PTTL only appears for preheating to 450 and below. This shows that the occupancy of deep electron traps at temperatures beyond 450 °C or 560 °C is low. The activation energy for peaks A1, A2 and A3 were calculated. The PTTL peaks were studied for thermal quenching and peaks A1 and A3 were found to be affected. The activation energies for thermal quenching were determined as 0.62 $\pm$ 0.04 eV and 0.65 $\pm$ 0.02 eV for peaks A1 and A3 respectively. The experimental dependence of PTTL intensity on illumination time is modelled using sets of coupled linear differential equations based on systems of donors and acceptors whose number is determined by preheating temperature.

Acknowledgments

First and foremost, I give thanks to the Almighty God who has guided me all through this project. I would like to express my deepest gratitude to my excellent supervisor Prof. M.L Chithambo, who has tirelessly supported and advised me at the course of this project at Rhodes University. His genuine enthusiasm and energy for scientific enquiry have inspired and guided me throughout. I feel very honoured to have been his PhD student.

I would like to express my gratitude to the University of Jos for the full time training leave granted to me and support to undertaken my PhD. programme in South Africa.

I gratefully acknowledge the support of Department of Physics and Electronics, Rhodes University for the award of Trevor Williams scholarship to the value of R25,000.00 for 2019 session which helped me tremendously in settle my outstanding fees.

My sincere appreciation also goes to Mr. Alexander Akoto, Theophilus Narh, Masok Felix, Ulrich and Dr. John Sanni and Ms Ncebakazi Ntsokota for their constant support. Sincerely, there are no words to quantify your love for me. Likewise I appreciates all research group member and well wishers who in different ways have assisted me throughout this study, thanks for being there for me.

These acknowledgments will be incomplete without words of appreciation to Densen, kids Ashik,

Ma'awe, Dongnaan and Na'anna who always prayed for my success in their daily devotion. Thank you for understanding and words of encouragement during this rough journey. Finally, I am indebted to uncle Alphonsus and Sylvanus Kilingdat, my younger brothers Vincent and Ezekiel for their constant support both in cash and kind to see to the success of this program.

Contents

List of Figures

List of Tables

CHAPTER 1

Introduction

Quartz has been a material of topical interest in luminescence research for a long time [1]. It can record the amount of ionizing radiation which it has been exposed to as a latent signal within the crystal lattice. It is useful as dosimetry material. However, to apply this material as a dosimeter, the latent signal must be erased by heating or exposure to daylight or high pressure [1]. Thus quartz can be used as a natural dosimeter to quantify the radiation history of a material. It also has a variety of applications in nuclear accident dosimetry [2], food irradiation control and dating of geological and archaeological material [3]. Quartz has been extensively studied because of its importance in dating and retrospective dosimetry. It contains various point defects that are involved in the luminescence process. Synthetic quartz, the subject of this thesis, is known to have fewer defects than natural quartz. This influences its optical characteristics.

The various methods used in measurement of the latent signals include thermoluminescence (TL), optically stimulated luminescence (OSL) and electron spin resonance (ESR). This study focussed on TL and OSL from quartz as a way to obtain useful information about mechanism luminescence and the point defects involved. Impurities present in the material are usually con-

sidered essential for TL or OSL to occur. These give rise to localised energy level within the forbidden energy gap which is crucial for the TL process [4]. A detailed explanation of TL and OSL shall be presented in chapter 2.

Despite numerous studies on TL and OSL properties of quartz, the problem regarding the nature of traps, the role of defects, and the processes of excitation and emission of light are still unclear [5, 6, 7].

Luminescence, is exploited in this study, is the emission of light from a semiconductor or insulator following the absorption of energy from an external source [4]. The absorption of the energy is from ionizing radiation, such as gamma-rays, X-rays, beta or alpha radiation or ultra-violet light. The emission can be classified as either fluorescence or phosphorescence. The classification depends on the characteristics lifetime between the absorption of the excitation energy and emission of the luminescence [4].

As explained earlier, the characterisation of luminescence depends on characteristic time (τ_c) of light emission after absorption of the irradiation. For fluorescence, $\tau_c < 10^{-8}$ s and phosphorescence $\tau_c > 10^{-8}$ s [4]. Fluorescence occurs simultaneously with the absorption of radiation and stops immediately the radiation stops [4]. In comparison, phosphorescence is characterised by a delay between the irradiation absorption and time (t) to reach full intensity. The phosphorescence can be subdivided into a long time ($> 10^{-4}$ s) and short time ($< 10^{-4}$ s) phosphorescence.

This study aims at investigating the underlying physical processes of the luminescence to gain extensive information about thermoluminescence, phototransferred thermoluminescence and various thermal effects that affect these processes.

1.1 Synthetic quartz

Quartz is a silicate mineral abundant in the earth's crust. It forms as a three-dimensional array of SiO_4 tetrahedron. Each of the oxygen (O) atoms is shared between the silicon (Si) atoms and each Si atom is connected to four O atoms. Synthetic quartz is hydrothermally grown as a single crystal at high pressure (700-900 kg $s^{-2}m^{-1}$) and elevated temperature (350-366 °C) [8]. The

defects present in synthetic quartz are mainly related to traces of Al and alkaline material [9].

1.2 Aims and objective

The aim of this research is to study the thermoluminescence and phototransferred thermoluminescence and attendant thermal effects in synthetic quartz. To achieve this goal, the following objectives were set.

(a) Characterisation of electron traps parameters using kinetics analysis in synthetic quartz.

(b) Study the influence of annealing on TL and OSL properties of synthetic quartz.

(c) Identification of electron traps and recombination centres in terms of point defects in synthetic quartz.

1.3 Thesis outline

This thesis consist of eight chapters as follows :

Chapter 2: The theoretical aspects of the luminescence; different types of luminescence and their models are described. The methods of kinetic analysis are also presented.

Chapter 3: A description of phototransferred thermoluminescence models.

Chapter 4: A description of the equipment used in this investigation and the samples studied is provided.

Chapter 5: The kinetic analysis of the TL of of unannealed synthetic quartz and of samples annealed at 500 and 900 °C described. The analysis of thermal quenching for the three samples and their dosimetric properties are also discussed.

Chapter 6: Thermal assistance studies of deep traps is presented. The effects of temperature on luminescence, the influence of annealing temperature, annealing time, preheating temperature, irradiation dose and stimulating time on thermal assistance and thermal quenching is presented.

Chapter 7: The general characteristics of phototransferred thermoluminescence are given. The kinetic analysis of the PTTL peaks and thermal quenching are presented. Mathematical models for the analysis of PTTL intensity profiles are given. The competitors effects during phototransferred TL are also described.

Chapter 8: The conclusions of the main findings are given. Area that need further study are outlined.

CHAPTER 2

Theoretical background

Presented in this chapter are the theoretical aspects and the models used to explained thermoluminescence. The methods of kinetic analysis of thermoluminescence and the phenomenon of thermal quenching are also discussed.

2.1 Energy bands and electron traps

In solid state physics, electronic levels that can be occupied consist of valence band and conduction band (see Figure 2.1). These are separated by the forbidden gas or the band gap. The valence is usually full and conduction band empty unless an external impulse such as ionization moves electrons to the conduction band. Presence of impurities and point defects causes localised energy levels to exit in the band gap. [10]. The electrical properties of each solid material depend entirely on the electronic band configuration [11]. The energy levels present in molecules or atoms can be divided into a near continuum levels termed as a band. The electrons are tightly bound to the constituent atoms of the crystal. In contrast, the outward electrons present in the atom are those in control of electrical conductively and chemical bonding. Figure 2.1 shows the

graphically electronic bands configuration in an insulator, semiconductor, and conductor. Examples of insulators are quartz, diamond, mica etc. In a semiconductor, the electron is loosely bound to the nucleus and therefore an amount of energy is needed to separate it from the nucleus. The band gap in a semiconductor is less than that in an insulator with the energy of 1-3 eV [12]. In both insulator and semiconductor, an indirect band gap exists. Conductors have free electrons even at room temperature. The electrons in the conductor are free to move thus participate in conduction.

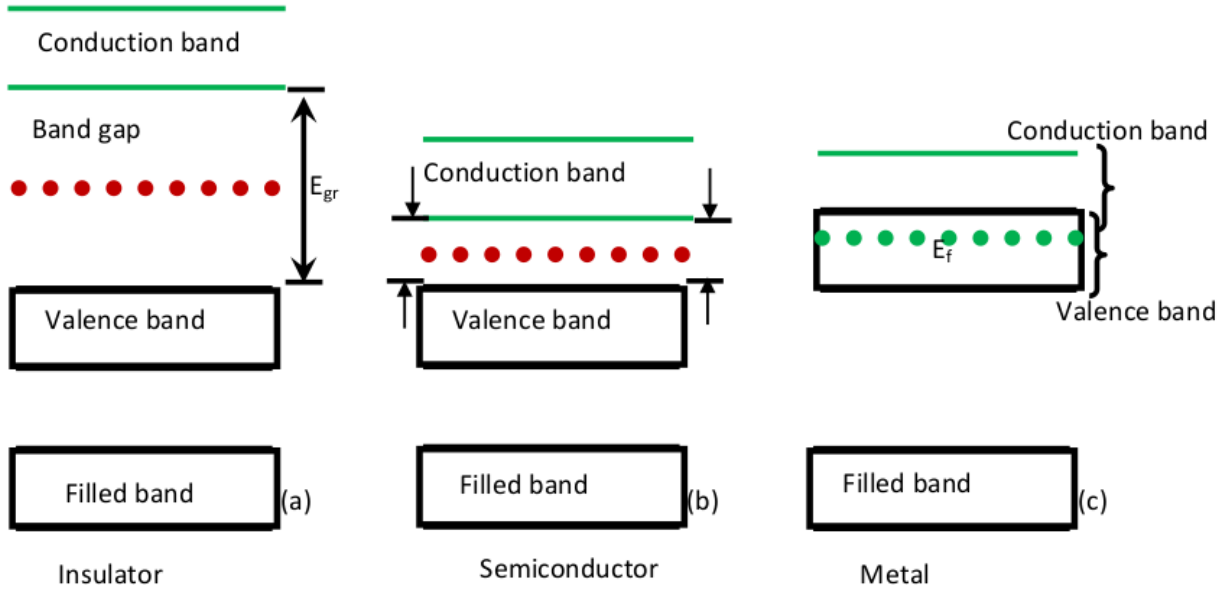

Figure 2.1: The energy band model of metals, semiconductor and insulator [1].

In real crystals, the presence of impurity centres cause metastable energy levels localised in the band gap. The metastable states may have a long lifetime. Electron transitions between conduction band and these levels is possible when the metastable levels are close to the conduction band. As a result of this excitation one level captures electrons and the other captures holes. The energies of these captured carriers are similar to the trapping states and are associated with imperfections and energies within the forbidden gap of the given crystal. The electron trapping

[1] https://micro.magnet.fsu.edu/primer/java/lasers/diodelasers/index.html

states are often close to the conduction band and the hole trapping states are close to the valence band. For the electron that is initially trapped to get liberated, an amount of extract energy is therefore needed. In these conditions, the hole trapping state is called luminescence or recombination center and electron trapping state is termed as an electron trap [13].

2.2 Thermoluminescence

Thermoluminescence (TL) is the emission of light from a previously irradiated insulator or semiconductor when heated at a controlled rate. There are several fundamental conditions for thermoluminescence to occur. Firstly the material must be an insulator or semiconductor. Secondly, the material must have at some time absorbed energy during exposure to radiation. Thirdly the luminescence emission is generated by heating at a controlled rate [4].

The graph of TL intensity (emitted light) as a function of measurement temperature is known as a glow curve. Each peak present in the TL glow curve represents a trap with a unique trap depth [4]. Peaks in a TL glow curve are analysed to derive important parameters that characterised the TL process in the material. These extracted parameters include activation energy (trap depth) E, frequency factor (attempt-to escape) s, the order of kinetics b, the capture cross-section for the traps and recombination centre [13].

2.2.1 Thermoluminescence models

The processes involved in thermoluminescence can be expressed mathematically by considering a simple model as described below.

Figure 2.2 shows a simple diagram consisting of one trapping state and one recombination centre. Let the concentrations of the electrons in trap be n (cm^{-3}) and the concentration of holes in the recombination centre be, m (cm^{-3}). The concentrations of trapping states and recombination centres are N and $M(cm^{-3})$ respectively. The activation energy and the frequency factor associated with the thermal liberation of the electron from traps are denoted by E (eV) and s (s^{-1}) respectively. The concentration of free electrons and hole are also respectively given by

$n_c(cm^-3)$ and $n_v(cm^{-3})$, the re-trapping probability coefficient of the electron is $A_n(cm^{-3}s^{-1})$, the recombination probability coefficient of electrons is $A_m(cm^{-3}s^{-1})$ and the trapping probability coefficient of holes in centres is $B\ (cm^{-3}s^{-1})$. The parameter $X(cm^{-3}s^{-1})$ is proportional to the dose rate of excitation and denotes the rate of production of electron-hole pairs [14].

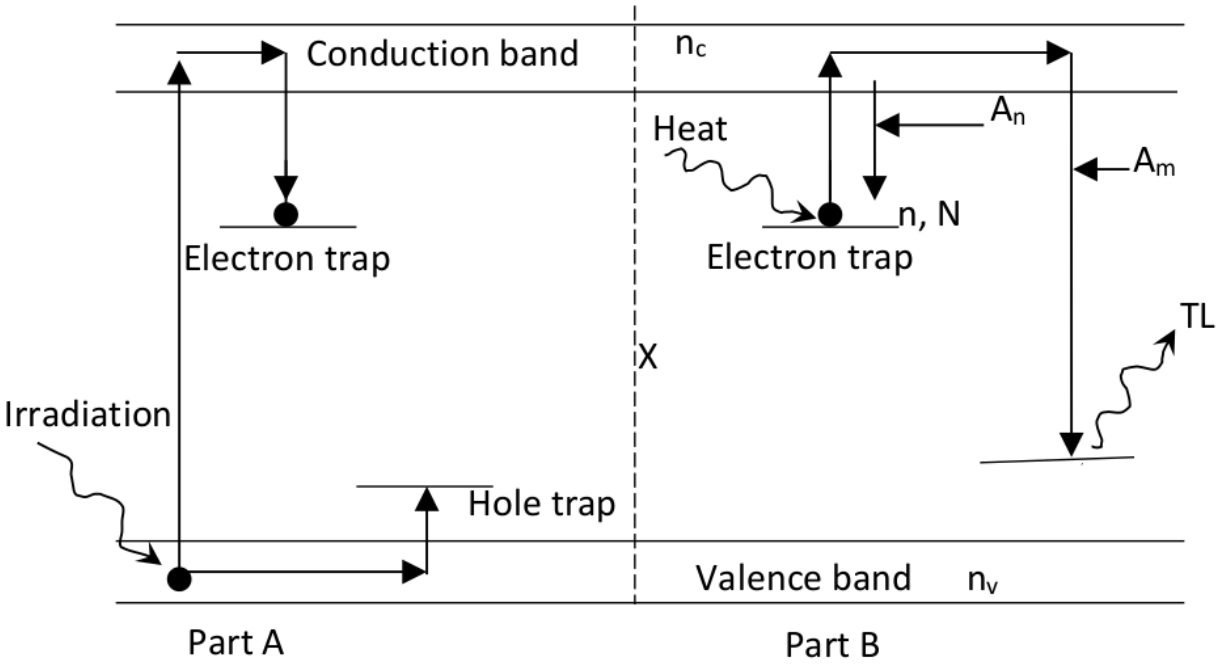

Figure 2.2: A simple TL model with one electron trap and one recombination centre. Part A represents the absorption stage during which interaction of ionizing radiation takes place and part B represent recombination stage during which the temperature is raised, electrons escape from their traps and recombine with trapped holed which act as a luminescence centre [14].

The set of differential equations that govern the process during irradiation is given as

$$\frac{dn}{dt} = A_n(N-n)n_c - ns\exp\left(\frac{-E}{kT}\right) \tag{2.1}$$

$$\frac{dm}{dt} = B(M-m)n_v - A_m M n_c \tag{2.2}$$

$$\frac{dn_c}{dt} = X - A_n(N-n)n_c - A_m M n_c \tag{2.3}$$

$$\frac{dn_v}{dt} = \frac{dn}{dt} + \frac{dn_c}{dt} - \frac{dm}{dt}. \tag{2.4}$$

The explanation of each of the equations (2.1 -2.4) is as follows;

Equation (2.1) is the rate of change in concentration of electrons in electron traps N. In equation (2.1), the first term represents re-trapping while the second term represents de-trapping from N to the conduction band. Equations (2.2) and (2.3) are the rate of change in concentration of holes at the recombination centre and free electrons in the conduction band respectively. Equation (2.4) express the charge neutrality condition. At low-temperature, the second term of equation(2.1) is negligible but when the temperature is high the term cannot be neglected. This set of differential equations can be solved analytically by making a simplifying assumption to approximate the dependence response to irradiation. After irradiation, the values of n, m, n_c and n_v become the initial values at the heating stage. At the heating stage, the function $T = T_o + \beta t$ varies linearly with time where β is the constant heating rate. When irradiation ends $X = 0$ and all hole have capture $n_v \approx 0$. The process during heating is governed by the equations given as

$$\frac{dn}{dt} = A_n(N - n)n_c - ns \exp\left(\frac{-E}{kT}\right). \tag{2.5}$$

The recombination rate is given by equation (2.2). Therefore, the TL intensity, $I(T)$ is proportional to the rate of change in concentration of free electron in the conduction band and recombination centres. Thus, the rate equation is given by

$$I(T) = -\frac{dm}{dt} = A_m m n_c. \tag{2.6}$$

For charge neutrality, $n_v \approx 0$ and hence equation (2.4) changes to

$$\frac{dm}{dt} = \frac{dn}{dt} + \frac{dn_c}{dt}. \tag{2.7}$$

The emitted signal depends on the trap and centres occupancies. This method is called ”quasi-equilibrium” or ”quasi-steady assumption” which can be stated as below

$$|\frac{dn_c}{dt}|\ll|\frac{dn}{dt}|,|\frac{dm}{dt}|; n_c \ll n. \tag{2.8}$$

Equation (2.8) implies that the rate of change of free carriers is significantly small compared to that of the trapped carriers and vice-versa. For the case where electrons are removed from the trap at the time of stimulation and proceed through the conduction band to the recombination site, the TL intensity is given by

$$I = -\frac{dm}{dt} = ns\exp\left(\frac{-E}{kT}\right)\frac{A_m m}{A_m m + A_n(N-n)}. \tag{2.9}$$

2.2.2 First-order kinetics

The first-order kinetics is the case where re-trapping is very slow or negligible. The simple assumption $n \cong m, \frac{dn}{dt} \cong \frac{dm}{dt}$ and $A_n m \gg (N-n)A_n$ (slow re-trapping). By using these simplifying assumption into equation (2.9), the first-order kinetics equation given as

$$I = -\frac{dn}{dt} = ns\exp\left(\frac{-E}{kT}\right). \tag{2.10}$$

If the stimulation is provided by heating at a linear rate ($\beta = dT/dt$), then the luminescence intensity is expressed as

$$I(T) = n_o s\exp\left(\frac{-E}{kT}\right)\exp\left[(-s/\beta)\int_{T_o}^{T}\exp\left(\frac{-E}{kT}\right)dT'\right] \tag{2.11}$$

where T_o is the initial temperatures, n_o is the initial electron and T' is a dummy integral variable temperature. Equation (2.11) is the solution of equation (2.10).

2.2.3 The second-order kinetics

The second-order kinetics is the case where re-trapping dominates. Garlick and Gibson [15] considered the case $(N-n)A_n \gg A_m m$, the trap is far from saturation $N \gg n$. Applying these conditions to equation (2.9) produces

$$I(T) = -\frac{dn}{dt} = \frac{A_m}{A_n N} n^2 s \exp\left(\frac{-E}{kT}\right). \tag{2.12}$$

Equation (2.12) indicates that the intensity $I(T)$ is proportional to n^2. This is referred to as second-order kinetics.

If the retrapping and recombination probability coefficients are equal i.e $A_m = A_n$ [14] then equation (2.12) reduces to

$$I(T) = -\frac{dn}{dt} = \frac{sn^2}{N} \exp(-E/kT) = s^{'} n^2 \exp\left(\frac{-E}{kT}\right) \tag{2.13}$$

where $s^{'} = s/N$ is a constant with unit a of $cm^{-3}s^{-1}$. The solution of equation (2.13) is express as

$$I(T) = \frac{n_o s^{''} \exp\left(\frac{-E}{kT}\right)}{[1 + (s'/\beta) \int_{T_o}^{T} \exp\left(\frac{-E}{kT}\right) dT']^2} \tag{2.14}$$

where $s^{''} = s^{'} n_o$ and all other terms are as early defined [13].

2.2.4 General-order kinetics

This is the general case where the kinetics are neither first nor second-order kinetics. May and Partridge [16] considered the general case for general-order of kinetics. They developed an expression known as the equation of general-order of kinetics given as

$$I(T) = n^b s^{'} \exp\left(\frac{-E}{kT}\right) \tag{2.15}$$

where $s^{'}$ has dimensions of $m^{3(b-1)}$ and b is defined as the general-order of kinetics [14]. If b is either 1 or 2, the expression reduces to first or second-order kinetics respectively. The solution of equation (2.15) with initial temperature from T_o and heating rate of β is given as

$$I(T) = s^{''} n_o \exp\left(\frac{-E}{kT}\right) [1 + (b-1)\frac{s^{''}}{\beta} \int_{T_o}^{T} \exp\left(\frac{-E}{kT}\right) dT']^{-\frac{b}{b-1}} \tag{2.16}$$

where $s'' = s' n_o^{b-1}$ is the effective frequency factor of general-order kinetics and all other terms are as defined earlier. The equation (2.15) is the general-order kinetics which is fully empirical and has no relation to actual physical models [14].

Another type of kinetics is called mixed-order kinetics. The assumption leading to second-order that is $m = n$. It has been shown by Chen et al. [17] that the assumption is unlike to occur in real samples due to the type of defects or impurities present. Mixed-order kinetics is not involved for any kinetic analysis in this work and is discussed further.

2.3 Quartz structure and impurities state

The defect pair model present in TL and OSL was proposed by Itoh et al [18] in discussing the production of the 110 and 325 °C TL peaks in quartz. The positions of the TL depends on the heating rate used. The model indicates that the energy for the two TL peaks and OSL is all stored by the same defect pairs. Peaks are formed as a result of irradiation and heating applied to defect pairs which are comprise of $[AlO_4]^-$ and $[X/M^+]^+$ [18] centres. The $[X/M^+]^+$ centre is an interstitial ion centre, in which the interstitial alkali ion (M^+) can stabilised by defect X [1]. The defect X may be Ti and M may be Na as both are impurities common in quartz. The luminescence signals from the TL peaks of 110 and 325 °C produced from radiolytic reaction and the recombination of defect pairs of $[AlO_4]^-$ and $[X/M^+]^+$. The TL peak of 110 °C is emitted at 380 nm. This follow as a result of a thermally-released electron captured by a hole centre following liberation of photon [19]. Among the several defects that stabilize alkalis which may be responsible for the 325 °C TL peak as X. The defect X may be Ti, which is known to contribute to the OSL [20]. The recombination of M^+ released from $[X/M^+]^+$ with $[AlO_4]^-$ emit a part of the energy stored by defect pairs as photons of 420 nm. In Itoh et al [18] model the 325 °C TL peak arise as a result of M^+ being thermally released and recombining at an $[AlO_4]^-$ centre. The TL peaks 110 and 325 °C in quartz arise from the same defect pairs and also have first-order kinetics as a common feature [18].

2.4 Methods of analysis thermoluminescence glow peaks

Thermoluminescence glow peaks can be analyzed to determine physical parameters responsible for the TL emission. These parameters provide useful information for an acceptable interpretation of the dynamics luminescence emission. These quantities include the order of kinetics b, activation energy E, frequency factor s. There are several methods used for the analysis of TL glow curves. This section describe some of these techniques.

2.4.1 The initial-rise method

The initial rise (IR) method relies on the TL in the low-temperature part of a TL glow peak. The number of electrons corresponding to the TL in this region is assumed to be approximately constant that is $n \approx n_o$ [14, 4]. As a rule of thumb, it has proposed that the initial-rise extends up to the point where TL intensity reaches about (5-15) % of the maximum [21]. In the lower-temperature region of the maximum intensity $I(T) \propto \exp(-E/kT)$. The dependence on temperature of the TL intensity can be expressed as

$$I(T) = C \exp\left(\frac{-E}{kT}\right) \tag{2.17}$$

where C is a constant, E is the activation energy (in eV), k is Boltzmann's constant (in eV/K) and T is absolute temperature (in K). The graph of $\ln(I)$ as a function $1/kT$ is expected to be a straight line. The slope of the plot gives the value of the activation energy, E. In employing this method, the TL peak should be well defined and separated from other peaks. When the peaks overlap, the methods of peak separation discussed by Mckeever [4] should be applied before using the IR method. These method of peak separation are thermal cleaning and partial heating method $(T_m - T_{stop})$ which shall be discussed later in the text.

2.4.2 The whole glow curve method

This method is also well known as the area method. The technique involves the transformation of a total glow peak into a straight line. The method can be applied to only a well defined and

clean glow peak. The value of the integral (area) $n(T)$ as a measure of the intensity of the TL intensity over a certain temperature region can be evaluated by the area under the glow curve from a given temperature T_o in the initial rise region up to the final temperature T_F as shown in Figure 5.5. The sum of the area $n(T)$ of the TL glow curve can be expressed mathematically as

$$n(T) = \int_{T_o}^{T_f} I dT. \tag{2.18}$$

Equation (2.18) can also be written in summation form as

$$n(T) = \sum_{i=T_o}^{T_f} I_i \frac{\Delta T}{\beta} \tag{2.19}$$

where $\Delta T = T_f - T_i$. The graph of $\ln(I/n)$ against $1/kT$ is expected to linear and the slope of the plot equal to the value of the activation energy E. The frequency factor s can be evaluated from the intercept $\ln(s/\beta)$ of the plot.

For the case of general-order kinetics, equation (2.15) can be re-written as

$$ln\frac{I}{n^b} = ln\left(\frac{s^{'}}{\beta}\right)\frac{E}{kT}. \tag{2.20}$$

The plot of $\ln(I/n^b)$ against $1/kT$ where b is the order of kinetics is expected to be linear. The value of b retained is the one that give the best fit. From the graph, the slope gives the value of the activation energy while the frequency factor can be evaluated from the intercept $\ln(s^{'}/\beta)$.

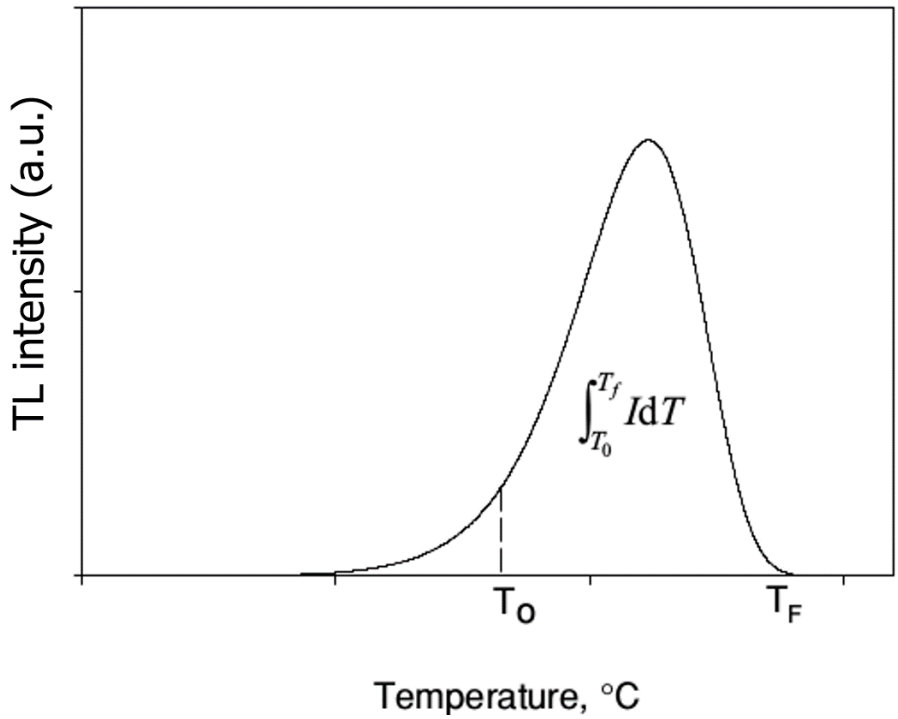

Figure 2.3: Calculation of area using whole glow peak method [21].

2.4.3 The peak-shape method

The peak-shape method was proposed by Chen [13] and is based on the geometrical properties or shape of the TL glow peak. This technique utilizes just two or three points from the peak. The points are the peak maximum T_m and either both the low and hight-temperature half-heights at T_1 and T_2 [13]. The quantities τ, δ and ω define the geometric features of the TL peak as $\tau = T_m - T_1$, $\delta = T_2 - T_m$ and $\omega = T_2 - T_1$ as illustrated in Figure 2.4.

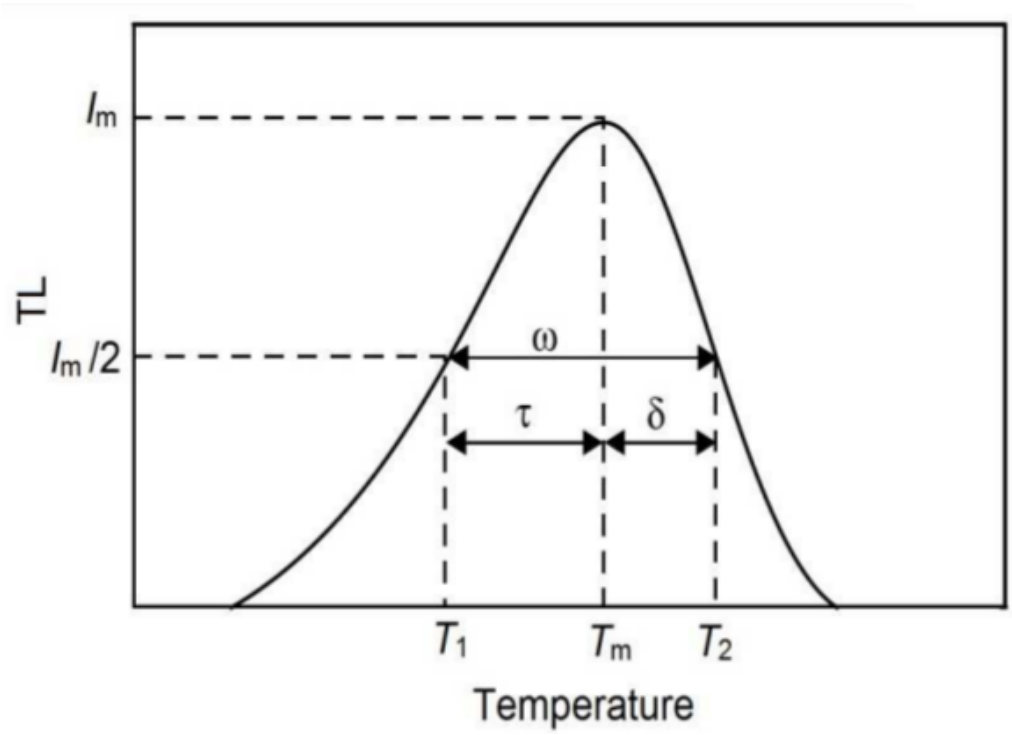

Figure 2.4: Glow peak showing the geometrical quanties τ, δ and ω [21].

The general expression for calculating the values of the activation energy is written as

$$E_\alpha = C_\alpha \left(\frac{kT_m^2}{\alpha} \right) - b_\alpha (2kT_m) \tag{2.21}$$

where α stand for τ, δ or ω. The values of C_α and b_α are summarized as shown below according to Chen [13]

$$C_\tau = 1.1510 + 3.0(\mu - 0.42), b_\tau = 1.58 + 4.2(\mu - 0.42) \tag{2.22a}$$

$$C_\delta = 0.976 + 7.3(\mu - 0.42), b_\delta = 0 \tag{2.22b}$$

$$C_\omega = 2.52 + 10.2(\mu - 0.42), b_\omega = 0. \tag{2.22c}$$

If $\mu = 0.42$ then, the TL peak is of first-order kinetics and if $\mu = 0.52$, it is of second-order kinetics [13].

2.4.4 The variable heating rate method

The heating rate changes the position of a peak. By maximising equation (2.11), i.e setting $\frac{dI}{dT} = 0$, one finds the following expression

$$\frac{\beta E}{kT_m^2} = s \exp\left(\frac{-E}{kT_m}\right). \tag{2.23}$$

Rearranging equation (2.23) gives

$$ln\left(\frac{T_m^2}{\beta}\right) = \left(\frac{E}{k}\right)\frac{1}{T_m} + ln\left(\frac{E}{sk}\right). \tag{2.24}$$

A plot of $\ln(T_m^2/\beta)$ as a function of $1/kT_m$ is expected to yield a straight line. The activation energy E can be found from the slope of the graph and the frequency factor s can be evaluated from the y-intercept $\ln(E/sk)$ [4, 13, 21]. Alternatively Chen and Winer [22] used the approximation for the integral present in the general-order kinetics to obtain the following expression

$$\frac{\beta E}{kT_m^2} = s[1 + (b-1)\Delta_m] \exp\left(\frac{-E}{kT_m}\right) \tag{2.25}$$

where $\Delta_m = 2kT_m/E$ and the term $[1+(b-1)\Delta_m]$ is treated to be approximately constant. The graph of $ln(T_m^2/k\beta)$ against $1/kT_m$ is expected to produce a straight line. The slope of the graph produces the value of activation energy. Similarly, by differentiating the general-order kinetics equation, it can be shown the maximum peak intensity of the TL (I_m) is related to heating rate (β) as

$$I_m^{b-1}\left(\frac{T_m^2}{\beta}\right)^b = \left(\frac{E}{bks}\right)^b \exp\left(\frac{E}{kT_m}\right). \tag{2.26}$$

The graph of $ln(I_m^{b-1}(T_m^2/\beta)^b$ as a function of $1/kT_m$ is supposed to give a straight line and the slope of the plot produced activation energy E. In this approach, the order of kinetic need to be known before the equation is applied [22].

2.4.5 Curve fitting

Curve fitting was developed by Mohan and Chen [23] for first and second-order peaks. The technique was further extended to general-order peaks by Shenker and Chen [24]. It was later

shown by Bull et al [25] that it can even apply on multiple peaks in the glow curve. If the trap levels are interact, the treatment of the glow curve as a superposition of several individual glow peaks is valid for first-order kinetics.

In using the curve fitting technique, a function that defines the quantities is usually fitted to the experimental TL glow curve. The fitting procedure commences with the formulation of an intelligent guess to figure the number of TL glow peaks in a given glow curve. The next task is to assign a correct mathematical function to the peaks identified.

If f(T) expresses the mathematical function of each TL glow peak, and if many TL glow peaks are involved in describing the glow curves, then the function can be written as

$$I(T) = \sum_{i=1}^{p} \gamma f_i(T) \tag{2.27}$$

where $f_i(T)$ is the mathematical function chosen to describe the number of TL grow peak, γ is a scaling factor, and p is the number of peaks present in the glow curve [13].

Kitis et al [26] developed equations for the first, second and general-order kinetics given as

$$I(T) = I_m \exp\left[1 + \frac{E}{kT}\frac{T - T_m}{T_m} - \frac{T^2}{T_m^2}\left(\frac{E}{kT}\frac{T - T_m}{T_m}\right)(1 - \Delta) - \Delta_m\right] \tag{2.28}$$

$$I(T) = 4I_m \exp\left(\frac{E}{kT}\frac{T - T_m}{T_m}\right)\left[\frac{T^2}{T_m^2}(1 - \Delta)\exp\left(\frac{E}{kT}\frac{T - T_m}{T_m}\right) + 1 + \Delta_m\right]^{-2} \tag{2.29}$$

$$I(T) = I_m b^{\frac{b}{b-1}} exp\left(\frac{E}{kT}\frac{T - T_m}{T_m}\right)\left[(b-1)(1 - \Delta)\frac{T^2}{T_m} exp\left(\frac{E}{kT}\frac{T - T_m}{T_m}\right) + Z_m\right]^{\frac{-b}{b-1}} \tag{2.30}$$

where Δ = 2kT/E, Δ_m = 2kT_m/E, $Z_m = 1 + (b-1)\Delta_m$, I_m is the peak maximum intensity and all others symbols are as defined earlier [26]. As recommended by Horowitz and Yossian [27], the figure of merit (FOM) is usually used to check for the goodness of the fit and is defined as

$$FOM = \sum \frac{|y_{expt} - y_{fit}|}{y_{fit}} \tag{2.31}$$

where y_{expt} is the experimental data and y_{fit} are the values from the fit. A fit is considered to be acceptable if the FOM is less than 3.5 % [28].

An expression for s can be obtained by taking the first derivative of the first equation (2.11) or equation (2.13) or equation (2.16) in that way. These equations for the frequency factor for the first, second and general-order kinetics are respectively given as

$$s = \frac{\beta E}{kT_m} \exp\left(\frac{E}{kT_m}\right) \tag{2.32}$$

$$s = \frac{\beta E}{kT_m^2(1 + \frac{2kT_m}{E})} \exp\left(\frac{E}{kT_m}\right) \tag{2.33}$$

$$s = \frac{\beta E}{kT_m^2(1 + \frac{2kT_m(b-1)}{E})} \exp\left(\frac{E}{kT_m}\right) \tag{2.34}$$

where all terms are as previously defined.

2.5 Analysis of phosphorescence

Chen [13] defined phosphorescence as the decay of thermally stimulated luminescence as a function of time at a constant temperature. A plot of the emitted light output (luminescence intensity) as a function of time at constant temperature is termed an isothermal decay curve.

Phosphorescence can be of first, second or general-order kinetics. The first-order behaviour for phosphorescence is given as

$$I(t) = I_o \exp(-pt) \tag{2.35}$$

where p^{-1} is the lifetime by the parameters p can be written as

$$p = s \exp\left(\frac{-E}{kT_i}\right). \tag{2.36}$$

Inserting equation (2.36) to equation (2.35) transforms into

$$I(t) = I_o \exp\left[-s \exp\left(\frac{-E}{kT_i}\right) t\right] \tag{2.37}$$

where all symbols retain their usual meanings. The plot of $I(t)$ as a function of time on a semilogarithmic scale should yield a straight line if the phosphorescence is of first-order. Its slope is equal to $-p$ at the given temperature.

$$p_i = s \exp\left(\frac{-E}{kT_i}\right) \tag{2.38}$$

A plot of $ln(p)$ against $1/kT_i$ is expected to yield a straight line and the slope of the graph is equal to the value of the activation energy E. The frequency factor s can be calculated from the y-intercept lns. If the measurement is carried out at two different temperatures, T_1 and T_2 then, the two slopes p_1 and p_2 can be obtained as

$$ln\left(\frac{p_1}{p_2}\right) = \frac{E}{k}\left(\frac{1}{T_2} - \frac{1}{T_1}\right). \tag{2.39}$$

From equation (2.39), the activation energy E can be evaluated.

For the case of second-order kinetics, the expression can be written as

$$I(t) = -\frac{dn}{dt} = p^{'} n^2 \tag{2.40}$$

where $p^{'} = s^{'} \exp(_E/kT)$ and the solution of the equation (2.40) is as follow

$$I(t) = \frac{I_o}{(1 + p^{'} n_o t)^2} \tag{2.41}$$

where $\sqrt{I_o/I(t)} = 1 + p^{'} n_o t$. The graph of $\sqrt{I_o/I(t)}$ against t is supposed to be a straight line and the slope of the graph gives $n_o p^{'} = n_o s^{"} \exp(-E/kT)$. The temperature can be varied and the quantities $s^{'} n_o$ and E can be evaluated [13].

The general-order kinetics for isothermal decay analysis has been suggested by May and Partridge [16], Takeuche et al. [29]. The order of kinetics can also be determined using phosphorescence method of analysis. By the integration of general-order kinetics i.e equation (2.15) with respective to time, t and keeping the temperature constant, one finds

$$I(t) = I_o \left[1 + s^{'} n_o^{b-1}(b-1)t \exp\left(\frac{-E}{kT_i}\right)\right]^{\frac{b}{1-b}} \tag{2.42}$$

where $I_o = s^{'} n_o^{b-1} \exp(-E/kT_i)$,$n_o$ is the initial concentration of the charge trapped and I_o is the initial TL intensity I of the TL intensity at time t [21]. The rearrangement of equation (2.42) produces

$$\left(\frac{I}{I_o}\right)^{\frac{b-1}{b}} = \left[1 + s^{'} n_o^{b-1}(b-1)t \exp\left(\frac{-E}{kT_i}\right)\right]. \tag{2.43}$$

Equation (2.43) indicated that the plot of $\ln(I/I_o)^{1-b/b}$ as a function of time, t is supposed to be linear if a suitable value of b is found. At different isothermal decay temperatures, a set of a straight lines produce slopes given as

$$p = s^{'} n_o^{b-1}(b-1) \exp\left(\frac{-E}{kT_i}\right). \tag{2.44}$$

A plot of $\ln(p)$ against $1/kT_i$ is expected to a be linear and the slope of the graph equal to the value of the activation energy E. May and Partridge [16] likewise provided an alternative way of determined order of kinetics, b as follows

$$ln\left(\frac{dI}{dt}\right) = lnC + \frac{2b-1}{b} ln(I). \tag{2.45}$$

The graph of $ln(dI/dt)$ against $ln(I)$ produces a straight line with the slope equal to $(2b-1)/b$ from which the value of b can be calculated.

2.5.1 The temperature-dependence of the area under an isothermal decay-curve

The method of calculating activation energy based on the temperature-dependence of the area under an isothermal decay-curve was reported by Chithambo [30]. This approach can also be used to calculate the activation energy, E as well as the activation energy for thermal quenching ΔE. The technique was specifically derived from first-order of kinetics and so indeed is most applicable for first-order kinetics. In the methods, only a small portion of the phosphorescence

decay-curve is required [30]. The small segment area Φ under the phosphorescence decay curve can be expressed mathematically as

$$\Phi = \kappa \exp\left(\frac{-E}{kT}\right) \tag{2.46}$$

where κ is a constant and all other terms are as previously defined. The plot of ln Φ against $1/kT$ is expected to be linear with a slope of the graph equal to the activation energy. Application of this method shall be discussed in the results section in this report.

2.6 Method of TL glow peak resolution

The methods of kinetics analysis discussed thus far a well-defined glow peak. However, TL glow peaks obtained during experiments may not be well isolated and defined. Therefore, it is important to employed techniques to separate any overlapping TL glow peaks.

2.6.1 Thermal cleaning

In this method, the sample is heated just to beyond the maximum of the first TL glow peak to empty the traps responsible for the peak. The sample is then immediately cooled and reheated again above the maximum of the subsequent TL glow peak, and so on throughout the whole glow curve. This usually produces a clean initial lower temperature part in each of the TL glow peaks.

2.6.2 T_m -T_{stop} technique

Mckeever [4] proposed a technique for peak resolution of a TL glow peak. In the method, a sample that has been previously irradiated is heated to a temperature T_{stop} on the lower-temperature end of the first peak. The procedure is redone on a freshly irradiated sample using a new value of higher temperature T_{stop}. In each case, the position of the maximum temperature is noted corresponding to the temperature T_m. The plot of T_m versus T_{stop} produces stepwise curve in most case . For the first-order peak, T_m versus T_{stop} is independent of the concentration of trapped

charge while for non-first order kinetics, the position of the peak shift to higher temperature i.e the initial trapped charge concentration is reduced.

2.7 Thermal quenching

The loss of luminescence efficiency with increase in temperature is is known as thermal quenching. Thermal quenching can be observed in many ways but mostly in measurements that monitor the intensity of TL, PL, OSL or RL as a function of temperature [31]. Thermal quenching appears as a decrease of emission intensity as temperature increases. The effects of the thermal quenching are only not restricted to decrease in intensity [32] but mean also affect trapping parameters. For example in the initial rise method, the activation energy can be underestimated to thermal quenching [33, 34]. The activation energies evaluated by peak shape method [13] can also be strongly underestimated [35].

The effects of thermal quenching can be revealed in TL when a set of TL glow curve is obtained at a various heating rates. The luminescence efficiency decreases and reduces the TL maximum peak height and area. This also shifts the TL peak to the higher temperature position with an increase in heating rate. The principles behind the Mott-Seitz mechanism of thermal quenching model have been summarized previously [31, 36]. The Mott-Seitz mechanism is shown schematically in Figure 2.5 using a configuration coordinate diagram and consists of an excited state of the recombination centre and the corresponding ground state. In this mechanism, electrons can undergo either one of two competing transitions as captured into an excited state of recombination centre. The first route resulting in the emission transition is a direct radiative recombination route following in the emission of light and is shown as a vertical arrow in Figure 2.5. The second route is an indirect thermally assisted non-radiative transition into the ground state of the

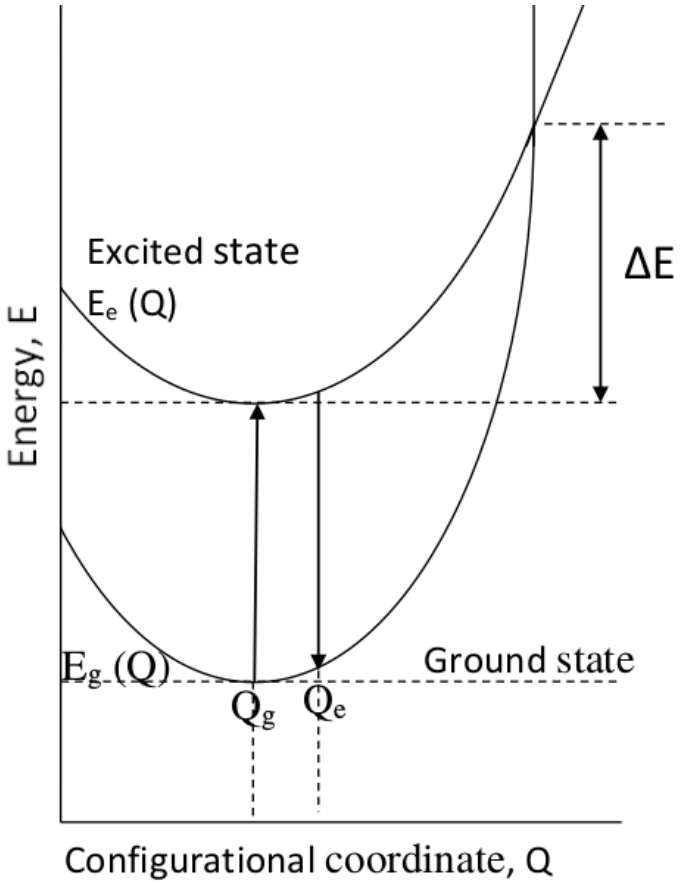

Figure 2.5: Variations of electron energy, E where E_g is the defect at ground state, E_e is defect at excited state with configuration coordinate Q_e for excited states, Q_g is for the ground states and ΔE is the activation energy of thermal quenching in a luminescence material [31]

recombination center; the activation energy ΔE for this non-radiative process is also illustrated in Figure 2.5. The energy given up in the non-radiative recombination is absorbed by the crystal as heat, rather than being emitted as photons. The fundamental assumptions of the Mott-Seitz mechanism is that the radiative and non-radiative processes compete within the bounds of the recombination centre called localized transitions [37].

The luminescence efficiency η is defined as the ratio of the probability for the radiative transition divide by the total transition probability given by

$$\eta = \frac{\tau}{\tau_o} = \frac{1}{1 + C\exp(\frac{-\Delta E}{kT})} \tag{2.47}$$

where $C = \tau_o \nu$.

The radiative luminescence intensity I is therefore given as

$$I = \frac{I_o}{1 + C \exp(\frac{-\Delta E}{kT})} \tag{2.48}$$

where I_o the unquenched intensity at a lower temperature. The thermal quenching efficiency $\eta(T)$ can be given as

$$\eta(T) = \frac{1}{1 + C \exp(\frac{-\Delta E}{kT})} \tag{2.49}$$

where C and ΔE are thermal quenching pre-exponential factor and activation energy of thermal quenching [38].

2.8 Stability of luminescence signal

The studied physical properties of TL materials for practical application in dosimeter or TL dating, one should be conscious of the probability of fading of the TL signal. The TL signal usually fade with time following or even at a time of the excitation of the sample [13]. This section briefly discussed the types of fading that normally occurs in TL for dosimetry or dating application.

2.8.1 Thermal fading

The effect of thermal fading usually occurs after irradiation of sample following a given excitation. The trapping state and the recombination centres are filled with charges of opposite sign carrier. However, thermal fading take effect at the temperature of excitation or even at room temperature. When a finite possibility that the charge carriers are thermally liberated from the trapping state into the de-localized band or any other excited state, from where they may recombine either radiative or non-radiative with carriers of the opposite sign in the recombination centres [13]. If the process of radiation is radiative, the measurable is associated with phosphorescence which decays with time as electron and holes are emptied. The reduction in the number of trapped carriers usually results in a commensurate decrease in the TL intensity measured during subsequent heating following certain waiting period between irradiation and readout.

In a practical scenario, any sample that is to be measured must be stored somewhere. In the case of TL, it may not be possible to do an immediate measurement after the initial exposure to ionizing radiation to fill the traps. But depending on the circumstances of the irradiation and measurement system, samples may need to be stored for (seconds or minutes or hours or days) or perhaps years at a time.

2.8.2 Anomalous fading

Many TL material sometimes fade at room temperature. The charge carried usually depleted from the traps less expected from the evaluation of lifetime. This behaviour is the term anomalous fading [13]. The anomalous fading has a serious effect on many application of TL and OSL dating. One feature of this anomalous fading is rapid decay and longer storage time of decay rate of TL or OSL signal. This investigation of anomalous fading normally required to complete long-term ageing studies of irradiated materials [13]. When the number of fading is observed which is over and above the normal level from thermal de-trapping alone, then anomalous fading is questionable. Anomalous fading was first observed by Wintle [39]. This abnormal behaviours usually occur both in natural as well as synthesized TL materials. It is often less for deep traps as compared to that of shallow traps as reported by Mckeever [4].

CHAPTER 3

Phototransferred thermoluminescence

In this chapter, we describe phototransferred thermoluminescence (PTTL) and models which have been proposed to explain its dynamics. The simple model and the phenomenological model reported by Chithambo et al [40, 41] is also described.

3.1 Phototransferred thermoluminescence

Phototransferred thermoluminescence (PTTL) is a widely observed phenomenon in many thermoluminescence materials. The PTTL is produced due to the transfer of electrons, optically from deep electron traps (donor traps) to previously empty shallower ones (acceptor traps). PTTL were useful in investigating some mechanisms involved in optically stimulated luminescence and thermoluminescence. It has also been useful for dosimetry and dating technique [42] and there is some renewed interest in its application for dosimetry [43].

The study of PTTL features leads to useful information regarding the optical energies expected to be capable in transferring charge between centres and help to identify the mechanisms involved in the optically stimulated and TL process [13].

3.1.1 Phototransferred thermoluminescence simple model

PTTL usually involved an electron trap (called acceptors) and a deep trap (called donors) and hole trap which act as recombination centre. Figure 3.1 shows a simple model for describing PTTL feature. The production of PTTL signal is a multiple-step process starting with irradiation of the sample, preheating, illumination and heating again.

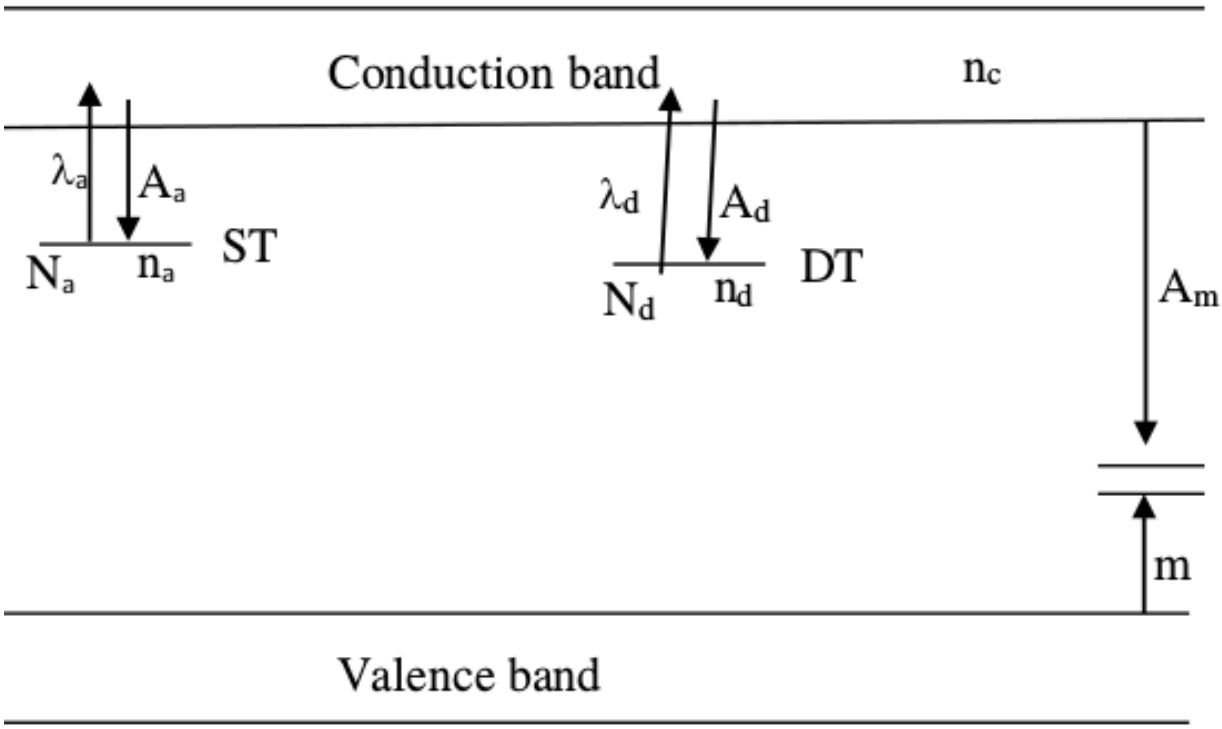

Figure 3.1: A simple PTTL model with one electron trap (level ST), one deep trap (DT) and one radiative recombination centre, where scrip a and d stand for acceptor and donor traps respectively; c, N_d and M are concentration of available acceptor traps, donor traps and recombination centre; n_a, n_d and m are concentration of the acceptor trsps, donor traps and hole; A_a, A_d and A_m are their respective probabilities [13].

The description of PTTL intensity profiles as a function of illumination time was proposed by Wintle and Murray [44] using a set of differential equations. This set of differential equations

describes the loss of an electron from the deep (donor traps) and the gain of an electron by shallow (acceptor traps). The set of differential equations Wintle and Murray [44] used are as follows;

$$\frac{dn_d}{dt} = -\lambda_d n_d \tag{3.1}$$

$$\frac{dn_a}{dt} = b\lambda_d n_d - \lambda_a n_a \tag{3.2}$$

where λ_d and λ_a are the rates of loss of an electron from donor traps and acceptor tarps respectively and b is constant during illumination. The loss mechanism for the donor and acceptor traps are optical excitations given as $\lambda_d = \Phi\sigma_d$ and $\lambda_a = \Phi\sigma_a$ where Φ is the intensity of the excitation light, σ_d and σ_a are the photoionization cross-section for the donor traps and acceptor trap respectively. The solution of the equation (3.1) and (3.2) is

$$n_a = b\frac{\lambda_d n_{do}}{\lambda_a - \lambda_d}[\exp(-\lambda_d t) - \exp(-\lambda_a t)]. \tag{3.3}$$

The characteristics of PTTL intensity profile as a function of illumination time as suggested by equation (3.3) is an increase and followed by a decrease to eventually to zero levels.[0.15cm] The production of PTTL involves multi-step i.e irradiation, preheating, illumination and heating. Chen and Mckeever [13] considered each of the stages in formulating their differential equation for the description of PTTL intensity profile. With the definition of all the parameters in Figure 3.1, Chen and Mckeever [13] set up differential equations as follows;

At time, $t = 0$, $n_{ai} = 0$ and $n_{doi} = m_o$, during illumination, the set of the couple differential equations for transfer of charge from the donor trap to acceptor trap level follows

$$\frac{dn_c}{dt} = -\frac{dn_a}{dt} - \frac{dn_d}{dt} + \frac{dm}{dt} \tag{3.4}$$

$$\frac{dn_a}{dt} = A_a(N_a - n_a)n_c - \lambda_a n_a \tag{3.5}$$

$$\frac{dn_d}{dt} = A_d(N_d - n_d)n_c - \lambda_d n_d \tag{3.6}$$

$$\frac{dm}{dt} = -A_m m n_c. \tag{3.7}$$

If there are no retrapping during excitation from donor traps to the acceptor traps then $A_d(N_d -$

$n_d)n_c \ll \lambda_d n_d$ and $A_a(N_a - n_a)n_c \ll \lambda_d n_d$, $\lambda_a n_a \approx= 0$. Also, according to the assumption of quasi- equilibrium given as;

$$| \frac{dn_c}{dt} | \ll | \frac{dm}{dt} |, | \frac{dn_c}{dt} | \approx 0. \tag{3.8}$$

Applying these assumptions to equations (3.4 - 3.7) becomes

$$\frac{dm}{dt} = \frac{dn_a}{dt} + \frac{dn_d}{dt} \tag{3.9}$$
$$\frac{dn_a}{dt} = A_a(N_a - n_s)n_c \tag{3.10}$$
$$\frac{dn_d}{dt} = -\lambda_d n_d \tag{3.11}$$
$$\frac{dm}{dt} = -A_m m n_c. \tag{3.12}$$

The solutions of equations (3.9 - 3.12) at the end of illumination becomes

$$n_a = N_a[1 - \exp(bt)] \tag{3.13}$$
$$n_d = n_{di} \exp(\lambda t) \tag{3.14}$$
$$m = m_o \exp(\frac{t}{\tau}) \tag{3.15}$$

where $b = n_c A_m$ and $\tau = (n_c A_m)^{-1}$ are all constants [13]. PTTL signal can only be observed if the sample is heated. When the sample is heated, the electron is thermally released from the shallow traps and recombine with a hole trap to produced PTTL intensity or be re-trapped into deep traps. The set of differential equations illustrating the flow of electrons during the heating stage are as follows;

$$\frac{dn_c}{dt} = -\frac{dn_a}{dt} - \frac{dn_d}{dt} + \frac{dm}{dt} \tag{3.16}$$
$$\frac{dn_a}{dt} = A_a(N_a - n_a)n_c - \gamma_a n_a \tag{3.17}$$
$$\frac{dn_d}{dt} = A_d(N_d - n_d)n_c \tag{3.18}$$
$$I = \frac{dm}{dt} = -A_m m n_c \tag{3.19}$$

The only difference between equations (3.4 - 3.7) and equations (3.16 - 3.19) is the thermal de-trapping term γ replaces the optical de-trapping λ. The thermal excitation is given as

$$\gamma_a = f_a \exp\left(\frac{-E_a}{kT}\right) \tag{3.20}$$

where f_a is the frequency factor and E_a activation energy associated with the acceptor trap [13]. Analytical solutions to these differential equations are only possible for a simplifying assumptions such as quasi-equilibrium [13]

$$|\frac{dn_c}{dt}| \ll |\frac{dm}{dt}|, |\frac{dn_c}{dt}| \approx 0. \tag{3.21}$$

The solutions of equations(3.16 - 3.19) are as follows

$$n_c = \frac{\gamma_a n_a}{[A_a(N_a - n_a) + A_d(N_d - n_d) + A_m m]} \tag{3.22}$$

$$I = -\frac{A_m \gamma_a n_a m}{A_a(N_a - n_a) + A_d(N_d - n_d) + A_m m} \tag{3.23}$$

$$N_d - n_d = \frac{N_d - n_{di}}{(\frac{m}{m_o})^{A_d/A_m}} \tag{3.24}$$

$$I_{PTTL} = -\frac{dm}{dt} = \gamma_a A_m m F(m) \tag{3.25}$$

where $F(m)$ is define as follows [13]

$$F(m) = \frac{(n_{ao} + n_{do} - m_o - N_d) + m + (N_d - n_{do})(m/m_o)^{A_d/A_m}}{A_a(N_a + N_d - n_{ao} - n_{do} + m_i) + (A_m - A_n)(N_d - n_{di})(m/m_o)^{A_d/A_m}}. \tag{3.26}$$

The subscript o indicates the charge concentration in the various traps at the start of heating. It can be observed that equation(3.23) and (3.26) contain variable m. The solutions of the set of the equations can only be solved numerically for a set of given input parameters. By simplifying the equations with the introduction of $\beta = dT/dt$ (heating rate), equation (3.23) can be written by changing the variable from t to T as

$$I_{PTTL} = -\beta \frac{dm}{dT} = \beta \gamma_a A_m m F(m) \tag{3.27}$$

The area under the PTTL curve is obtained by the integration of equation (3.27) from the initial temperature T_o to the final temperature T_f as given below

$$S_{PTTL} = \int_{T_o}^{T_f} I_{PTTL} dT. \tag{3.28}$$

Equations (3.25), (3.26) and (3.27) are combined to yield;

$$S_{PTTL} \approx \frac{A_m m_o n_{ao}}{A_d (N_d - n_{do})}. \tag{3.29}$$

The equation (3.29) can be used to describe the profile of PTTL intensity as a function of illumination time and equation (3.29) can be written in this form

$$S_{PTTL} = C \frac{m(t) n_a(t)}{N_d - n_d(t)} \tag{3.30}$$

where C is a constant of integration of PTTL [13]. Using a similar approach as above, it can also be written as

$$S_{PTTL} = C \frac{\exp(-t/\tau) N_a [1 - \exp(-bt)]}{(N_d/n_{do}) - \exp(-\lambda t)} \tag{3.31}$$

Chen and Mckeever [13]showed that for longer illumination time, $t \to \infty$, $n_d \to 0$, $m \to n_a$ and S_{PTTL} will start from 0 at $t = 0$ and increase smoothly to a maximum, given as

$$S_\infty = \frac{C n_a^2}{N_d} \tag{3.32}$$

The above equations described making use of various assumptions in describing the variation of PTTL intensity as a function of illumination time.

3.1.2 Empirical model of PTTL

Wintle and Murray [44], Alexander and Mckeever [45] developed PTTL models for the description of PTTL intensity as a function of illumination time. The validities of their models depend

on numbers of assumptions in describing the behaviours of PTTL intensity profiles as a function of illumination time. Recently, Chithambo et al [40] developed a model that explains the PTTL intensity profile as a function of illumination time using a set of coupled differential equations. The solutions of differential equations are linear and were formulated base on the number of multiple donor traps and acceptor traps following preheating temperature. The solutions of the differential equations can be applied directly on the experimental data.

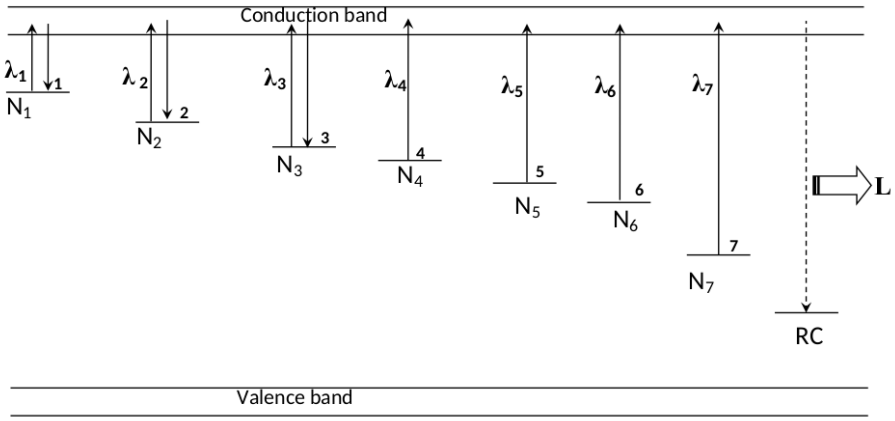

Figure 3.2: The energy band scheme used to describe PTTL in annealed synthetic quartz. Electron levels 1 through 7 are associated with electron concentration N_i as shown. The parameters λ_i are each the probability of optical stimulation. Luminescence L is emitted from the recombination centre RC. Where $N_1, N_2, N_3, N_4, N_5, N_6$, and N_7 are concentrations of electrons at levels 1 through 7. The parameters λ_1 through λ_7 are probabilities of optical stimulation from these levels respectively.

The analysis is based on the assertion that only a portion of charge stimulated from a donor is transferred to an acceptor and that any retrapping of stimulated electrons is negligible. The change of PTTL intensity as a function of illumination time will be explained with respect to the energy band diagram shown in Figure 3.2 N_1 to N_7 are each the concentration of electrons at levels 1 to 7 whereas λ_1 through λ_7 are the corresponding probabilities of optical stimulation.

The sample of synthetic quartz studied in this investigations have six peaks and the deep traps making seven levels. The peaks are labeled I, II, III, IV, V and VI position at 90, 120, 180, 210,

240 and 340 °C respectively. The application of this model shall be discussed in the results part of this thesis.

3.1.2.1 PTTL following preheating to 250 °C

When the sample was preheated to 250 °C following irradiation to removed peak I-V, we expect a PTTL peak to be reproduced when at least one shallow trap has been depleted and one or more donors are intact. But in this case, there was no PTTL peak after removal of I-IV. PTTL peak was only reproduced following preheating to 250 to remove peaks I-V, but peak V was not completely remove. The PTTL was only reproduced at 90 °C. The donors here are at levels 5, 6 and 7 with only one acceptor at level 1.

The family of differential equations describing the transfer of charge from donors to the acceptor responsible for PTTL peak 1 will be given as

$$\frac{dN_7}{dt} = -\lambda_7 N_7 \tag{3.33}$$

$$\frac{dN_6}{dt} = -\lambda_6 N_6 \tag{3.34}$$

$$\frac{dN_5}{dt} = -\lambda_5 N_5 \tag{3.35}$$

$$\frac{dN_1}{dt} = -\lambda_1 N_1 + \alpha_5\lambda_5 N_5 + \alpha_6\lambda_6 N_6 + \alpha_7\lambda_7 N_7 \tag{3.36}$$

where α_5, α_6 and $\alpha_7$are constants of proportionality. The first term in equation (3.36) concerns the optical removal of electrons during illumination. The rest of the terms describe the retrapping of charge from donors. The solution for the set of differential equations (3.33)-(3.36) for PTTL peak 1 is

$$N_1 = A_1[\exp(-\lambda_5 t) - \exp(-\lambda_1 t)] + A_2[\exp(-\lambda_6 t) - \exp(-\lambda_1 t)] + A_3[\exp(-\lambda_7 t) - \exp(-\lambda_1 t)] \tag{3.37}$$

where $A_1 = \alpha_5\lambda_5 N_{5i}/(\lambda_1 - \lambda_5)$, $A_2 = \alpha_6\lambda_6 N_{6i}/(\lambda_1 - \lambda_6)$ and $A_3 = \alpha_7\lambda_7 N_{7i}/(\lambda_1 - \lambda_7)$, N_{5i}, N_{6i} and N_{7i} are each the concentration of electrons at electron traps levels 5, 6 and 7 at the start of illumination.

3.1.3 PTTL following preheating to 350 °C

To empty peaks I-VI, the sample was preheated to 350 °C to remove peaks. Two PTTL peaks were reproduced at peak I and III. Under this preheating, it was observed that peak VI could not be properly removed and still reappeared although the intensity of the peak extremely reduced. Thus levels 6 and 7 are considered as donors for the PTTL peaks I and III. In this case, there are two separate systems of two donors and two acceptors.

The set of coupled differential equations describing the case for PTTL peak I is

$$\frac{dN_7}{dt} = -\lambda_7 N_7 \tag{3.38}$$
$$\frac{dN_6}{dt} = -\lambda_6 N_6 \tag{3.39}$$
$$\frac{dN_1}{dt} = -\lambda_1 N_1 + b_6\lambda_6 N_6 + b_7\lambda_7 N_7 \tag{3.40}$$

where b_6 and b_7 are constants of proportionality. The solution of equations (3.38 - 3.40) is given by

$$N_1 = D_1[\exp(-\lambda_6 t) - \exp(-\lambda_1 t)] + D_2[\exp(-\lambda_7 t) - \exp(-\lambda_1 t)] \tag{3.41}$$

where $D_1 = b_6\lambda_6 N_{6i}/(\lambda_1 - \lambda_6)$ and $D_2 = b_7\lambda_7 N_{7i}/(\lambda_1 - \lambda_7)$ and all symbols are as initially defined. The set of coupled differential equations explaining PTTL peak III is expressed as

$$\frac{dN_7}{dt} = -\lambda_7 N_7 \tag{3.42}$$
$$\frac{dN_6}{dt} = -\lambda_6 N_6 \tag{3.43}$$
$$\frac{dN_3}{dt} = -\lambda_3 N_3 + k_6\lambda_6 N_6 + k_7\lambda_7 N_7 \tag{3.44}$$

The PTTL intensity as a function of illumination time for the acceptor associated with PTTL peak III is

$$N_3 = H_1[\exp(-\lambda_6 t) - \exp(-\lambda_3 t)] + H_2[\exp(-\lambda_7 t) - \exp(-\lambda_3 t)] \tag{3.45}$$

where $H_1 = \delta_6\lambda_6 N_{6i}/(\lambda_3 - \lambda_6)$ and $H_2 = \delta_7\lambda_7 N_{7i}/(\lambda_3 - \lambda_7)$.

3.1.4 PTTL following preheating to 500 °C: Sampling deep electron traps

If all the peaks in the glow curve were removed by preheating to 500 °C, two PTTL peaks were reproduced again at position I and III. The deep trap is level 7 in this case is the donor. The transfer of charge from the deep trap to acceptors at peak I can be expressed as

$$\frac{dN_7}{dt} = -\lambda_7 N_7 \tag{3.46}$$

$$\frac{dN_1}{dt} = -\lambda_1 N_1 + \mu_7 \lambda_7 N_{7i} \tag{3.47}$$

where μ_7 is a constant of proportionality and all other parameters are as previously defined. The solution of the differential equation (3.46 - 3.47) is given as

$$N_1 = D_1[\exp(-\lambda_7 t) - \exp(-\lambda_1 t)]. \tag{3.48}$$

The dependence of PTTL intensity as a function of illumination time for acceptor III can be found as

$$N_3 = P_1[\exp(-\lambda_7 t) - \exp(-\lambda_3 t)] \tag{3.49}$$

where $D_1 = \mu_7 \lambda_7 N_{7i}/(\lambda_1 - \lambda_7)$, $P_1 = \delta_7 \lambda_7 N_{7i}/(\lambda_3 - \lambda_7)$, μ_7 and δ_7 are constants of proportionality. The application of these models shall be discussed in chapter 7.

CHAPTER 4

Instrumentation and experimental methods

This chapter briefly described the equipment and the samples used during the investigation. Risø TL/OSL luminescence Reader model TL/OSL DA-20 was used throughout for the measurement of both thermoluminescence and optical stimulated luminescence.

4.1 The Risø TL/OSL Luminescence Reader system

The measurement of thermoluminescence and optical stimulated luminescence was carried out using the Risø TL/OSL luminescence Reader model TL/OSL DA-20. The system consists of a light detection unit, a luminescence stimulation unit (thermal and optical) and an irradiation source. The reader can accommodate up to 48 samples. Samples can be heated individually between room temperature to 700 °C on a carousel. Figure 4.1 shows schematic diagram of TL/OSL Reader. Figure 4.2 shows the Risø TL/OSL reader. The labelled parts are (a) controller, (b) carousel, (c) photomultiplier tube and (d) beta irradiation source.

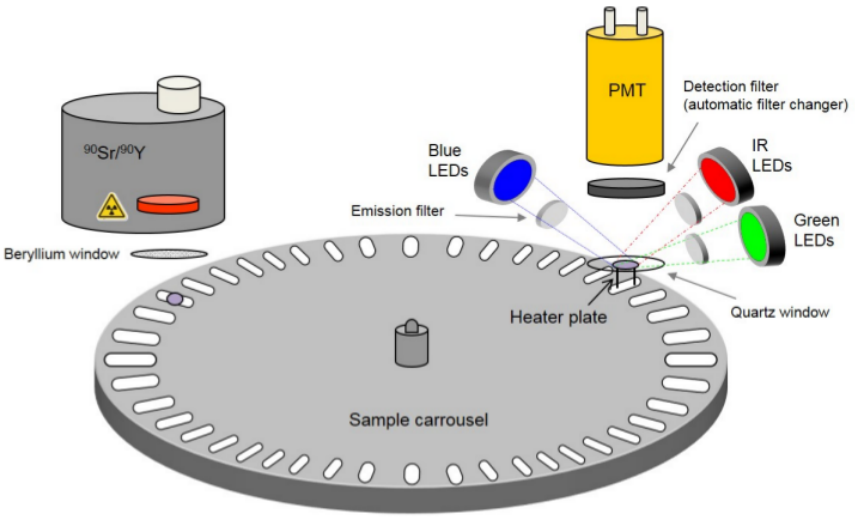

Figure 4.1: The schematic diagram of Risø TL/OSL luminescence reader [1].

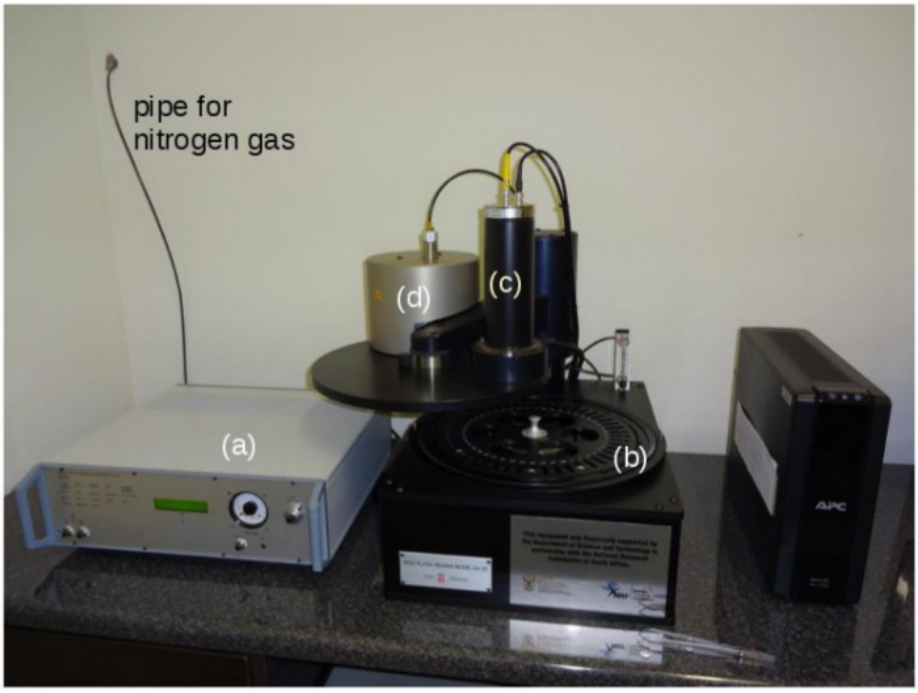

Figure 4.2: The Risø TL/OSL Luminescence Reader system, model DA-20.

[1] User manual of the Risø TL/OSL-DA-20 Reader 2011. Technical university of Denmark.

4.1.1 Light detection system

The light detection system consists of the photomultiplier (PMT) and a detection filter. The luminescence is detected by a photomultiplier tube (EM1 9235 QA). The photomultiplier tube has a maximum detection efficiency between 200 and 400 nm [46]. This make it suitable for the detection of luminescence from quartz. Figure 4.3 shows the quantum efficiency as a function of incident photon wavelength for the EM1 9235 QA photomultiplier. Detection filters placed in front of the photomultiplier prevent scattered stimulation light from reaching the photomultiplier tube. The detection filter Hoya U-340 (7.5 nm thick) was used throughout this work. This filter has transmission band between 270 and 389 nm (FWHM).

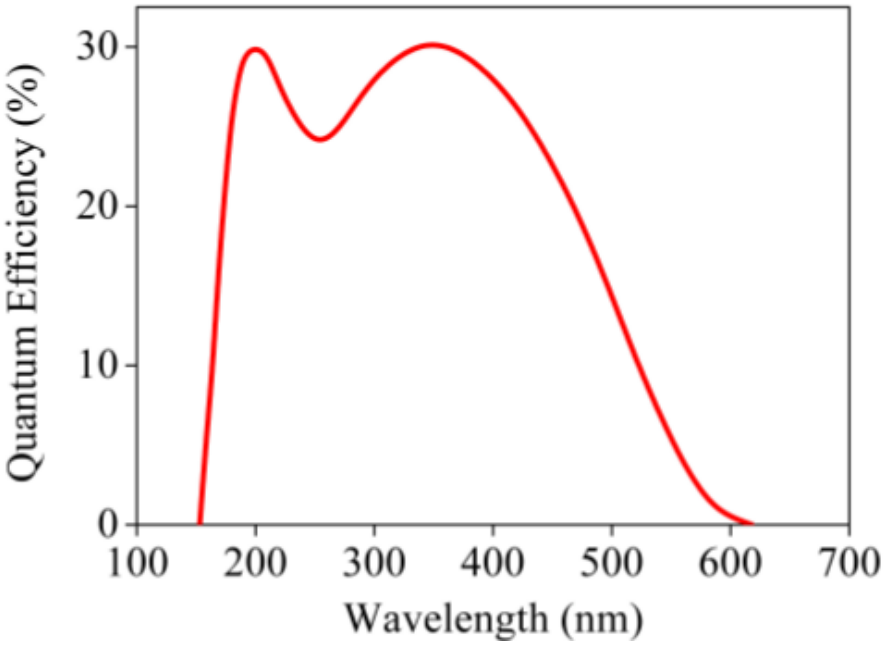

Figure 4.3: The quantum efficiency of photomultiplier tube EM1 9235Qb as a function of photon wavelength and energy [2].

[2]User manual of the Risø TL/OSL-DA-20 Reader 2011. Technical university of Denmark.

4.1.2 Thermal stimulation system

The thermal stimulation system consist of the heating element that heats the sample. During measurement, this positioned underneath the photomultiplier tube (Figure 4.1). The system lifts the sample into the measurement position. Heating the sample is achieved by feeding a controlled current through the heating element. This system can heat the sample from room temperature up to 700 °C at heating rates between 0.1 and 10 °C s^{-1}. The flow of nitrogen during measurement prevents spurious luminescence from air.

4.1.3 Optical stimulation system

The basis for OSL is the stimulation of an irradiated sample with a light source providing a selected wavelength. The sensitivity of the traps depends on the wavelength of stimulation used. Shorter wavelength of stimulation has a greater chance of evicting charge from traps. In all the OSL measurements presented in this thesis, 470 nm blue light and set at a power density of 72 $mWcm^{-2}$ was used. The sample was stimulated at constant light intensity (continuous wave CW-OSL mode).

4.1.4 The irradiation source

Samples were irradiated using an inbuilt beta source of isotopes ^{90} Sr $/^{90}$ Y. The irradiation is software controlled and allows single irradiation of a sample at a time. The beta source in our Reader emits beta particles at a nominal dose rate of 0.1028 Gy s^{-1}.

4.2 Samples and the experimental details

The samples of synthetic quartz used for this investigation are commercial (Sawyer Research Products, Ohio USA). The samples were used in powder form. The as-received sample are henceforth called unannealed quartz. Other aliquots of the samples were annealed at 500, 900 and 1000 °C for 10 minutes. Sample annealed at 900 °C for 30 and 60 minutes were also used

in this investigation. Measurement were made on the mass of 0.080 g, 0.090 g, 0.070 g, 0. 068 g and 0.082 g aliquot of the unannealed sample, annealed at 500 °C, annealed at 900 °C for 10 minutes, annealed at 900 °C for 30 minutes, annealed at 900 °C for 60 minutes and annealed at 1000 °C respective. Annealing is a thermal treatment procedure that involves heating the samples to a predetermined temperature, keeping them at that temperature for a defined period of time and then cooling the samples to room temperature. Samples were annealed to erase any remanent signal and to effect their sensitivity. In all the measurements carried out in this investigation, samples were mounted on stainless steel disks. All measurements were made in a nitrogen atmosphere to prevent false signals from the air and to improve thermal contact between the sample holder and the heater.

CHAPTER 5

Thermoluminescence: Kinetic analysis

This chapter report the results of Kinetic analysis of the main peak of thermoluminescence glow curve. The unannealed sample and the samples annealed at 500 and 900 °C were studied. Analysis of thermal quenching for the three samples and their dosimetric properties are also discussed. The aim is to study the influence of annealing on TL properties of synthetic quartz. The investigation on TL properties of synthetic quartz is to determine kinetic parameters.

5.1 Introduction

The synthetic quartz used for this thesis is the same one used in previous studies [47, 48, 49] and also the one published by Dawam and Chithambo [50]. The authors found that luminescence lifetimes in synthetic quartz determined using time-resolved spectra increase with annealing temperature. The results were interpreted as evidence of increase in dominance of particular recombination centres. Recently, Chithambo and Niyonzima [49] using radioluminescence identified seven emission bands at 2.04, 2.54, 2.77, 3.04, 3.75 and 3.91 eV and showed that the intensity of the emission bands changes with annealing temperature. This investigation is to

examine whether TL features of the sample including non- radiative transitions are affected by annealing and if they are to attempt to offer some explanation.

5.2 Glow curve characteristics

The investigations on the thermoluminescence of synthetic quartz were carried out on the unannealed sample, samples annealed at 500 and 900 °C. Annealing the sample to 500 °C is a heat treatment to remove any residual signal and enhances the sensitivity of the sample. The synthetic quartz sample used in this study changes its sensitivity owing to thermal activation [51]. If the sample is not heated beyond a thermal activation, around 300 °C, the sensitivity is very low. Heating it above 500 °C during measurement of TL activates it. Annealing refers to heating the sample and holding it at a specific temperature for a given time. Since other annealing temperatures were used in this study, a similar treatment had to be done at 500 °C to assess the influence of annealing on properties and not simply to thermally activate the sample. If a comparison is made based on annealing, all samples have to be treated in the same way. The study did not compare samples annealed at 500 °C and those simply heated to 500 °C.

Figure 5.1 shows a glow curve of synthetic quartz annealed at 900 °C recorded at 1 °C s^{-1} after irradiation to 40 Gy. There is a single prominent peak at 84 °C and other weaker intensity ones at 164 and 240 °C. The inset shows a semi-logarithmic plot of the same glow curve as well as ones measured from the unannealed quartz and the sample annealed at 500 °C revealed that there are more than three peaks with additional one around 210 and 340 °C . For comparison, the unannealed quartz and the sample annealed at 500 have peaks at similar positions at 70, 180 and 310 °C. All three cases show one high intensity peak. This investigation focuses only on the kinetic analysis of the main peak. The other weaker peaks are not reliable for the study. The motivation of this work is to study the influence of annealing on kinetic parameters and in particular to study the effect of annealing on non-radiative transitions. Part of the work in this chapter has been published previously [50].

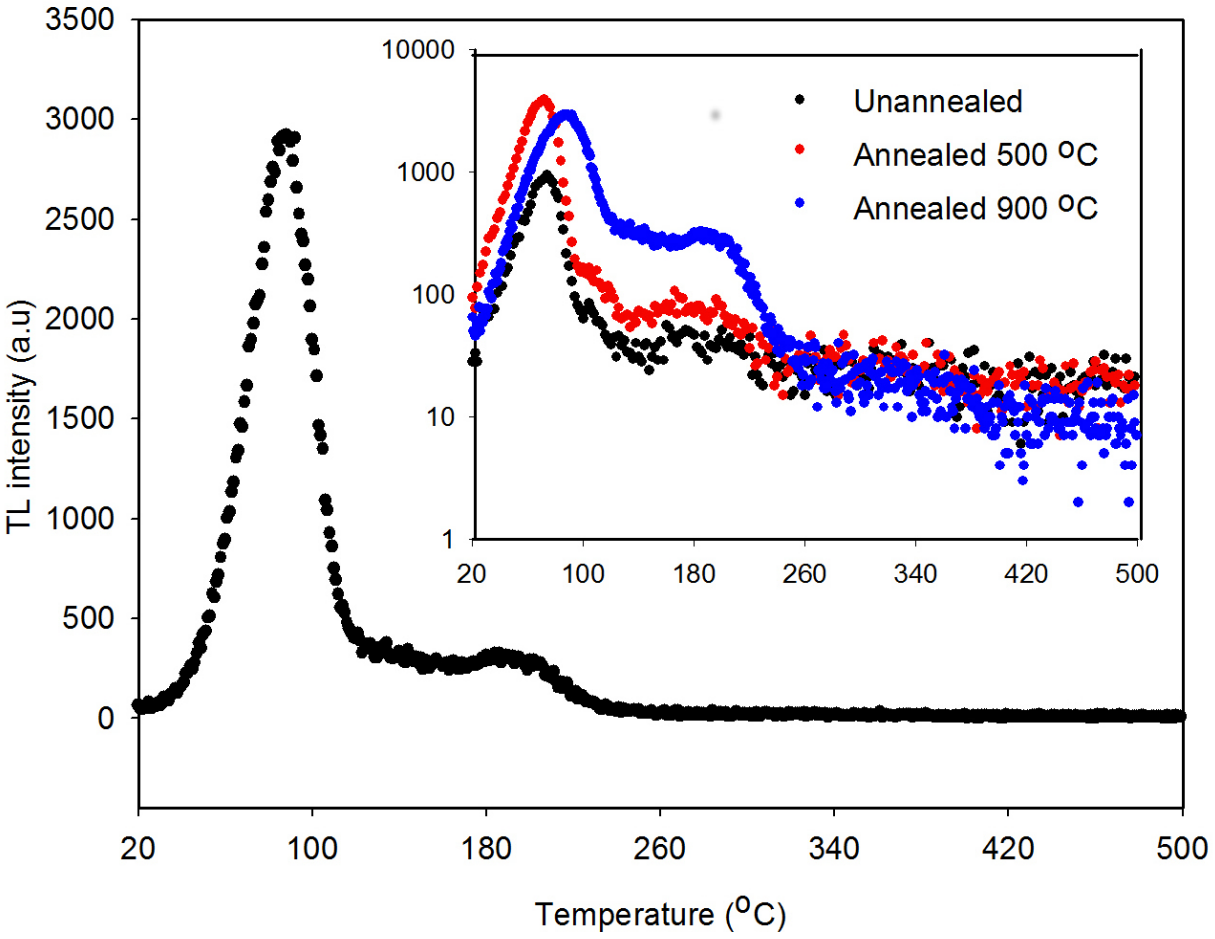

Figure 5.1: A glow curve measured at 1 °C s^{-1} from a sample annealed at 900 °C. The inset shows semi-logarithmic plots comparing this result with ones measured from the unannealed sample and the sample annealed at 500 °C.

5.3 Order of kinetics

The order of kinetics of the main peak was first investigated using dependence of the peak position (T_m) on the preheating temperature (T_{stop}) and peak position as a function of irradiation dose. Other methods of assessment of order of kinetics used shall be discussed in the subsequent sections.

5.3.1 Assessment using the dependence of T_m on dose

The order of kinetics of the main peak was first assessed using the dependence of its position T_m on irradiation dose from 10 to 200 Gy. The position for the main peak for the unannealed quartz, and samples annealed at 500 and 900°C were monitored as a function of irradiation dose. It was found that in all cases the peak position is independent of irradiation dose at an average of 84.5 ±1.3 °C for the sample annealed at 900 °C and 70.5 ±0.8 °C for the unannealed sample and the sample annealed at 500 °C. Figure 5.2 shows the dependence peak position on the irradiation dose for the three cases. Since the plot of peak position as a function of irradiation is independent of irradiation dose, the peak is subject to first-order kinetics in each case [4].

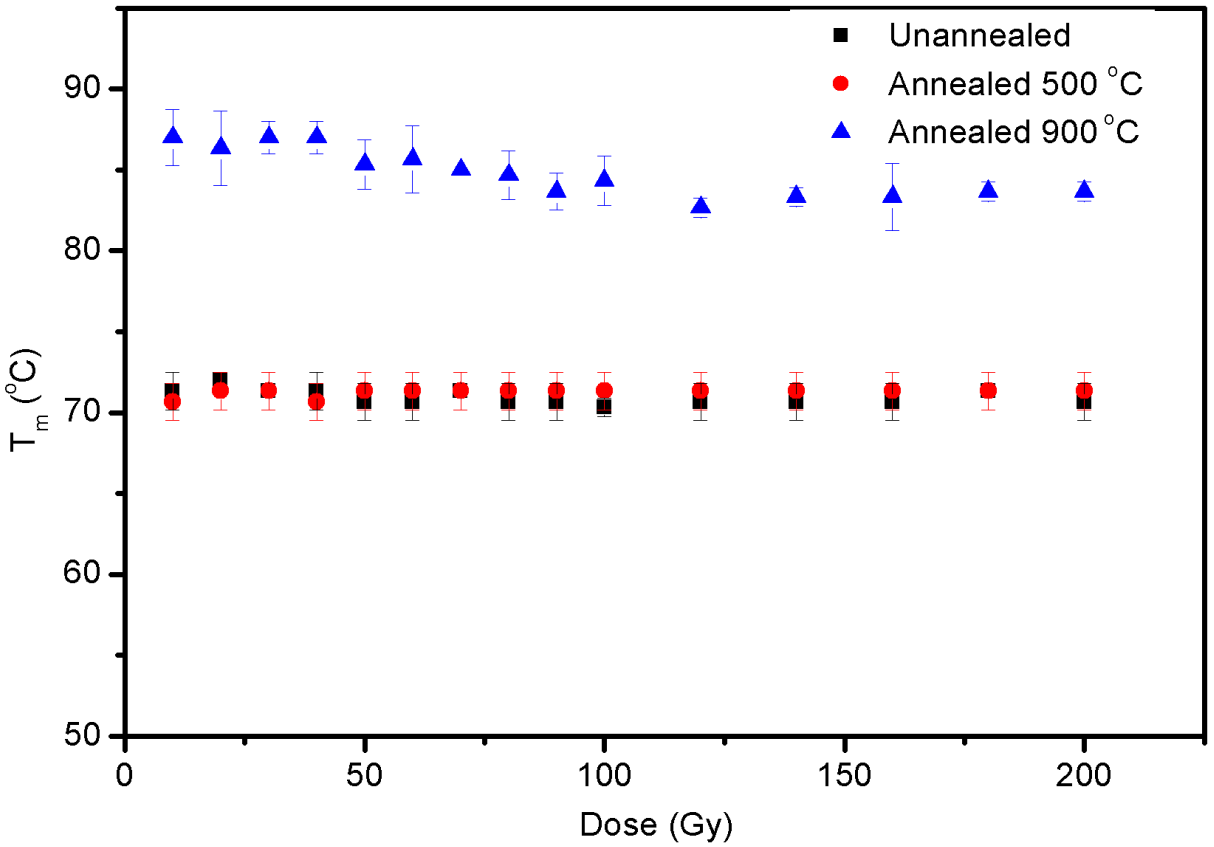

Figure 5.2: The variation of peak position with the irradiation dose for the unannealed sample and samples annealed at 500 and 900 °C.

5.3.2 Assessment using the T_m-T_{stop} method

The partial heating method, $(T_m - T_{stop})$ was also used to study the order of kinetics. The sample was irradiated to 40 Gy and partially heated from 40 to 42 °C and after cooling heated again to 500 °C to obtain the complete glow curve. The position, T_m of the resultant peak was noted.

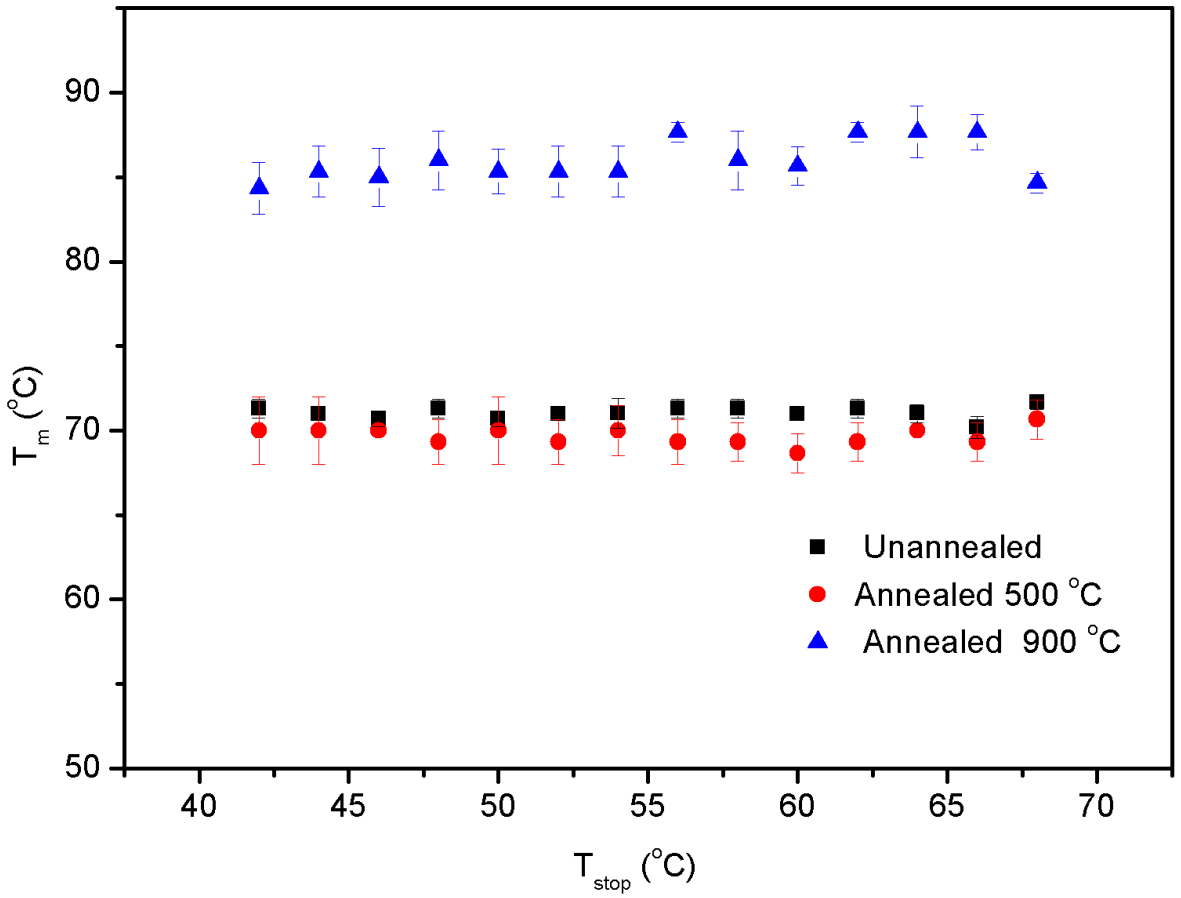

Figure 5.3: Plots of T_m against T_{stop} for measurements corresponding to 40 Gy. Each data point is an average of three measurements for the unnealed sample and samples annealed at 500 and 900°C.

The procedure was repeated with T_{stop} changed from 40 to 70 °C at intervals of 2 °C. The measurements were run three times and the average of T_m was obtained with the uncertainty ΔT as the standard deviation. Figure 5.3 shows the graph of T_m as a function of preheat temperature (T_{stop}) for samples. As shown T_m is independent of preheat temperature and is evidence of first-

order kinetics [4].

The averages of these positions were found to be 70.8±0.2 °C for the unannealed sample and the sample annealed at 500 °C while 85.4 ±1.4 °C for the sample annealed at 900 °C. The peak was thus confirmed to follow first-order kinetics.

5.4 Kinetic analysis

The kinetic analysis of the main peak was carried out using the initial rise, whole glow peak, peak shape, variable heating rate and curve fitting methods for comparison.

5.4.1 The initial rise method

The initial rise method is based on assumption that in the rising part of a glow peak, the thermoluminescence intensity $I(T)$ depends exponentially on temperature, T as given by equation (2.17). The initial rise method was used on data within the range 5-10 % (between 20 and 36 °C) of the maximum the main peak.

Figure 5.4 shows graphs of $\ln(I)$ against $1/kT$ for the unannealed sample and samples annealed at 500 and 900 °C. The activation energy of the main peak was determined as 0.91 ± 0.01 eV, 0.83 ± 0.02 eV and 0.77 ± 0.03 eV for the unannealed sample and samples annealed at 500 and 900 °C respectively. The values of the activation energy reported in our study are comparable with those reported by other researchers for synthetic quartz. For example Petrov and Baillif [52] calculated the value of activation energy of the main peak range from 0.80 to 0.99 eV, Kitis et al [53] reported as 0.79 eV and Yazici et al [54] as 0.90 eV. A preliminary conclusion in our study is that the activation energy slightly decreases with annealing temperature.

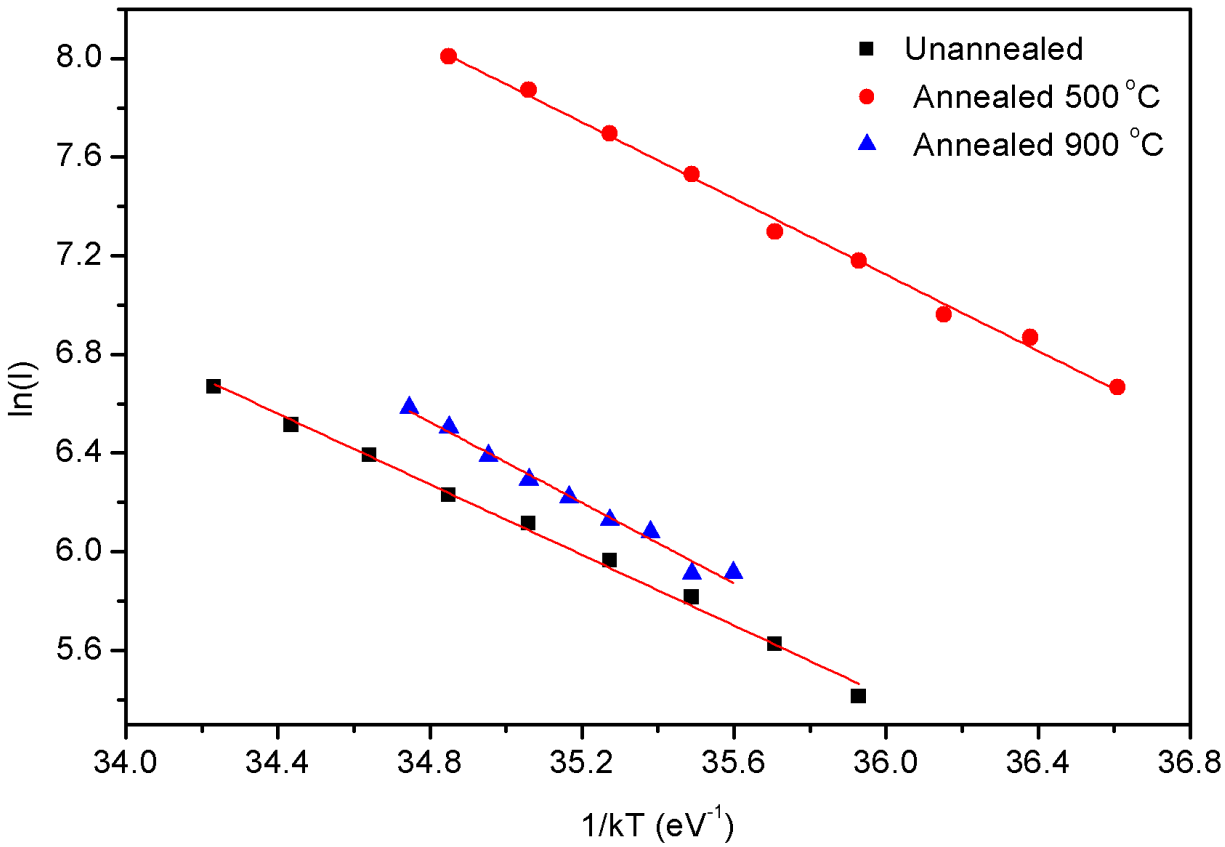

Figure 5.4: $\ln(I)$ against $1/kT$ for the unannealed sample and samples annealed at 500 and 900 °C. The solid lines represent the best fit in each cases for the main peak.

5.4.2 Whole glow curve method

The analyses were also carried out using the whole glow peak method. Figure 5.5 shows plots of $\ln(I/n^b)$ against $1/kT$ for the sample annealed at 900 °C. The best fit for the sample annealed at 900 °C was obtained with be b = 1.1 and E = 0.68±0.02 eV, s' = 5.2×10^{11} s^{-1}. The same approach was applied for the unannealed sample and the sample annealed at 500 °C which gave E = 0.90±0.02 eV, s' = 3.2 × $10^{10}s^{-1}$, b = 1.2 and 0.91±0.01 eV, s' = 2.3 × $10^{9}s^{-1}$ b = 1.1 respectively. The values of the activation energy for the main peak again decreased with increased with annealing temperature.

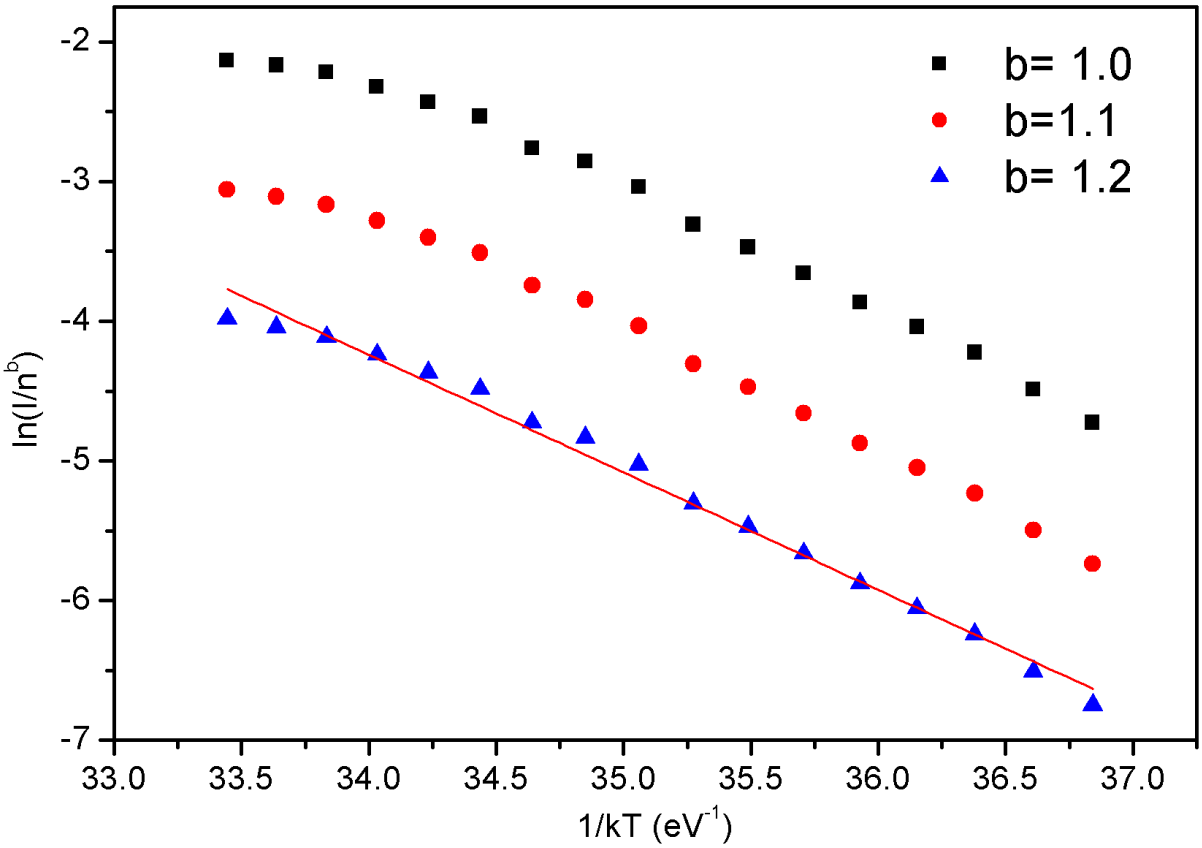

Figure 5.5: A plot of $\ln(I/n^b)$ versus $1/kT$ for different values of b for the sample annealed at 900 °C.

5.4.3 Peak shape method

The main peak was again analysed using the peak-shape method. The activation energy, E_α was calculated using the equation (2.21). The values of C_α and b_α are given in equations (2.22a-2.22c). The values of the geometrical factor for the unannealed sample and the samples annealed at 500 and 900 °C are $\mu_g = 0.40 \pm 0.03$, 0.42 ± 0.03 and 0.42 ± 0.02 respectively indicating first-order kinetics for the main peak. The values of the activation energy were evaluated as $E_\tau = 0.92 \pm 0.03$ eV, $E_\delta = 0.86 \pm 0.04$ eV and $E_\omega = 0.90 \pm 0.05$ eV respectively for unannealed sample. Similar calculations for the other samples gave $E_\tau = 0.92 \pm 0.06$ eV, $E_\delta = 0.89 \pm 0.04$ eV and $E_\omega = 0.91 \pm 0.04$ eV respectively for the sample annealed at 500 °C and for the one annealed at 900 °C, $E_\tau = 0.68 \pm 0.04$ eV, $E_\delta = 0.67 \pm 0.08$ eV, and $E_\omega = 0.68 \pm 0.06$ eV. These results

again suggest that the activation energy decreases when the annealing temperature is increased to 900°C.

5.4.4 Analysis using the variable heating rate method

Kinetic parameters were also analysed using the variable heating rate method which relies on the relationship between peak position and heating rate using equation (2.24). This technique was employed using heating rates from 0.2 to 5.0 °C s^{-1}. Figure 5.6 shows the plots of $\ln(T_m^2/\beta)$ against $1/kT_m$ for the unannealed quartz and samples annealed at 500 and 900 °C.

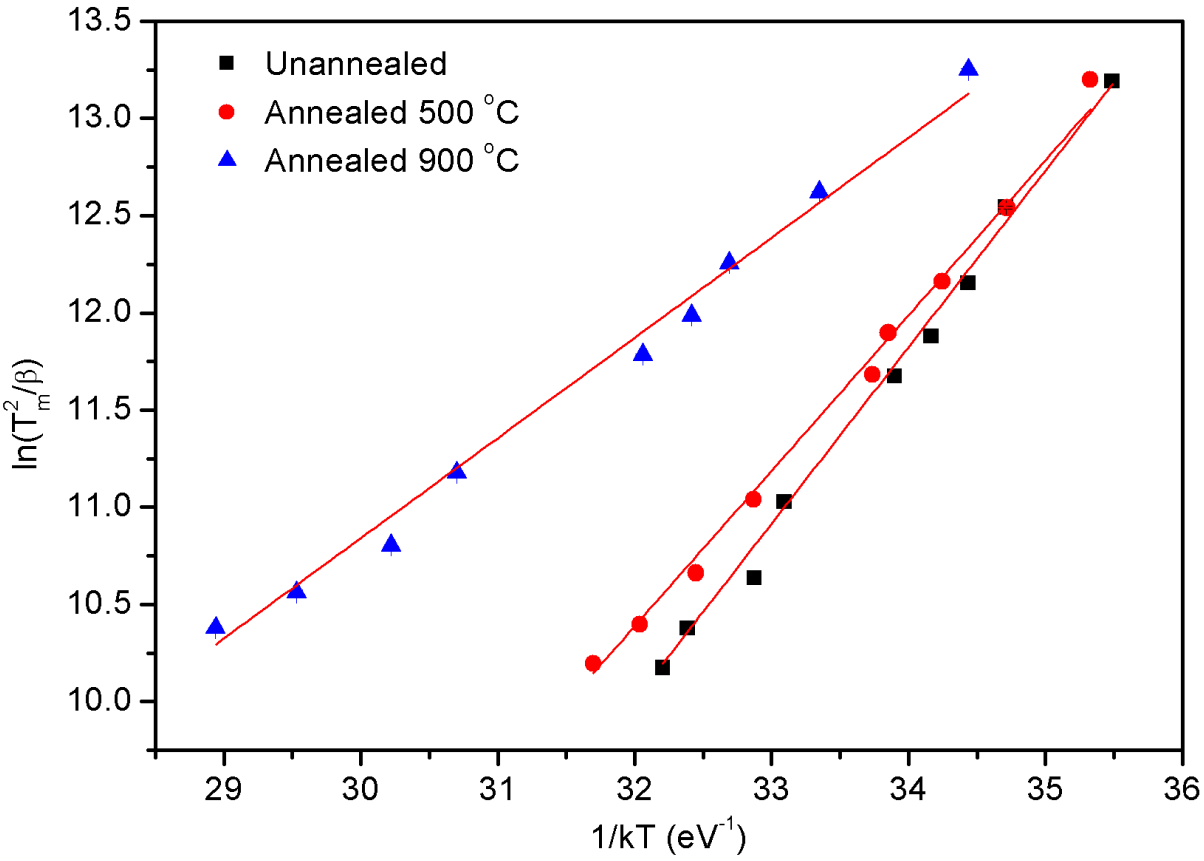

Figure 5.6: Plots of $\ln(T_m^2/\beta)$ against $1/kT_m$ used to evaluate values of E and s for the unnealed sample and samples annealed at 500 and 900 °C.

The activation energy for the sample annealed at 900 °C was found as 0.52 ± 0.02 eV. In comparison, for the unannealed sample and the sample annealed at 500 °C, the values were 0.80 ±

0.03 eV and 0.82 $\pm$ 0.03 eV. The results using this method appear to underestimate the values of E compared with the other methods used. However, the value of E still seems to decrease with annealing to 900 °C.

5.5 Analysis using phosphorescence-based methods

This section deal with the analysis of phosphorescence. The samples were annealed at 500, 900 °C and unannealed following irradiation to 40 Gy. Phosphorescence was carried out by simply looking at decay behaviour (first-order kinetics) [13] and temperature-dependence of the area under an isothermal decay-curve [30].

5.5.1 Analysis of phosphorescence using first-order kinetics

Phosphorescence is the decay of thermally stimulated luminescence as a function of time at a constant temperature. To further check the order of kinetics of the main peak, phosphorescence was measured between 40 and 60 °C from samples irradiated to 40 Gy.

For first-order kinetics, the phosphorescence decay follows a simple exponential decay as given in equation (2.35). Figure 5.7(a) shows the plot of $\ln(I)$ against t for the sample annealed at 900 °C. The linear form confirm first-order kinetics for this data. Figure 5.7(b) shows a graphs of $\ln(p)$ against $1/kT$ used to evaluate the kinetic parameters for the unannealed sample and samples annealed at 500 and 900 °C. The slopes of each plot is equal to the activation energy. For the sample annealed at 900 °C, this was found as 0.63 $\pm$ 0.04 eV. This can be compared with 0.96 $\pm$ 0.03 eV and 1.05 $\pm$ 0.05 eV determined using the same method for the sample annealed at 500 °C and for the unannealed sample respectively. Again, we notice a decrease in the activation energy with annealing temperature.

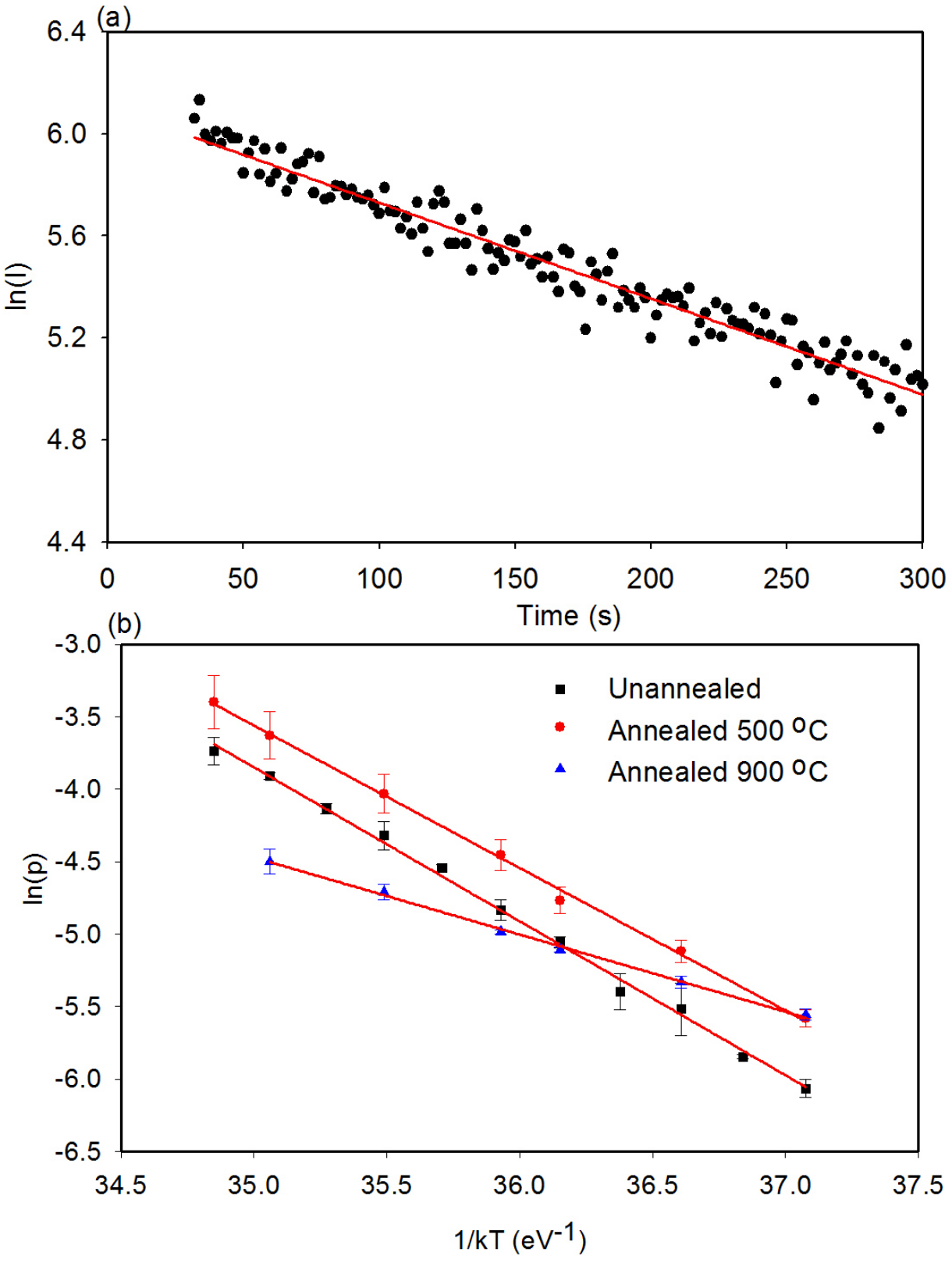

Figure 5.7: A graph of ln(I) against t for the sample annealed at 900 °C. (a) Plots of ln(p) against $1/kT$ for the samples annealed at 500, 900 °C and for the unannealed sample (b).

5.5.2 Analysis using the area under an isothermal decay-curve

The phosphorescence was further analysed using the temperature-dependence of the area under an isothermal decay-curve [30]. The temperature-dependence of the area Φ under a small segment of a phosphorescence decay curve is described by equation (2.46).

Figure 5.8 shows such graphs for the samples annealed at 500 and 900 °C and the unannealed sample. Using this method, the activation energy was found as 0.85 $\pm$ 0.02 eV, 0.79 $\pm$ 0.12 eV and 0.62 $\pm$ 0.03 eV respectively for unannealed sample and samples annealed at 500 and 900 °C. It is also evident here that the activation energy decreases with annealing to 900 °C.

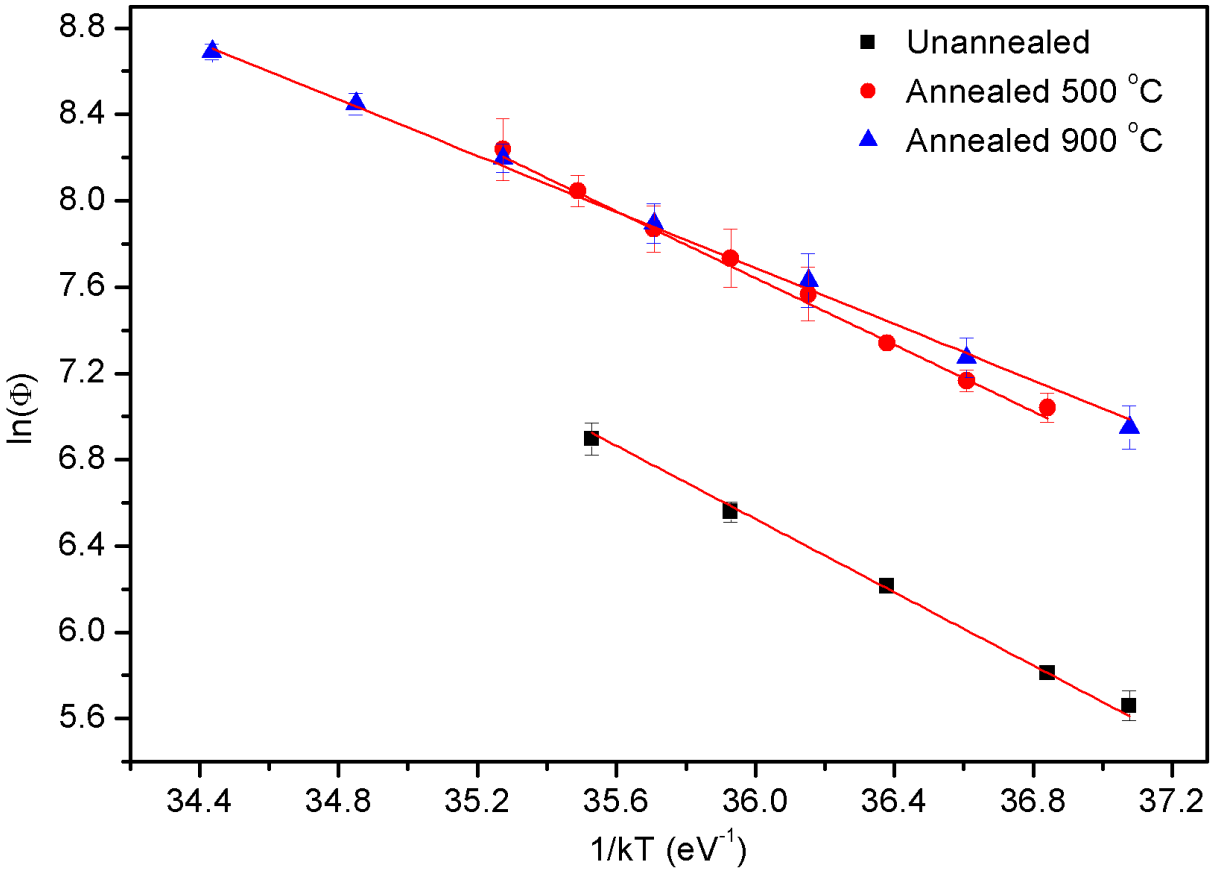

Figure 5.8: Plots of $\ln(\Phi)$ against $1/kT$ for the unnannealed sample and the samples annealed at 500 and 900 °C.

5.6 Thermal quenching and inverse thermal quenching

This section describe the influence of heating rates on thermoluminescence intensity. The unannealed sample and the samples annealed at 500 and 900 °C were used. The activation energy of thermal quenching was evaluated from the variable heating rate method [21] and using the temperature dependence of the area under isothermal decay curve [30].

5.6.1 Analysis for thermal quenching using the influence of heating rate on the thermoluminescence intensity

The influence of heating rate on thermoluminescence intensity (noted as peak area) is shown in Figure 5.9 of the unannealed sample and samples annealed at 500 and 900 °C . Results for the unannealed sample and the sample annealed at 500 °C is shown in Figure 5.9(a) & (b). The result for the sample annealed at 900 °C is shown in Figure 5.9(c). The intensity decreases with the heating rate for the unannealed sample and the sample annealed at 500 °C. This behaviour is ascribed to thermal quenching and applies for first order kinetics.

If $A_q(T)$ is the experimental quenched TL intensity and A_{uq} represent unquenched TL intensity at the lower heating rates, the two are related as

$$\frac{A_q}{A_{uq}} = \frac{1}{1 + Cexp\left(\frac{-\Delta E}{kT_m}\right)} \tag{5.1}$$

where ΔE is the activation energy of thermal quenching, C is a constant and all other terms are as previously defined [21]. A plot of ln[(A_{uq}/A_q)-1] against 1/kT_m should yield a straight line with slope ΔE. Figure 5.10 shows a plots for the unannealed sample and the sample annealed at 500 °C from which ΔE and C were found as 0.82 ±0.02 eV and 2.2×10^{13} for the sample annealed at 500 °C . The results for the unannealed sample was evaluated as 0.95 ± 0.06 eV and 3.2×10^{14}. These parameters compare well with ΔE = 0.80 eV [47] for the same quartz.

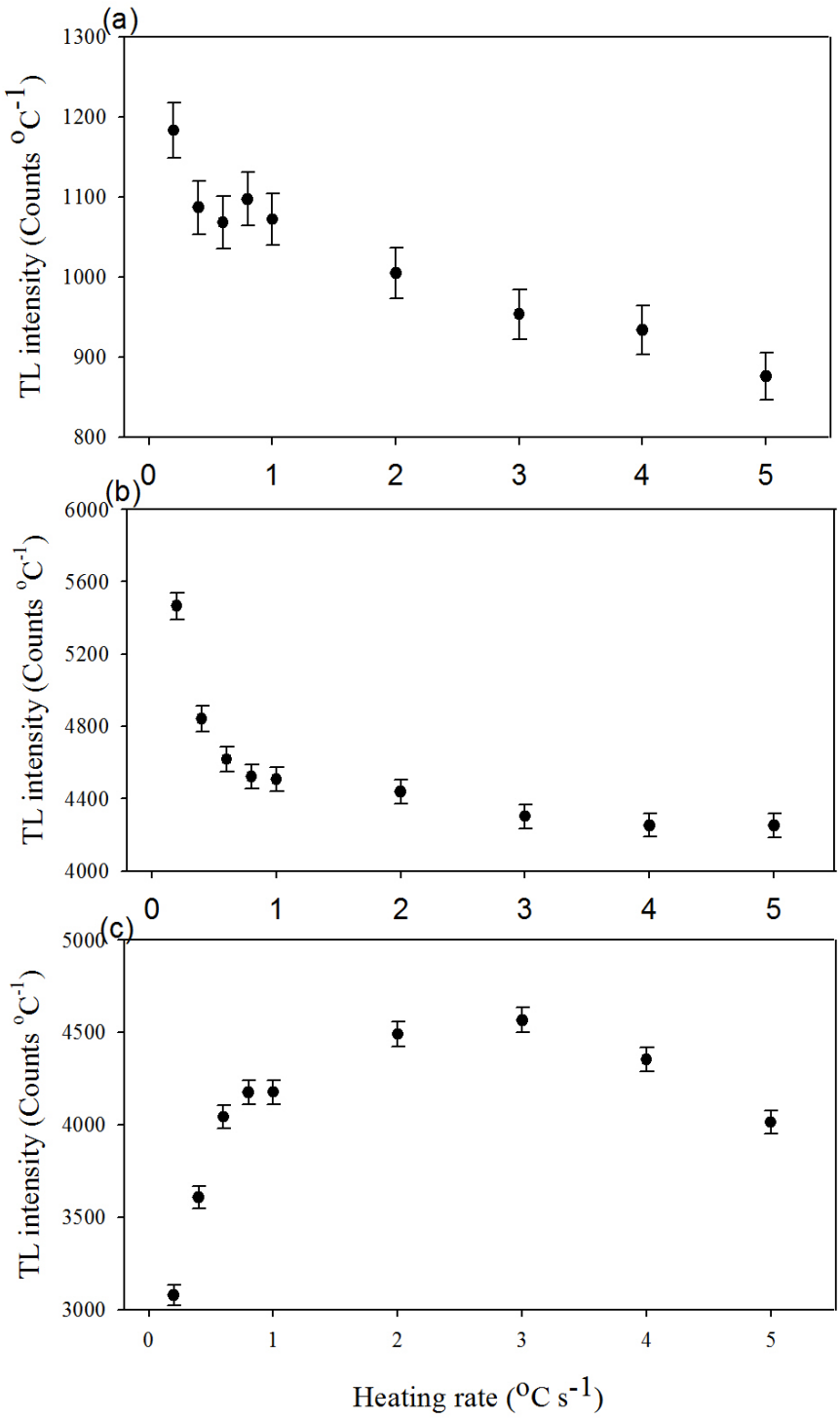

Figure 5.9: The variation of peak intensity with heating rate forunannealed sample (a) the sample annealed at 500 °C (b) and the sample annealed at 900 °C (c).

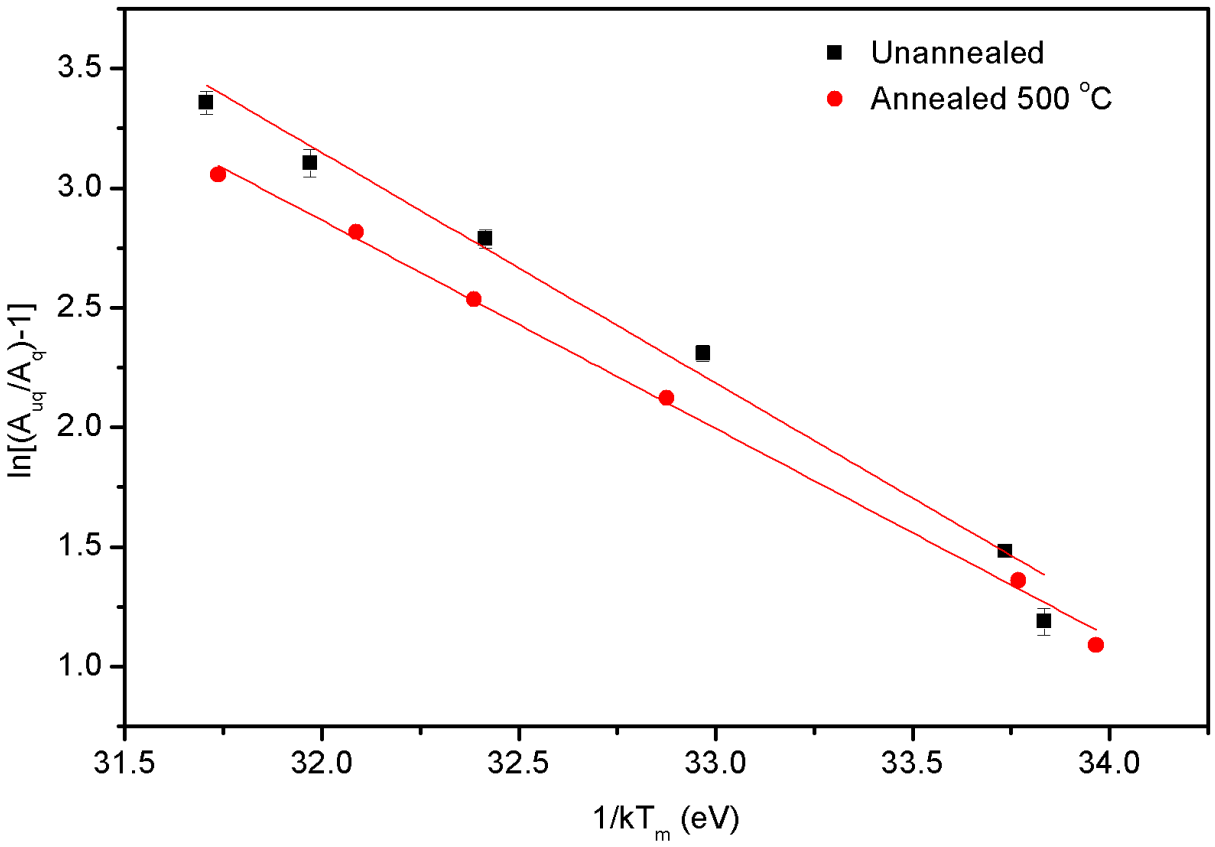

Figure 5.10: The graph of $\ln[(A_q/A_{uq}) - 1]$ against $1/kT_m$ used to evaluate the quenching parameters for unannealed sample and the sample annealed at 500 °C.

5.6.2 Inverse thermal quenching: Investigations of thermal quenching in synthetic quartz annealed at 900 °C

The study reported in this section was published by Dawam and Chithambo [50]. The increase of TL intensity with the heating rate in the sample annealed at 900 °C may imply the absence of thermal quenching. Therefore, such a preliminary conclusion needs to be verified by alternative tests. However, for the same dose of 40 Gy, the intensity of the sample annealed at 900 °C behaves differently with the heating rate as shown in Figure 5.9(c). The TL intensity for the sample annealed at 900 °C increases with heating rate. This could mean that the sample in question is not affected by thermal quenching.

It is known that luminescence emission involves competing radiative and non-radiative routes summarised as

$$\frac{1}{\tau} = \frac{1}{\tau_{rad}} + \frac{1}{\tau_{th}} exp\left(\frac{-\Delta E}{kT}\right) \tag{5.2}$$

where $1/\tau_{rad}$ is the probability of radiative emission, $1/\tau_{th}$ is the probability of thermal excitation and ΔE is the activation energy of thermal quenching [55]. The implications of the competing pathways were illustrated for α-Al_2O_3:C [40]. The hypothesis is that if the number of electrons undergoing radiative transitions is very low, the luminescence intensity cannot be high enough to mask any loss due to non-radiative transitions. For this reason, any effect due to non-radiative transition i.e thermal quenching will be manifest and can be studied.

For this test, the dependence of TL intensity on heating rate was measured again but this time with the dose significantly reduced from 40 Gy to 3 Gy. Figure 5.11(a) shows the result. Unlike before, the TL intensity decreases with the heating rate. The thermal quenching was quantified as before. Figure 5.11(b) shows the plot of ln[(A_{uq}/A_q)-1] against $1/kT_m$ from which ΔE = 0.65$\pm$0.02 eV and C = 2.4 $\times 10^{10}$. It is evident that when a high dose is used, the effect of thermal quenching does not appear. This is an important finding of the present study, that thermal quenching has an apparent dependence on dose in the sample annealed at 900 °C.

Since the manifestation of thermal quenching depends on the irradiation dose on the sample annealed at 900 °C, the question here is up to what level of irradiation would the TL intensity decrease or increase with the heating rate. In this investigation we, studied this effect using irradiation dose of 10, 15 and 20 Gy. Figure 5.12 shows the plots of TL intensity as a function of the heating rate. It is evident that for the sample irradiated 10 Gy, the TL intensity decreases with increase in heating rate as shown with irradiation of 3 Gy. However, when the sample was irradiated with doses between 15 and 20 Gy, the TL intensity increases as a function of the heating rate and resembles that for 40 Gy.

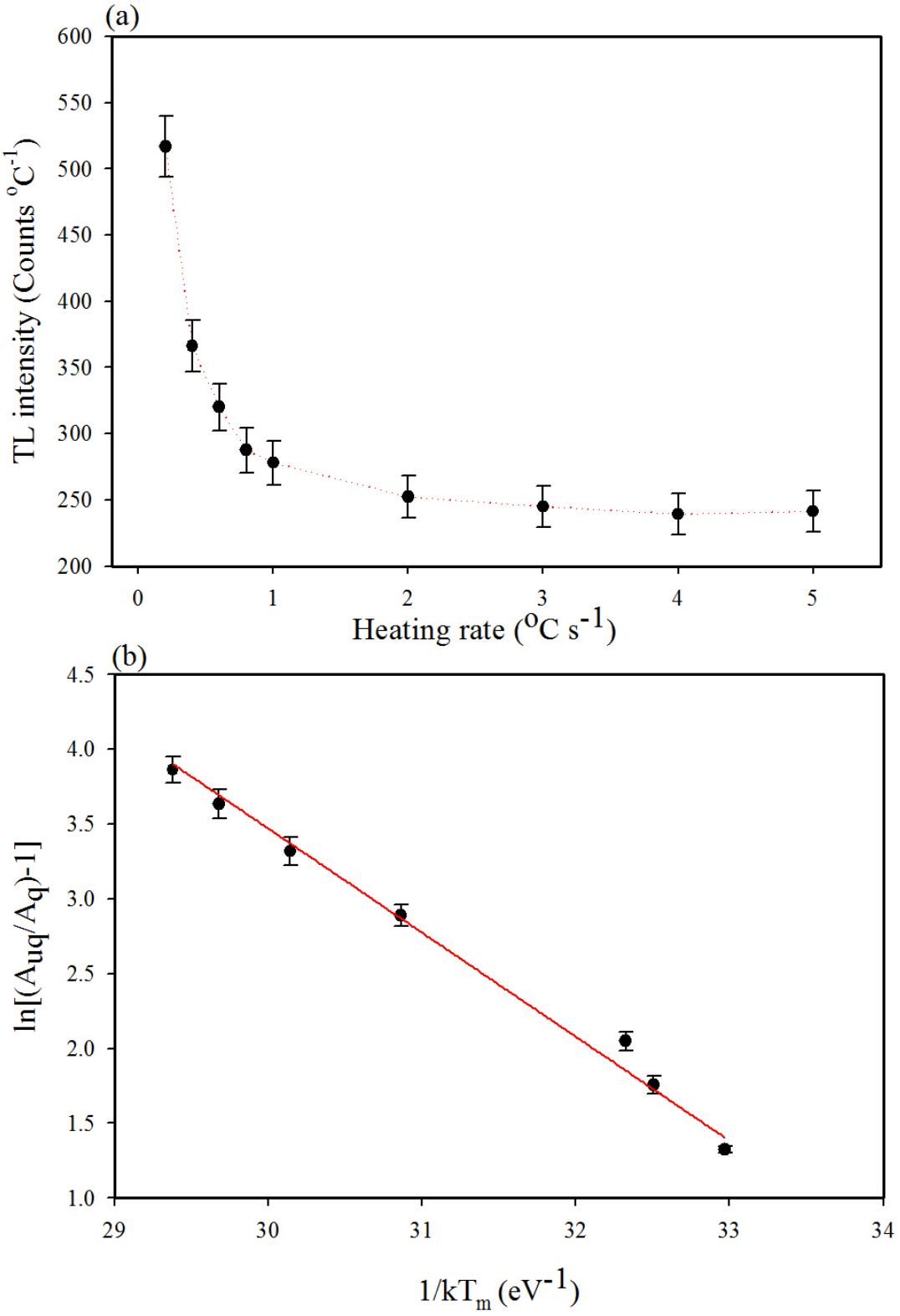

Figure 5.11: The dependence of peak intensity as a function of heating rate for the sample annealed at 900 °C (a) The graph of $\ln[(A_q/A_{uq})-1]$ against $1/kT_m$ used to evaluate the quenching parameters (b). The dose used here was 3 Gy.

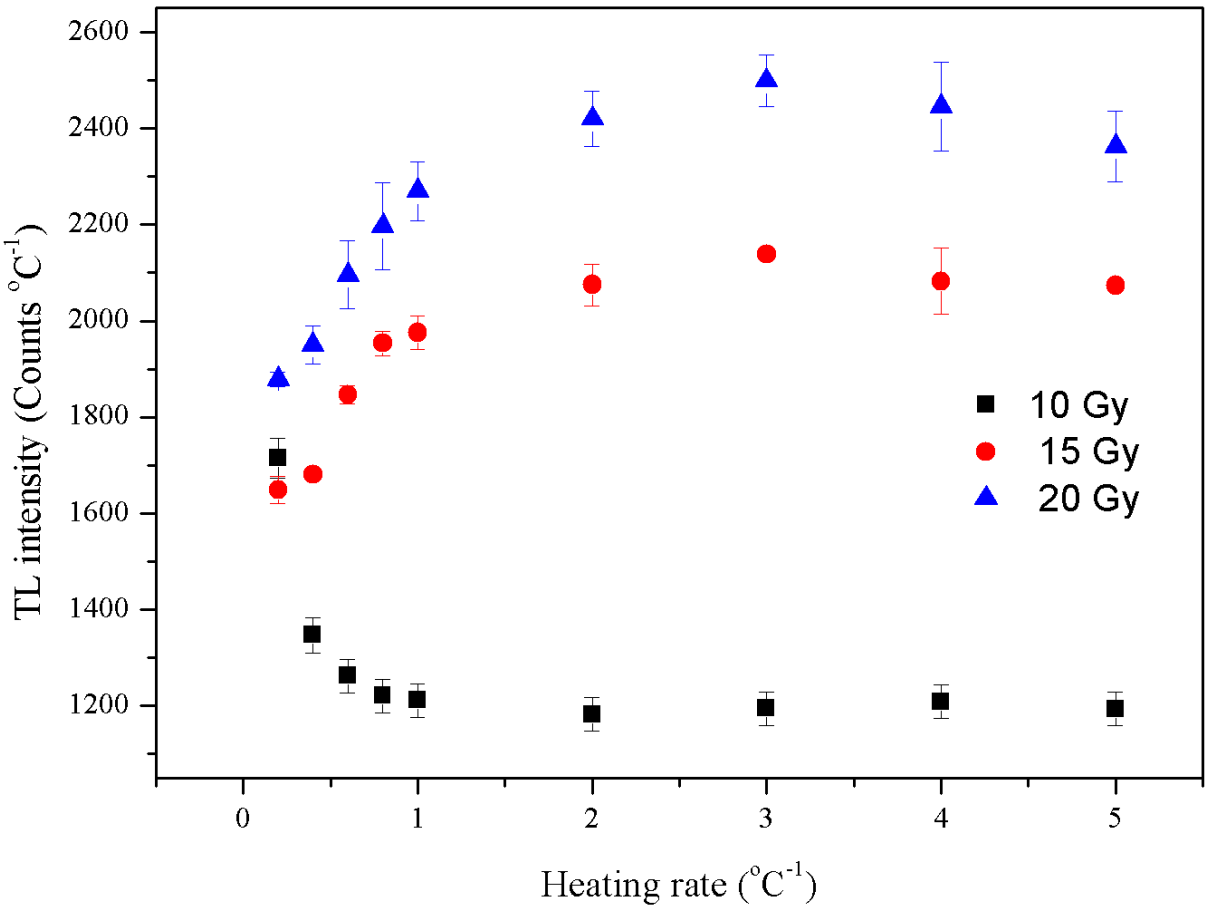

Figure 5.12: The dependence of peak intensity as a function of heating rate for the sample annealed at 900 °C irradiated to dose of 10, 15 and 20 Gy.

The activation energy of thermal quenching of all the sample irradiated to 10, 15 and 20 Gy were evaluated using the temperature dependence of the area under isothermal decay curve as reported by Chithambo [30]. This is discussed in the next section. The values of the activation energy of thermal quenching were found as $\Delta E = 0.67 \pm 0.02$, 0.64 ± 0.02 and 0.68 ± 0.03 eV for irradiation to 10, 15 and 20 Gy respectively. These results are consistent.

5.6.3 Quantifying thermal quenching using phosphorescence

The study reported in this section was published by Dawam and Chithambo [50]. The activation energy for thermal quenching in the quartz annealed at 900 °C was again evaluated using an

alternative method based on the use of phosphorescence [30]. If Φ_q is the fractional area under a phosphorescence decay curve at a particularly high temperature where thermal quenching is most effective and Φ_{uq} is the fractional area under a phosphorescence decay curve measured at lower temperatures where thermal quenching is less of an effect, these two parameters are related as

$$\frac{\Phi_q}{\Phi_{uq}} \approx \frac{1}{C} exp\left(\frac{\Delta E}{kT}\right) \tag{5.3}$$

where all symbols are as previously defined [30]. The plot of ln(Φ_q/Φ_{uq}) against 1/kT should be linear with slope equal to the activation energy of thermal quenching. The ratio Φ_q/Φ_{uq} was calculated for measurements between 40 and 60 °C at 2 °C interval. Figure 5.13 shows the graph of ln(Φ_q/Φ_{uq}) against $1/kT$ for the unannealed quartz, quartz annealed at 500 and 900 °C label (a), (b) and (c) respectively.

It should be noted that this method is useful where equation (5.1) cannot be applied, for example, if the TL intensity increases with heating rate. The values of the activation energy of thermal quenching evaluated using this method were 0.82±0.03 eV 0.78 ± 0.02 eV and 0.65 ± 0.03 eV for the unannealed sample, and samples annealed at 500 and 900 °C respectively. The value of ΔE (0.65 ± 0.03 eV) using the phosphorescence method is in excellent agreement with that from the heating rate method (0.65 ± 0.03 eV). In general, it also seems that the value of ΔE decreases with annealing temperature.

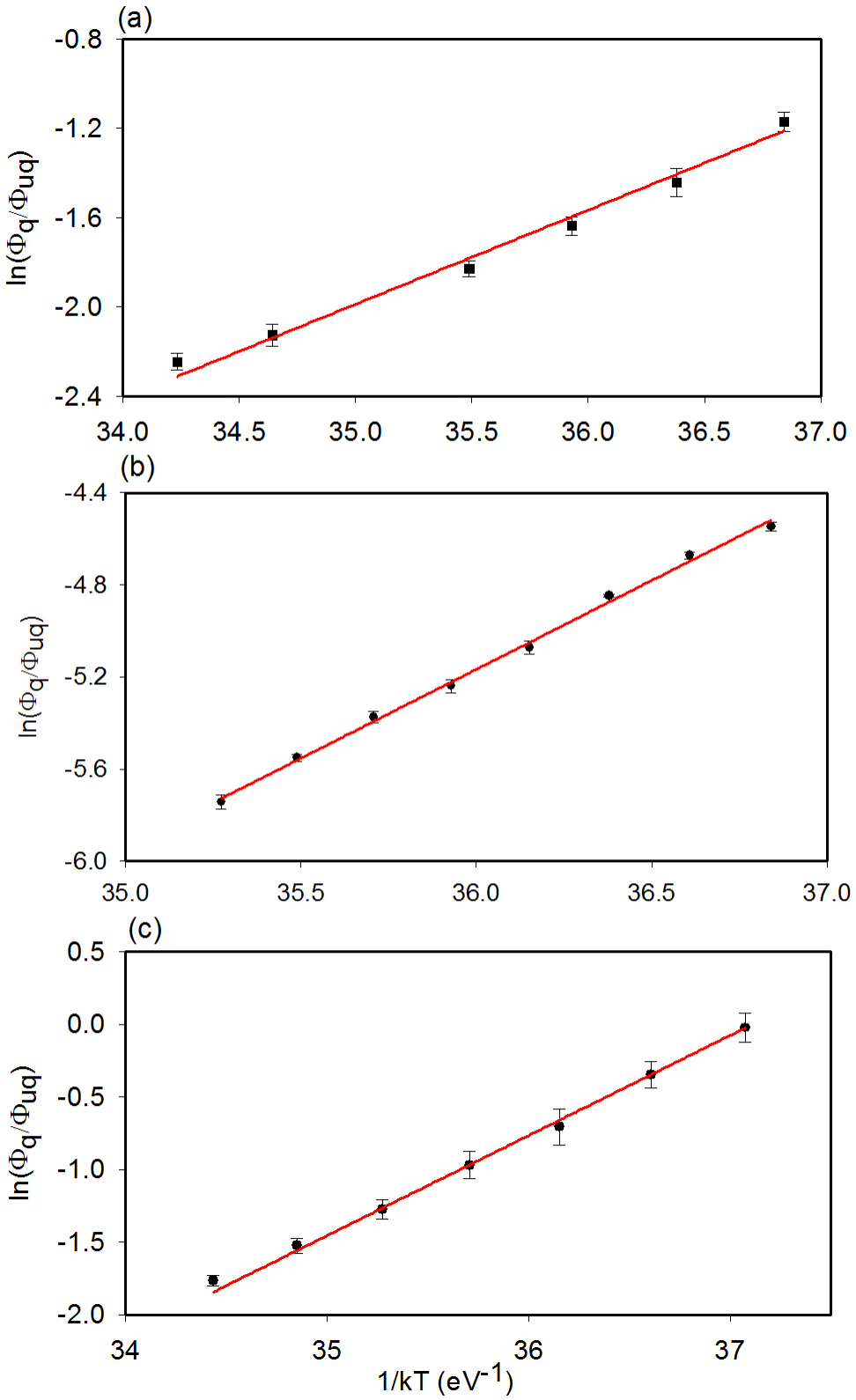

Figure 5.13: The graph $\ln(\Phi_q/\Phi_{uq})$ against $1/kT$ used to calculate the activation energy of thermal quenching for the (a) unannealed sample (b) the sample annealed at 500 °C (c) the sample annealed at 900 °C.

If the area Φ is directly plotted against measurement temperature, one finds another method of calculating kinetic parameters.

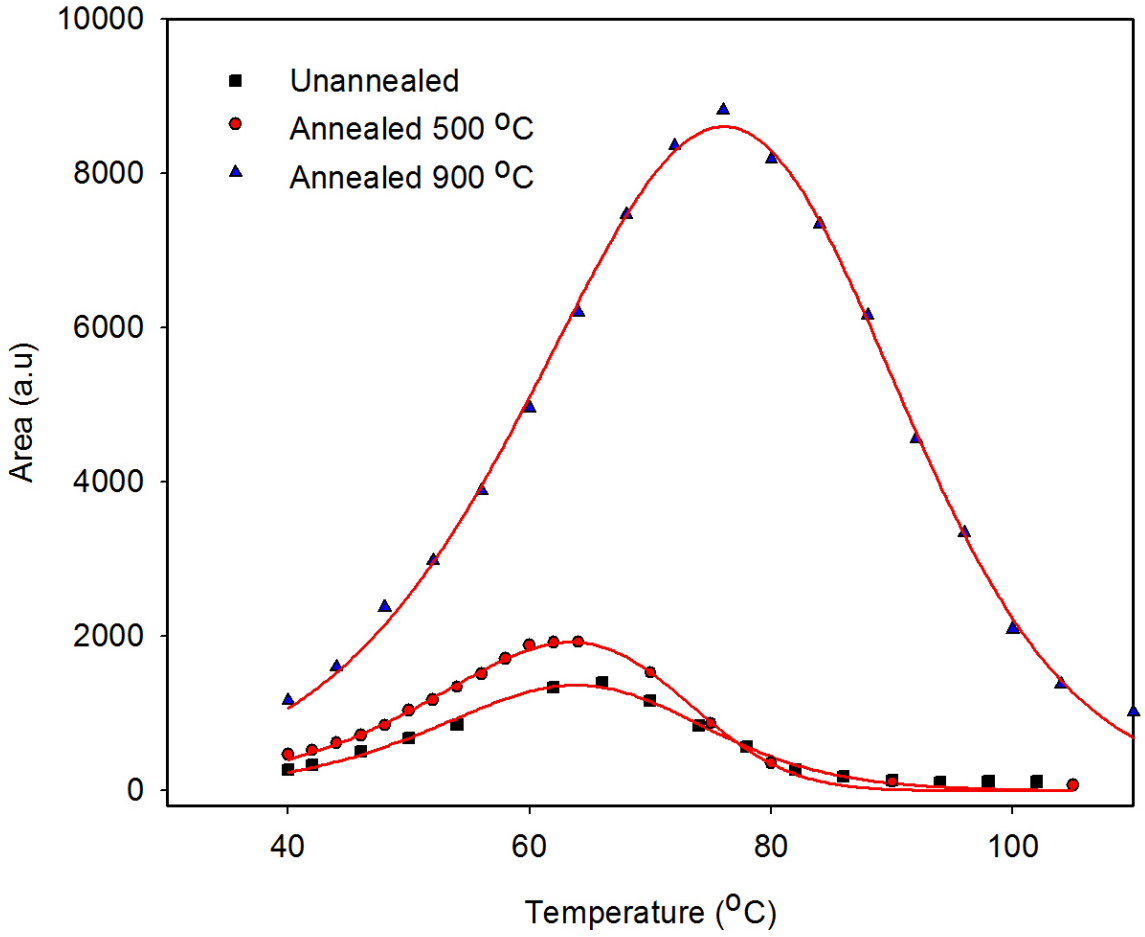

Figure 5.14: The dependence of area (Φ) on the measurement temperature made of the unannealed sample, sample annealed at 500 and 900 °C as indicated in the figure. The solid line through the data points in case is the best fit of general-order glow curve using Kitis [26]

Figure 5.14 shows the plot of area(Φ) against measurement temperature which resembles a TL glow peak. This peak was analysed using curve fitting method [26] where E and b found as 1.00 $\pm$0.02 and 1.05$\pm$ 0.03 for unannealed sample. For sample annealed at 500 °C, $E = 0.99 \pm 0.02$ eV, $b = 1.15 \pm 0.04$ and for sample annealed at 900 °C $E = 0.80 \pm 0.03$ eV, $b = 1.13 \pm 0.03$. These results also show that the values of activation energy decrease with annealing.

5.6.4 Curve fitting of the main peak

The main peak was also analysed by curve fitting. The main peak was isolated from the weaker ones and then fittings only with the general kinetics equation (2.30). The solid line passing through the data points is the best fit. The fitted were carried out on the unannealed sample, sample annealed at 500 and 900 °C. Figure 5.15 shows the TL glow curve fitted with equation (2.30) for unannealed sample, sample annealed at 500 and 900 °C. The residuals for all the three samples are plotted and shown top of Figure 5.15. The values of the activation energy were E = 1.03 $\pm$ 0.03, 0.96 $\pm$ 0.02 and 0.80 $\pm$ 0.04 eV for the unannealed quartz, and the one annealed at 500 and 900 °C respectively. The associated order of kinetics are b =1.12 $\pm$0.05, 1.06 $\pm$ 0.03 and 1.14 $\pm$ 0.06 respectively, this is again first order kinetics. Using the parameters obtained above, the frequency factor was evaluated from the equation (2.34) as 1.1 $\times 10^{13}$, 1.7 $\times 10^{12}$ and 2.7 $\times 10^{10}$ s^{-1} for unannealed sample, sample annealed at 500 and 900 °C respectively. These results are also consistent with those from the other methods.

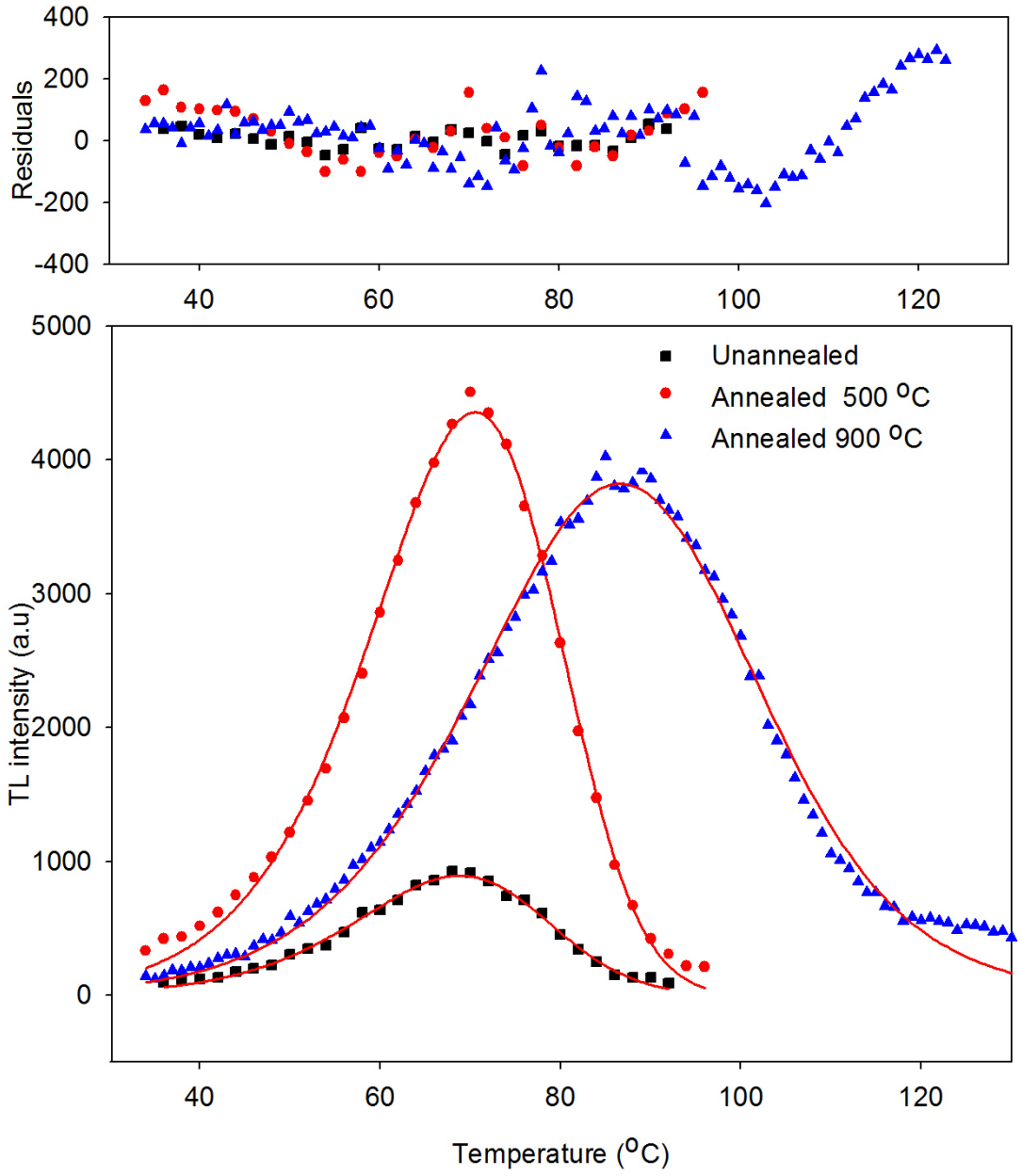

Figure 5.15: The TL glow curve of the main peak measured from unannealed sample and samples annealed at 500 and 900 °C. The data is shown fitted with equation (2.30). The residuals plot shows the goodness of the fits.

5.7 Dosimetric features

In this section, the influence of dose on the intensity on the unannealed sample and the samples annealed at 500 and 900 °C is reported. The dose response was described qualitatively by the super-linearity index in all the three samples. Influence of delay time between irradiation on the main TL peak was also studied for the three samples.

5.7.1 Dose response of the main peak

The dose response of the main peak of the three samples was studied. Each sample was irradiated to different doses between 10 and 200 Gy. In each case, the maximum intensity of each peak was noted. Each data point is an average of three identical measurements and the error bars are the standard deviation. Figure 5.16 shows the dependence of maximum intensity as a function of irradiation dose for the unannealed sample and the samples annealed at 500 and 900 °C respectively. The TL intensity in each case increases with the irradiation dose.

The growth curve of the dose response can be express as

$$I_m = aD^k \tag{5.4}$$

where I_m represent the peak intensity, D is the irradiation dose and a, k are constants [21].

The qualitative analysis of dose response was carried out using super-linearity index for

$$g(D) = [(Dy^{''}(D)/y^{'}(D)) + 1] \tag{5.5}$$

where $g(D)$ is super-linearity index, $y^{'}(D)$ and $y^{''}(D)$ indicates the first and second derivative of the function $y(D)$. The super-linearity index $g(D)$ gives the change in the slope of dose response.

A value of $g(D) < 1$ indicates sub-linearity while $g(D) > 1$ indicate super-linearity while $g(D) = 1$ signifies the linearity [21]. As seen in Figure 5.16 for all the three samples, $g(D)$ shows sublinear behaviours.

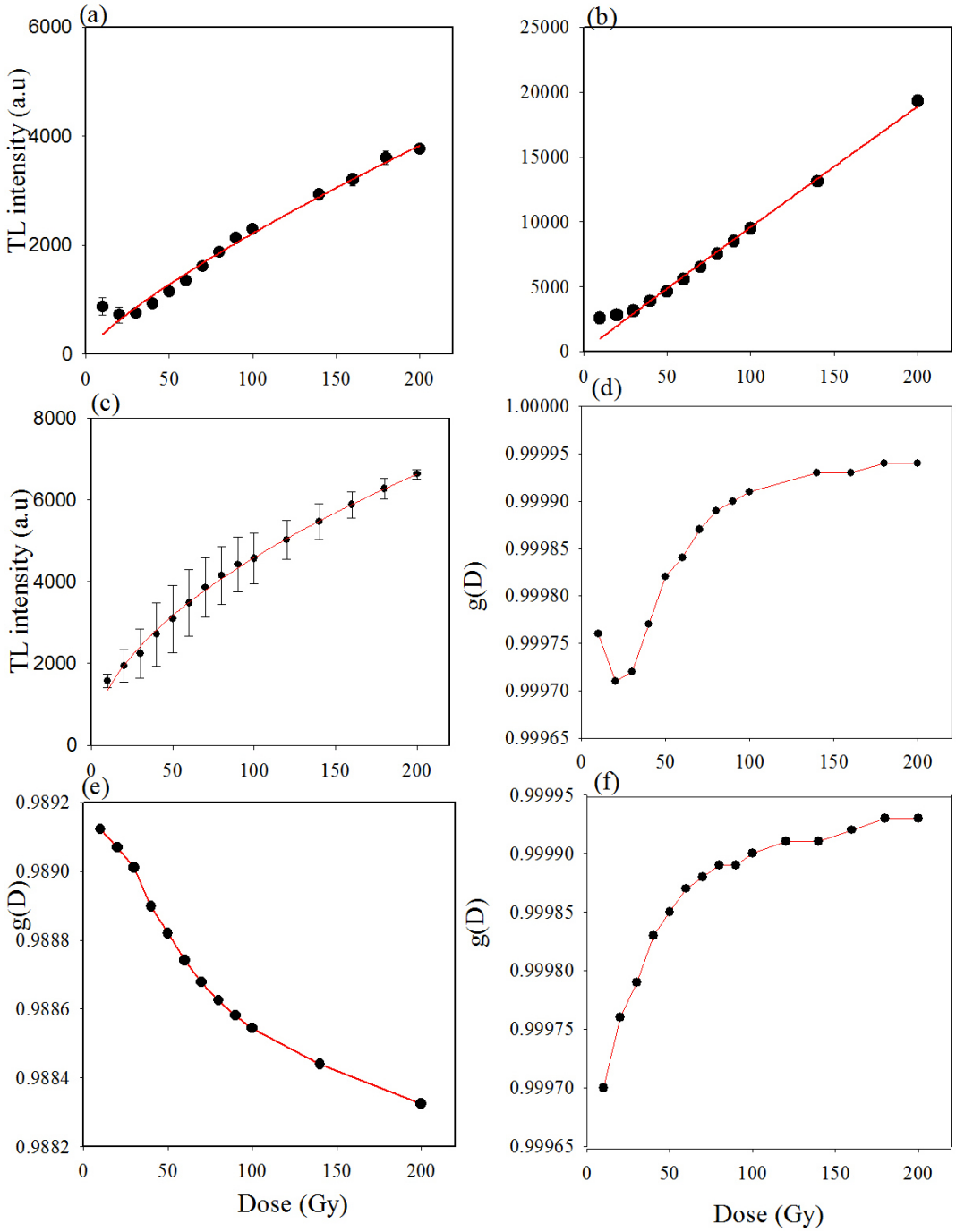

Figure 5.16: The dose response of (a) the unannealed sample (b) the sample annealed at 500 °C (c) the sample annealed at 900 °C (d) plot of g(D) as a function of irradiation for unannealed sample (e) plot of g(D) as a function of irradiation for sample annealed at 500 °C (f) and plot of g(D) as a function of irradiation for sample annealed at 900 °C. The solid line passing through the data point are the best fit.

5.7.2 Fading

The influence of delay time between irradiation and measurement on the main TL peak was studied from the unannealed sample and the samples annealed at 500 and 900 °C. The fading of the main peak could be described by an exponential function of the form

$$I(t) = I_o \exp(\lambda t) \tag{5.6}$$

where I(t) is the TL intensity at time t, I_o is the initial TL intensity and λ is the decay constant [13]. The intensity of the main peak was observed to decreases with time until it reaches minimum values after 5 hours. Figure 5.17 shows the fitted form of equation (5.6) where the solid line through the data points is the best fit of I(t). The decay constants were obtained from the best fits as 2.85 $\times 10^{-3}$ s^{-1}, 2.92 $\times 10^{-3}$ s^{-1} and 3.10 $\times 10^{-3}$ s^{-1} hence mean lifetime of the main TL peak in each case are $\approx$ 1 hour.

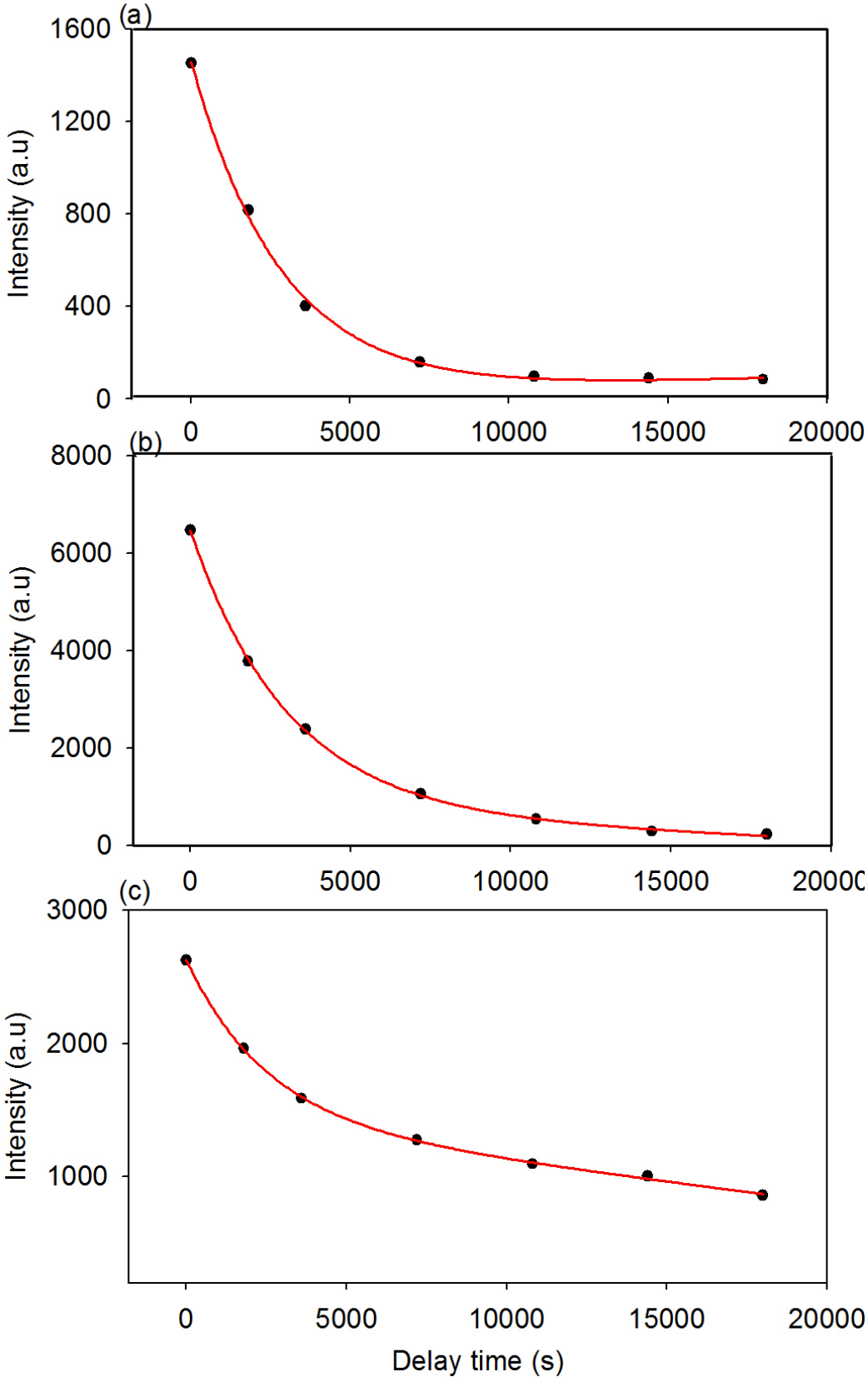

Figure 5.17: Plots of TL intensity against delay time for (a) the unnannealed sample (b) the sample annealed 500 °C (c) the sample annealed at 900 °C.

5.8 The effect of annealing on kinetic paramters and thermal quenching

Kinetic parameters evaluated using various methods are summarised in Table 5.1. These values of the activation energy can be compared with 0.82 $\pm$ 0.04 eV for a peak at 110 °C in synthetic quartz annealed at 900 °C [53] determined using the heating rates 0.5-4 °C. A direct comparison of the values from different samples is not instructive but evidently the order of magnitude of the activation energy is similar. For the unannealed sample, the values of ΔE compare well with ΔE = 0.80 eV [47] for the sample quartz annealed at 600 °C.

This study has been published previously [50]. Our results show that the values of E and ΔE decrease with annealing temperature. It is necessary to account for this. Regarding thermal quenching, previous studies on this quartz showed that lifetime determined from time-resolved spectral change with annealing temperature [48] as do emission bands [49]. In particular, the sample shows at least seven emission band between 2.04 and 3.91 eV whose amplitude depends on annealing up to 1000 °C. The change in lifetime with annealing is ascribed to change in dominant recombination centre involved in the luminescence [48, 56]. Since the activation energy for thermal quenching depends on the emission wavelength [49], the change of ΔE can be ascribed to change in dominant recombination centre with annealing.

The effect of annealing on electron traps is of interest. Computational simulations which accounted for the increase in TL sensitivity with annealing e.g Chen and Fogel [57] implicitly assumed that kinetic parameters are unaffected by annealing. On the other hand, Toktamiş and Yazici [58], who studied the effect of annealing on trap depth in synthetic quartz and natural quartz, reported that annealing affected the trap depth of all glow peaks and that the trap depth increased after annealing. Hence Toktamiş and Yazici [58] results show that the activation energy in quartz can be affected by annealing.

The cause of change in the activation energy of an electron trap with annealing is possible due to a complex combination of structural and electron modification of associated point-defects due to annealing. Previous studies using positron annihilation on the sample studied here showed that

annealing did not produce a new defects in the sample [48]. It is likely then that the change in activation energy is due to electronic modification of the electron trap(s). For example, oxygen or silicon vacancies in quartz can catalyse the formation of other unstable defects which can act as electron traps (for example see Table 2 in Preusser et al [1]). Examples of possible electron traps in quartz are extensive and inclusive the family of E-centers and othersstabilised by the presence of, for example H. Removal or displacement of a stabilising species can affect the electron trap and potential it is associated with as discussed elsewhere [1]. If annealing causes a change in the electronic configuration of an electron trap or its site, then a change in its potential with respect to the conduction band can be reflected as a change in the activation energy as observed.

T_A (∘C)	Method	E (eV)	b	s(s^{-1})	ΔE (eV)	Reference.
20	T_m -dose		1			Figure 5.2
20	$T_m - T_{stop}$		1			Figure 5.3
20	Initial rise	0.91 ± 0.01				Figure 5.4
20	Whole glow peak	0.90 ± 0.02	1.2	3.2 $\times 10^{10}$		Section 7.4.1
20	Peak shape	0.92 ± 0.03x				Section 5.4.3
20		0.86 ± 0.04y				Section 5.4.3
20		0.90 ± 0.05z				Section 5.4.3
20	Variable heating rate	0.80 ± 0.03			0.95± 0.06	Figure (5.6 & 5.10)
20	Curve fitting	1.03 ± 0.03	1.12 ± 0.05	1.1 $\times 10^{13}$		Figure 5.15
20	Phos first-order	0.96 ± 0.05				Figure 5.7(b)
20	Phos area method	0.85 ± 0.02			0.82 ± 0.03	Figure (5.8 & 5.13(a))
20	Curve fitting Area Phos	1.00 ± 0.02	1.04 ± 0.03			Figure 5.14
500	T_m -dose		1			Figure 5.2
500	$T_m - T_{stop}$		1			Figure 5.3
500	Initial rise	0.83 ± 0.02				Figure 5.4
500	Whole glow peak	0.91 ± 0.01	1.1	2.3 $\times 10^{9}$		Section 7.4.1
500	Peak shape	0.92 ± 0.06x				Section 5.4.3
500		0.89 ± 0.06y				Section 5.4.3

500		0.91 ± 0.04z				Section 5.4.3
500	Variable heating rate	0.82 ± 0.03			0.82 ± 0.02	Figure (5.6 & 5.10)
500	Curve fitting	0.96 ± 0.02	1.06 ± 0.03	1.7 $\times 10^{12}$		Figure 5.15
500	Phos first-order	0.96 ± 0.03				Figure 5.7(b)
500	Phos area method	0.79± 0.12			0.78± 0.02	Figure (5.8 & 5.13(b))
500	Curve fitting Area Phos	0.99 ± 0.03	1.15 ± 0.04			Figure 5.14
900	T_m -dose		1			Figure 5.2
900	$T_m - T_{stop}$		1			Figure 5.3
900	Initial rise	0.77 ± 0.03				Figure 5.4
900	Whole glow peak	0.67 ± 0.02	1.1	2.3 $\times 10^{9}$		Figure 5.5
900	Peak shape	0.68 ± 0.04x				Section 5.4.3
900		0.67 ± 0.08y				Section 5.4.3
900		0.68 ± 0.06z				Section 5.4.3
900	Variable heating rate	0.52 ± 0.02			0.65 ± 0.02	Figure (5.6 & 5.11 (b))
900	Curve fitting	0.80 ± 0.04	1.14 ± 0.06	2.7 $\times 10^{12}$		Figure 5.15
900	Phos first-order	0.63 ± 0.04				Figure 5.7(b)
900	Phos area method	0.62 ± 0.03			0.65 ± 0.03	Figure (5.8 & 5.13(c))
900	Curve fitting Area Phos	0.80 ± 0.03	1.13 ± 0.03			Figure 5.14

Table 5.1: Kinetic parameters determined using various methods. The indices x, y, z corresponding to the peak shape method refer to E_δ, E_δ and E_ω respectively, T_A stands for the annealing temperature which the unannealed sample is shown as 20 °C

5.9 Summary

The thermoluminescence of synthetic quartz annealed at 900 °C has been reported. Measurements were also made on quartz annealed at 500 °C as well as from an unannealed sample. Glow curves recorded at 1 °C s^{-1} following beta irradiation to 40 Gy from all these samples show three peaks with a prominent peak at just below 100 °C. Kinetic analysis was carried out on this main peak only in each case. Using various methods, the order of kinetics of this peak was determined to be first order. It has been observed that the activation energy decreases from an average of 0.90 ± 0.02 eV to when the annealing temperature is changed from room temperature 0.65 ±0.02 eV to 900 °C. The intensity of the main peak corresponding to 40 Gy decreases with the heating rate in a manner observed for thermal quenching for the sample annealed at 500 °C as well as the unannealed one. In contrast, the intensity increases with the heating rate for the same dose in the sample annealed at 900 °C, a result that may suggest an absence of thermal quenching in this case. When the experiment on the sample annealed at 900 °C is instead made using a low dose of 3 to 10 Gy, the intensity decreases with heating rate. The activation energy for thermal quenching for samples annealed at 900 °C, 500 °C and the unannealed one were evaluated as 0.65 ±0.02 eV, 0.82 ±0.02 eV and 0.95 ±0.06 eV showing that annealing also affects recombination centres.

CHAPTER 6

Thermal assistance and quenching related to deep electron traps

In this chapter, we present the characteristics related to deep traps in synthetic quartz. The study was carried out using optical stimulation luminescence. The aim of this chapter is to determine kinetics information using CW-OSL signals from samples annealed at 500 °C, 900 °C for 10, 30, 60 minutes and a sample annealed at 1000 °C. We present results of investigations on the OSL signal obtained by optical stimulation of deep traps in synthetic quartz using 470 nm blue LEDs. The activation energy of thermal assistance and that of thermal quenching were evaluated.

6.1 Introduction

The application of dosimetric techniques such as thermoluminescence has numerous limitations during experimental work. Some of these limitations are anomalous fading, changes in the properties of the sample due to heating or non-linear dose dependence [59]. To overcome some of these limitations, Huntley et al [60] used a method of optically stimulated luminescence (OSL).

Deep traps which are the focus of this chapter, refer to those traps that are thermally inaccessible when the luminescence material is heated from room temperature to a high temperature of say 500 °C [61]. It is difficult to examine deep traps using conventional TL. However, the OSL signal from deep traps can be measured [62]. The OSL signal observed after preheating quartz to 500 °C is apparently due to deep traps since the shallow and the main traps which would give rise to this OSL signal are empty. The only likely source of the OSL are there deep traps. The presence of deep traps using thermally assisted OSL has been reported in many luminescent materials, such as Al_2O_3:C [38, 63] and natural quartz [62, 64]. The measurements of the OSL as a function of temperature provides an alternative method for estimating some kinetic parameters like the activation energy of thermal assistance, the activation energy of thermal quenching and the frequency factor of the non-radiative process [65, 66].

This chapter is concerned with the study of deep electron traps using thermally assisted OSL. The effects of annealing temperature, duration of annealing, stimulation time and irradiation dose on the activation energy of thermal assistance and the activation energy of thermal quenching were investigated. Previous studies on this same quartz using time-resolved luminescence showed that lifetime changes with annealing temperature [48]; the amplitude of emission bands increases with annealing temperature and the intensity increases with duration of annealing temperature above 700 °C as noted using radioluminescence [49]. The activation energy of thermal quenching also seems to decrease with annealing temperature (recombination centres affected) as concluded using thermoluminescence [50]. The influence of the factors stated above on the profiles of OSL as a function of measurement temperature is also of importance. Measurements were made using CW-OSL and the role of thermal assistance in the process was examined.

6.2 Thermal assistance and thermal quenching

Thermal assistance and thermal quenching are two separable thermodynamic effects that affect stimulation of luminescence simultaneously [67]. Thermal assistance affects the rate of optical eviction of charge and thereby drastically affects the initial luminescence intensity. In terms of

intensity, the process of thermal assistance was initially discussed by Spooner [68].

The derivation of thermal assistance and thermal quenching processes used in this section is described in the work published by Chithambo [66]. This is according to the Mott-Seitz configuration coordinate model as described for fluorescence and adapted for stimulation luminescence processes. The distribution of luminescence lifetimes with temperature T consists of radiative, phonon-assisted and non-radiative terms as

$$\frac{1}{\tau} = \frac{1}{\tau_{rad}} + \gamma coth\left(\frac{\hbar\omega}{kT}\right) + \nu \exp\left(\frac{\Delta E}{kT}\right) \tag{6.1}$$

where τ is the lifetime of the excited state at the luminescence, τ_{rad} is the radiative lifetime at absolute zero temperature, γ is a constant, ω is the phonon vibration frequency, $\hbar$ is planck's constant, k is Boltzmann's constant, ΔE is the activation energy of thermal quenching and ν is the frequency factor of non- radiative process [66, 55].

The temperature dependence of the excited state mean lifetime is expressed as follows if the phonon-assistance contribution is ignored

$$\tau(T) = \frac{\tau_{rad}}{1 + C\exp(\Delta E/kT)} \tag{6.2}$$

where $C = \nu\tau_{rad}$.

The intensity in time-resolved can be written as

$$I(t) = \int_0^\infty I_i \exp(-t/\tau_i)dt = I_i\tau_i \tag{6.3}$$

where τ_i and I_i are lifetime and amplitude of the ith component respectively. The intensity at any constant temperature T for constant lifetime τ_o is $I(T) = I_i\tau_o = I_o$. It follows that the temperature dependence of luminescence corresponding to the process explained in equation (6.2) is

$$I = \frac{I_o}{1 + C\exp\left(-\Delta E/kT\right)} \tag{6.4}$$

where all parameters are as previously defined [67].

In some cases, the luminescence intensity initially increases with measurement temperature due to the effect of thermal assistance [68]. The overall intensity goes through a peak as a function

of measurement temperature. To account for this behaviour, an additional Boltzmann term needs to be added to the total probability of luminescence emission in equation (6.1) as

$$\frac{1}{\tau} = \frac{1}{\tau_{rad}} + \left[\nu \exp\left(\frac{-\Delta E}{kT}\right)\right] \exp\left(\frac{E_a}{kT}\right) \tag{6.5}$$

from which

$$\tau = \frac{\tau_{rad} \exp(E_a/kT)}{1 + \nu\tau_{rad} \exp(-\Delta E/kT)} \tag{6.6}$$

and by similar arguments, leading to equation (6.4), one finds

$$I = \frac{I_o \exp\left(-E_a/kT\right)}{1 + C \exp\left(-\Delta E/kT\right)} \tag{6.7}$$

where all terms are as previously defined [66, 68]. The advantages of using equation (6.7) is that, it enables the evaluation of multiple kinetic parameters such as E_a, ΔE and C. The value of the constant C provides a means to determine the frequency factor for the non-radiative process [66]. The effect of thermal assistance and thermal quenching are independent of each other [68, 69, 70]. Chithambo and Galloway [67] studied thermal assistance and thermal quenching separately. In their study, they confirmed that the effects are truly independent. Equation (6.7) describes the effects of the two processes i.e thermal assistance and thermal quenching.

6.2.1 Profile of deep traps in CW-OSL

The characteristic profiles of luminescence (CW-OSL) from deep traps in annealed synthetic quartz was monitored using the following steps:

Step 1: The sample was first heated to 500 °C to clear the background signal.

Step 2: The sample was irradiated to 100 Gy at room temperature to populate electron traps.

Step 3: The sample was heated to 500 °C to clear the main trap and all secondary electron traps.

Step 4: The sample was illuminated using 470 nm blue LEDs for 10 s at room temperature during which the CW-OSL from deep traps was recorded.

Step 5: Heating to 500 °C to record the PTTL peak induced by phototransfer after the CW-OSL

measurement. The procedure was repeated for temperature between 30-200 °C.

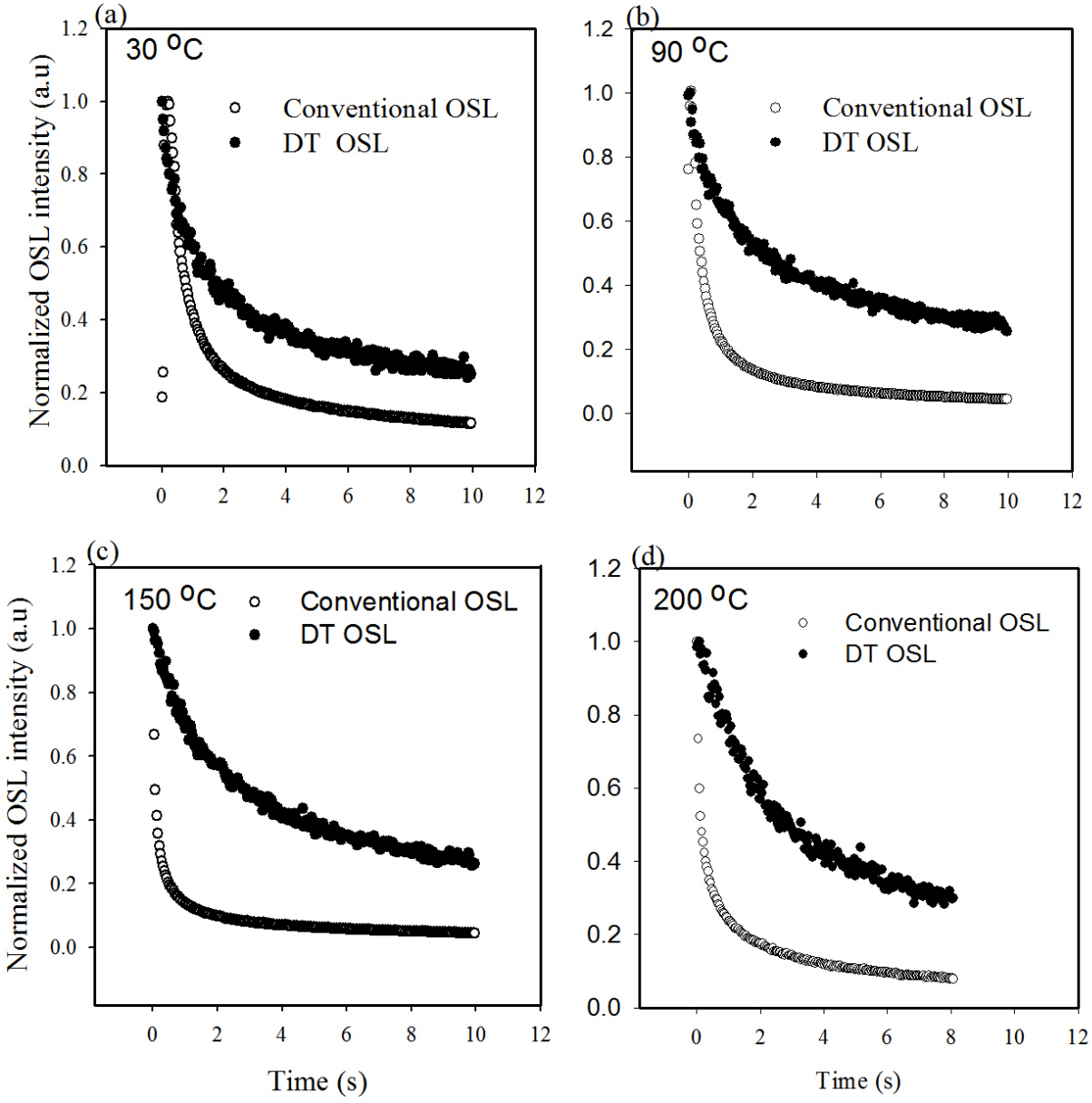

Figure 6.1: Variation of conventional and deep traps of CW-OSL intensity measured during stimulation 470 nm blue LEDs.

For comparison, the same procedure above was repeated skipping step 3 to monitor conventional or shallow traps OSL. Figure 6.1 shows the plots of OSL intensity against stimulation time for the sample annealed at 900 °C comparing conventional OSL intensity (shallow traps) with that from the deep traps. It can be observed that the profile of deep traps in CW-OSL intensity is different from that of the conventional OSL regardless of the measurement temperature. The conventional OSL signal decays faster than that from deep traps for all measurement temperatures.

6.2.2 Dependence of luminescence intensity on temperature

The influence of temperature during stimulation on the intensity of continuous wave optically stimulated luminescence (CW-OSL) was investigated. The measurement was carried out on the sample annealed at 900 °C for 10 minutes. The sample was irradiated to 100 Gy prior to heating to 500 °C to empty all electron traps in this range. The high dose was used to effectively fill deep traps. The sample was then exposed to 470 nm blue LEDs for 10 s at room temperature and finally heated to 500 °C to clear residual signal from electron traps. Similarly the sequence of the measurements was made with the temperature reversed from 200 to 30 °C. The entire OSL decay curve was integrated to obtain the intensity at each measurement temperature. Figure 6.2 shows the plots of the integrated OSL intensity as a function of measurement temperature for the two sequences. In both cases, the integrated OSL intensity against measurement temperature goes through a peak at a maximum temperature of 130 °C for the two measurements. The difference in OSL intensity between the two runs of the measurements represents a loss of OSL signal as reported elsewhere [67] and that loss in OSL intensity could be due to a sequence of measurements at elevated temperature.

The solid line through the data points is the best fit of equation (6.7). The activation energy of thermal assistance, thermal quenching and constant C were evaluated from the fits. These values are $E_a = 0.089 \pm 0.004$ eV, $\Delta E = 0.82 \pm 0.03$ eV and $C = 1.42 \times 10^6$ for the measurement runs from 30-200 °C. When the measurement sequence was reversed, the activation energy of thermal assistance, thermal quenching and the constant C were calculated as 0.075 ± 0.002 eV, $\Delta E = 0.84 \pm 0.03$ eV and $C = 5.46 \times 10^6$ respectively. These sets of kinetic parameters are

consistent. The values of activation energy of thermal quenching is in good agreement with that of Chithambo et al [48] obtained using TR-OSL for the sample annealed at 500 °C reported as 0.82 ± 0.03 eV or that of Petrov and Bailiff [34] reported as 0.78 ± 0.01 eV for the annealed sample of synthetic quartz.

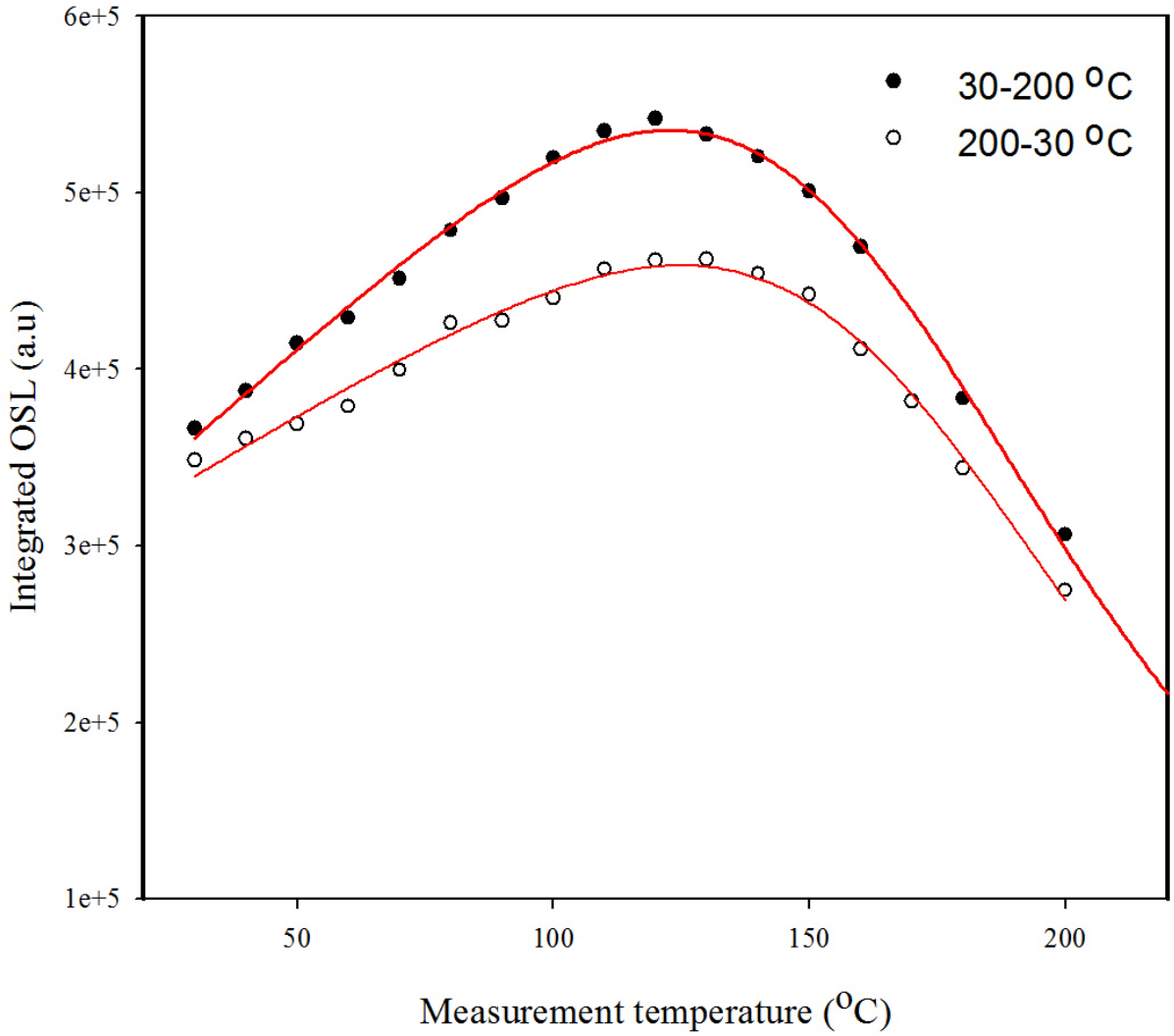

Figure 6.2: The relationship between integrated OSL intensity and measurement temperature for the sample annealed at 900 °C. The lines through data are the best fit of equation (6.7).

6.2.3 Analysis on the conventional OSL decay curves

A study of the behaviour of conventional OSL decay curves was carried out on the sample annealed at 900 °C for 10 minutes. The same experimental procedure described in section 6.2.1 was carried out, skipping step 3. The measurement was repeated for the stimulation temperature between 30-200 °C. Figure 6.3 shows the CW-OSL intensity plotted against stimulating time for the temperatures 130 and 200 °C and the inset is the same plot for the temperature of 30 °C. It can be observed that for the temperature of 30 °C, the profile of CW-OSL intensity as a function of stimulating time is peak shape like. However, as the temperature increases, the CW-OSL intensity decreases monotonically and weakens in intensity as illustrated in Figure 6.3 for 200 °C.

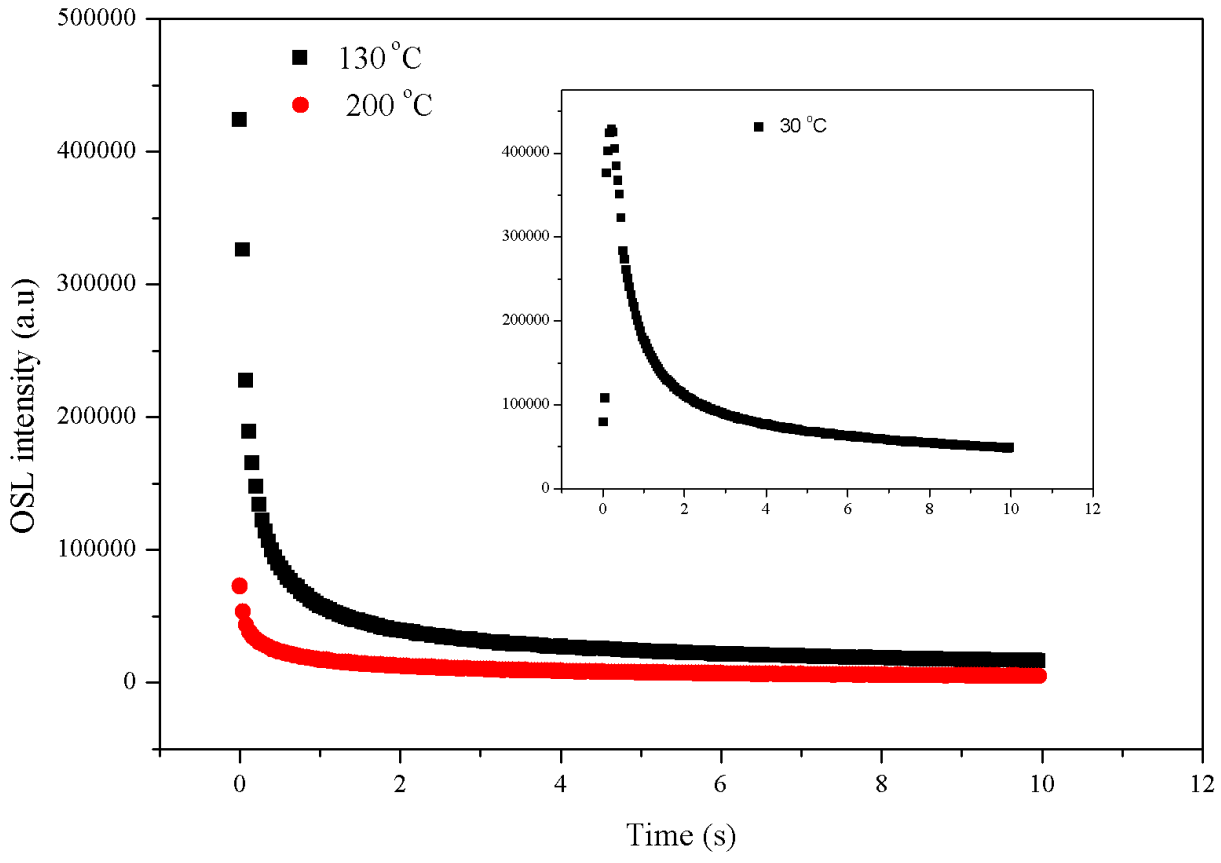

Figure 6.3: The OSL intensity as function of stimuation time for measurement temperature of 130 and 200 °C. Inset is same plot for the temperature of 30 °C.

The CW-OSL intensity for each measurement temperature in the interval of 10 °C was again obtained by integrating the entire CW-OSL as a function of stimulating time. The integrated OSL intensity was then plotted against stimulated temperature as shown in Figure 6.4. The OSL intensity increases between 30 and 70 °C and decreases thereafter. The change in OSL intensity could not be satisfactory fitted with equation (6.7). Quantitatively, the intensity increase owing to thermal assistance.

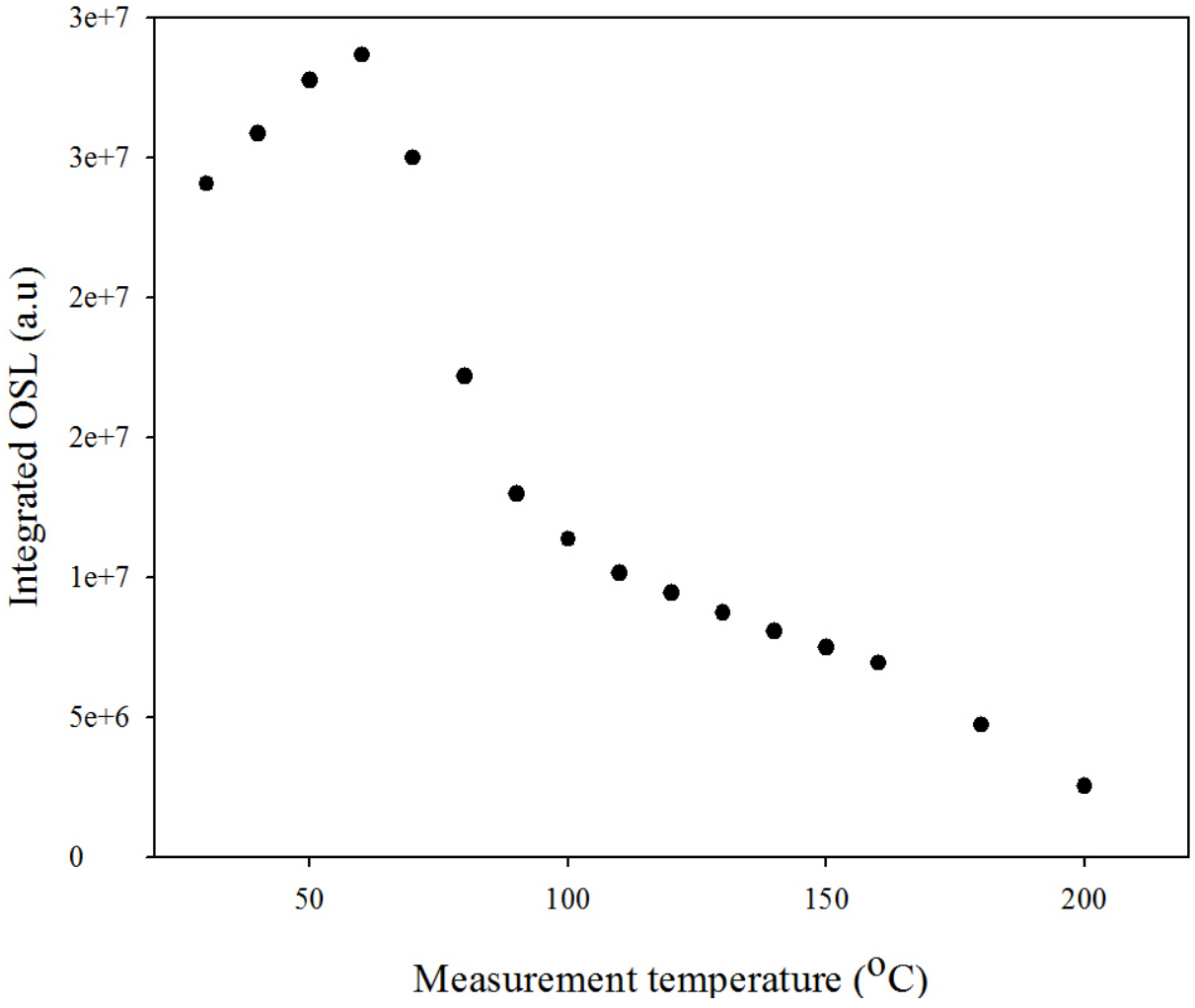

Figure 6.4: The graph of Integrated OSL intensity against measurement temperature 30-200 °C.

6.2.4 Effect of annealing temperature on the luminescence intensity

Figure 6.5 shows the observed luminescence intensity for samples annealed at 500, 900 and 1000 °C for 10 minutes before use. Samples were irradiated to 100 Gy each time before measurement at each temperature, preheated to 500 °C followed by CW-OSL using 470 nm light for 10 s and finally heated to 500 °C to measure the residual signal. In each of the measurements, the integrated OSL intensity was obtained and plotted as a function of measurement temperature.

The CW-OSL intensity increases with increase in annealing temperature at 500, 900 and 1000 °C. This observation is important because annealing induces change in luminescence sensitivity. This change in the luminescence intensity can be explained by a mechanism involving an alteration in the concentration of recombination centres. Quartz undergoes phase inversion at 573 and 870 °C [1] leading to significant changes in the OSL signal. It has been pointed out by Aitken and Smith [71] that thermal treatment influences sensitivity in OSL of quartz.

The kinetic parameters for samples corresponding to different annealing temperature were calculated again by fitting. The resulting values of the activation energy of thermal assistance and the activation energy of thermal quenching (E_a and ΔE) are $E_a = 0.40 \pm 0.03$ eV, $\Delta E = 0.59 \pm 0.02$ eV for the sample annealed at 500 °C. The constant C for the sample was calculated to be 2.26×10^7. For the sample annealed at 900 °C, the kinetic parameters are respectively $E_a = 0.075 \pm 0.005$ eV, $\Delta E = 0.82 \pm 0.02$ eV and $C = 5.46 \times 10^6$. Similarly, when the annealing temperature was increased to 1000 °C the activation energy of thermal assistance, thermal quenching and constant are given as $E_a = 0.216 \pm 0.002$ eV, $\Delta E = 0.59 \pm 0.03$ eV and $C = 3.40 \times 10^6$. These values of the activation energies of thermal quenching are consistent for the different annealing temperature. It is not immediately clear why some E_a values are large. This may be due to the problem with the fitting.

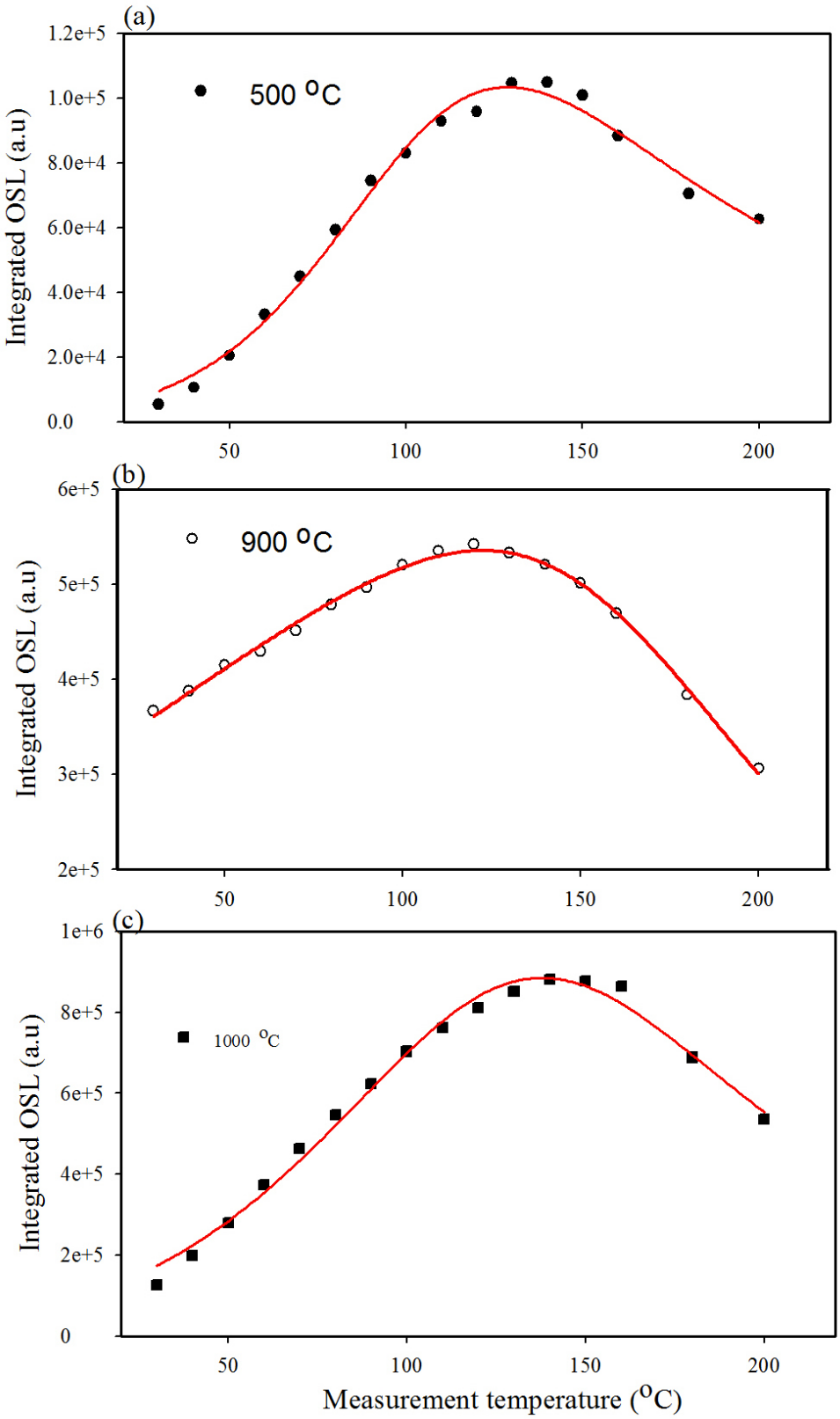

Figure 6.5: Variation of integrated OSL intensity as a function of measurement temperature for samples annealed at (a) 500°C (b) 900 °C and (c) 1000 °C.

6.2.5 Influence of duration of annealing on CW-OSL intensity

The influence of duration of annealing on synthetic quartz was investigated. Samples were annealed at 900 °C for 10, 30 and 60 minutes prior to use. The same experimental procedure of section 6.2.1 was used for this investigation. Figure 6.6 shows the graphs of integrated OSL intensity against measurements temperature for the samples annealed for 10, 30 and 60 minutes. The intensity decrease with increase in duration of annealing as seen in Figure 6.6.

The activation energy of thermal assistance and the activation energy of thermal quenching were also quantified by fitting the data with equation (6.7). Figure 6.6 shows the best fits of CW-OSL intensity as a function of temperature for samples annealed for 10, 30 and 60 minutes respectively. The activation energy of thermal assistance and that of thermal quenching for the sample annealed for 10 minutes were evaluated as $E_a = 0.074 \pm 0.002$ eV, $\Delta E = 0.65 \pm 0.02$ eV. When the duration of annealing was increased to 30 and 60 minutes, the kinetic parameters were found to be $E_a = 0.094 \pm 0.005$ eV, $\Delta E = 0.74 \pm 0.03$ eV and $E_a = 0.063 \pm 0.004$ eV, $\Delta E = 0.75 \pm 0.02$ eV. The values for the constant C for the samples annealed for 10, 30 and 60 minutes were $3.91 \times 10^6, 1.89 \times 10^6$ and 3.70×10^6 respectively. These values of the activation energy of thermal assistance and quenching are consistent for the three different duration of annealing. The values of the activation energy of thermal quenching are consistent duration of annealing. This show that the recombination centre is not affected by duration of annealing.

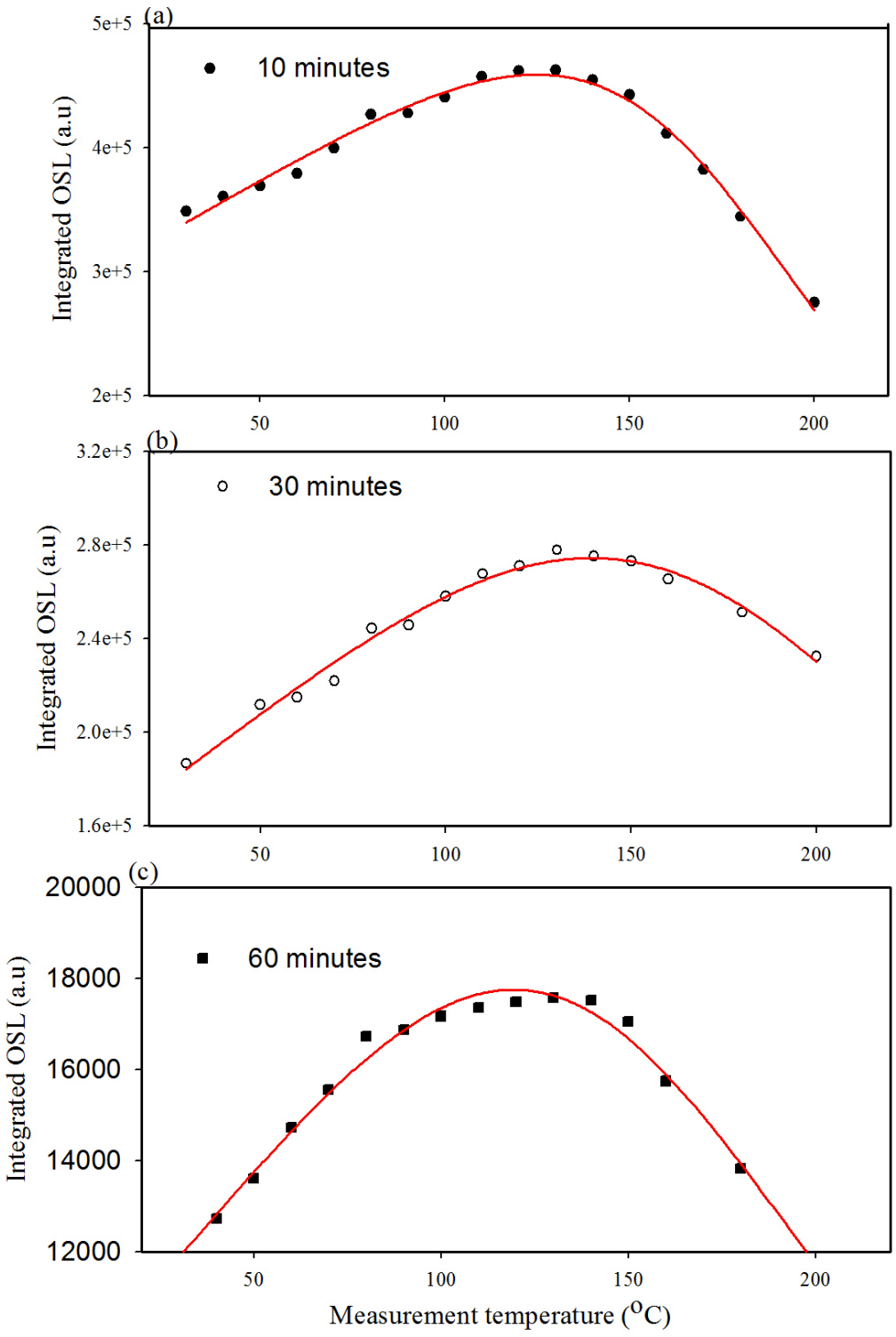

Figure 6.6: The dependence of integrated OSL intensity on measurement temperature for sample annealed at 900 °C for (a) 10 minutes (b) 30 minutes and (c) 60 minutes.

6.2.6 Effect of radiation dose on OSL intensity

Figure 6.7 shows the plots of integrated OSL intensity against measurement temperature for doses of 40 and 50 Gy. The study was carried out on the sample annealed at 900 °C for 10 minutes. The OSL intensity increases with the irradiation dose. The values of the activation energy of thermal assistance and thermal quenching were again calculated from fitting the data with equation (6.7). The activation energy of thermal assistance for the two separate doses of 40 and 50 Gy are 0.033 ± 0.002 eV and 0.023 ± 0.003 eV respectively. The values of the activation energy of thermal quenching for the sample irradiated to 40 and 50 Gy respectively are 0.73 ± 0.03 eV and 0.72 ± 0.03 eV. These values of activation energies for thermal quenching for the two separate doses 40 and 50 Gy can be compare with those reported by Dawam and Chithambo [50] as 0.65 ± 0.02 eV using TL analysis. The values of the activation energy of thermal quenching for the two separate doses are similar to each other.

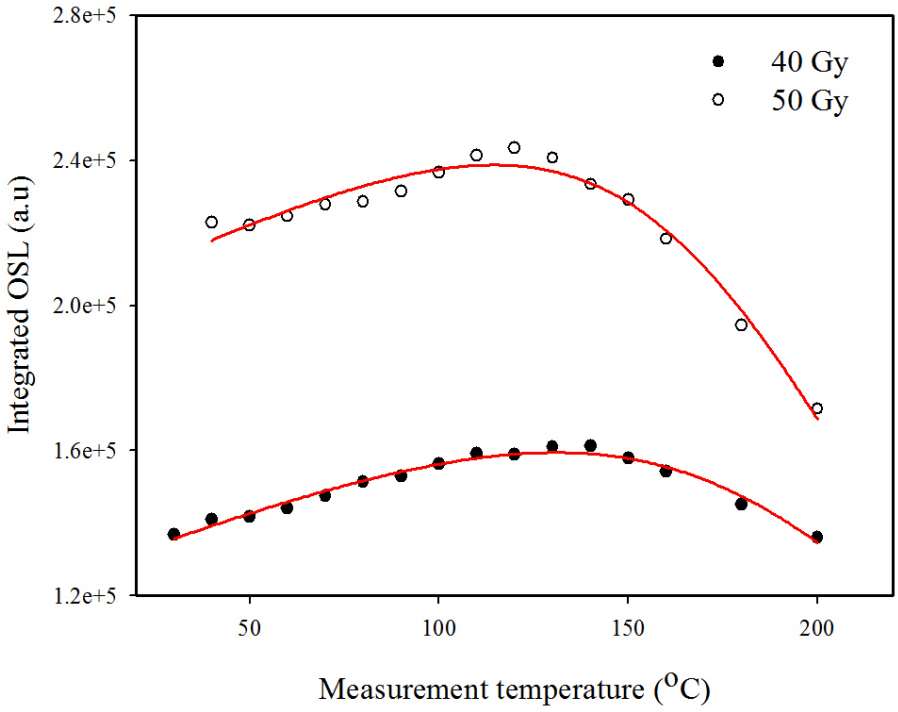

Figure 6.7: Variation of integrated OSL intensity with measurement temperature for a sample irradiated to a dose of 40 and 50 Gy

6.2.7 Influence of illumination time on CW-OSL intensity

The sample annealed at 900 °C for 10 minutes was irradiated to 100 Gy prior to heating to 500 °C. The OSL was then measured for stimulation time of 100 s and finally heated to 500 °C to clear residual charge. The measurement was repeated for the temperature between 30-200 °C. The whole exercise was repeated but, in this case, the stimulation time was changed to 500 s. Figure 6.8 shows the variation of integrated CW-OSL with measurement temperature. The observed profiles are similar for longer illumination time. It can be observed that the OSL intensity increase with illumination time.

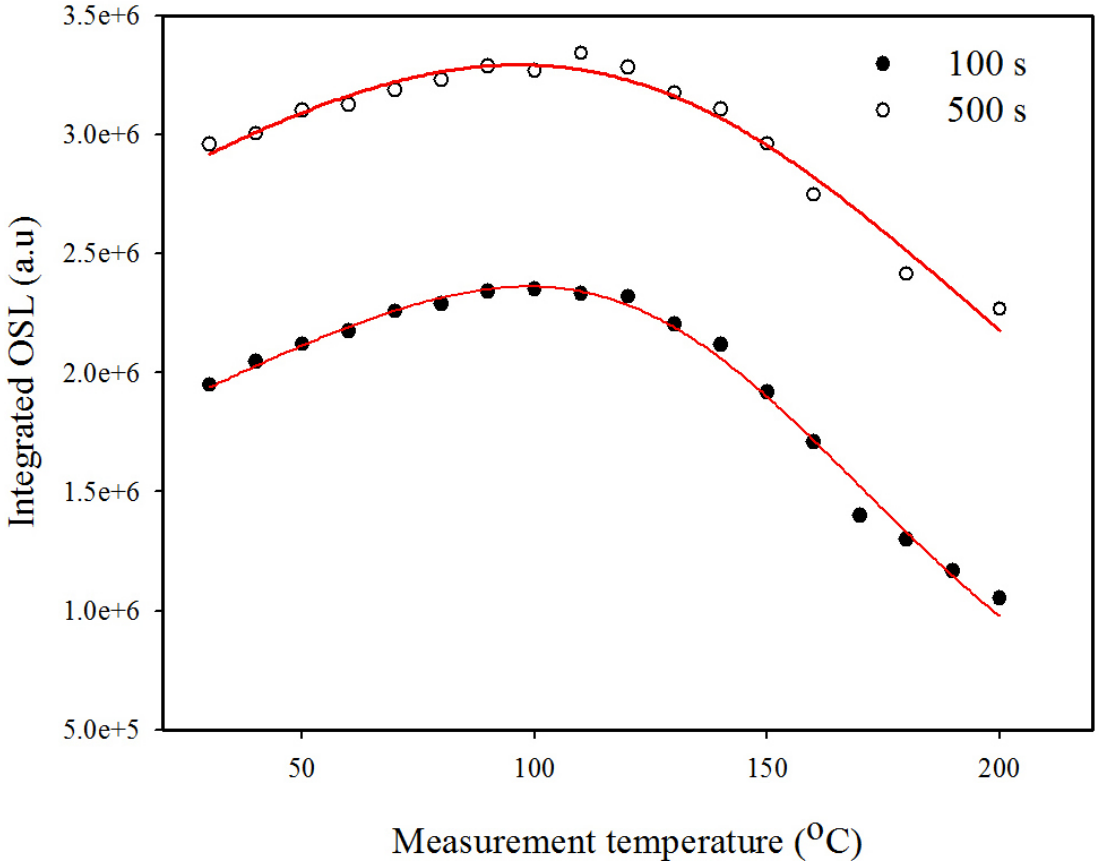

Figure 6.8: The graphs of integrated OSL intensity as a function of measurement temperature for stimulation time of 100 s and 500 s.

The activation energy of thermal assistance and thermal quenching was dertermined by fitting equation (6.7). The values of activation energy of thermal assistance for the illumination time of 100 and 500 s were 0.089 ± 0.003 eV and 0.079 ± 0.004 eV respectively. Additionally, the activation energies of thermal quenching were estimated respectively as 0.85 ± 0.03 eV and 0.64 ± 0.04 eV for stimulation time of 100 and 500 s and the constants C were also evaluated as 1.18×10^6 and 1.51×10^5 respectively. It can be observed that the activation energy of thermal quenching vary slightly with an increase in illumination time.

6.2.8 Effect of preheating on CW-OSL intensity

The influence of preheating temperature on the CW-OSL was investigated on the samples annealed at 500, 900 and 1000 °C for 10 minutes. The experimental procedure follows the same steps as in sections 6.2.1, except that in step 3 the sample was preheated to 300 °C. The exercise was done for the stimulation temperature between 30 - 200 °C. The effect of preheating temperature between 20 to 200 °C on lifetime was investigated by Ogundare and Chithambo [72]. Their investigation revealed that lifetime is independent of preheating temperature. However, our interest in this section is to study the effect of preheating temperature on the activation energy of thermal assistance and the activation energy of thermal quenching using OSL from deep traps.

Figure 6.9 shows the plots of integrated OSL intensity for the three samples annealed at 500, 900 and 1000 °C. Interestingly, under identical investigation, CW-OSL intensity increases with an increase in annealing temperature at 500, 900 and 1000 °C. These changes in sensitivity can be ascribed to alteration in the concentration of recombination centres [73, 74].

The kinetic parameter was evaluated by fitting the data with equation (6.7) and the lines through the data points are the best fits. The fitting parameters associated with the activation energy of thermal assistance, thermal quenching and constant C were evaluated as 0.095 ± 0.004 eV, 0.79 ± 0.03 eV and 1.71×10^6 respectively for the sample annealed at 500 °C. For the sample annealed at 900 °C, the parameters were 0.121 ± 0.003 eV, 0.64 ± 0.03 eV and $C = 2.58 \times 10^7$ and for the sample annealed at 1000 °C, the kinetic parameters were also evaluated as 0.081 ± 0.03 eV, 0.69 ± 0.03 eV and $C = 1.78 \times 10^7$. These results are presented in Table 6.1. The values

of activation energy of thermal quenching after preheating to 300 °C is in satisfactory agreement with that of the sample preheated to 500 °C. This shows that preheating to 300 °C has a negligible influence on the values of the activation energy of thermal quenching. The values of activation energy of thermal quenching reported in the present work are in agreement with those reported by Chithambo [75, 47] using time-resolved on the same sample of synthetic quartz.

The kinetic parameters for the samples annealed at 500, 1000 and 900 °C for 10, 30 and 60 minutes are listed in Table 6.1. In particular, the value of the activation energy of thermal quenching using thermally assisted OSL is consistent with that for the main peak using TL analysis as reported by Dawam and Chithambo [50]. There is no systematic dependence of the activation energies of thermal assistance and the activation energy of thermal quenching on the annealing temperature or duration of annealing or irradiation dose. The values of the activation energy of thermal quenching with illumination time decreases with increase in the duration of illumination. The value of constant C from the fit provide a means to evaluate the frequency factor for non-radiative process given as

$$C = \nu\tau_{rad} \tag{6.8}$$

where τ_{rad} is the luminescence lifetime of radiative transition, ν is the frequency factor for the non-radiative and C is the dimensionless constant [66]. Since the value of τ_{rad} for this particular sample was measured by Chithambo et al [48], equation (6.8) can be use to evaluate the frequency factor for non-radiative Table 6.1 summarises the values of activation energies of thermal assistance, thermal quenching and the frequency factor on non-radiative process calculated.

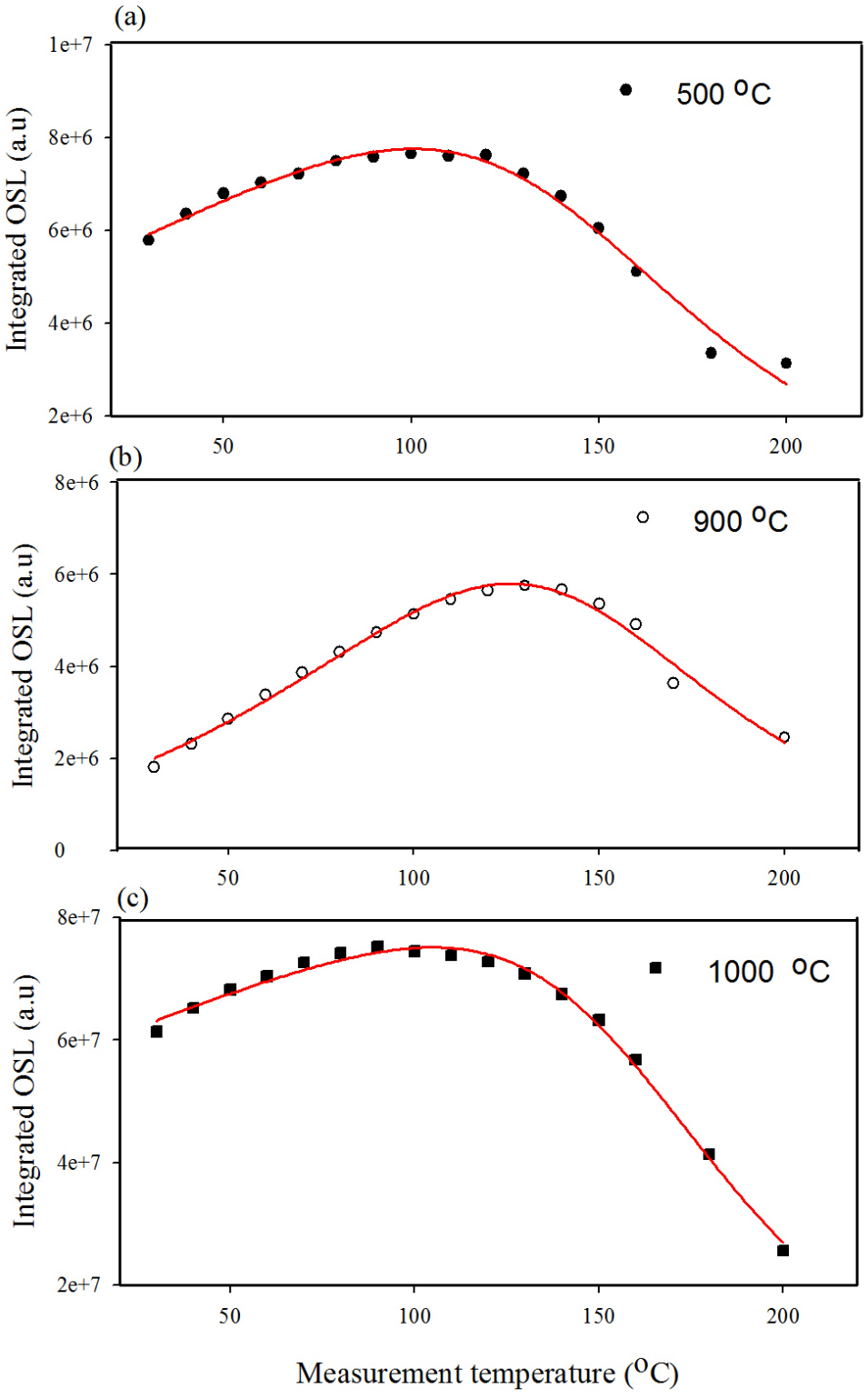

Figure 6.9: Integrated OSL intensity as a function of measurement temperature after preheating to 300 °C for sample annealed at (a) 500 °C (b) 900 °C and (c) 1000 °C.

6.3 Effect of measurement temperature on phototransferred thermoluminescence

The influence of measurement temperature on phototransferred thermoluminescence induce by the CW-OSL was investigated on the sample annealed at 900 °C for 10 minutes. The experimental procedure was that the sample was irradiated anew at for a run at each temperature to 100 Gy followed by preheating to 300 °C to remove peaks I-V in the glow curve. The sample was then exposed to 470 nm blue LEDs for 10 s at room temperature and finally heated to 500 °C to record any PTTL peaks. Three PTTL peaks were reproduced at 80, 136 and 200 °C and labelled A1, A2 and A3. The PTTL peaks were monitored for each measurement temperature between 30 and 200 °C at constant illumination time of 10 s. The PTTL peak position was constant. Figure 6.10 shows the plots of PTTL intensity against measurement temperature for the three PTTL peaks reproduced. As shown in Figure 6.10(a) the PTTL intensity initially increases with measurement temperature and thereafter decreases monotonically for peaks A1 and A2. However, for peak A3, the PTTL intensity increases with measurement temperature between 30 -100 °C and then subsequently decreases monotonically to 200 °C. The increase in the PTTL intensity with measurement temperature is associated with the phenomenon of thermal assistance. The decrease beyond 100 °C may be due to the combination effect of less retrapping at the main trap of charges stimulated from the deep traps and thermal quenching at recombination sites at higher temperature.

The activation energy of thermal assistance and thermal quenching of peak A3 was evaluated also by fitting the data of PTTL intensity as a function of measurement using equation (6.7). The parameters were found as $E_a = 0.044 \pm 0.002$ eV, $\Delta E = 0.76 \pm 0.01$ eV and $C = 4.39 \times 10^{13}$ illustrated in Figure 6.10(b). The values of the activation energy of thermal assistance and thermal quenching are consistent with the calculated ones reported in the previous sections. The detailed explanation regarding PTTL profiles and their analysis shall be presented in chapter 7.

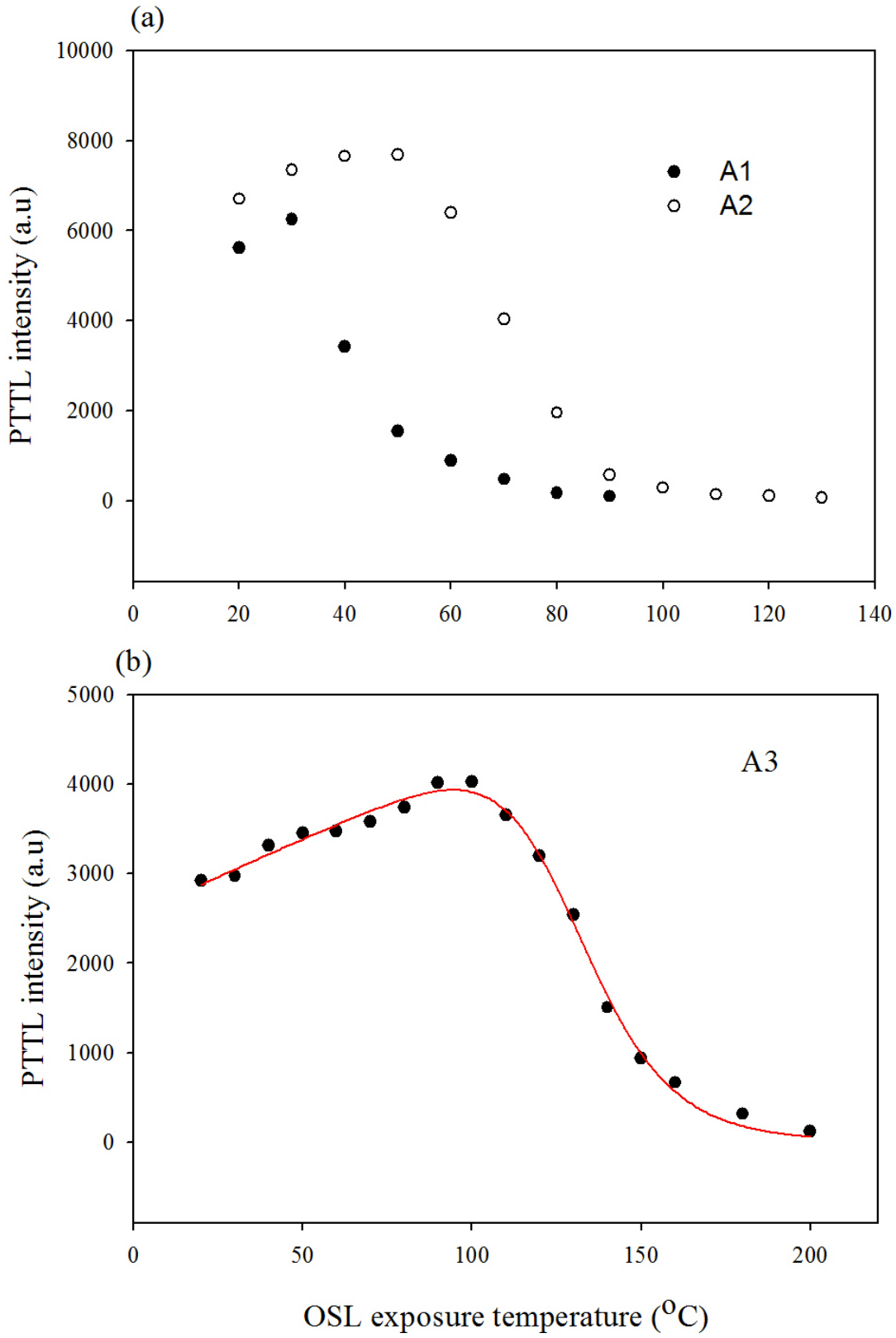

Figure 6.10: Plots of PTTL intensity as a function of measurement temperature after preheating to 300 °C for peak (a) A1 and A2 (b) A3 fitted with equation (6.7).

Dose (Gy)	Temp. range (°C)	Annealing time (minutes)	Annealing temp. (°C)	Preheat (°C)	Stim. time (s)	E_a(eV)	ΔE (eV)	ν (s^{-1})	Reference
100	30-200	10	900	No	10	0.285 ± 0.020	0.42 ± 0.07	2.15×10^{11}	Figure 6.3(b)
100	30-200	10	900	500	10	0.064 ± 0.002	0.64 ± 0.02	4.79×10^{11}	Figure 6.2
100	200-30	10	900	500	10	0.045 ± 0.002	0.68 ± 0.02	3.06×10^{11}	Figure 6.2
100	30-200	10	500	500	10	0.359 ± 0.020	0.59 ± 0.02	3.34×10^{10}	Figure 6.5(a)
100	30-200	10	1000	500	10	0.216 ± 0.030	0.59 ± 0.03	3.80×10^{10}	Figure 6.5(c)
100	30-200	30	900	500	10	0.076 ± 0.005	0.61 ± 0.03	1.38×10^{10}	Figure 6.6(b)
100	30-200	60	900	500	10	0.086 ± 0.004	0.54 ± 0.04	1.95×10^{10}	Figure 6.6(c)
40	30-200	10	900	500	10	0.033 ± 0.002	0.73 ± 0.03	7.45×10^{10}	Figure 6.7
50	30-200	10	900	500	10	0.023 ± 0.003	0.72 ± 0.03	1.14×10^{11}	Figure 6.7
100	30-200	10	900	500	100	0.050 ± 0.003	0.64 ± 0.03	9.58×10^{9}	Figure 6.8
100	30-200	10	900	500	500	0.047 ± 0.004	0.58 ± 0.04	1.09×10^{10}	Figure 6.8
100	30-200	10	500	300	10	0.056 ± 0.003	0.59 ± 0.02	3.14×10^{10}	Figure 6.9(a)
100	30-200	10	900	300	10	0.134 ± 0.020	0.59 ± 0.03	4.73×10^{11}	Figure 6.9(b)
100	30-200	10	1000	300	10	0.034 ± 0.003	0.75 ± 0.03	3.27×10^{11}	Figure 6.9(c)

Table 6.1: Comparison of activation energies of thermal assistance, thermal quenching and the frequency factors of the non-radiative process evaluated from the fits CW-OSL

6.4 Dependence of photoionisation cross-section on measurement temperature

The results reported in this section are data obtained after preheating to 300 and 500 °C in section 6.2.8. The data was fitted with a sum of three components i.e fast, medium and slow components using the following expression

$$I_{OSL} = A\exp(\frac{-t}{\tau_A}) + B\exp(\frac{-t}{\tau_B}) + C\exp(\frac{-t}{\tau_C}) \tag{6.9}$$

where A, B and C are scaling constants and τ_A, τ_B and τ_C are the decay constants in the unit of (s) for fast, medium and slow components respectively. The decay rate does not provide information about the optical properties of the traps involved in the OSL process. Therefore, we need to examine the photoionisation cross-section and its dependence on the stimulation temperature. The photoionisation cross-section refers to electron transition from a discrete bound defect state to the quasi-continuum density of states in the conduction band (electron emission) or to electron transition from the valence band to a localized level (hole emission)[14]. The decay rate yields the information about the interaction between the incident photons and the charge trapping states in the synthetic quartz. Since the decay constant is $\tau = 1/\sigma\Phi$, where σ is photoionisation cross-section and Φ is the intensity of stimulating light [76, 31], these values of decay constants were obtained by fitting the experimental data of CW-OSL intensity as a function of illumination time as shown in Figure 6.11(a) & (b) after preheating to 300 and 500 °C respectively . The values of decay rate at each measurement temperature were then used to calculate the photoionisation cross-section corresponding to the fast, medium and slow components.

Figure 6.12 shows the plots of photoionisation cross-section (σ) as a function of measurement temperature obtained after preheating to 300 °C for the fast, medium and slow component respectively. As seen in Figure 6.12(a), photoionisation cross-section increases between 30-140 °C and thereafter decreases. The increase is similar to a manner of thermal assistance and decrease as thermal quenching respectively for the fast component. However, for the medium and slow components it decreases with measurement temperature.

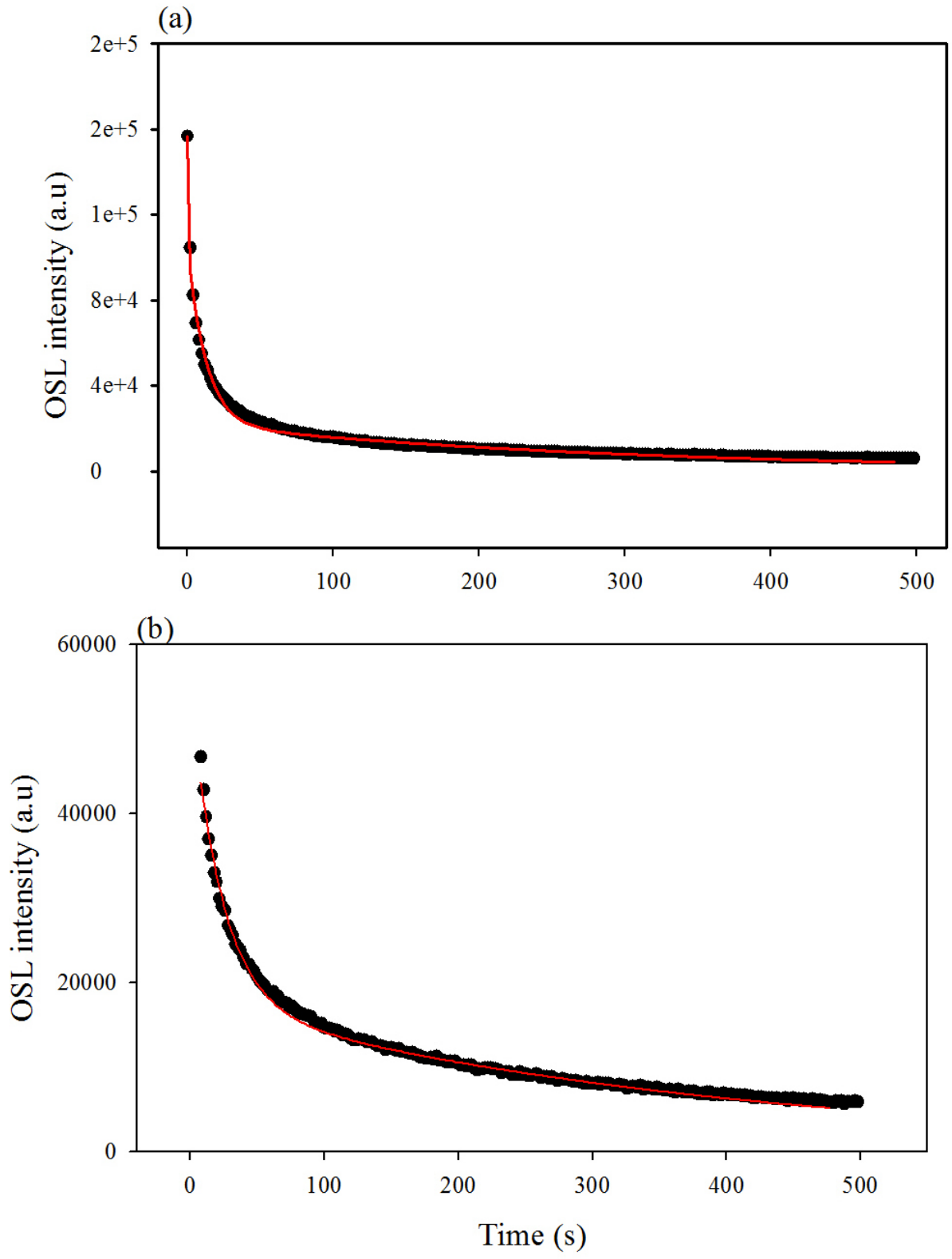

Figure 6.11: OSL intensity against time fitted with equation (6.9) after preheating to (a) 300 °C and (b) 500 °C

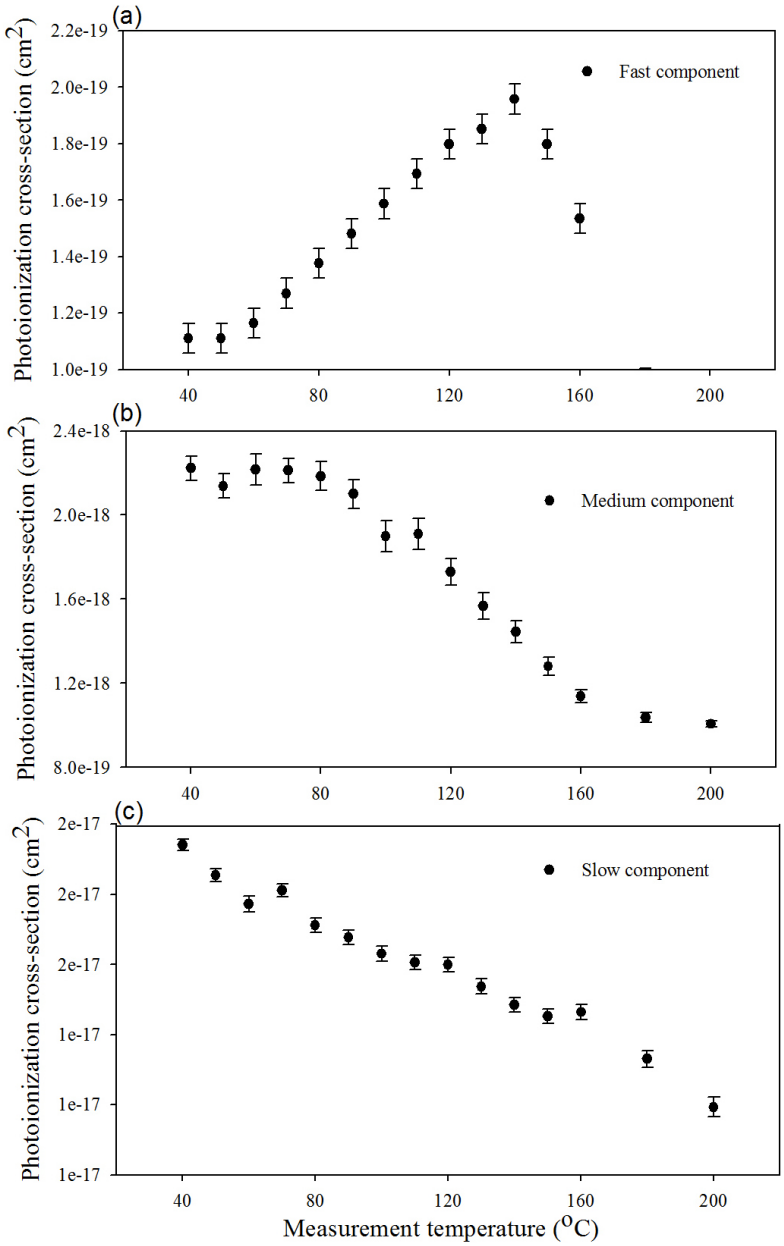

Figure 6.12: Dependence of photoionisation cross-section (σ) against measurement temperature after preheating to 300 °C for (a) fast component (b) medium component and (c) slow component

In a similar way, the data for the sample preheating to 500 °C were fitted using equation (6.9). Coincidentally, the values for decay rate for the fast components of the OSL were all negligible for all the measurement temperature under investigation. Figure 6.13 shows the plots of

photoionisation cross-section against measurement temperature for the medium and slow components. The negligible values for the decay rate of the fast component could be attributed to

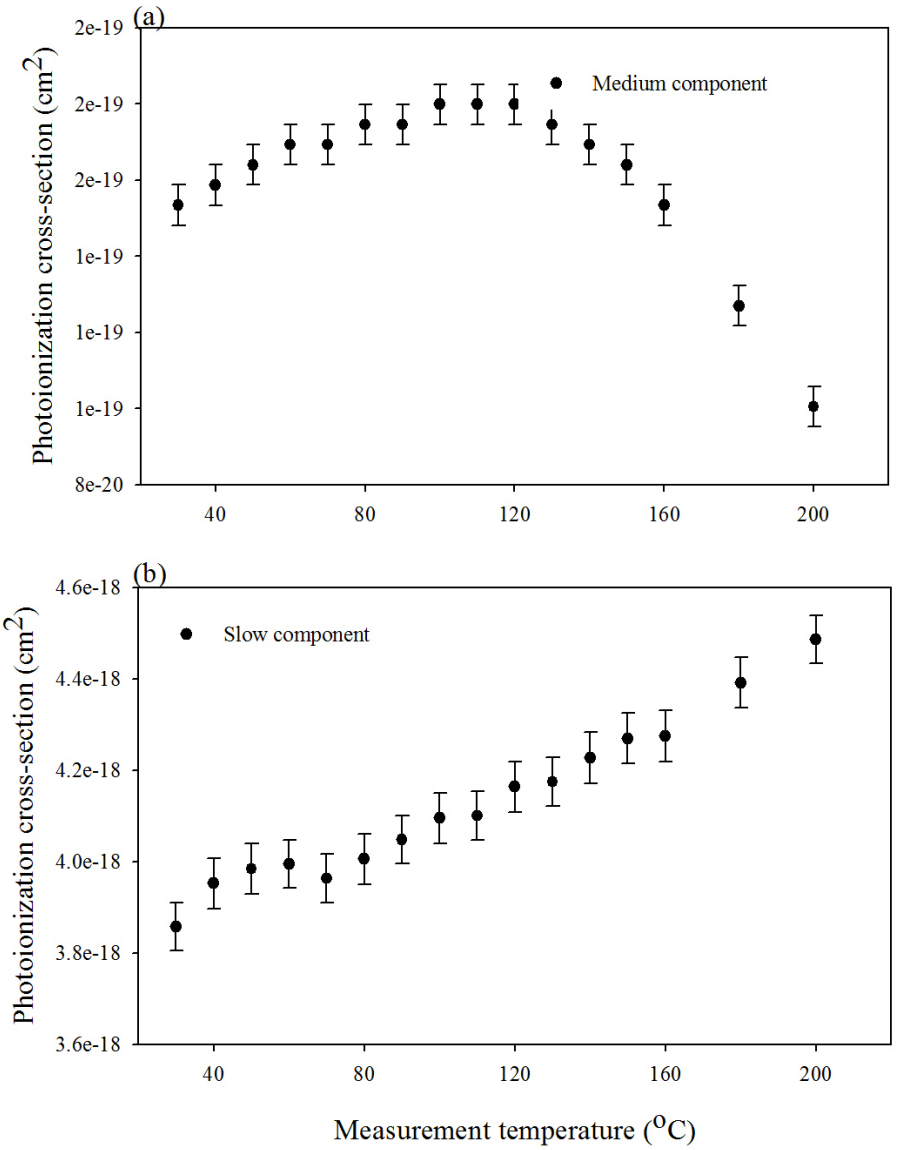

Figure 6.13: Dependence of photoionisation cross-section on the measurement temperature after preheating to 500 °C.

depletion of the main trap leaving on only the deep trap active. As it is shown in Figure 6.13, the photoionisation cross-section for the medium component increases from room temperature to 120 °C. This behaviour of photoionisation cross-section was reported by Singarayer and Bailey

[77]. For the case of slow component, the photoionisation cross-section increases with measurement temperature.

6.5 Summary

Thermally assisted CW-OSL from the sample of annealed synthetic quartz has been studied. Measurements were carried out using 470 nm light at temperatures between 30 and 200 °C. The sample was irradiated to 100 Gy followed by preheating to either 300 or 500 °C in all cases. The preheating temperature to 500 °C was to enable measurement of signal of deep traps present in synthetic quartz. In all cases, the CW-OSL goes through a peak as a function of measurement temperature. Using CW-OSL, the intensity was found to increase with stimulation time and annealing temperature.

The activation energies of thermal assistance and thermal quenching have been evaluated. The values of activation energies of thermal quenching are consistent for all the experimental conditions. The values of activation energies of thermal assistance characterise the trapping process during optical stimulations were also evaluated.

The PTTL intensity as a function of measurement temperature was monitored between 30-200 °C. Peak A3 increases with measurement temperature between 30 - 130 °C and afterwards decreases monotonically in a manner of thermal assistance and quenching respectively. The activation energy of thermal assistance and thermal quenching were evaluated as $E_a = 0.044 \pm 0.002$ eV, $\Delta E = 0.76 \pm 0.01$ eV.

The OSL data obtained after preheating to 300 and 500 °C were fitted with the sum of several first-order exponential decay components to examine the variation of photoionisation cross-sections. Photoionisation cross-section increase for the fast component and thereafter decreases for preheating to 300 °C. For the medium and slow component the photoionisation cross-section all show a decrease with increase in measurement temperature. In contrast, preheating to 500 °C removes the fast component leaving only the medium and the slow components from the decay curve.

CHAPTER 7

Phototransferred thermoluminescence

The detailed analysis of phototransferred thermoluminescence (PTTL) is presented in this chapter. Samples were annealed at 500 °C for 10 minutes, 900 °C for 10, 30 , 60 minutes and annealed at 1000 °C for 10 minutes. The kinetic parameters of the PTTL peaks were determined. The dependence of the PTTL intensity profile on illumination time is modelled using various combinations of an acceptor and donors using coupled linear differential equations following the empirical model of Chithambo et al [40].

7.1 Introduction

Phototransferred thermoluminescence has been used for various objectives such as the study of TL mechanisms [40] understanding annealing induced changes in the concentration of deep electron traps [78, 79] and for dosimetry [42]. The appeal of PTTL for dosimetry is exemplified in recent reports [43, 80] . Whereas the basis for dosimetry for irradiated samples is the link between irradiation dose and intensity, that under PTTL is the dose due to optical transfer from a donor.

The PTTL observed in natural and synthetic quartz has been associated with the emptying of electron traps at 325 °C [45, 81] or 375 °C [82]. Alexander and McKeever [45] described PTTL using a theoretical case of two-electron traps and one recombination centre, the same set-up used by Wintle and Murray [44] to account for PTTL in natural quartz. Their model was essentially a system of one donor and one acceptor. In comparison, Chithambo et al [40, 41] used sets of coupled linear differential equations to explain experimental results of PTTL from $Al_2O_3 : C$ and unannealed synthetic quartz using systems of an acceptor and multiple donors.

The method described by Chithambo et al [40, 41] differs from that of Alexander and Mckeever [45]. Alexander and Mckeever [45] described the transport of electrons involved in the PTTL process during irradiation, preheating, illumination and heating using sets of non-linear differential equations. These equations do not have analytical solutions. As such, numerical approximations are used to predict the behaviour of the PTTL intensity as a function of illumination time. The method of Chithambo et al [40] was formulated to describe the transfer by light, of a portion of electrons from a donor to an acceptor only during illumination. The differential equations are set up based on the number of donors corresponding to an acceptor during illumination. The number of acceptors or donors is not fixed but varies depending on experimental results. The system of coupled differential equations devised this way has analytical solutions which can be applied directly to experimental data.

This chapter aims to study PTTL from annealed synthetic quartz. In this investigation, the sample of synthetic quartz was annealed at 500 °C for 10 minutes, 900 °C for 10, 30, 60 minutes and finally 1000 °C for 10 minutes. The influence of annealing and that of the duration of annealing on the PTTL are thus of interest in this investigation. The dependence of the PTTL intensity profile on illumination time is modelled using various combinations of an acceptor and donors using coupled linear differential equations following the empirical model of Chithambo et al. [40]. The system of an acceptor and donors is determined by experiment. Complementary studies of the kinetic analysis of the PTTL peaks, thermal quenching and competition effects are also described.

7.2 Glow curve characteristics

Figure 7.1 shows glow curves of synthetic quartz annealed at 500 °C for 10 minutes, 900 °C for 10, 30, 60 minutes and 1000 °C for 10 minutes recorded at 1 °Cs^{-1} after irradiation to 200 Gy. The high dose was used to facilitate the measurement of PTTL. There are three distinguishable peaks at or near 76, 120 and 180 °C for the samples annealed at 500 °C. The inset shown in Figure 7.1(a), on a semi-logarithmic scale is the same glow curve for the sample annealed at 500 °C. The latter shows that there are in fact more than just three peaks with additional ones apparent near 200, 240 and 350 °C. For the sample annealed at 900 °C for 10 minutes , the glow curve has six peaks at positions of 90, 122, 176, 210, 240 and 340 °C. The sample annealed at 900 °C for 30 minutes has peaks at 80, 110, 136, 196, 240 and 330 °C while for the sample annealed at 900 °C for 60 minutes the peaks are at the position 80, 110, 134, 188, 235 and 340 °C. Similarly when the sample was annealed to 1000 °C for 10 minutes it also showed six peaks at the position of 74, 120, 135, 190, 220 and 345 °C . The presence of six peaks in the glow curves was confirmed by the thermal cleaning, a method for separating peaks described by Mckeever [4] and was also reported by Chithambo and Niyonzima [41] on the same sample of quartz. Part of the work in this chapter has been published [83].

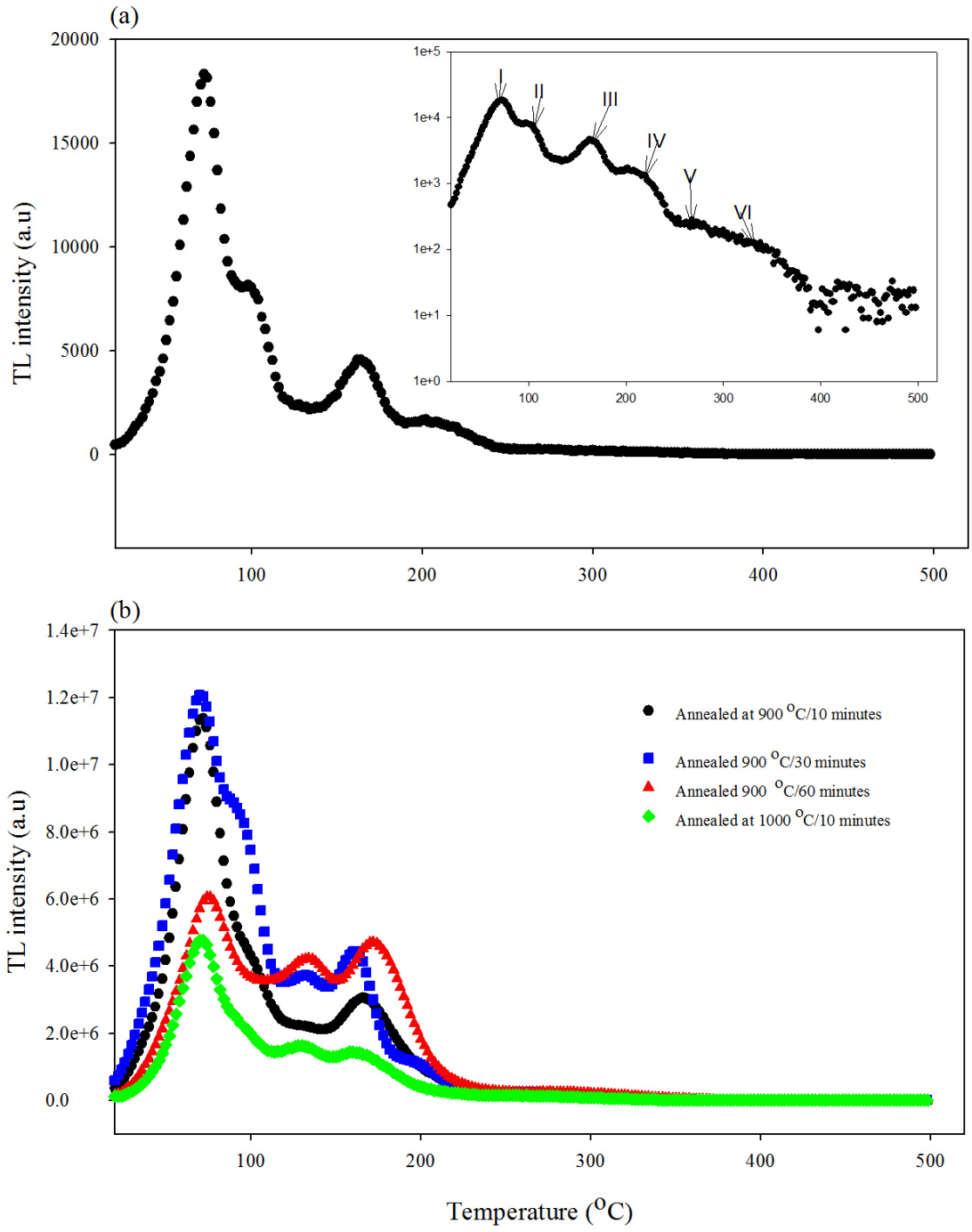

Figure 7.1: The TL glow curves measured from samples annealed at (a) 500 °C and in the inset shown on a semi-logarithmic scale, is the same TL glow curve of the sample annealed at 500 °C to better show the presence of other peaks (b)The samples annealed at 900 °C for 10, 30, 60 minutes and 1000 °C at a heating rate of 1 °C s^{-1} following beta irradiation of 200 Gy.

7.3 General features of PTTL

The PTTL test measurements were made by preheating a sample irradiated to 200 Gy in turn to 120,180, 250, 350 and 500 °C to remove peaks I, I-III, I-V and I-VI in succession. The proximity of peaks II and IV to the next in the series restricted preheating to remove one peak at a time. After each preheat, and cooling to room temperature, the sample was exposed to 470 nm blue light for a given time and reheated to 500 °C to measure the complete glow curve. Any presence of PTTL peak(s) was monitored at this stage. The PTTL corresponding to preheating to 500 °C, that is, from any deep electron traps was studied only for the quartz annealed at 900 °C for 10 minutes. The signal in the samples annealed at 500, 1000 °C and that of the samples annealed at 900 °C for 30 and 60 minutes was too low for reliable study.

When the sample annealed at 500 °C was preheated to 120 °C to completely remove peak I, there was no PTTL peak observed. This search for PTTL peak was continued for peaks I, II and III following preheating to 180 °C. But when peaks I-IV were completely removed after preheating to 250 °C , a PTTL peak was observed at 74 °C. When peaks I-V were removed following preheating to 280 °C, a PTTL peak was again reproduced at the same position as before at 76 °C and label A1. Following the removal of peaks I-VI by preheating to 340 °C, a PTTL peak was found at 76 °C but its intensity was too low for reliable study.

When the sample annealed at 900 °C for 10 minutes was preheated to 120 °C to remove peak I, no PTTL was observed. Furthermore, no PTTL was seen after removal of peaks I, II and III following preheating to 180 °C. However, after complete removal of peaks I-IV following preheating to 250 °C and indeed after completely removing the first five peaks by preheating to 350 °C, two PTTL peaks were observed at 90 °C and 176°C. We label these peaks as A1 and A3. Although the purpose of preheating to 250 and 350 °C was to remove peaks I-V and I-VI respectively, each preheat still left a remnant of peak V and VI. Further, when all the peaks (I - VI) were removed by preheating to 500 °C, only two PTTL peaks were seen at 100 and 176 °C. Figure 7.2(a) shows examples of PTTL peaks reproduced after preheating to 350 and 500 °C in the sample annealed at 900 °C for 10 minutes.

For the sample annealed at 900 °C for 30 minutes, only peak A1 was reproduced at 80 °C after preheating to either 250 or 350 °C. No clear PTTL peak was observed after preheating to 500 °C. Whereas, for the sample annealed at 900 °C for 60 minutes, PTTL peaks were observed at 80, 134 and 188 °C after preheating to either 250 or 350 or 450 °C. Figure 7.2(b) shows the PTTL peaks induced after preheating to 350 °C in the sample annealed at 900 °C for 60 minutes and labelled A1, A1 and A3. In summary, three PTTL peaks were reproduced for the sample annealed at 900 °C for 60 minutes, whereas two for the sample annealed at 900 °C for 10 minutes and only one peak for the sample annealed at 900 °C for 30 minutes. Interestingly PTTL peaks were not reproduced when samples annealed at 900 °C for 30 and 60 minutes were preheated to or above 500 and 560 °C . The latter result either means that the occupancy of any available deep electron traps is negligible even for a dose of 200 Gy.

Additionally, when the sample was annealed at 1000 °C, again three PTTL peaks were reproduced after preheating to either 250 or 350 °C. The peaks were reproduced at the position 74, 124 and 196 °C labelled A1, A2 and A3 respectively. In comparison, the PTTL of the same synthetic quartz but unannealed was studied by Chithambo et al[41]. In their study, PTLL was investigated at a preheating temperature below 450 °C and only one peak was reproduced. This same quartz was annealed to 500 °C, 900 °C for 10, 30, 60 minutes and 1000 °C for 10 minutes but two to three PTTL peaks were reproduced. This could be attributed to the effects of annealing on the samples. Also, PTTL was investigated for preheated temperature beyond 500 °C for the sample annealed at 900 °C for 10 minutes.

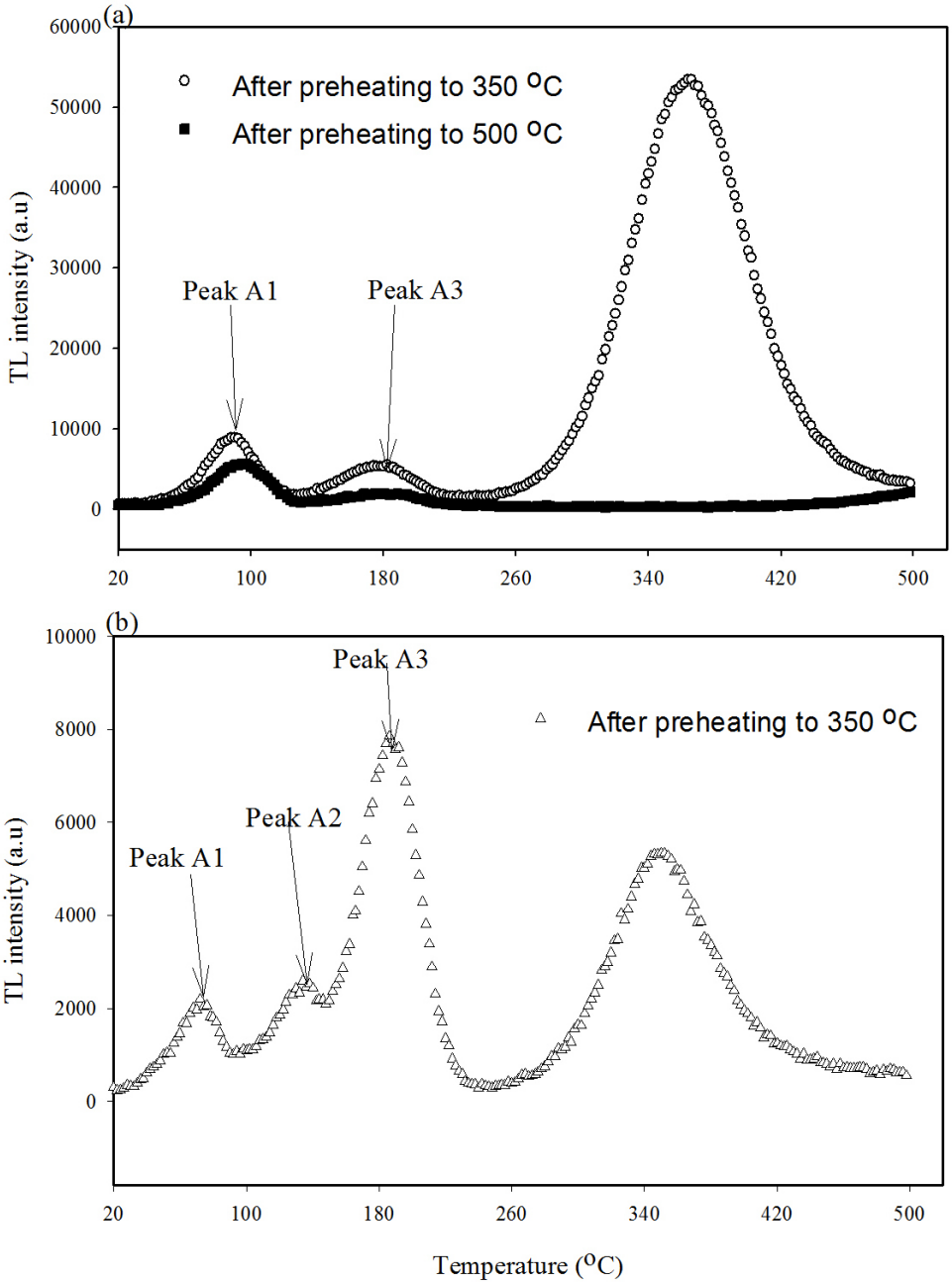

Figure 7.2: The glow curves measured after preheating to 350 and 500 °C following irradiation to 200 Gy and exposure to 470 nm blue light for 20 s (a) Sample annealed at 900 °C for 10 minutes (b) Sample annealed at 900 °C for 60 minutes.

7.4 Kinetic analysis of PTTL peaks

The conventional TL for the quartz used in this work has been studied previously [50]. Thus, the kinetic parameters of its most prominent peak are known. In this study, kinetic analysis of PTTL peaks A1, A2 and A3 was carried out to compare the parameters with ones from conventional TL and to confirm if the peaks in question are the ones reproduced under PTTL. In particular, peak I in the conventional TL was shown to follow first-order kinetics and to be affected by thermal quenching [50]. The kinetic analysis to be described was carried out using the whole glow peak, variable heating rate, curve fitting and by using phosphorescence related to phototransfer methods for the samples annealed at 500 °C for 10 minutes, 900 °C for 10, 30, 60 minutes and that of 1000 °C for 10 minutes.

7.4.1 Analysis using whole glow peak method

In the whole glow peak (WGP) method the PTTL intensity I is related to temperature according to equation (2.20). Figure 7.3 shows the graph of $ln(I/n^b)$ against $1/kT$ for the sample annealed at 900 °C for 10 minutes after preheated to 500 °C. The values of activation energy of the two PTTL peaks were 0.66 ± 0.01 eV and 0.68 ± 0.03 eV. The order of kinetics for the two peaks was found to be $b = 1.2$ each. Similarly, for the sample annealed at 900 °C for 30 minutes the activation energy and the order of kinetics were found to be $E = 0.67 \pm 0.01$ eV and $b = 1.0$ after preheating to 350 °C. Following the same approach, for the sample annealed at 900 °C for 60 minutes after preheating to 350 °C the kinetic parameters were evaluated as $E = 0.66 \pm 0.02$ eV, 1.06 ± 0.04 eV and b = 1.0 each for peaks A1 and A3 respectively. When the samples were annealed at 500 and 1000 °C the activation energy of peaks A1 following preheating to 250 °C was evaluated as 0.68 $\pm$ 0.03 eV and 0.78 ± 0.02 eV respectively. Their order of kinetics was evaluated as $b = 1.1$ and 1.2. These results shows that PTTL peaks A1 and A3 are subjected to first-order kinetics for all annealing temperature and duration of annealing.

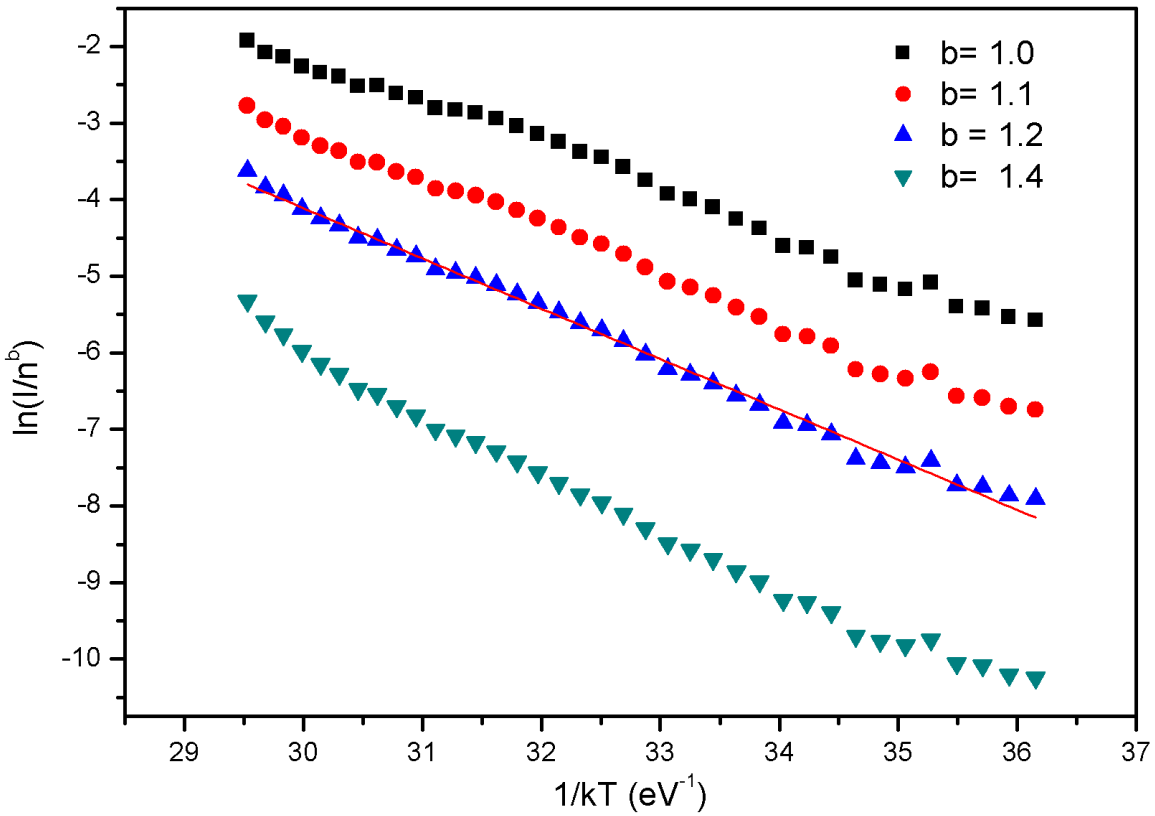

Figure 7.3: The graph of $ln(I/n^b)$ against $1/kT$ used to calculate the activation energy and the order of kinetics. The best fit has for $b = 1.2$ for the sample annealed at 900 °C for 10 minutes.

7.4.2 Analysis using phototransferred phosphorescence

Phosphorescence related to PTTL was measured between 40-60 °C. These temperatures correspond to the rising edge of PTTL peak A1. This is phosphorescence owing to charge at a shallower trap transferred there optically from deeper traps. Phototransferred phosphorescence has previously been studied on synthetic quartz annealed at 500 °C [84]. The activation energy of the PTTL peak was calculated from the time dependence of phosphorescence intensity $I(t)$ for first-order kinetics from the equation (2.35). The measurements were made on samples irradiated to 200 Gy. Figure 7.4(a) shows a graph of $ln(I)$ against t for the sample annealed at 900 °C for 10 minutes. The result is linear, consistent with first order kinetics. Figure 7.4(b) is the corresponding plot of $ln(p)$ versus $1/kT$. From the slope of such a plot, the activation energy

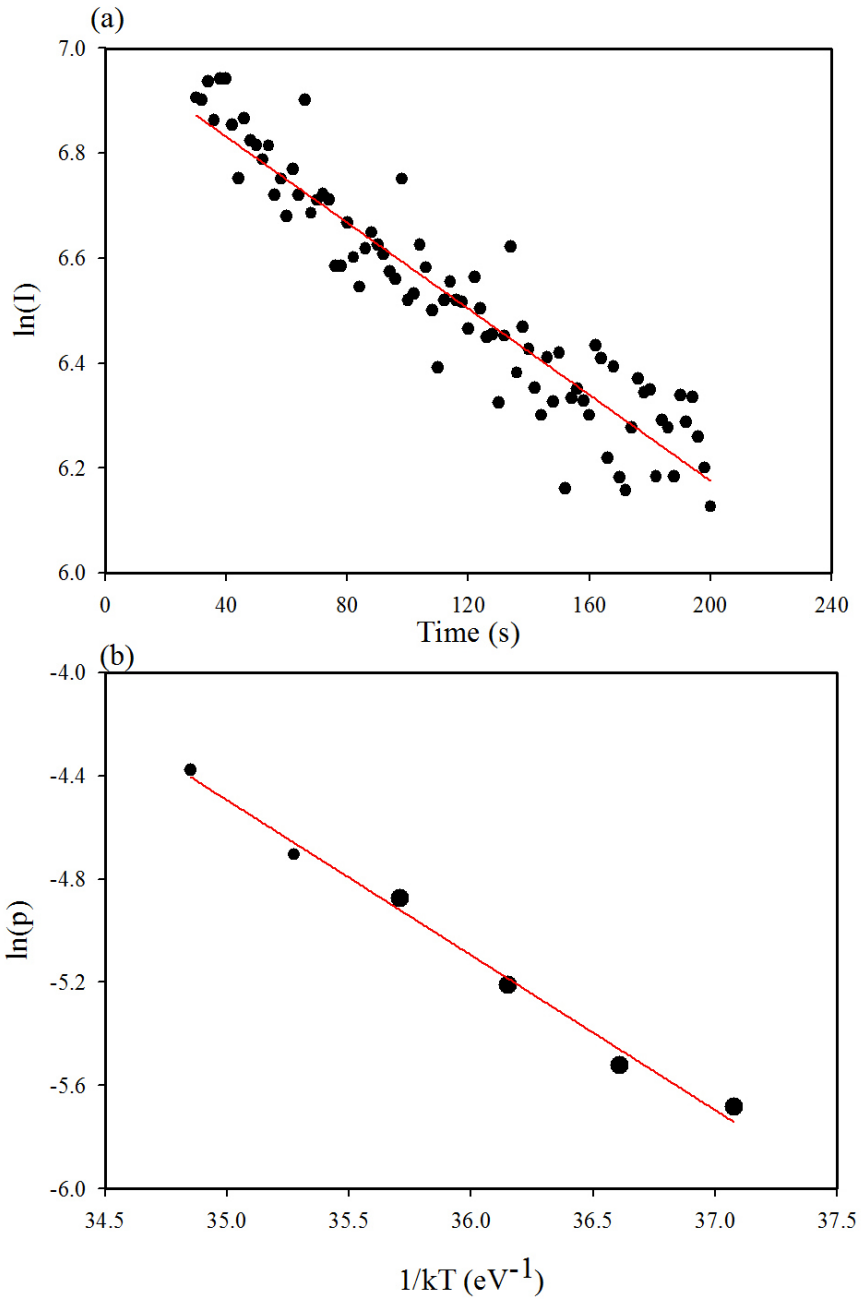

Figure 7.4: The graph of $ln(I)$ against t (a). The plot of $ln(p)$ versus $1/kT$ used to calculate the activation energy from the sample annealed at 900 °C for 10 minutes (b).

for the electron trap corresponding to peak A1 was determined as 0.60 $\pm$ 0.02 eV for the sample annealed at 900 °C for 10 minutes. This can be compared with that from the WGP method for

peak A1. Furthermore, the activation energies for samples annealed at 500, 1000 °C and that of the sample annealed at 900 °C for 30 and 60 minutes is discussed in Table 7.1.

7.4.3 Analysis using variable heating rate

In the variable heating rate method which depends on the peak position and the heating rate, the activation energy was found using equation (2.24). Figure 7.5 shows the plots of $ln(T_m^2/\beta)$ against $1/kT_m$ for the sample annealed at 900 °C for 60 minutes on peak A1, A2 and A3 recorded at the heating rates between 0.2 - 5.0 °C s^{-1}.

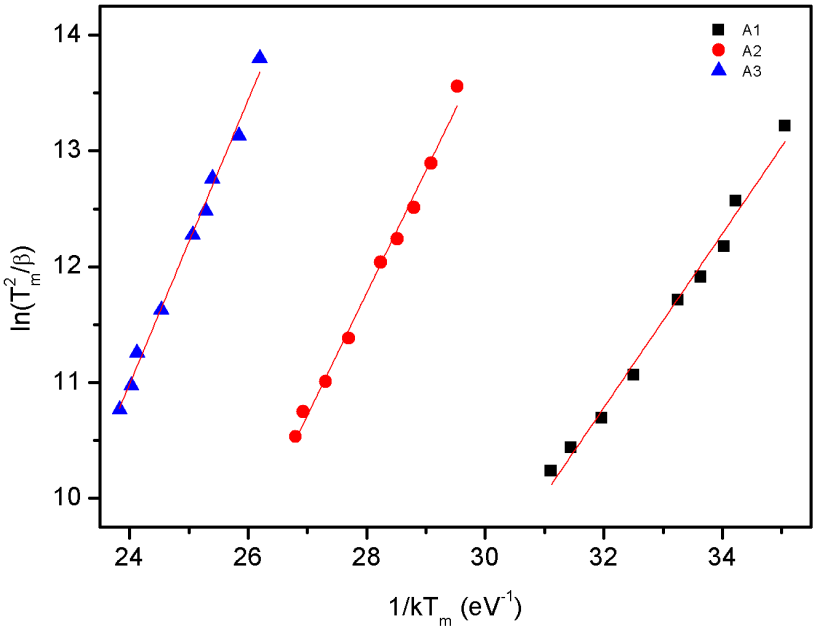

Figure 7.5: The Plot of $ln(T_m^2/\beta)$ against $1/kT_m$ for the sample annealed at 900 °C for 60 minutes after preheating to 350 °C used to the activation energies for PTTL peak A1, A2 and A3.

The activation energy corresponding to peaks A1, A2 and A3 were found as 0.72 ± 0.02, 0.89 ± 0.02 and 1.09 ± 0.02 eV respectively after preheating to 250 °C. In a similar manner, the activation energy for samples annealed at 500 °C for 10 minutes, 900 °C for 10, 30 minutes and that of sample annealed at 1000 °C for 10 minutes were evaluated. These results are presented

in Table 7.1.

7.4.4 Influence of heating rate on PTTL intensity Evidence of thermal quenching

Figure 7.6(a) shows the influence of heating rate on PTTL intensity of peaks A1 and A3 for samples annealed at 900 °C for 10 minutes. The measurements were made with heating rates from 0.2-5.0 °Cs^{-1}, the latter being the reasonable upper limit of heating rate in TL experiments. The intensity decreases with heating rate. The change as seen in Figure 7.6(a), for first order kinetics which applies to peaks A1 and A3, indicates that the peaks are affected by thermal quenching. In the same ways, the samples annealed at 500 °C, 900 °C for 30, 60 minutes and 1000 °C, the PTTL intensities decrease with increase in heating rates. These decrease with heating rates indicates that PTTL peaks of all the samples were affected by thermal quenching.

If we assume that the PTTL intensity at lower heating rates I_uq (in units of counts $^{\circ}C^{-1}$) are less affected by thermal quenching and if I_q represents a PTTL intensity measured at the highest heating rate where the quenching is most effective, then equation (5.1) is used to evaluate the quenching parameters. Figure 7.6(b) shows plots of $ln[(I_{uq}/\mathrm{I}_q$)-1] against $1/kT_m$ for peaks A1 and A3. The activation energy of thermal quenching was determined as 0.62 $\pm$ 0.04 eV and as 0.65 $\pm$ 0.05 eV using peaks A1 and A3 in the sample annealed at 900 °C for 10 minutes. Similarly, for the sample annealed at 900 °C for 30 and 60 minutes, the activation energy of thermal quenching was found as 0.63 $\pm$ 0.02 eV and 0.66 $\pm$ 0.03 eV. In both cases the sample was preheated to 250 °C. Furthermore, the activation energy of thermal quenching of peak A1 for samples annealed at 500 and 1000 °C was evaluated as 0.80 ± 0.02 and 0.73 ± 0.03 eV respectively. These values of activation energy of thermal quenching are consistent with the one 0.65 $\pm$ 0.02 eV using peak 1 in the conventional TL [50]. The results show that the emission is from a common recombination centre. This is consistent with a previous study using radioluminescence [49] which showed that changing the duration of annealing only alters the intensity not the position of the emission band. However, the values obtained in this study and by Dawam and Chithambo[50] are typical of natural quartz e.g 0.64 $\pm$ 0.03 eV[67] or 0.636 $\pm$ 0.003 eV [44]

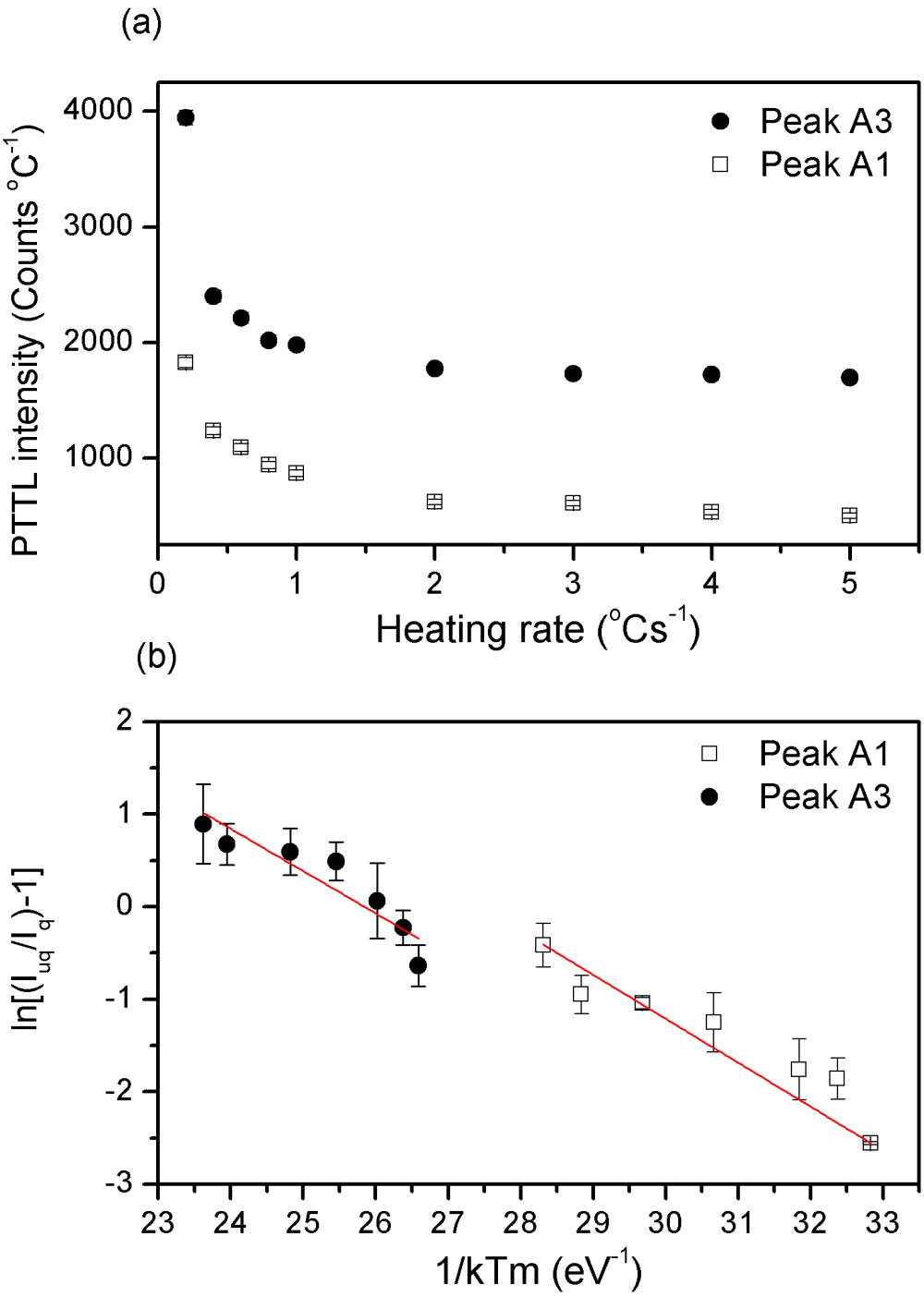

Figure 7.6: The Plot of PTTL intensity as a function of heating rate for sample annealed at 900 °C for 10 minutes after preheating to 500 °C (a). A graph of $ln[(I_{uq}/I_q) - 1]$ against 1/kT_m used to calculate the activation energy of thermal quenching of peaks A1 and A3 (b).

and differ somewhat from values obtained for synthetic quartz e.g 0.82 $\pm$ 0.01 eV [48] or 0.78 $\pm$ 0.01 eV [34]. The cause of differences is yet to be systematically studied but could be due to variations in pre-measurement treatment such as annealing.

Thermal quenching has been quantified using TL emission near 90 and 180 °C. Use of emission near ambient to study thermal quenching as done before [40] requires some comments. The emission of luminescence is subject to competing radiative and non-radiative transitions described by equation (5.2).

The analysis of thermal quenching provides a means to determine the frequency factor for the non-radiative process since $C = \nu\tau_{rad}$ where τ_{rad} is the luminescence lifetime [66]. The value of C can be obtained by fitting as explained earlier. The value of C was found as 9. 8 $\times 10^7$ for peak A1 and 6.5 $\times 10^7$ for peak A3 respectively. Since τ_{rad} for this particular sample was measured as 54.5 μs [48], $\nu = 1.8 \times 10^{11}$ s^{-1} using peak A1 and $\nu = 1.2 \times 10^{11}$ s^{-1} using peak A3 for the sample annealed at 900 °C for 10 minutes.

7.4.5 Curve fitting

Phototransferred peaks A1 and A3 obtained after preheating to either 350 °C or 500 °C for samples annealed at 500 °C, 900 °C for 10, 30, 60 minutes and the sample annealed at 1000 °C were further analysed by curve fitting. The data were corrected for the effect of thermal quenching before fitting. The general order-kinetics equation (2.30) was used. The goodness of fits were tested by the 'figure of merit' FOM using equation (2.31). The FOM for the fits were evaluated as 0.88, 1.08 and 1.02 % for samples annealed at 900 °C for 10, 30 and 60 minutes respectively. For the samples annealed at 500 and 1000 °C, the FOM was evaluated as 1.34 and 1.58 % respectively. Since, for a good fit, FOM should be $\leq$ 3.5 % [28], all fits were deemed acceptable. Figure 7.7 shows a glow curve of PTTL obtained after preheating to 500 °C for the sample annealed at 900 °C for 10 minutes. The activation energy for peaks A1 and A3 were obtained as 0.64 $\pm$0.02 eV and 0.73 $\pm$ 0.04 eV and their order of kinetics as b1 = 1.20 $\pm$ 0.04 and b2 =1.10 $\pm$ 0.1 respectively. The full set of results for that of the samples annealed at 500

°C, 900 °C for 30, 60 minutes and that of the sample annealed at 1000 °C are discussed in Table 7.1. By using this method, the order of kinetic is first-order for peaks A1 and A3. The kinetic parameters evaluated using this method are consistent with that from WGP and phosphorescence methods.

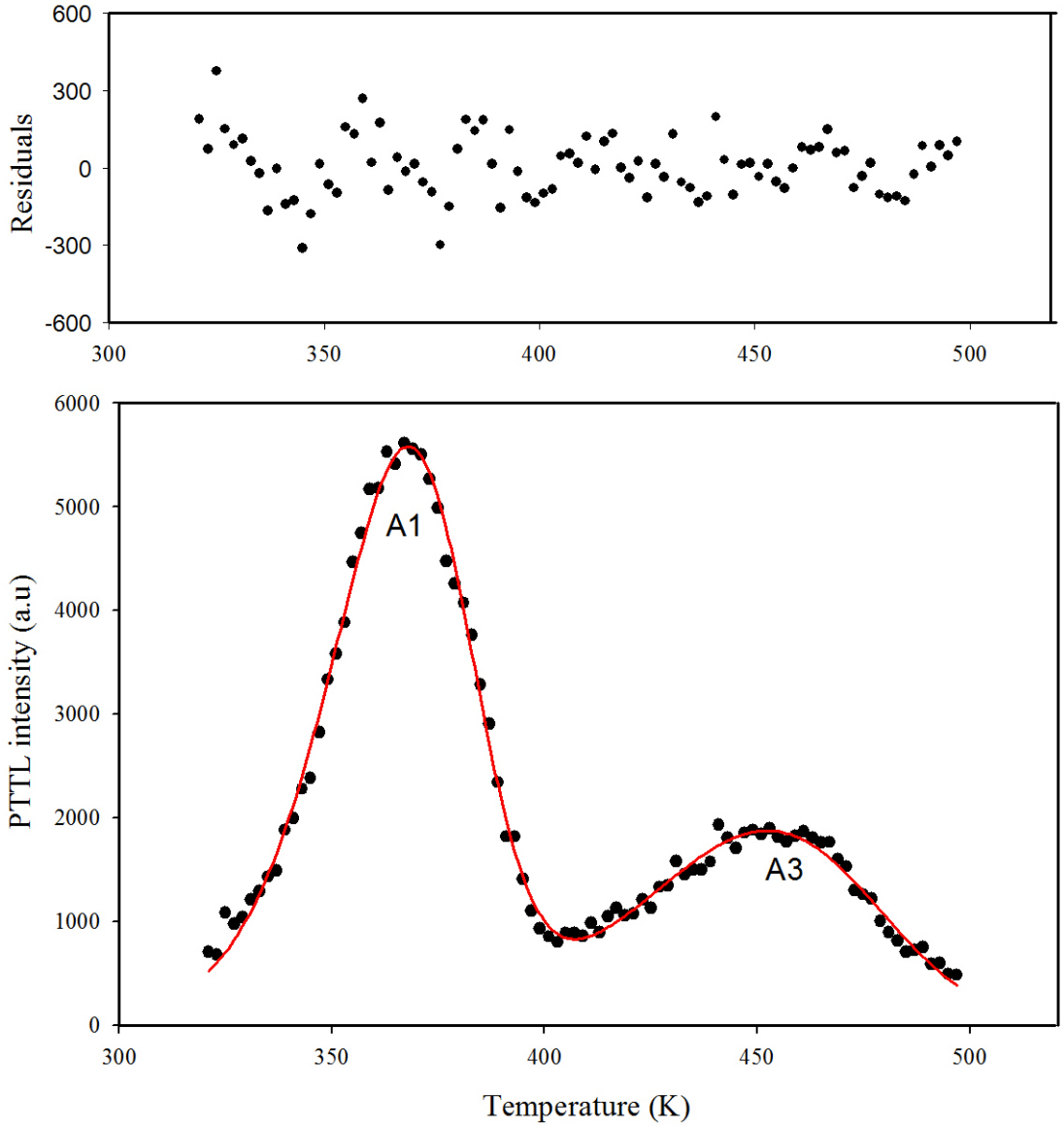

Figure 7.7: A glow curve for the sample annealed at 900 °C for 10 minutes measured preheated to 500 °C. The line is the best fit of equation (2.30).

The results of kinetic analysis for peaks A1, A2 and A3 for samples annealed at 500 °C, 900

°C for 10, 30, 60 minutes and that of the sample annealed 1000 °C are listed in Table 7.1. In particular, the value of the activation energy for peak A1 is consistent with that for the main peak under conventional TL, i.e. 0.67 ± 0.02 eV as reported by Dawam and Chithambo [50]. That study also showed that the peak is affected by thermal quenching with an activation energy of 0.65 ± 0.02 eV. Thus the main peak is properly reproduced under phototransfer. There is no systematic dependence of the activation energy, the activation energy of thermal quenching, or the order of kinetics on the temperature or duration of annealing.

Peak	Annealing time (minutes)	Annealing temp. (°C)	Preheat temp. (°C)	T_m (°C)	Method	b	E (eV)	ΔE (eV)	ν (s^{-1})	Reference.
A1	10	500	250	74	WGP	1.1	0.69 ± 0.02			Section 7.4.1
A1	10	900	250	90	WGP	1.2	0.66 ± 0.01			Figure 7.3
A1	30	900	250	80	WGP	1.1	0.67 ± 0.01			Section 7.4.1
A1	60	900	250	80	WGP	1.2	0.66 ± 0.02			Section 7.4.1
A1	10	1000	250	76	WGP	1.1	0.76 ± 0.02			Section 7.4.1
A1	10	900	350	90	WGP	1.1	0.76 ± 0.02			Section 7.4.1
A1	60	900	350	80	WGP	1.2	0.76 ± 0.02			Section 7.4.1
A1	10	900	500	100	WGP	1.1	0.66 ± 0.02			Section 7.4.1
A1	10	500	250		Phos	1	0.67 ± 0.03			Section 7.4.2
A1	10	900	250		Phos	1	0.60 ± 0.02			Figure 7.4
A1	30	900	250		Phos	1	0.62 ± 0.03			Section 7.4.2
A1	60	900	250		Phos	1	0.52 ± 0.01			Section 7.4.2
A1	10	1000	250		Phos	1	$0.7\,2 \pm 0.01$			Section 7.4.2
A1	10	500	250		VHR		0.62 ± 0.04	0.72 ± 0.04	1.2×10^{11}	Section 7.4.3
A1	10	900	250		VHR		0.62 ± 0.02	0.65 ± 0.02	1.8×10^{11}	Section 7.4.3
A1	30	900	250		VHR		0.63 ± 0.02	0.64 ± 0.02	1.2×10^{11}	Section 7.4.3
A1	60	900	250		VHR		0.72 ± 0.02	0.62 ± 0.02	1.2×10^{11}	Figure 7.5
A1	10	1000	250		VHR		0.75 ± 0.03	0.68 ± 0.03	1.2×10^{11}	Section 7.4.3

A1	10	500	250	74	CF	1.1 ± 0.03	0.75 ± 0.04			Section 7.4.5
A1	10	900	350	90	CF	1.2 ± 0.03	0.73 ± 0.02			Figure 7.7
A1	30	900	350	80	CF	1.1 ± 0.03	0.75 ± 0.04			Section 7.4.5
A1	60	900	350	80	CF	1.2 ± 0.03	0.57 ± 0.03			Section 7.4.5
A1	10	1000	350	76	CF	1.1 ± 0.02	0.87 ± 0.02			Section 7.4.5
A2	60	900	350		VHR		0.89 ± 0.02	0.62 ± 0.02	8.7×10^{10}	Figure 7.5.
A2	10	1000	350		VHR		0.99 ± 0.02	0.64 ± 0.02	5.6×10^{10}	Section 7.4.3
A3	10	900	250	176	WGP	1.2	0.68 ± 0.03			Section 7.4.1
A3	60	900	250	176	WGP	1.2	1.06 ± 0.04			Section 7.4.1
A3	10	1000	250	196	WGP	1.1	1.12 ± 0.04			Section 7.4.1
A3	10	1000	350		VHR		1.23 ± 0.04	0.68 ± 0.03	6.8×10^{11}	Section 7.4.3
A3	10	900	500		VHR		0.82 ± 0.02	0.66 ± 0.02	1.2×10^{11}	Section 7.4.3
A3	60	1000	350		VHR		1.23 ± 0.04	0.64 ± 0.03	4.9×10^{10}	Figure 7.5
A3	10	1000	350		VHR		1.09 ± 0.02	0.67 ± 0.02	8.4×10^{11}	Section 7.4.3
A3	10	900	500	176	CF	1.06 ± 0.03	0.68 ± 0.03			Section 7.4.3
A3	60	900	350	136	CF	1.06 ± 0.05	1.12 ± 0.04			Section 7.4.5

Table 7.1: Kinetic parameters of PTTL peaks A1, A2 and A3 determined using whole glow peak method (WGP), phosphorescence method (Phos), variable heating rate (VHR) and curve fitting (CF)

7.5 Analysis of phototransfered thermoluminescence

In this section, the analysis of PTTL using pulse annealing to identify acceptors and donors traps was presented. The PTTL intensity profile as a function of illumination time is modelled using various combinations of an acceptor and donors using coupled linear differential equations following the empirical model of Chithambo et al [40]. The competition effects involved in the PTTL are also discussed.

7.5.1 Pulse annealing

The so called pulse annealing technique [85, 86] was carried out to determine the role of electron traps as donors or acceptors in the PTTL process. A sample irradiated to 200 Gy was preheated to a particular temperature to remove a trapped charge from specific electron traps. The sample was then exposed to 470 nm blue light for 20 s to transfer electrons from deep traps to empty shallow traps and then heated again to 500 °C to monitor any PTTL. This procedure was repeated with the preheat temperature varied from 100 to 500 °C in steps of 10 °C. Although the glow curve of each sample has multiple peaks, the most intense one, peak I, was studied in the pulse annealing experiment. Thus the maximum intensity for any reproduced peak A1 was noted for each of the preheating temperatures. The removal of charge from a donor by preheating should cause the TL intensity of the corresponding acceptor trap to decrease.

Figure 7.8 shows the peak intensity as a function of preheating temperature for samples annealed at 500 °C for 10 minutes, 900 °C for 10, 30, 60 minutes and the sample annealed at 1000 °C for 10 minutes. Figure 7.8(a) shows the plot of intensity against preheat temperature for the sample annealed at 500 °C. It can be observed that the intensity increases with preheating temperature between 100 - 130 °C and thereafter decreases. The increase in intensity between 100-130 °C could be due to the accumulation of electron and therefore suggests that peak I and II are not donor traps. The intensity is vary slowly in that region with preheating between 100 and 120 °C as illustrated in Figure 7.8, since no significant amount of charge is removed from any putative donor at these temperatures.

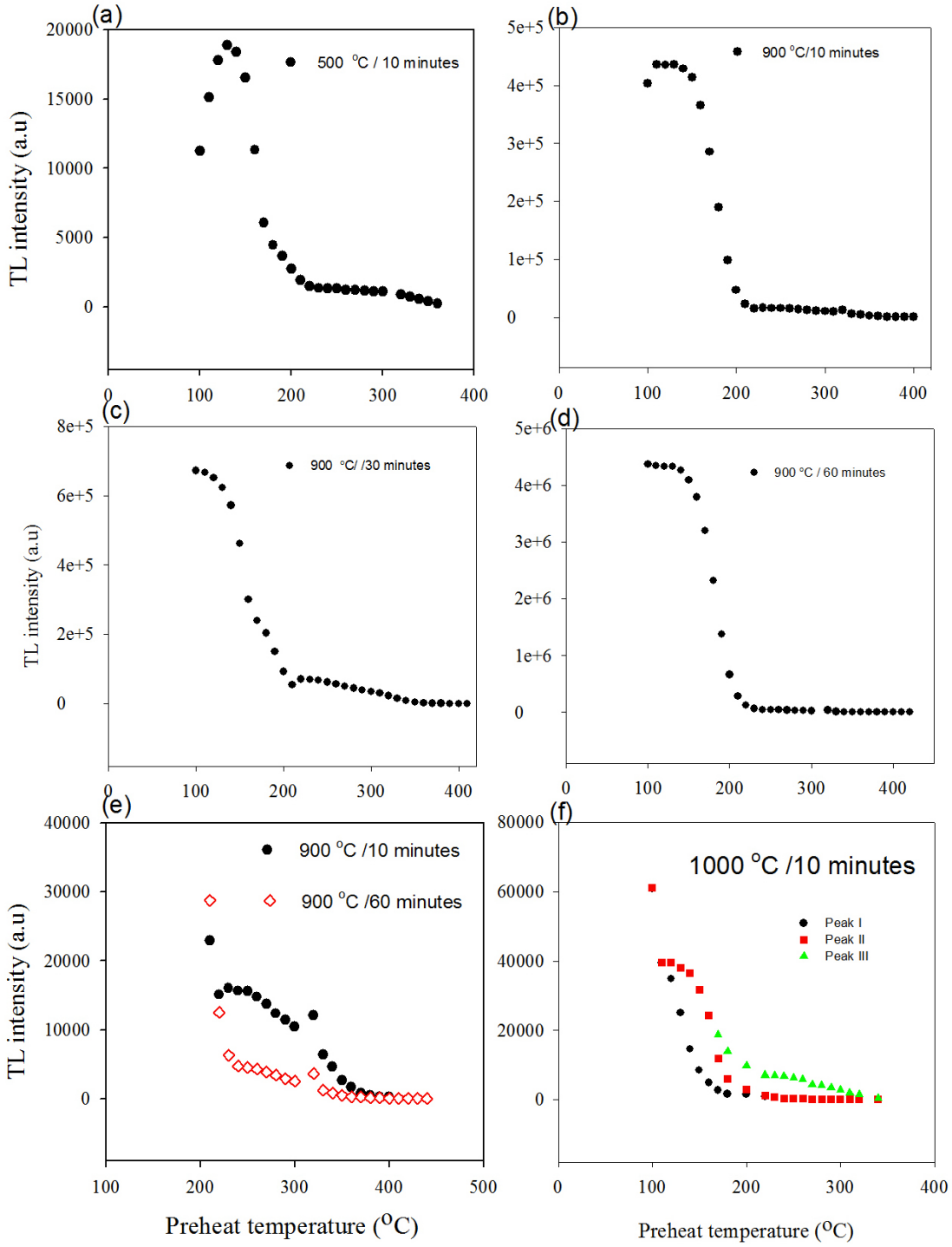

Figure 7.8: The variation of peak intensity against preheating temperature for the sample annealed at (a) 500 °C for 10 minutes (b) 900 °C for 10 minutes (c) 900 °C for 30 minutes (d) 900 °C for 60 minutes (e) The same plot for the samples annealed at 900 °C for 10 and 60 minutes between 200 to 440 °C (f) 1000 °C for peaks I-III.

Preheating between 120-190 °C causes the intensity to decrease sharply. The decrease reflects a reduction in occupancy at source or donor traps which at this stage would be electron traps corresponding to peaks II and III. For preheating to 200 °C and above, the TL intensity of A1 is apparently approximately independent of preheat temperature. In fact, as Figure 7.8(e) shows, the intensity continues to decrease with preheating temperature up to 350 °C. This is evidence that electron traps associated with peaks IV to VI also act as donors. The same outline applies to the results in Figure 7.8(c, d and f).

We also present the results of pulse annealing of the integrated OSL intensity as a function of preheating temperature. The aim of these results is to observe the behaviours of the OSL with the increase in preheating temperature which could determine the active OSL traps involves for PTTL emission. Figure 7.9 shows the plots of normalised integrated OSL intensity for comparison as a function of preheating temperature for the samples annealed at 500 °C, 900 °C for 10, 30, 60 minutes and the sample annealed at 1000 °C.

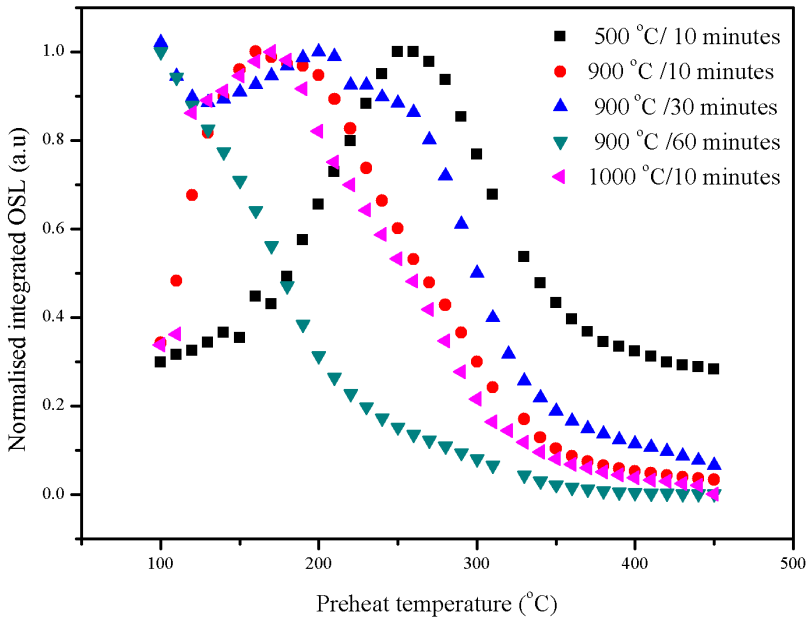

Figure 7.9: The plots of integrated OSL intensity as a function of preheating temperature for the samples annealed at 500 °C, 900 °C for 10, 30 , 60 minutes and the sample annealed at 1000 °C.

It can be observed that OSL intensity increase with increasing preheat temperature between 100-

300 °C and subsequently decreases continuously for the sample annealed at 500 °C. For the sample annealed at 900 °C for 10 minutes, the OSL intensity increase from 100 to 170 °C and then decreases for the remaining preheating temperature. When the duration of annealing was increased to 30 minutes, the OSL intensity decreases from 100-120 °C and then increases between 130-200 °C and finally decreases sharply. As the annealing temperature increases to 1000 °C, the OSL intensity increases between 100-160 °C and then decreases. In contrast for the sample annealed at 900 °C for 60 minutes, the intensity decreases throughout with preheating temperature. The decrease of OSL intensity with preheating temperature suggests the behaviour of donor traps.

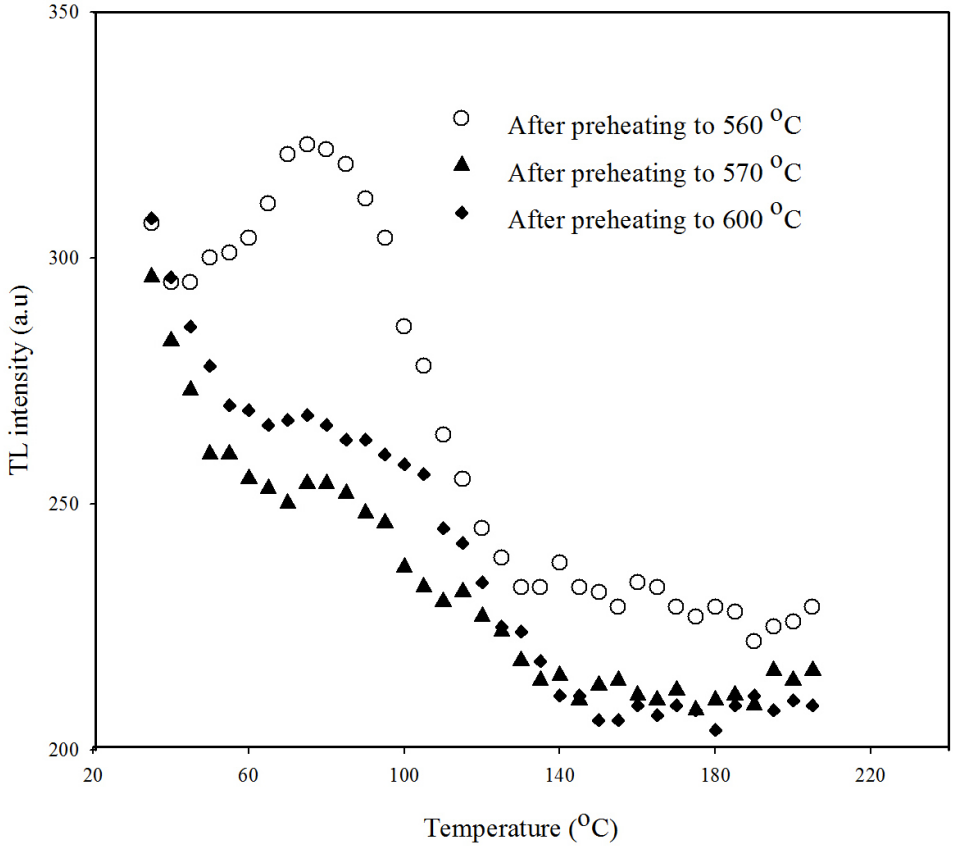

Figure 7.10: The glow curve measured after preheating to 560, 570 and 600 °C.

In order to examine the presence of donor traps above 500 °C, pulse annealing was done between 510 and 600 °C at 10 °C intervals. By removing all peaks, it should be expected that phototransfer

would only ensue from source traps beyond 500 °C. The intensity of PTTL obtained this way was quite weak and cannot be represented as a function of preheating temperature. Instead, we only show some glow curves so obtained. Figure 7.10 shows examples of glow curves showing PTTL measured after preheating to 560, 570 and 600 °C for the sample annealed at 900 °C for 10 minutes. A weak phototransferred peak is measured following preheating to 560 °C. When the preheating temperature is increased to 570 or 600 °C, PTTL is still observed but is ill defined. This indicates that, as donors, deep electron traps in the region beyond 570 °C make only a minimal contribution to the PTTL recorded from this sample.

7.6 Analysis of illumination-time dependence of PTTL intensity

The profile of PTTL intensity as a function of illumination time takes various forms. The archetypal experimental one is an increase followed by a decrease (e.g[87, 40, 44]). The range of experimental forms is considerable and cannot be accounted for by a single model. Alexander and Mckeever [45] described the illumination-time dependent curves of PTTL intensity using sets of non-linear differential equations. They developed their model for a system of one acceptor and one donor. Using a number of assumptions they described various dependences of PTTL intensity on illumination time. In comparison, Chithambo et al. [40] explained the behaviour of PTTL as a function of illumination time using sets of coupled linear differential equations formulated based on multiple donors and acceptors. These differential equations, being linear, have analytical solutions which can be applied directly to experimental data. In this report, we will use the model of Chithambo et al.[40]. The analysis is based on the assertion that only a portion of charge stimulated from a donor is transferred to an acceptor and that any retrapping of stimulated electrons is negligible. The change of PTTL intensity as a function of illumination time will be explained with respect to the energy band diagram in chapter 3 shown in Figure 3.2.

Here $N_1, N_2, N_3, N_4, N_5, N_6$, and N_7 are concentrations of electrons at levels 1 through 7 and that the PTTL intensity is proportional to N. The parameters λ_1 through λ_7 are probabilities of

optical stimulation from these levels respectively. If an acceptor with index j is associated with n donors, the change of trapped charge at the acceptor trap can be compactly described as

$$\frac{dN_j}{dt} = -\lambda_j N_j + \sum_{k=i}^{n} \alpha_k \lambda_k N_k \tag{7.1}$$

where α_k are constants of proportionality. The terms $\lambda_k N_k$ represent the amount of charge stimulated from a donor, a portion ($\alpha_k N_k$) of which is captured at an acceptor. Used together with a set of equations describing the loss of charge from donors, the coupled equations provide a particular solution that can be applied directly to experimental data. Since this is empirically based, the equations describing loss of electrons from donors need to be based on experimental results rather than be formulated as general expressions [40]. Another point to note is that since peaks A1 and A3 follow first-order kinetics as shown in section 7.4 retrapping can indeed be neglected.

7.6.1 PTTL following preheating to 250 °C

When the sample annealed at 500 °C was preheated to 250 °C following the irradiation to 200 Gy to removed peak I-V, but only peaks I-IV were completely removed. Peak V remained with its intensity drastically reduced. The PTTL was only reproduced at 74 °C. The donors here are at levels 5, 6 and 7 with only one acceptor at level 1.

The family of differential equations describing the transfer of charge from donors to the acceptor responsible for PTTL peak A1 is given as

$$\frac{dN_7}{dt} = -\lambda_7 N_7 \tag{7.2}$$

$$\frac{dN_6}{dt} = -\lambda_6 N_6 \tag{7.3}$$

$$\frac{dN_5}{dt} = -\lambda_5 N_5 \tag{7.4}$$

$$\frac{dN_1}{dt} = -\lambda_1 N_1 + \alpha_5 \lambda_5 N_5 + \alpha_6 \lambda_6 N_6 + \alpha_7 \lambda_7 N_7 \tag{7.5}$$

where α_5, α_6 and α_7 are constants of proportionality. The stimulation probability of each of the processes can be expressed as $\lambda = \Phi\sigma$ where σ is the photoionisation cross-section and Φ is the

intensity of stimulation light [31]. The first term in equation (7.5) concerns the optical removal of electrons during illumination. The rest of the terms describe the retrapping of charge from donors. The solution for the set of differential equations (7.2)-(7.5) for peak A1 is

$$N_1 = A_1[\exp(-\lambda_5 t) - \exp(-\lambda_1 t)] + A_2[\exp(-\lambda_6 t) - \exp(-\lambda_1 t)] + A_3[\exp(-\lambda_7 t) - \exp(-\lambda_1 t)] \tag{7.6}$$

where $A_1 = \alpha_5\lambda_5 N_{5i}/(\lambda_1 - \lambda_5)$, $A_2 = \alpha_6\lambda_6 N_{6i}/(\lambda_1 - \lambda_6)$ and $A_3 = \alpha_7\lambda_7 N_{7i}/(\lambda_1 - \lambda_7)$, N_{5i}, N_{6i} and N_{7i} are each the concentration of electrons at electron traps levels 5, 6 and 7 at the start of illumination.

Meanwhile, for the sample annealed at 900 °C for 10 minutes after preheating to 250 °C to remove peaks I-V, only peaks I-IV were properly removed and peak V remained although much reduced in intensity. PTTL peaks were reproduced at 90 °C and 176 °C. Conceptually therefore, the donors here are levels 5, 6 and 7 and the acceptors are levels 1 and 3. Peak A1 reproduced after preheating as same in the sample annealed at 500 °C with the same number of donors. Hence, equation (7.6) holds for peak A1 for the sample annealed at 900 °C. By the same arguments for peak A1 for the samples annealed at 900 °C for 30 and 60 minutes and that of the sample annealed at 1000 °C, equation (7.6) holds.

Following the same procedure as above, the dependence of electron concentration at level 2 for peak A2 in the sample annealed at 900 °C for 60 minutes is found to be

$$N_2 = B_1[\exp(-\lambda_5 t) - \exp(-\lambda_2 t)] + B_2[\exp(-\lambda_6 t) - \exp(-\lambda_2 t)] + B_3[\exp(-\lambda_7 t) - \exp(-\lambda_2 t)]. \tag{7.7}$$

where $B_1 = \omega_5\lambda_5 N_{5i}/(\lambda_2 - \lambda_5)$, $B_2 = \omega_6\lambda_6 N_{6i}/(\lambda_2 - \lambda_6)$ and $B_3 = \omega_7\lambda_7 N_{7i}/(\lambda_2 - \lambda_7)$, ω_5, ω_6, and ω_7 are constants of proportionality and other symbols have their original meanings.

For the sample annealed at 900 °C for 10 minutes and 1000 °C, the dependence of PTTL intensity on the illumination time for the electron concentration at level 3 for peak A3 is given as

$$N_3 = C_1[\exp(-\lambda_5 t) - \exp(-\lambda_3 t)] + C_2[\exp(-\lambda_6 t) - \exp(-\lambda_3 t)] + C_3[\exp(-\lambda_7 t) - \exp(-\lambda_3 t)] \tag{7.8}$$

where $C_1 = \gamma_5\lambda_5 N_{5i}/(\lambda_1 - \lambda_5)$, $C_2 = \gamma_6\lambda_6 N_{6i}/(\lambda_1 - \lambda_6)$ and $C_3 = \gamma_7\lambda_7 N_{7i}/(\lambda_1 - \lambda_7)$, γ_5, γ_6, and γ_7 are constants of proportionality and other symbols have their original meanings.

Figure 7.11 shows the plots of PTTL intensity as a function of illumination time after preheating to 250 °C. All plots go through a peak with illumination time except peak A1 for the sample annealed at 1000 °C for 10 minutes. The detailed behaviour differs and is certainly affected by number and contribution of donors. The quartz whose PTTL is studied here each show at least six peaks I-VI. Thus qualitatively when say, peak I, is removed by preheating, it might be expected that phototransfer will reproduce and this does not happen. Instead PTTL is only observed when a certain number of peaks have been removed. Indeed, not all peaks removed by preheating re-appear under phototransfer. The results of Figure 7.11 are therefore discussed with reference to the preheating temperature used in the PTTL procedure, for preheating to 250 °C. In these plots, we assume as previously [40, 44] that the PTTL intensity is proportional to the concentration of charge at an acceptor.

Here and throughout Figure 7.11, the curve-fitting was based on the Marquardt-Levenberg minimization routine [88]. The time-dependent profiles of the PTTL intensity for peak A1 corresponding to preheating to 250 °C are shown in Figure 7.11(a) and Figure 7.11(b) respectively for the samples annealed at 500 °C and 900 °C for 10 minutes. The solid line through data in Figure 7.11(a) is the best fit of equation (7.6) and also that of Figure 7.11(b). The plot for peak A3 for the sample annealed at 900 °C for 10 minutes is shown in Figure 7.11(c) fitted with equation (7.8). Figure 7.11(d) are for measurement for the sample annealed at 900 °C for 30 minutes. The acceptor A1 for the sample annealed at 900 °C for 60 minutes was fitted with equation (7.6) and illustrated in Figure 7.11(e). Figure 7.11(f) exemplifies the best fit of equation (7.7) for PTTL measured from peak A2 for the sample annealed at 900 °C for 60 minutes. When the annealing temperature was increased to 1000 °C two PTTL peaks were also reproduced shown in Figure 7.11(g) and 7.11(h) fitted with equation (7.6) and equation (7.8).

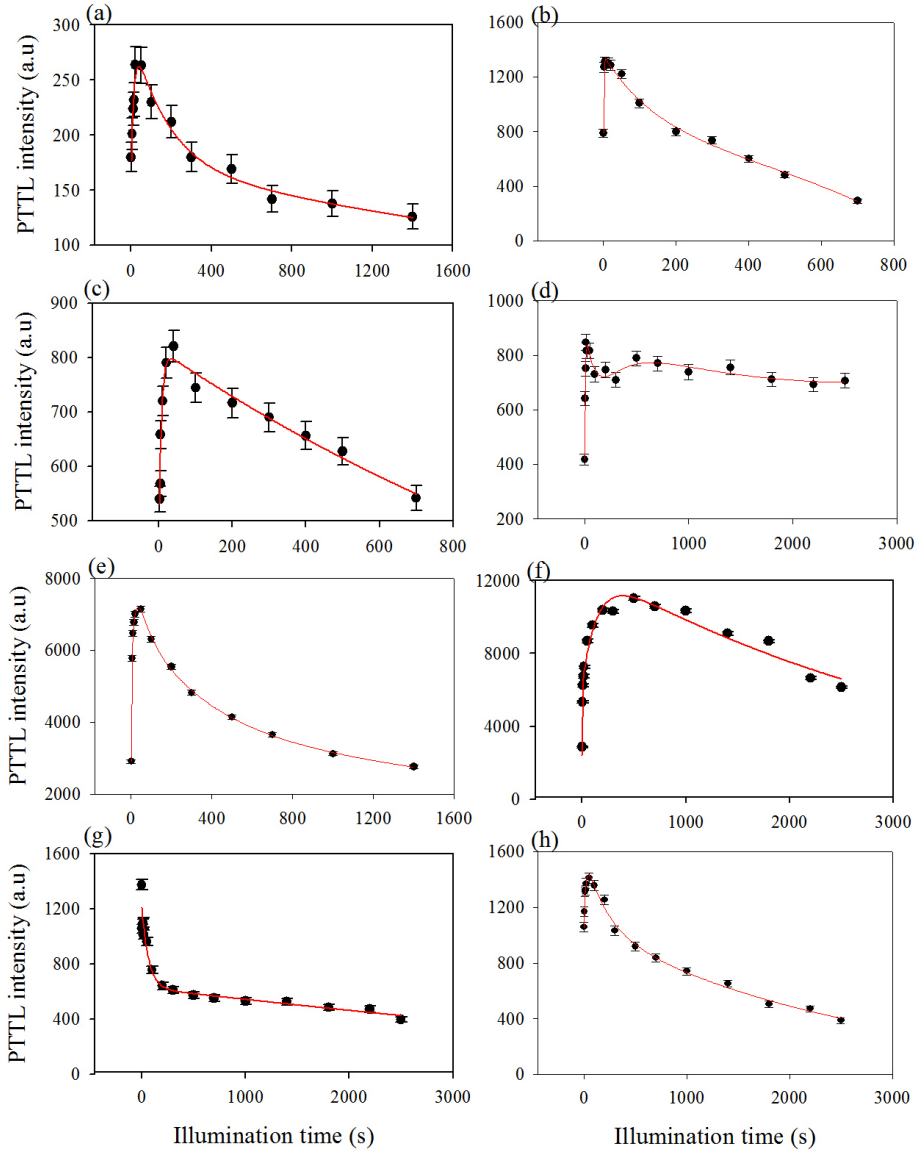

Figure 7.11: The dependence of PTTL intensity on illumination time measured after preheating to 250 °C for peak (a) A1 for the sample annealed at 500 °C (b) A1 for the sample annealed at 900 °C for 10 minutes (c) A3 for the sample annealed at 900 °C for 10 minutes (d) A1 for the sample annealed at 900 °C for 30 minutes (e) A1 for the sample annealed at 900 °C for 60 minutes (f) A2 for the sample annealed at 900 °C for 60 minutes (g) A1 for the sample annealed at 1000 °C and (h) A2 for the sample annealed at 1000 °C.

All cases shown in Figure 7.11 mathematically explained the experimental data fairly well.

The fitting parameters obtained from the fits were used to calculate photoionisation cross-sections. The analysis of the PTTL as described provides a means to determine the photoionisation cross section. The photoionisation cross-section, a parameter that describes the ease with an electron trap can be optically stimulated. The relevant fitting parameters were presented in Table 7.2 with the associated photoionisation cross-sections. The values of photoionisation cross-section are comparable with the ones previously published for natural quartz [31, 89].

7.6.2 PTTL following preheating to 350 °C

In the measurement where the sample annealed at 900 °C for 10 minutes was preheated to 350 °C to remove peak I-VI, two PTTL peaks were reproduced at 90 °C and 176 °C. Under this preheating, it was noted that peak VI could not be properly removed and still reappeared although the intensity of the peak extremely reduced. Thus levels 6 and 7 are considered as donors for the PTTL peaks A1 and A3. In this case, there are two separate systems of two donors and two acceptors.

The set of coupled differential equations describing the case for peak A1 is

$$\frac{dN_7}{dt} = -\lambda_7 N_7 \tag{7.9}$$

$$\frac{dN_6}{dt} = -\lambda_6 N_6 \tag{7.10}$$

$$\frac{dN_1}{dt} = -\lambda_1 N_1 + b_6\lambda_6 N_6 + b_7\lambda_7 N_7 \tag{7.11}$$

where b_6 and b_7 are constants of proportionality. The solution of equations (7.9 - 7.11) is given by

$$N_1 = D_1[\exp(-\lambda_6 t) - \exp(-\lambda_1 t)] + D_2[\exp(-\lambda_7 t) - \exp(-\lambda_1 t)] \tag{7.12}$$

where $D_1 = b_6\lambda_6 N_{6i}/(\lambda_1 - \lambda_6)$ and $D_2 = b_7\lambda_7 N_{7i}/(\lambda_1 - \lambda_7)$ where all symbols are as initially defined.

When the quartz annealed at 900 °C for 60 minutes was preheated to 350 °C to remove peaks I-

VI, three PTTL peaks A1, A2 and A3 was measured at 80, 134 and 188 °C. This preheating could not completely remove peak VI and so its associated electron trap is still regarded as a donor. The concentration of the acceptor traps follows the same behaviour with sample annealed at 900 °C for 10 minutes and as such, equation (7.12). However, the dependence of PTTL intensity on illumination time for electron concentration at the acceptor related to peak A2 in the sample annealed at 900 °C for 60 minutes is expressed as

$$N_2 = E_1[\exp(-\lambda_6 t) - \exp(-\lambda_2 t)] + E_2[\exp(-\lambda_7 t) - \exp(-\lambda_2 t)] \tag{7.13}$$

where $E_1 = \delta_6 \lambda_6 N_{6i}/(\lambda_2 - \lambda_6)$, $E_2 = \delta_7 \lambda_7 N_{7i}/(\lambda_2 - \lambda_7)$, δ_6 and δ_7 are constants of proportionality. Similarly, it can be shown that the PTTL intensity as a function of illumination time for the acceptor associated with peak A3 in the sample annealed at 900 °C for 10 minutes is

$$N_3 = G_1[\exp(-\lambda_6 t) - \exp(-\lambda_3 t)] + G_2[\exp(-\lambda_7 t) - \exp(-\lambda_3 t)] \tag{7.14}$$

where $G_1 = \delta_6 \lambda_6 N_{6i}/(\lambda_3 - \lambda_6)$ and $G_2 = \delta_7 \lambda_7 N_{7i}/(\lambda_3 - \lambda_7)$.

Figure 7.12(a-h) shows the dependence of PTTL intensity on illumination time for the measurements after preheating to 350 °C. It is interesting to note that the PTTL (for the 10 minute sample) monitored here is more intense than that recorded after preheating to 250 °C. This points to the possibility of level 6 (responsible for peak VI) influencing the process as a competitor for electrons released from deep traps since this is the only additional peak removed when the preheating temperature is changed from 250 to 350 °C. Figure 7.12(a) is for peak A1 in the sample annealed at 900 °C for 10 minutes, while Figure 7.12(b) is for peak A3 in the same sample. The data are satisfactorily fitted by equation (7.12) and equation (7.14) respectively. The intensity of peaks A1, A2 and A3, which appears in the sample annealed for 60 minutes, is shown against illumination time in Figure 7.12(c-e). The intensity of peak A2 goes through an extended growth to the maximum. The solid line through the data points are fitted by equations (7.12), (7.13) and (7.14). The results for the sample annealed at 1000 °C for the peaks A1, A2 and A3 are also fitted by equations (7.12), (7.13) and (7.14) and presented in Figure 7.12(f-h) respectively.

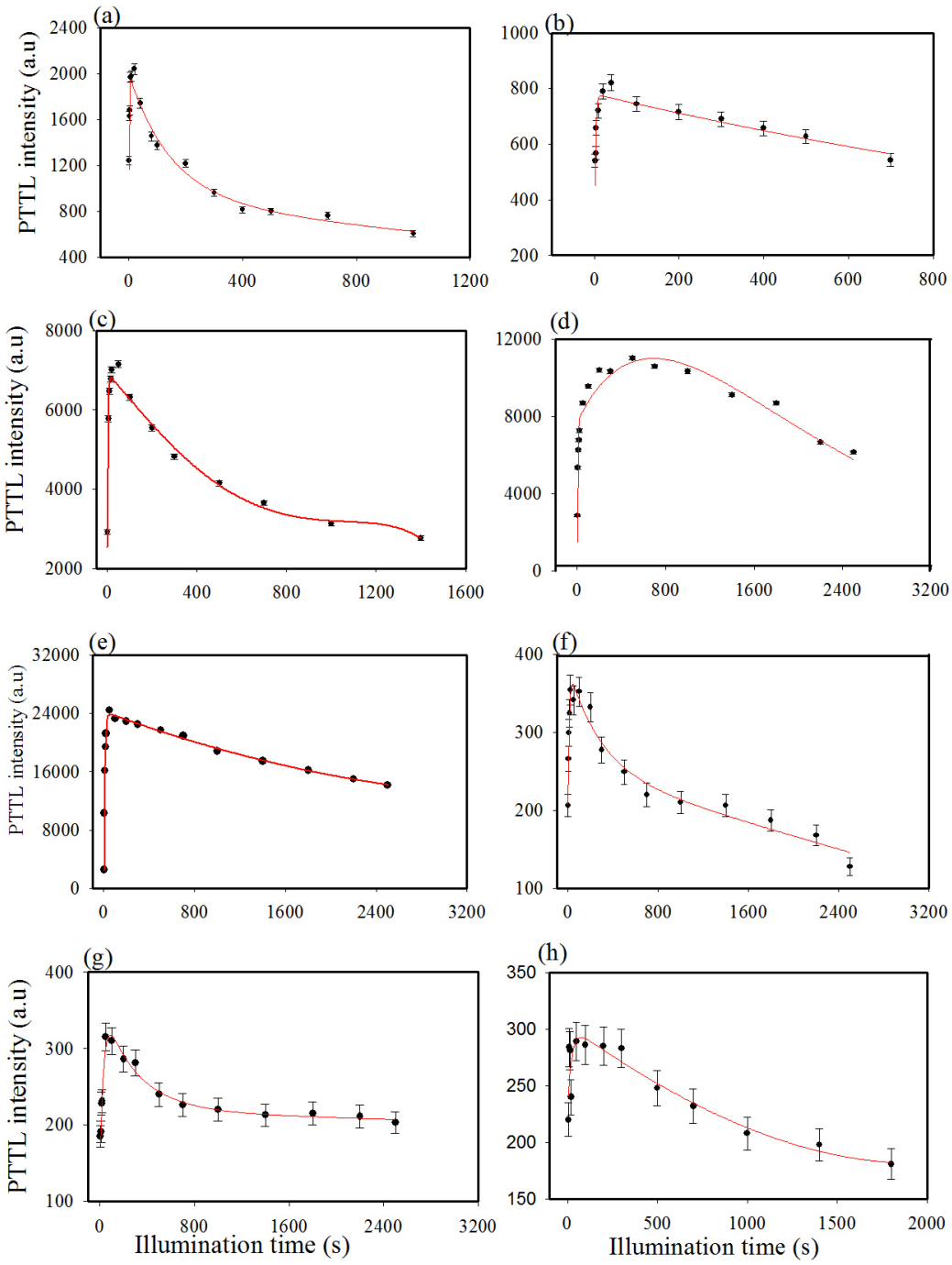

Figure 7.12: The dependence of PTTL intensity against illumination time measured after preheating to 350 °C for peak (a) A1 for the sample annealed at 900 °C for 10 minutes (b) A3 for the sample annealed at 900 °C for 10 minutes(c) A1 for the sample annealed at 900 °C for 60 minutes (d) A2 for the sample annealed at 900 °C for 60 minutes (e) A3 for the sample annealed at 900 °C for 60 minutes (f) A1 for the sample annealed at 1000 °C (g) A2 for the sample annealed at 1000 °C (h) A3 for the sample annealed at 1000 °C.

7.6.3 PTTL following preheating to 450 °C

Preheating an irradiated sample annealed at 900 °C for 60 minutes to 450 °C significantly depletes the TL intensity. The aim of such preheat was to remove all the peaks completely. The PTTL peaks A1, A2 and A3 were measured after preheating at 84, 136 and 202 °C respectively. Peak VI could not be completely remove again. The donor traps here are levels 6 and 7 .

The acceptors A1, A2 and A3 are associated with donors, levels 6 and 7. Using a similar approach as before, the equations describing the PTTL intensity against illumination time for acceptors A1, A2 and A3 are respectively given as

$$N_1 = G_1[\exp(-\lambda_6 t) - \exp(-\lambda_1 t)] + G_2[\exp(-\lambda_7 t) - \exp(-\lambda_1 t)] \tag{7.15}$$

$$N_2 = H_1[\exp(-\lambda_6 t) - \exp(-\lambda_2 t)] + H_2[\exp(-\lambda_7 t) - \exp(-\lambda_2 t)] \tag{7.16}$$

$$N_1 = P_1[\exp(-\lambda_6 t) - \exp(-\lambda_3 t)] + P_2[\exp(-\lambda_7 t) - \exp(-\lambda_3 t)]. \tag{7.17}$$

Figure 7.13(a) and Figure 7.13(b) shows the influence of illumination time on the peaks A1, A2 and A3 for the sample annealed at 900 °C for 60 minutes. The peaks A1, A2 and A3 correspond to the system of two donors and multiple acceptors. The solid line through the data points is thus the best fit of equations (7.15), (7.16) or (7.17) as illustrated in Figure 7.13. The important fitting parameters are presented in Table 7.2.

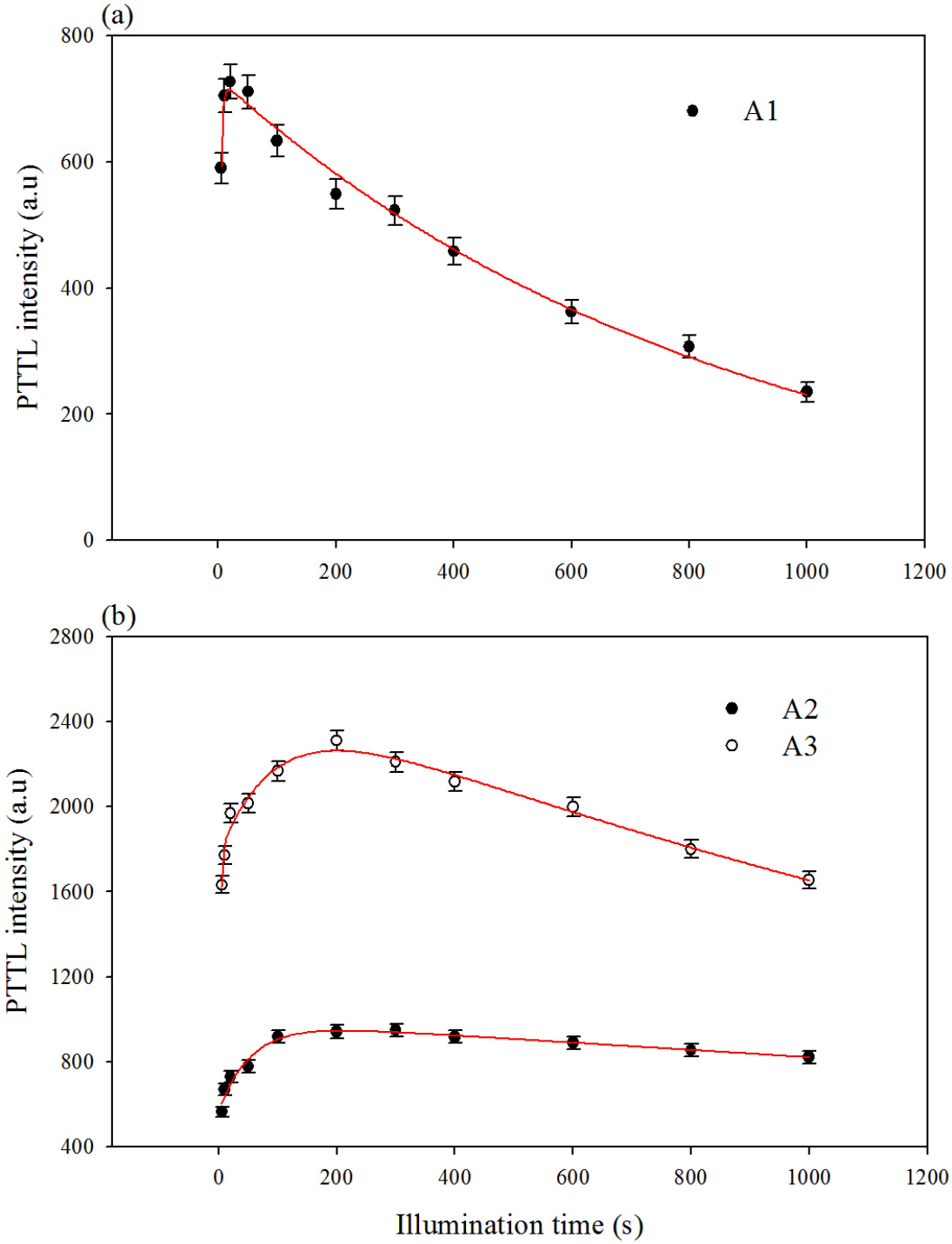

Figure 7.13: The dependence of PTTL intensity as a function of illumination time measured after preheating to 450 °C for the sample annealed at 900 °C for 60 minutes for peak (a) A1 (b) A2 and A3.

7.6.4 PTTL following preheating to 500 °C Sampling deep electron traps

When all the peaks in the glow curve were removed by preheating to 500 °C in the sample annealed at 900 °C for 10 minutes, two PTTL peaks were reproduced at 100 °C and 176 °C. The supposed deep trap (level 7) in this case is the donor. The acceptors are A1 and A3. The transfer of charge from the deep trap to acceptors A1 can be expressed as

$$\frac{dN_7}{dt} = -\lambda_7 N_7 \tag{7.18}$$

$$\frac{dN_1}{dt} = -\lambda_1 N_1 + \mu_7 \lambda_7 N_{7i} \tag{7.19}$$

where μ_7 is a constant of proportionality and all other parameters are as previously defined. The solution of the differential equation (7.18 - 7.19) is given as

$$N_1 = D_1^*[\exp(-\lambda_7 t) - \exp(-\lambda_1 t)] \tag{7.20}$$

where $D_1^* = \mu_7 \lambda_7 N_{7i}/(\lambda_1 - \lambda_7)$.

In the same way, for peak A3 for the sample annealed for 10 minutes, we have

$$N_3 = G_1^*[\exp(-\lambda_7 t) - \exp(-\lambda_3 t)] \tag{7.21}$$

where $G_1^* = \delta_7 \lambda_7 N_{7i}/(\lambda_3 - \lambda_7)$, μ_7 and δ_7 are constants of proportionality.

The PTTL intensity as a function of illumination time observed after preheating to 500 °C is shown in Figure 7.14 for peaks A1 and A3 for the sample annealed 900 °C for 10 minutes. The result of Figure 7.14(a) is properly modelled by equation (7.20) as evident from the solid line through data. The same comments apply for Figure 7.14(b) for peak A3 where the data is fitted by equation (7.21). This is a simpler case of one acceptor and one donor. The PTTL intensity for samples annealed at 500 °C , 900 °C for 30 and 60 minutes and that of the sample annealed at 1000 °C was too weak for any systematic study following preheating to 500 °C. The fitted parameters are conferred in Table 7.2 with associated photoionisation cross-section.

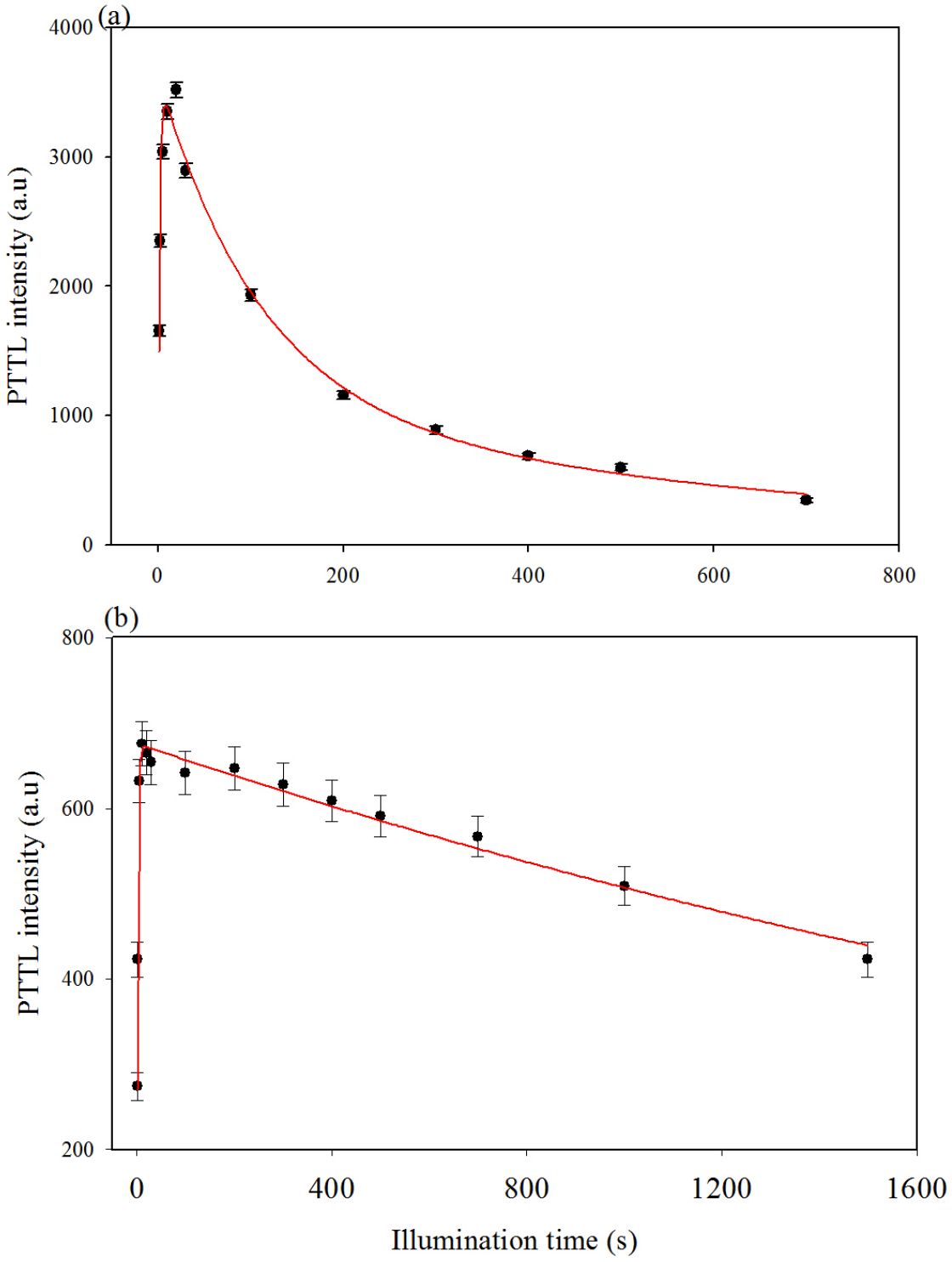

Figure 7.14: The influence of illumination time on PTTL intensity following preheating to 500 °C for the sample annealed at 900 °C for 10 minutes (a) peak A1 (b) peak A3.

Peak	Annealing time (minutes)	Annealing temp. (°C)	Preheat temp. (°C)	T_m (°C)	λ_a (s^{-1})	λ_d (s^{-1})	σ_a (cm^2) $\times 10^{-18}$	$\sigma_d(cm^2)$ $\times 10^{-20}$	Reference
A1	10	500	250	74	0.48 ± 0.03	0.082 ± 0.003	2.54 ± 0.16	4.34 ± 0.32	Figure 7.11(a)
A1	10	900	250	90	0.88 ± 0.03	0.021 ± 0.003	4.56 ± 0.16	1.11 ± 0.26	Figure 7.11(b)
A1	30	900	250	80	0.64 ± 0.05	0.021 ± 0.004	3.34 ± 0.26	1.11 ± 0.11	Figure7.11(d)
A1	60	900	250	80	0.46 ± 0.02	0.031 ± 0.006	2.43 ± 0.11	1.64 ± 0.11	Figure 7.11(e)
A1	10	1000	250	76	0.54 ± 0.03	0.061 ± 0.005	2.86 ± 0.16	3.23 ± 0.11	Figure 7.11(g)
A1	10	900	350	90	0.43 ± 0.04	0.081 ± 0.002	2.28 ± 0.21	4.29 ± 0.16	Figure 7.11(a)
A1	60	900	350	80	0.83 ± 0.02	0.019 ± 0.002	4.39 ± 0.11	1.01 ± 0.16	Figure 7.11(c)
A1	60	900	450	84	0.41 ± 0.04	0.081 ± 0.002	2.17 ± 0.21	4.29 ± 0.21	Figure 7.13(a)
A1	10	1000	350	76	0.60 ± 0.04	0.007 ± 0.003	3.23 ± 0.21	0.37 ± 0.32	Figure 7.12(f)
A1	10	900	500	100	0.56 ± 0.03	0.019 ± 0.003	2.96 ± 0.16	1.01 ± 0.21	Figure 7.14(a)
A2	60	900	250	134	0.44 ± 0.06	0.012 ± 0.004	2.32 ± 0.32	0.63 ± 0.21	Figure 7.11(f)
A2	10	1000	250	122	0.58 ± 0.05	0.091 ± 0.006	3.07 ± 0.21	4.81 ± 0.53	Figure 7.11(h)
A2	60	900	350	134	0.64 ± 0.03	0.052 ± 0.004	3.39 ± 0.16	2.75 ± 0.11	Figure 7.12(f)
A2	10	1000	350	120	0.47 ± 0.04	0.062 ± 0.004	2.49 ± 0.21	3.28 ± 0.16	Figure 7.12(h)
A2	60	900	450	122	0.41 ± 0.06	0.024 ± 0.001	2.17 ± 0.32	1.17 ± 0.32	Figure 7.13(b)
A3	10	900	250	176	0.34 ± 0.04	0.058 ± 0.002	1.80 ± 0.21	3.07 ± 0.11	Figure 7.11(c)
A3	10	900	350	176	0.43 ± 0.04	0.063 ± 0.003	2.28 ± 0.32	3.33 ± 0.26	Figure 7.12(b)
A3	60	900	350	188	0.82 ± 0.04	0.013 ± 0.006	4.33 ± 0.37	0.69 ± 0.16	Figure 7.12(e)

A3	10	1000	350	196	0.61 ± 0.03	0.023 ± 0.002	3.22 ± 0.26	1.22 ± 0.16	Figure 7.12(h)
A3	60	900	450	188	0.47 ± 0.05	0.033 ± 0.005	2.49 ± 0.26	1.75 ± 0.11	Figure 7.13(b)
A3	10	900	500	176	0.46 ± 0.03	0.073 ± 0.003	2.43 ± 0.16	3.86 ± 0.32	Figure 7.14(b)

Table 7.2: A list of fitting parameters of PTTL peaks A1, A2 and A3 from time-dependence of PTTL intensity and their corresponding calculated values of photoionisation cross-sections for the acceptor and donor traps

7.6.5 Competition effects during phototransfer

Phototransfered TL at peak A1 was only observed after the removal of peaks I-IV. There was no PTTL after removal of peaks I, I and II or I to III. In principle, we should expect a PTTL peak to be reproduced when at least one shallow trap has been depleted and one or more supposed donors are intact. That the PTTL only appeared after some supposed donors were removed suggests that some of these may act as effective competitors for charge that would otherwise be captured at an acceptor. In order to investigate this possibility, the intensities of peaks III to VI are plotted against preheating temperature in Figure 7.15.

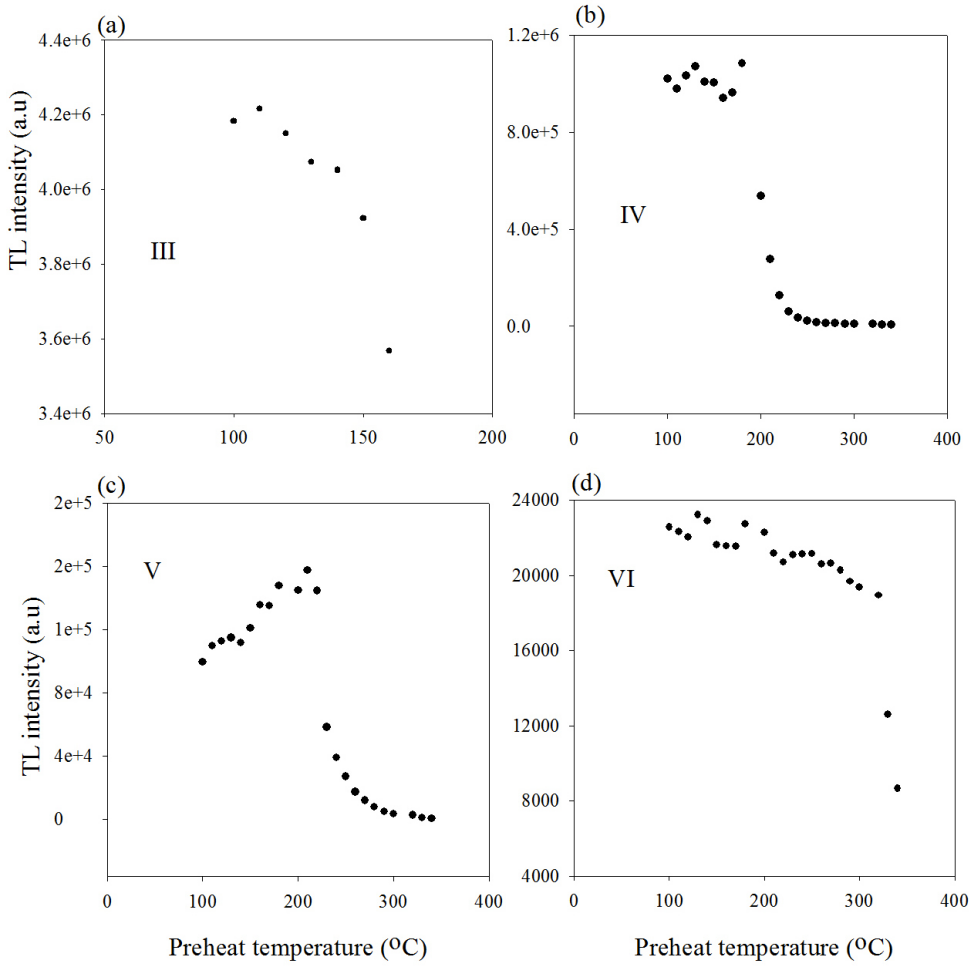

Figure 7.15: The dependence of TL intensity as a function of preheating for putative donors peak for the sample annealed at 900 °C for 10 minutes(a) III (b) IV (c) V and (d) VI.

If a preheat temperature is below the position of a particular peak, it is expected that the peak will contribute as a donor and its intensity should decrease or remain unchanged if that contribution is negligible. Figure 7.15(a) shows that the intensity of peak III decreases with preheating temperature. This is expected of a good donor where any retrapping is negligible. The kinetic analysis in the previous section showed that peak A3 follows first-order kinetics. The change of intensity with preheating temperature shown in Figure 7.15(a) is consistent with this conclusion. The intensity of peak IV in Figure 7.15(b) remain unchanged and latter decrease as expected. On the other hand, if an electron trap competes for phototransferred charge while also acting as a donor, the extent to which it also acts as an acceptor will be reflected in a plot of intensity against preheating temperature. The intensity of peak V, in Figure 7.15(c), increases by 58 % when the heating is changed from 100 to 210 °C. Since the position of this peak is at 240 °C and the preheating temperatures are below this, the increase in intensity must be due to accumulation of charge at its associated electron trap. Beyond 210 °C, the intensity decreases owing to depletion of its charge by preheating and possibly by loss of charge by phototransfer.

The influence of possible competitors can also be examined in illumination-time profiles as shown in Figure 7.16. In Figure7.16(a), the intensity of peak A1 increases with preheating temperature. This is counter-intuitive because increasing the preheat temperature should cause a gradual depletion of donors. This should be seen as a decrease in the intensity of an acceptor peak. The results of Figure 7.16(a) must mean that the effect of any competitor trap is reduced as its trap is depleted as was observed for peak IV in Figure 7.15(b). In contrast, the intensity of peak A3 decreases with preheating temperature as illustrated in Figure 7.16(b). This can be ascribed to the reduction of charge at donors as the preheating temperature is increased.

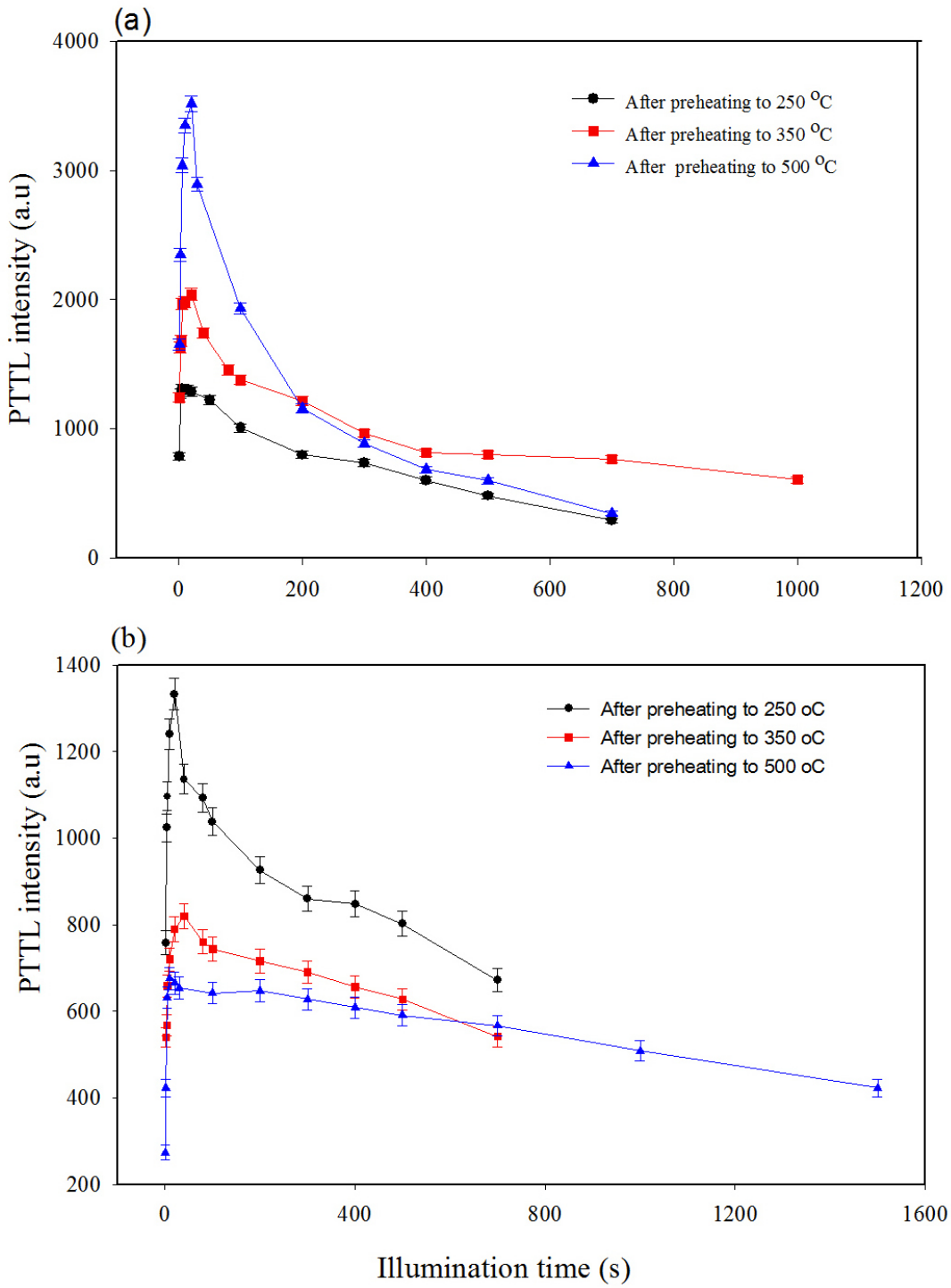

Figure 7.16: Time-response profiles for the sample annealed at 900 °C for 10 minutes for peak (a) A1 (b) A3. The lines are visual guides only.

7.7 Summary

Phototransferred thermoluminescence of annealed synthetic quartz induced using 470 nm blue light has been studied. The samples were annealed at 500 °C for 10 minutes, 900 °C for 10, 30, 60 minutes and 1000 °C for 10 minutes. The conventional TL measured at 1 °C s^{-1} after irradiation to 200 Gy for all samples shows six peaks each. However, only three PTTL peaks were reproduced for the sample annealed at 900 °C for 60 minutes and 1000 °C. When the duration of annealing of the sample annealed at 900 °C was reduced to 10 minutes, only two PTTL peaks were induced. But for an intermediate duration of 30 minutes, the sample annealed at 900 °C and that of the sample annealed at 500 °C only one PTTL peak was reproduced. Deep traps beyond 600 °C make a negligible contribution to the PTTL. All the PTTL peaks studied were affected by thermal quenching. The activation energy of thermal quenching for peaks A1 and A3 were evaluated as 0.62 $\pm$ 0.02 eV and 0.65 $\pm$ 0.02 eV respectively. The PTTL intensity goes through a peak as a function of illumination time. The experimental change of PTTL intensity as a function of illumination time is modelled using sets of coupled linear differential equations. This is in good agreement with the experiment and the model based on systems of donors and acceptors whose number is determined by preheating temperature.

CHAPTER 8

Conclusion

8.1 Conclusion

The motivation of this study was to study physical mechanism of luminescence in synthetic quartz and the extraction of physical information using TL, PTTL and OSL techniques. Efforts centered on the relevant properties of luminescence to physical mechanism was investigated. Summaries of the studied undertaken are presented at the end of each result chapters. In this conclusion section, the general findings are summarised and directions for future study are suggested.

The TL of samples annealed at 900 , 500 °C and unannealed sample were investigated. In all the three samples, the main peak position was below 100 °C with the other weaker peaks. The kinetic analyses was carried out on the main peak only. In all cases, the peak was subjected to first order kinetics using various techniques. The main peak for the unannealed sample and sample annealed at 500 °C decreases with increases with the heating rates, a phenomena called thermal quenching following irradiation to 40 Gy. However, for the sample annealed at 900 °C,

the peak shows an inverse quenching. When the sample was irradiated to lower dose for example 3 Gy, the peak decreases with heating rate i.e thermal quenching. The activation energy of the main peak for the three samples were evaluated which slightly decreases with increase in annealing temperature. Likewise, the activation energy of thermal quenching were evaluated and the increase in annealing also affects the values of activation energy of thermal quenching.

Thermally assisted CW-OSL from the samples of annealed synthetic quartz using 470 nm blue LEDs has also been investigated. The OSL was measured from a temperature between 30 - 200 °C after preheating to either 300 or 500 °C. The preheated temperature to 500 °C is evident of deep traps presence in the samples. In all cases, the CW-OSL goes through a peak as a function of measurement temperature. The integrated OSL intensity was found to increase with irradiation dose, stimulation time and annealing temperature. But, the increase in the duration of annealing decreases the OSL intensity. The values of the activation energies of thermal assistance obtained have some discrepancy while that of activation energy of thermal quenching are consistent for change with annealing temperature, duration of annealing and stimulation time.

The PTTL of annealed synthetic quartz induced using 470 nm blue light has been studied. The samples were annealed at 500 °C for 10 minutes, 900 °C for 10, 30, 60 minutes and 1000 °C for 10 minutes before use. The conventional TL measured at 1 °C s^{-1} after irradiation to 200 Gy for all samples shows six peaks. However, only three PTTL peaks were reproduced for the sample annealed at 900 °C for 60 minutes and the sample annealed at 1000 °C for 10 minutes. For the sample annealed at 900 °C for 10 minutes two peaks were reproduced under PTTL. So also, for the samples annealed at 500 and 900 °C for 30 minutes, only one peak was reproduced under PTTL. The PTTL peaks were studied for thermal quenching and peaks A1 and A3 were determined to be subject to thermal quenching. The activation energies of thermal quenching for peaks A1 and A3 were evaluated as 0.62 ± 0.02 eV and 0.65 ± 0.02 eV respectively. The results for the two peaks A1 and A3 are similar to each other in both case. This means that they have the same recombination centre for the electron traps responsible for both peaks. The PTTL intensity goes through a peak as a function of illumination time in most cases. The experimental change of PTTL intensity with illumination time is modelled using sets of coupled linear differential

equations based on systems of donors and acceptors whose number is determined by preheating temperature.

8.2 Possible areas for future study

For better understanding of physical mechanism and nature of defects using luminescence techniques, the following are essential for future studies where equipments are available;

- The spectral measurement are required to gain a comprehensive nature and identification of the recombination centres participating during the TL or OSL in quartz. This could also be useful to determine more precisely the detection window occupied during TL and OSL measurements.
- For the OSL mechanism, additional information is likely to be obtained by performing temperature dependence measurement using various wavelength. Also, optically and thermally stimulated exo-electronic emission may help to understand if electrons are transported directly into the conduction band. Finally, measurement of the optical depth of the traps could clarify the importance of an electron-phonon interaction.
- It could be of interest to determine the optical trap depth of the donor traps using the dependence of the PTTL intensity on the photon energy of the light used for inducing the phototransfer. Such studies may require photon flux of light at different wavelengths.

Bibliography

[1] Frank Preusser et al. “Quartz as a natural luminescence dosimeter”. In: *Earth-Science Reviews* 97.1 (2009), pp. 184–214.

[2] Yu A. Marazuev, A. B Brik, and V. Ya Degoda. “Radioluminescent dosimetry of α-quartz”. In: *Radiation measurements* 24.4 (1995), pp. 565–569.

[3] Martin Jim Aitken. *Thermoluminescence dating*. Academic press, 1985.

[4] S. W. S Mckeever. *Thermoluminescence of solid*. Cambridge, 1985.

[5] Owen M. Williams and Nigel A. Spooner. “Defect pair mechanism for quartz intermediate temperature thermoluminescence bands”. In: *Radiation Measurements* 108 (2018), pp. 41 –44.

[6] Marco Martini, Mauro Fasoli, and Irene Villa. “Defect studies in quartz: Composite nature of the blue and UV emissions”. In: *Nuclear Instruments and Methods in Physics Research Section B: Beam Interactions with Materials and Atoms* 327 (2014), pp. 15 –21.

[7] Nigel A. Spooner, Owen M. Williams, and Jillian E. Moffatt. “Pulsed optically stimulated luminescence for mechanisms studies in quartz”. In: *Radiation Measurements* 128 (2019), pp. 106–176.

[8] Prasenjit Saha, N Annamalai, and Animesh Kumar Guha. “Synthetic quartz production and applications”. In: *Transactions of the Indian Ceramic Society* 50.5 (1991), pp. 129–135.

[9] Roland Stalder and Jürgen Konzett. “OH defects in quartz in the system quartz–albite–water and granite–water between 5 and 25 kbar”. In: *Physics and Chemistry of Minerals* 39.10 (2012), pp. 817–827.

[10] Anthony R West. *Solid state chemistry and its applications*. John Wiley & Sons, 2014.

[11] Eduardo Calabrese and W. Beall Fowler. “Electronic energy-band structure of α quartz”. In: *Phys. Rev. B* 18 (6 1978), pp. 2888–2896.

[12] Charles Kittel, Paul McEuen, and Paul McEuen. *Introduction to solid state physics*. Vol. 8. Wiley New York, 1996.

[13] Reuven Chen and Stephen W S McKeever. *Theory of thermoluminescence and related phenomena*. World Scientific, 1997.

[14] Reuven Chen and Vasilis Pagonis. *Thermally and optically stimulated luminescence: a simulation approach*. John Wiley & Sons, 2011.

[15] G. F. J Garlick and A. F Gibson. “The electron trap mechanism of luminescence in sulphide and silicate phosphors”. In: *Proceedings of the physical society* 60.6 (1948), p. 574.

[16] C. E May and J. A Partridge. “Thermoluminescent kinetics of alpha-irradiated alkali halides”. In: *The Journal of Chemical Physics* 40.5 (1964), pp. 1401–1409.

[17] R Chen et al. “Mixed first and second order kinetics in thermally stimulated processes”. In: *Journal of luminescence* 23.3-4 (1981), pp. 293–303.

[18] N Itoh, D Stoneham, and AM Stoneham. “Ionic and electronic processes in quartz: mechanisms of thermoluminescence and optically stimulated luminescence”. In: *Journal of Applied Physics* 92.9 (2002), pp. 5036–5044.

[19] N Itoh, D Stoneham, and AM Stoneham. “The predose effect in thermoluminescent dosimetry”. In: *Journal of Physics: Condensed Matter* 13.10 (2001), p. 2201.

[20] N. R. J Poolton et al. “Luminescence sensitivity changes in natural quartz induced by high temperature annealing: a high frequency EPR and OSL study”. In: *Journal of Physics D: Applied Physics* 33.8 (2000), p. 1007.

[21] Vasilis Pagonis, George Kitis, and Claudio Furetta. *Numerical and practical exercises in thermoluminescence*. Springer Science, 2006.

[22] Reuven Chen and S .A .A Winer. “Effects of various heating rates on glow curves”. In: *Journal of applied physics* 41.13 (1970), pp. 5227–5232.

[23] N. S Mohan. “Numerical curve fitting for calculating glow parameters”. In: *J. Phys. D: Appl. Phys.* 3 (1940), p. 243.

[24] D Shenker and R Chen. “Numerical curve fitting of general order kinetics glow peaks”. In: *Journal of Physics D: Applied Physics* 4.2 (1971), p. 287.

[25] R. K Bull et al. “Thermoluminescence kinetics for multipeak glow curves produced by the release of electrons and holes”. In: *Journal of Physics D: Applied Physics* 19.7 (1986), p. 1321.

[26] G. Kitis, J. M Gomez-Ros, and J. W. N Tuyn. “Thermoluminescence glow-curve deconvolution functions for first, second and general orders of kinetics”. In: *Journal of Physics D: Applied Physics* 31.19 (1998), p. 2636.

[27] Yigal S Horowitz and D Yossian. *Computerised glow curve deconvolution: application to thermoluminescence dosimetry*. Nuclear Technology Publ., 1995.

[28] H. Garo Balian and Nelson W. Eddy. “Figure-of-merit (FOM), an improved criterion over the normalized chi-squared test for assessing goodness-of-fit of gamma-ray spectral peaks”. In: *Nuclear Instruments and Methods* 145.2 (1977), pp. 389–395.

[29] Nozomu Takeuchi, Katsuyuki Inabe, and Hidehito Nanto. “Note on the isothermal decay method for determining trap depth from glow curves”. In: *Journal of Materials Science* 10.1 (1975), pp. 159–159.

[30] M. L Chithambo. “A method for kinetic analysis and study of thermal quenching in thermoluminescence based on use of the area under an isothermal decay-curve”. In: *Journal of Luminescence* 151 (2014), pp. 235–243.

[31] L. Bøtter-Jensen, S. W. S. McKeever, and A. G. Wintle. *Optically stimulated luminescence dosimetry*. Elsevier, 2003, p. 355. ISBN: 9780444506849.

[32] B Subedi, G Kitis, and V Pagonis. “Simulation of the influence of thermal quenching on thermoluminescence glow-peaks”. In: *physica status solidi (a)* 207.5 (2010), pp. 1216–1226.

[33] G Kitis, V Pagonis, and C Drupieski. “Cooling rate effects on the thermoluminescence glow curves of Arkansas quartz”. In: *physica status solidi (a)* 198.2 (2003), pp. 312–321.

[34] S. A Petrov and I. K Bailiff. “Determination of trap depths associated with TL peaks in synthetic quartz (350-550 K”. In: *Radiation Measurements* 2 (), pp. 185–191.

[35] G. Kitis et al. “The influence of heating rate on the response and trapping parameters of alpha-Al2O3: C”. In: *Radiation Protection Dosimetry* 55.3 (1994), pp. 183–190.

[36] V Pagonis et al. “Modelling the thermal quenching mechanism in quartz based on time-resolved optically stimulated luminescence”. In: *Journal of luminescence* 130.5 (2010), pp. 902–909.

[37] D. L Dexter, C. C Klick, and G. A Russell. “Criterion for the occurrence of luminescence”. In: *Physical Review* 100.2 (1955), p. 603.

[38] M. S Akselrod et al. “Thermal quenching of F-center luminescence in $Al_2O_3 : C$”. In: *Journal of applied physics* 84.6 (1998), pp. 3364–3373.

[39] A. G Wintle. “Detailed study of a thermoluminescent mineral exhibiting anomalous fading”. In: *Journal of Luminescence* 15.4 (1977), pp. 385–393.

[40] M. L Chithambo, C Seneza, and J. M Kalita. “Phototransferred thermoluminescence of α-Al_2 O_3: C: Experimental results and empirical models”. In: *Radiation Measurements* 105.Supplement C (2017), pp. 7–16.

[41] M. L Chithambo, P Niyonzima, and J. M Kalita. “Phototransferred thermoluminescence of synthetic quartz: Analysis of illumination-time response curves”. In: *Journal of Luminescence* 198 (2018), pp. 146–154.

[42] I. K. Bailiff et al. “The phototransfer technique and its use in thermoluminescence dating”. In: *Journal of Electrostatics* 3.1-3 (1977), pp. 269–280.

[43] Lily Bossin, Ian .K Bailiff, and Ian Terry. “Phototransferred TL properties of alumina substrates”. In: *Radiation Measurements* 120 (2018), pp. 41–46.

[44] A. G. Wintle and A. S. Murray. “The relationship between quartz thermoluminescence, photo-transferred thermoluminescence, and optically stimulated luminescence”. In: *Radiation Measurements* 27.4 (1997), pp. 611–624.

[45] C. S Alexander and S. W. S McKeever. “Phototransferred thermoluminescence”. In: *Journal of Physics D: Applied Physics* 31.20 (1998), p. 2908.

[46] Mayank Jain and Lars Bøtter-Jensen. “Luminescence instrumentation”. In: *Defect and Diffusion Forum*. Vol. 357. Trans Tech Publ. 2014, pp. 245–260.

[47] M. L Chithambo. “Time-resolved luminescence from annealed synthetic quartz under 525nm pulsed green light stimulation”. In: *Radiation Measurements* 38.4 (2004), pp. 553–555.

[48] M. L Chithambo, P Sane, and F Tuomisto. “Positron and luminescence lifetimes in annealed synthetic quartz”. In: *Radiation Measurements* 46 (2011), pp. 310–318.

[49] M. L Chithambo and P Niyonzima. “Radioluminescence of annealed synthetic quartz”. In: *Radiation Measurements* 106 (2017), pp. 35–39.

[50] R.R. Dawam and M.L. Chithambo. “Thermoluminescence of annealed synthetic quartz: The influence of annealing on kinetic parameters and thermal quenching”. In: *Radiation Measurements* 120 (2018), pp. 47–52.

[51] M. L Chithambo and P Niyonzima. “On isothermal heating as a method of separating closely collocated thermoluminescence peaks for kinetic analysis”. In: *Journal of luminescence* 155 (2014), pp. 70–78.

[52] S. A Petrov and I. K Bailiff. “The 110 °C TL peak in synthetic quartz”. In: *Radiation Measurements* 24.4 (1995), pp. 519–523.

[53] G. Kitis et al. “Detailed kinetic study of the thermoluminescence glow curve of synthetic quartz”. In: *Radiation protection dosimetry* 100.1-4 (2002), pp. 225–228.

[54] A Necmeddin Yazici and Mustafa Topaksu. “The analysis of thermoluminescence glow peaks of unannealed synthetic quartz”. In: *Journal of Physics D: Applied Physics* 36.6 (2003), p. 620.

[55] Fernando Agulló-López, Charles Richard Arthur Catlow, and Peter David Townsend. *Point defects in materials*. Academic Press, 1988.

[56] R. B Galloway. “Luminescence lifetimes in quartz: dependence on annealing temperature prior to beta irradiation”. In: *Radiation Measurements* 35.1 (2002), pp. 67–77. ISSN: 1350-4487.

[57] R Chen and G Fogel. “Supralinearity in thermoluminescence revisited”. In: *Radiation Protection Dosimetry* 47.1-4 (1993), pp. 23–26.

[58] Hüseyin Toktamiş and A Necmeddin Yazici. “Effects of annealing on thermoluminescence peak positions and trap depths of synthetic and natural quartz by means of the various heating rate method”. In: *Chinese Physics Letters* 29.8 (2012), p. 087802.

[59] Reuven Chen. “Advantages and Disadvantages in the Utilisation of Thermoluminescence (TL) and Optically Stimulated Luminescence (OSL) for Radiation Dosimetry”. In: Croatia: Croatian Radiation Protection Association, 2001, pp. 1–8.

[60] David J Huntley, Dorothy I Godfrey-Smith, and Michael L. W Thewalt. “Optical dating of sediments”. In: *Nature* 313.5998 (1985), p. 105.

[61] A. N Nyirenda and M. L Chithambo. “Factors influencing the shape of CW-OSL signal obtained by stimulation of very deep traps in carbon-doped aluminium oxide: An experimental study”. In: *Journal of Luminescence* 192 (2017), pp. 436–442.

[62] George S. Polymeris et al. “Thermal assistance in TA OSL signals of feldspar and polymineral samples; comparison with the case of pure quartz”. In: *Radiation Measurements* 81 (2015), pp. 270–274.

[63] G. S. Polymeris et al. “Thermally assisted OSL from deep traps in $Al_2O_3 : C$”. In: *Radiation Measurements* 45.3-6 (2010), pp. 519–522.

[64] G. S Polymeris et al. “Properties of quartz TA–OSL signal with a peculiar decay shape for SAR TA–OSL applications”. In: *Radiation Measurements* 120 (2018), pp. 176–180.

[65] B. W Smith and E. J Rhodes. “Charge movements in quartz and their relevance to optical dating”. In: *Radiation Measurements* 23.2-3 (1994), pp. 329–333.

[66] M. L Chithambo. “The analysis of time-resolved optically stimulated luminescence: II. Computer simulations and experimental results”. In: *Journal of Physics D: Applied Physics* 40.7 (2007), p. 1880.

[67] M. L Chithambo and R. B Galloway. “On the slow component of luminescence stimulated from quartz by pulsed blue light-emitting diodes”. In: *Nuclear Instruments and Methods in Physics Research Section B: Beam Interactions with Materials and Atoms* 183.3-4 (2001), pp. 358–368.

[68] Nigel A Spooner. “On the optical dating signal from quartz”. In: *Radiation Measurements* 23.2-3 (1994), pp. 593–600.

[69] A. S Murray and A. G Wintle. “Factors controlling the shape of the OSL decay curve in quartz”. In: *Radiation Measurements* 29.1 (1998), pp. 65–79.

[70] D. J Huntley, M. A Short, and K Dunphy. “Deep traps in quartz and their use for optical dating”. In: *Canadian Journal of Physics* 74.3-4 (1996), pp. 81–91.

[71] M. J Aitken and B. W Smith. “Optical dating: recuperation after bleaching”. In: *Quaternary Science Reviews* 7.3-4 (1988), pp. 387–393.

[72] F. O. Ogundare and M. L. Chithambo. “Time resolved luminescence of quartz from Nigeria”. In: *Optical Materials* 29.12 (2007), pp. 1844 –1851.

[73] L. Bøtter-Jensen et al. “Luminescence sensitivity changes in quartz as a result of annealing”. In: *Radiation Measurements* 24.4 (1995), pp. 535–541.

[74] Y. D Kale and Y. H Gandhi. “Influence of pre-measurement thermal treatment on OSL of synthetic quartz measured at room temperature”. In: *Journal of Luminescence* 128.3 (2008), pp. 499–503.

[75] M. L Chithambo. “The influence of annealing and partial bleaching on luminescence lifetimes in quartz”. In: *Radiation Measurements* 37.4 (2003), pp. 467–472.

[76] J.H Choi, G. A. T Duller, and A. G Wintle. “Analysis of quartz LM-OSL curves”. In: *Ancient TL* 24.1 (2006), pp. 9–20.

[77] J.S. Singarayer and R.M. Bailey. “Component-resolved bleaching spectra of quartz optically stimulated luminescence: preliminary results and implications for dating”. In: *Radiation Measurements* 38.1 (2004), pp. 111 –118.

[78] J. M Kalita and M. L Chithambo. “Phototransferred thermoluminescence in $\alpha - Al_2O_3$: C, Mg under 470 nm blue light stimulation”. In: *Journal of Luminescence* 188 (2017), pp. 371–377.

[79] J. M Kalita and M. L Chithambo. “Phototransferred thermoluminescence and thermally-assisted optically stimulated luminescence dosimetry using $\alpha - Al_2O_3$: C, Mg annealed at 1200 C”. In: *Journal of Luminescence* 205 (2019), pp. 1–6.

[80] S. W. S McKeever, R Minniti, and S Sholom. “Phototransferred thermoluminescence (PTTL) dosimetry using Gorilla® glass from mobile phones”. In: *Radiation Measurements* 106 (2017), pp. 423–430.

[81] A. J. J Santos, J. F de Lima, and M. E. G Valerio. “Phototransferred thermoluminescence of quartz”. In: *Radiation measurements* 33.4 (2001), pp. 427–430.

[82] Alan D. Franklin. “On the interaction between the rapidly and slowly bleaching peaks in the TL glow curves of quartz”. In: *Journal of Luminescence* 75.1 (1997), pp. 71–76.

[83] ML Chithambo and RR Dawam. “Phototransferred thermoluminescence of annealed synthetic quartz: Analysis of illumination-time profiles, kinetics and competition effects”. In: *Radiation Measurements* 131 (2020), p. 106236.

[84] E. F. M Kombe-Atang and M. L Chithambo. “Phototransferred thermoluminescence and phosphorescence related to phototransfer in annealed synthetic quartz.” In: SAIP, 2016, pp. 49–54.

[85] G. A. T Duller. “A new method for the analysis of infrared stimulated luminescence data from potassium feldspars”. In: *Radiation Measurements* 23.2-3 (1994), pp. 281–285.

[86] Sheng-hua Li, Man-Yin W Tso, and Nelson W. L Wong. “Parameters of OSL traps determined with various linear heating rates”. In: *Radiation Measurements* 27.1 (1997), pp. 43–47.

[87] M. Bertucci, I. Veronese, and M. C. Cantone. “Photo-transferred thermoluminescence from deep traps in quartz”. In: *Radiation Measurements* 46.6 (2011), pp. 588–590.

[88] Donald W Marquardt. “An algorithm for least-squares estimation of nonlinear parameters”. In: *Journal of the society for Industrial and Applied Mathematics* 11.2 (1963), pp. 431–441.

[89] C. K Kuhns, N Agersnap Larsen, and S. W. S McKeever. “Characteristics of LM-OSL from several different types of quartz”. In: *Radiation Measurements* 32.5-6 (2000), pp. 413–418.

APPENDIX A

Part of the work presented in this thesis was published in some international journals. Attached below are the published papers.

Radiation Measurements 120 (2018) 47–52

Contents lists available at ScienceDirect

Radiation Measurements

journal homepage: www.elsevier.com/locate/radmeas

Thermoluminescence of annealed synthetic quartz: The influence of annealing on kinetic parameters and thermal quenching

R.R. Dawam, M.L. Chithambo*

Department of Physics and Electronics, Rhodes University, P.O.Box 94, Grahamstown, 6140, South Africa

ARTICLE INFO

Keywords:
Synthetic quartz
Thermal quenching
Kinetic parameters
Phosphorescence

ABSTRACT

The thermoluminescence of synthetic quartz annealed at various temperatures up to 900 °C is reported. Glow curves measured at 1 $^{o}Cs^{-1}$ following beta irradiation to 40 Gy from a sample annealed at 500 °C and from an unannealed one consist of a prominent peak at 70 °C and secondary peaks at 110, 180 and 310 °C. In comparison, the glow peak from the sample annealed at 900 °C consists of three peaks but with the main peak at 86 °C and other lower intensity peaks at 170 and 310 °C. Kinetic analysis was carried out on the main peak only in each case. The order of kinetics of this peak was determined to be first order using various methods. The activation energy was evaluated as an average of 0.90 ± 0.02 eV for the unannealed sample and the one annealed at 500 °C. However, when the synthetic quartz is annealed at 900 °C, the activation energy decreases to 0.65 ± 0.02 eV. The main point of interest however concerns thermal quenching. It was noted that for the sample annealed at 500 °C as well as the unannealed one, the maximum intensity of the main peak decreases with heating rate. This phenomenon is associated with thermal quenching. When the same experiment is carried out using quartz annealed at 900 °C and irradiated to the same dose, namely 40 Gy, the intensity increases with heating rate. This would imply that this sample is not affected by thermal quenching. Using the notion that the radiative and non-radiative recombination routes are competitive, we repeated the experiment using a low dose of 3 Gy. In this case, the intensity decreased with heating rate showing that the process can be tuned. The activation energy for thermal quenching for the samples annealed at 900 °C, 500 °C and unnannealed one was found as 0.65 ± 0.02 eV, 0.82 ± 0.02 eV and 0.95 ± 0.06 eV. Evidently, annealing affects recombination processes in synthetic quartz.

1. Introduction

Natural and synthetic quartz have been extensively studied because of their importance in dating and retrospective dosimetry. Natural and synthetic quartz contain various point-defects that are involved in the luminescence process. In particular, synthetic quartz is prepared to have fewer defects than natural quartz and this affects its optical characteristics. Annealing affects various properties of quartz including its sensitivity and lifetime (Chithambo et al., 2011; Galloway, 2002) as well as its emission bands (Chithambo and Niyonzima, 2017). Annealing sometimes causes a decline in the sensitivity of TL in some materials including synthetic quartz (Yang and McKeever, 1990).

The synthetic quartz used for this report is the same one used in previous studies (Chithambo, 2004; Chithambo et al., 2011; Chithambo and Niyonzima, 2017). Luminescence lifetimes in synthetic quartz determined using time-resolved spectra increase with annealing temperature. This change is interpreted as evidence of increase in dominance of particular recombination centres from one associated with a lower lifetime. Chithambo and Niyonzima (2017) using radioluminescence identified seven emission bands at 2.04, 2.54, 2.77, 3.04, 3.75 and 3.91 eV and showed that the intensity of the emission bands changes with annealing temperature. Our interest now is to examine whether TL features of the sample including non-radiative transitions are affected by annealing and if they are to attempt to offer some explanation.

The aim of this work is to investigate the effect of annealing on kinetic parameters and thermal quenching in synthetic quartz. The study focusses on quartz annealed at 900 °C but complementary measurements made on a sample annealed at 500 °C and an unnannealed one are also reported.

2. Experimental details

Commercially available synthetic quartz (Sawyer Research Products, Ohio,USA) ground into coarse grain was used. Prior to use, samples were annealed at 900 °C for 10 min. For comparison,

* Corresponding author.
E-mail address: m.chithambo@ru.ac.za (M.L. Chithambo).

https://doi.org/10.1016/j.radmeas.2018.06.004
Received 2 December 2017; Received in revised form 9 May 2018; Accepted 2 June 2018
Available online 04 June 2018

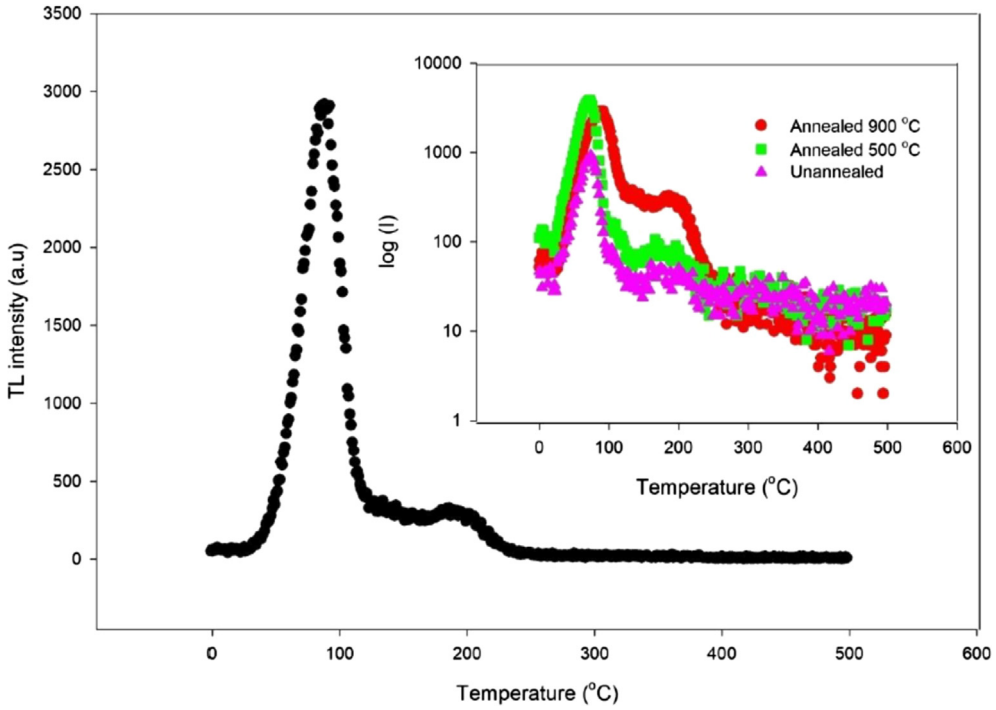

Fig. 1. A glow curve measured at 1 °Cs^{-1} from a sample annealed at 900 °C. The inset shows semi-logarithmic plots comparing this result with ones measured from the unannealed sample and the sample annealed at 500 °C.

measurements were also made on unannealed samples and synthetic quartz annealed at 500 °C. Also for 10 min. TL measurements were made using a RISØ TL/OSL DA-20 Luminescence Reader. The luminescence was detected by a photomultiplier tube (EMI 9635QA) through a 7 mm Hoya U-340 filter (transmission band 250–390 nm FWHM). Samples were irradiated using a ^{90}Sr/^{90}Y beta source at a dose rate of 0.10 Gy s^{-1}.

3. Results and discussion

3.1. Glow curve characteristics

Fig. 1 shows a glow curve of synthetic quartz annealed at 900 °C recorded at 1°Cs^{-1} after irradiation to 40 Gy. There is a single prominent peak at 86 °C. The inset shows a semi-logarithmic plot of the same glow curve as well as of ones measured from the unannealed quartz and the sample annealed at 500 °C. All three cases show one high intensity peak although the presence of other weaker-intensity peaks can be deduced. This report focuses only on the kinetic analysis of the main peak. The aim of the work is to study the influence of annealing on kinetic parameters and in particular to study the effect of annealing on non-radiative transitions.

3.2. Assessment of order of kinetics

3.2.1. Assessment using the dependence of T_m on dose

The order of kinetics of the main peak was first assessed using the dependence of its position T_m on irradiation dose from 10 to 200 Gy. The peak position was found to be independent of dose at an average of 84.5 ± 1.3 °C for the sample annealed at 900 °C and at 70.5 ± 0.8 °C for the unannealed sample and the sample annealed at 500 °C. This shows that the peak is subject to first order kinetics in each case.

3.2.2. Assessment using the $T_m - T_{stop}$ method

The partial heating method, $T_m - T_{stop}$ (Mckeever, 1985), was also used to study the order of kinetics by monitoring how the peak position was affected by partially heating the sample to a temperature T_{stop}. In measurements where T_{stop} was changed from 40 to 60 °C at 2 °C intervals, the peak position was also found to be unaffected by change in T_{stop} being at an average of 70.8 ± 0.2 °C for the unannealed sample and the sample annealed at 500 °C and at 85.4 ± 1.4 °C for the sample annealed at 900 °C. This result confirms that the main peak in each case follows first order kinetics and that it is a genuinely single peak without any overlapping components.

3.3. Kinetic analysis

The kinetic analysis of the main glow peak was carried out using the initial rise, peak shape and variable heating rate methods (Mckeever, 1985), isothermal analysis (Chithambo, 2014), whole glow peak method (Pagonis et al., 2006) and curve fitting (Kitis et al., 1998). For relevant theory, the reader is referred to the cited works.

3.3.1. Initial rise method

The initial rise method was used on data within the range 5–10% of the peak maximum (between 20 and 36 °C). The activation energy for the sample annealed at 900 °C was determined as 0.77 ± 0.03 eV. The values for the unannealed sample and the one annealed at 500 °C were found as 0.91 ± 0.01 eV and 0.83 ± 0.02 eV respectively. A preliminary conclusion is that the activation energy decreases with annealing temperature.

3.3.2. Whole glow curve method

The analyses were also done using the whole glow peak method where the area n under a glow peak can be expressed as

$$ln\left(\frac{I}{n^b}\right) = ln\left(\frac{s'}{\beta}\right) - \left(\frac{E}{kT}\right) \quad (1)$$

where b is the order of kinetics, s' is the effective frequency factor in units of (m$^{3(b-1)}$s^{-1}), β is the heating rate, I is the TL intensity and E is the activation energy. A plot of $\ln I/n^b$ against $1/kT$ should be linear for specific values of b. Its slope is equal to the activation energy whereas s' can be found from the intercept on the y axis. The results for the sample

annealed at 900 °C were $b = 1.1$, $E = 0.67 \pm 0.02$ eV and $s' = (5.2 \pm 2.3) \times 10^{11}$ s^{-1}. The same method applied for the unannealed sample and the sample annealed 500 °C gave $b = 1.2$, $E = 0.90 \pm 0.02$ eV, $s' = (3.2 \pm 1.3) \times 10^{10}$ s^{-1} and $b = 1.1$, $E = 0.91 \pm 0.01$ eV and $s' = (2.3 \pm 1.0) \times 10^{9}$ s^{-1} respectively.

3.3.3. Peak shape method

In the peak-shape method, the activation energy, E_α was estimated using the equation

$$E_\alpha = C_\alpha\left(\frac{kT_m^2}{\alpha}\right) - b_\alpha(2kT_m) \tag{2}$$

where T_m is the peak position, α stands for any of $\tau = T_m - T_1$ or $\delta = T_2 - T_m$ and $\omega = T_2 - T_1$ where T_1 and T_2 are the lower and higher temperature at half height respectively (Mckeever, 1985). The values of C_α and b_α are given elsewhere (Mckeever, 1985). The values of the geometrical factor μ_g for the unannealed sample and the samples annealed at 500 and 900 °C are 0.40 ± 0.03, 0.42 ± 0.03 and 0.42 ± 0.02 respectively indicating that the main peak follows first order kinetics. The values of the activation energy were evaluated as $E_\tau = 0.92 \pm 0.03$ eV, $E_\delta = 0.86 \pm 0.04$ eV and $E_\omega = 0.90 \pm 0.05$ eV respectively for unannealed sample. Similar calculations gave $E_\tau = 0.92 \pm 0.06$ eV, $E_\delta = 0.89 \pm 0.04$ eV and $E_\omega = 0.91 \pm 0.04$ eV respectively for the sample annealed at 500 °C. For the one annealed at 900 °C; $E_\tau = 0.68 \pm 0.04$ eV, $E_\delta = 0.67 \pm 0.08$ eV, and $E_\omega = 0.68 \pm 0.06$ eV. In these results as well, the activation energy decreases with annealing temperature.

3.3.4. Analysis using the variable heating rate method

The variable heating rate method was applied using heating rates from 0.2 to 5.0 °Cs^{-1}. These rates are within the upper limit of 5 °C/s identified by Betts and Townsend (1993) and Betts et al. (1993) as advisable to minimize effects of temperature gradients between the ends of a sample. The activation energy for the sample annealed at 900 °C was found as 0.52 ± 0.02 eV. In comparison, for the unnannealed sample and the sample annealed at 500 °C, the values were 0.80 ± 0.03 eV and 0.82 ± 0.03 eV. The value of E still seems to decrease with annealing to 900 °C. This method appears to underestimate the values of E in comparison with other techniques used. Pagonis et al. (2013) have also shown that the heating rate method can systematically underestimate the value of the activation energy.

3.3.5. Curve fitting

The main peak was also analysed by curve fitting using the equation

$$I(T) = I_m b^{(b/b-1)} exp\left(\frac{E}{kT}\frac{T - T_m}{T_m}\right) \left[(b-1)(1-\Delta)\frac{T^2}{T_m}\exp\left(\frac{E}{kT}\frac{T-T_m}{T_m}\right) + Z_m\right]^{-b/b-1} \tag{3}$$

where $\Delta = 2kT/E$, $\Delta_m = 2kT_m$, $Z_m = 1 + (b-1)\Delta_m$, I_m is the intensity at peak maximum and all others symbols are as defined earlier (Kitis et al., 1998). The goodness of fit was tested by the 'figure of merit' FOM given by

$$FOM = \sum \frac{|y_{expt} - y_{fit}|}{y_{fit}} \tag{4}$$

where y_{fit} denote values from the fitting function and y_{exp} represent the experimental data. Using this method, the values of the activation energy and its margin of error were determined as 1.03 ± 0.03 eV, 0.96 ± 0.02 eV and 0.80 ± 0.04 eV for the unannealed quartz, and the one annealed at 500 and 900 °C respectively. The associated order of kinetics was found as $b = 1.12 \pm 0.05$, 1.06 ± 0.03 and 1.14 ± 0.06 respectively that is, first order kinetics. Using the parameters obtained above, the frequency factor was evaluated from the expression

$$s = \frac{\beta E}{kT_m^2(1 + 2kT_m(b-1)/E}\, exp\left(\frac{E}{kT_m}\right) \tag{5}$$

as 1.1×10^{13}, 1.7×10^{12} and 2.7×10^{12} s^{-1}. These results are also consistent with those from the other methods.

3.4. Analysis using phosphorescence-based methods

3.4.1. Analysis of phosphorescence using first-order kinetics

Phosphorescence is the decay of thermally stimulated luminescence as a function of time at a constant temperature. In order to further check the order of kinetics of the main peak, phosphorescence was measured between 40 and 60 °C from a sample irradiated to 40 Gy. First order kinetics for phosphorescence can be expressed as $I(t) = I_0\exp(-pt)$ where I_o is the initial intensity, t is time and p is the probability of thermal stimulation (Mckeever, 1985) given as $p = sexp(-E/kT)$. Having verified that first order kinetics applies, the activation energy, equal to the slope in a plot of $\ln(p)$ against $1/kT$, was found as 0.63 ± 0.04 eV. This can be compared with 0.96 ± 0.03 eV and 1.05 ± 0.05 eV determined using the same method for the sample annealed at 500 °C and for the unannealed sample respectively. The activation energy is similar to those from curve fitting. Again, we notice a decrease in the activation energy with annealing temperature.

3.4.2. Analysis using the area under an isothermal decay-curve

The phosphorescence was further analysed using the temperature-dependence of the area under an isothermal decay-curve (Chithambo, 2014). The partial area Φ under a small segment of a phosphorescence decay curve can be expressed as $\Phi = \kappa\exp(-E/kT)$ where κ is a constant and all other terms are as previously defined. A plot of $\ln\Phi$ against $1/kT$ should be linear with slope equal to the activation energy. Fig. 2 shows such a graph for the sample annealed at 900 °C. Using this method, the activation energy was found as 0.85 ± 0.02 eV, 0.79 ± 0.12 eV and 0.62 ± 0.03 eV respectively for the unannealed sample and samples annealed at 500 and 900 °C. It is also evident here that the activation energy seems to decrease with annealing to 900 °C.

3.5. Influence of annealing on thermal quenching

3.5.1. Analysis for thermal quenching using the effect of heating rate on the thermoluminescence intensity

Fig. 3 shows the influence of heating rate on the intensity of the

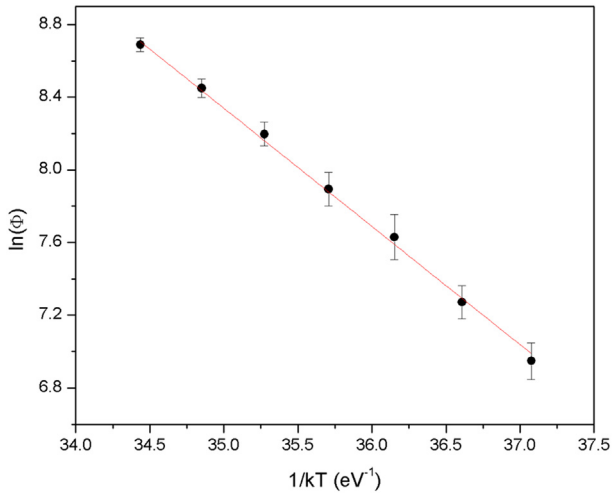

Fig. 2. The plot of $\ln\phi$ against $1/kT$ for phosphorescence measured between 40 and 60 °C from a sample annealed at 900 °C.

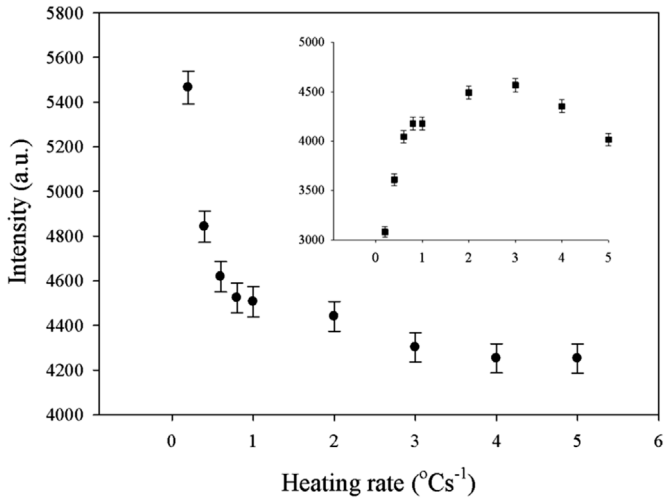

Fig. 3. The dependence of peak intensity on heating rate for the sample annealed at 500 °C (a) and for the sample annealed at 900 °C (inset).

main peak (noted as peak area) for the sample annealed at 500 °C. This and all data were corrected for heating rate. The intensity decreases with heating rate. The change was similar for the unannealed sample. For first-order peaks, this behaviour is ascribed to thermal quenching. However, for the same dose (40 Gy), the intensity of the sample annealed at 900 °C (Fig. 3, inset), behaves differently with heating rate. This was the motivation for further investigations which will be presented in the next section.

If A_q is the experimental 'quenched' TL intensity and A_{uq} represent 'unquenched' TL intensity at the slowest heating rate, the two are related as $A_q/A_{uq} = 1/(1 + Cexp(-\Delta E/kT))$ where ΔE is the activation energy of thermal quenching, C is a constant and all other terms are as previously defined (Pagonis et al., 2006). A plot of $\ln[(A_q/A_{uq}) - 1]$ against $1/kT_m$ should be a straight line with slope ΔE. Fig. 4 shows a plot (solid symbols) for the sample annealed at 500 °C from which ΔE and C were found as 0.82 ± 0.02 eV and 2.2×10^{13} respectively. The results for the unannealed sample were 0.95 ± 0.06 eV and 3.2×10^{14}.

3.5.2. Investigation of thermal quenching in synthetic quartz annealed at 900 °C

The increase of TL intensity with heating rate in the sample annealed at 900 °C may imply absence of thermal quenching. However, such a deduction needs to be tested. The emission of luminescence involves competing radiative and non-radiative routes summarised as

$$\frac{1}{\tau} = \frac{1}{\tau_{rad}} + \frac{1}{\tau_{th}} \exp\left(\frac{-\Delta E}{kT}\right) \quad (6)$$

where $1/\tau_{rad}$ is the probability of radiative emission, $1/\tau_{th}$ is the probability of thermal excitation and ΔE is the activation energy of thermal quenching (Agulló-López et al., 1988). The result of the competing pathways on TL intensity can be distinguished as was illustrated in a study on Al_2O_3:C by Chithambo et al. (2017). The hypothesis is that if the number of electrons undergoing radiative transitions is made very low, the luminescence intensity cannot be high enough to mask any loss due to non-radiative transitions. In that way, any effect due to non-radiative transition, that is, thermal quenching will be manifest and can be studied.

For this test, the dependence of TL intensity on heating rate was measured again but this time with the dose significantly reduced from 40 Gy to 3 Gy. Fig. 4 (inset (a), open squares) shows the result. Unlike before (Fig. 3, inset), the TL intensity decreases with heating rate and the thermal quenching could be quantified. The open circles (inset b) in Fig. 4 shows a plot of $\ln[(A_q/A_{uq}) - 1]$ against $1/kT_m$ from which $\Delta E = 0.65 \pm 0.02$ eV and $C = 2.4 \times 10^{10}$. It is evident that when a high dose is used, the effect of thermal quenching in the sample annealed at 900 °C does not appear. The important point here is that the increase of TL intensity with heating rate should not be used to conclude that a sample is not affected by thermal quenching.

3.5.3. Analysis of thermal quenching using phosphorescence

The activation energy for thermal quenching in the quartz annealed at 900 °C was again evaluated using an alternative method based on the use of phosphorescence (Chithambo, 2014). If Φ_q is the fractional area under a phosphorescence decay curve at a particular high temperature where thermal quenching is most effective and Φ_{uq} is the fractional area under a phosphorescence decay curve measured at lower temperatures where thermal quenching is less of an effect, these two parameters are related as $\Phi_q/\Phi_{uq} \approx 1/(1 + Cexp(-\Delta E/kT))$ where all symbols are as previously defined (Chithambo, 2014). The plot of $\ln(\Phi_q/\Phi_{uq})$ against 1/kT should be linear with a slope equal to the activation energy of thermal quenching. The ratio Φ_q/Φ_{uq} was calculated for measurements between 40 and 60 °C made at 2 °C interval. Fig. 5 shows a graph of $\ln(\Phi_q/\Phi_{uq})$ against $1/kT$ for the quartz annealed at 900 °C. It should be noted that this method does not depend on heating rate. The values of the activation energy of thermal quenching evaluated using this method

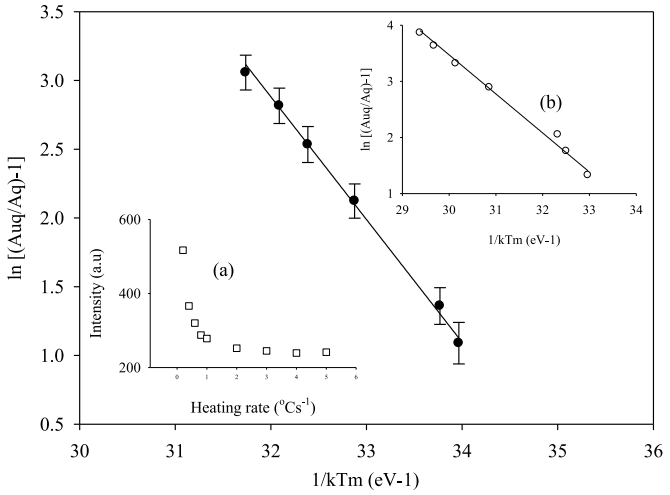

Fig. 4. A graph of $\ln[(A_q/A_{uq}) - 1]$against $1/kT_m$for sample annealed at 500 °C (solid symbols) and in the insets, the dependence of TL intensity on heating rate for the sample annealed at 900 °C (inset a) and the corresponding plot of $\ln[(A_q/A_{uq}) - 1]$against $1/kT_m$ (inset b).

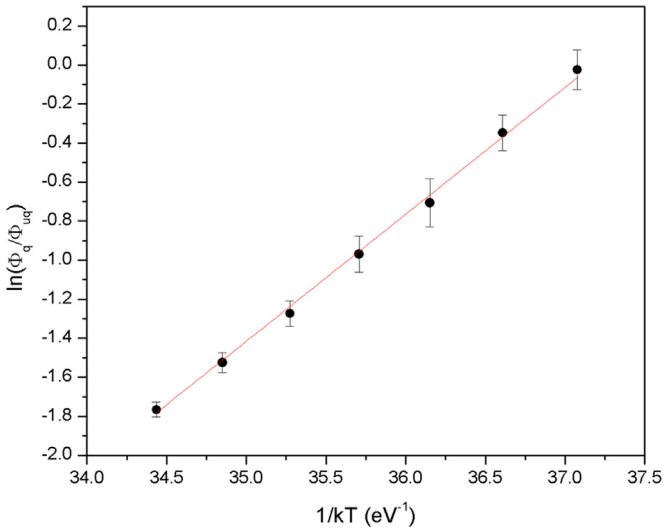

Fig. 5. A plot of $\ln(\Phi_q/\Phi_{uq})$against $1/kT$ for the sample annealed at 900 °C.

Table 1
Kinetic parameters found using various methods. The indices a, b, c corresponding to the peak shape method refer to Eτ, E_δ and Eω respectively, T_A stands for the annealing temperature which for the unannealed sample is shown as 20 °C.

sT_A (°C)	Method	E (eV)	b	s (s^{-1})	ΔE (eV)	Reference
20	Tm-dose		1			Sect. 3.2.1
	Tm-Tstop		1			Sect. 3.2.2
	Initial rise	0.91 ± 0.01				Sect. 3.3.1
	Whole peak	0.90 ± 0.02	1.2	3.2×10^{10}		Sect. 3.3.2
	Peak-shape	0.92 ± 0.03a				Sect. 3.3.3
		0.86 ± 0.04b				Sect. 3.3.3
		0.90 ± 0.05c				Sect. 3.3.3
	Var.heat rate	0.80 ± 0.03			0.95 ± 0.06	Sect. 3.3.4, 3.5.1
	Curve fitting	1.03 ± 0.03	1.12 ± 0.05	1.1×10^{13}		Sect. 3.3.5
	PS, firdt-order	1.05 ± 0.05				Sect. 3.3.5
	PS, Area	0.85 ± 0.02			0.82 ± 0.03	Sect. 3.4.1
500	Tm-dose		1			Sect. 3.2.1
	Tm-Tstop		1			Sect. 3.2.2
	Initial rise	0.83 ± 0.02				Sect. 3.3.1
	Whole peak	0.91 ± 0.01	1.1	2.3×10^{9}		Sect. 3.3.2
	Peak shape	0.92 ± 0.06a	1†			Sect. 3.3.3
		0.89 ± 0.06a	1†			Sect. 3.3.3
		0.91 ± 0.04c	1†			Sect. 3.3.3
	Var.heat rate	0.82 ± 0.03			0.82 ± 0.02	Sect. 3.3.4, Fig. 4
	Curve fitting	0.96 ± 0.02	1.06 ± 0.03	1.7×10^{12}		Sect. 3.3.5
	PS, firdt-order	0.96 ± 0.03				Sect. 3.4.1
	PS, Area	0.79 ± 0.12			0.78 ± 0.02	Sect. 3.4.2, 3.5.3
900	Tm-dose		1			Sect. 3.2.1
	Tm-Tstop		1			Sect. 3.2.2
	Initial rise	0.77 ± 0.03				Fig. 2
	Whole peak	0.67 ± 0.02	1.1	5.2×10^{11}		Fig. 2, inset
	Peak shape	0.68 ± 0.04a	1†			Sect. 3.3.3
		0.67 ± 0.08b	1†			Sect. 3.3.3
		0.68 ± 0.06a	1†			Sect. 3.3.3
	Var. heat rate	0.52 ± 0.02				Sect. 3.3.4
					0.65 ± 0.02	Fig. 4, inset
	Curve fitting	0.80 ± 0.04	1.14 ± 0.06	2.7×10^{12}		Sect. 3.3.5
	PS, first-order	0.63 ± 0.04				Sect. 3.4.2
	PS, Area	0.62 ± 0.03			0.65 ± 0.03	Sect. 3.4.2, Fig. 5

were 0.82 ± 0.03 eV, 0.78 ± 0.02 eV and 0.65 ± 0.03 eV for the unannealed sample, and samples annealed at 500 and 900 °C respectively. The value of ΔE (0.65 ± 0.03eV) using the phosphorescence method is in excellent agreement with that from heating rate method (0.65 ± 0.02 eV). In general, the value of ΔE decreases with annealing temperature.

4. The effect of annealing on kinetic parameters and thermal quenching

Kinetic parameters evaluated using various methods are summarised in Table 1. These can be compared with, say, E = 0.82 ± 0.04 eV for a peak at 110 °C in synthetic quartz annealed at 900 °C (Kitis et al., 2002) determined using the variable heating rate method using heating rates 0.5–4 °C. A direct comparison of values from different samples is not instructive but evidently the order of magnitude of the activation energy is similar. For the unannealed sample, the values of ΔE compare well with ΔE = 0.80 eV (Chithambo, 2004) for the same quartz annealed at 600 °C.

Our results show that values of *E* and ΔE decrease with annealing temperature. It is necessary to account for this. Regarding thermal quenching, previous studies on this quartz showed that lifetimes determined from time-resolved spectra change with annealing temperature (Chithambo et al., 2011) as do emission bands (Chithambo and Niyonzima, 2017). In particular, the sample shows at least seven emission bands between 2.04 and 3.91 eV whose amplitude depends on annealing up to 1000 °C. The change in lifetime with annealing is ascribed to change in the dominant recombination centre involved in the luminescence (Chithambo et al., 2011; Galloway, 2002). Since the activation energy for thermal quenching depends on the emission wavelength (Chithambo, 2007), the change of ΔE can be ascribed to change in dominant recombination centre with annealing.

The effect of annealing on electron traps is of interest. Computational simulations which accounted for the increase in TL sensitivity with annealing e.g. Chen and Fogel (1993) implicitly assumed that kinetic parameters are unaffected by annealing. On the other hand, Toktamiş and Yazici (2012), who studied the effect of annealing on trap depth in synthetic and natural quartz, reported that annealing affected the trap depth of all glow peaks and that the trap depth increased after annealing. These examples show that the activation energy in quartz can be affected by annealing.

The cause of change in the activation energy of an electron trap with annealing is possibly due to a complex combination of structural and electronic modification of associated point-defects due to annealing. Previous studies using positron annihilation on the sample studied here showed that annealing did not produce new defects in the sample (Chithambo et al., 2011). It is likely then that the change in activation energy is due to electronic modification of the electron trap(s). For example, oxygen or silicon vacancies in quartz can catalyse the formation of other unstable defects which can act as electron traps (e.g. see Table 2 in Preusser et al., 2009). Examples of possible electron traps in quartz are extensive and include the family of E-centres and others stabilised by presence of, for example, H. Removal or displacement of a stabilising species can affect the electron trap and potential it is associated with as discussed elsewhere e.g (Preusser et al., 2009 and references therein). If annealing causes a change in the electronic configuration of an electron trap or its site, then a change in its potential with respect to the conduction band can be reflected as a change in the activation energy as observed.

5. Conclusions

The thermoluminescence of synthetic quartz annealed at 900 °C has been reported. Complementary measurements were made on quartz annealed at 500 °C as well as from an unnannealed sample. Glow curves recorded at 1 Cs^{-1} following beta irradiation to 40 Gy from all these samples show three peaks with a prominent peak at just below 100 °C. Kinetic analysis was carried out on this main peak only in each case. Using various methods, the order of kinetics of this peak was determined to be first order. It has been observed that the activation energy decreases from an average of 0.90 ± 0.02 eV to 0.65 ± 0.02 eV when the annealing temperature is changed from room temperature to 900 °C. The intensity of the main peak corresponding to 40 Gy decreases with heating rate in a manner observed for thermal quenching for the sample annealed at 500 °C as well as the unannealed one. In contrast, the intensity increases with heating rate for same dose in the sample annealed at 900 °C, a result that may suggest absence of thermal quenching in this case. When the experiment on the sample annealed at 900 °C is instead made using a low dose of 3 Gy, the intensity decreases with heating rate. The result is explained with reference to change in competition between the radiative and non-radiative transitions. The activation energy for thermal quenching for samples annealed at 900 °C, 500 °C and the unnannealed one were evaluated as 0.65 ± 0.02 eV, 0.82 ± 0.02 eV and 0.95 ± 0.06 eV showing that annealing also affects recombination centres.

Acknowledgements

We gratefully acknowledge financial support from the National Research Foundation and Rhodes University.

Appendix A. Supplementary data

Supplementary data related to this article can be found at http://dx.doi.org/10.1016/j.radmeas.2018.06.004.

References

Agulló-López, F., Catlow, C.R.A., Townsend, P.D., 1988. Point defects in Materials. Academic Press.
Betts, D.S., Townsend, P.D., 1993. Temperature distribution in thermoluminescence experiments. I: some calculational models. J. Phys. D Appl. Phys. 26, 849–857.
Betts, D.S., Couturier, L., Khayrat, A.H., Luff, B.J., Townsend, P.D., 1993. Temperature distribution in thermoluminescence experiments. I: experimental results. J. Phys. D Appl. Phys. 26, 843–848.
Chen, R., Fogel, G., 1993. Superlinearity in thermoluminescence revisited. Radiat. Protect. Dosim. 47, 23–26.
Chithambo, M.L., 2004. Time-resolved luminescence from annealed synthetic quartz under 525nm pulsed green light stimulation. Radiat. Meas. 38, 553–555.
Chithambo, M.L., 2007. The analysis of time-resolved optically stimulated luminescence. II: Computer Simulations and Experimental Results. J. Phys. D.: Appl. Phys. 40, 1880–1889.
Chithambo, M.L., 2014. A method for kinetic analysis and study of thermal quenching in thermoluminescence based on use of the area under an isothermal decay-curve. J. Lumin. 151, 235–243.
Chithambo, M.L., Niyonzima, P., 2017. Radioluminescence of annealed synthetic quartz. Radiat. Meas. 106, 35–39.
Chithambo, M.L., Sane, P., Tuomisto, F., 2011. Positron and luminescence lifetimes in annealed synthetic quartz. Radiat. Meas. 46, 310–318.
Chithambo, M.L., Seneza, C., Kalita, J.M., 2017. Phototransferred thermoluminescence of Al_2O3:C: experimental results and empirical models. Radiat. Meas. 105, 7–16.
Galloway, R.B., 2002. Luminescence lifetimes in quartz: dependence on annealing temperature prior to beta irradiation. Radiat. Meas. 35, 67–77.
Kitis, G., Gomez-Ros, J., Tuyn, J., 1998. Thermoluminescence glow-curve de-convolution functions for first, second and general orders of kinetics. J. Phys. D Appl. Phys. 31, 2636.
Kitis, G., Pagonis, V., Cartey, H., Tatsis, E., 2002. Detailed kinetic study of the thermoluminescence glow curve of synthetic quartz. Radiat. Protect. Dosim. 100, 225–228.
Mckeever, S.W.S., 1985. Thermoluminescence of Solid. Cambridge. .
Pagonis, V., Kitis, G., Furetta, C., 2006. Numerical and Practical Exercises in Thermoluminescence. Springer Science.
Pagonis, V., Blohm, L., Brengle, M., Mayonado, G., Woglam, P., 2013. Anomalous heating rate effect in Thermoluminescence intensity using a simplified semi-localized transition (SLT) model. Radiat. Meas. 51, 40–47.
Preusser, F., Chithambo, M.L., Götte, T., Martini, M., Ramseyer, K., Sendezera, E.J., Susino, G.J., Wintle, A.G., 2009. Quartz as a natural luminescence dosimeter. Earth Sci. Rev. 97, 196–226.
Toktamiş, H., Yazici, A.N., 2012. Effects of annealing on thermoluminescence peak positions and trap depths of synthetic and natural quartz by means of the various heating rate method. Chin. Phys. Lett. 29 087802.
Yang, X., McKeever, S., 1990. Point defects and the pre-dose effect in quartz. Radiat. Protect. Dosim. 33, 27–30.

Radiation Measurements 131 (2020) 106236

Contents lists available at ScienceDirect

Radiation Measurements

journal homepage: http://www.elsevier.com/locate/radmeas

Phototransferred thermoluminescence of annealed synthetic quartz: Analysis of illumination-time profiles, kinetics and competition effects

M.L. Chithambo *, R.R. Dawam

Department of Physics and Electronics, Rhodes University, P.O. Box 94, Grahamstown, 6140, South Africa

ARTICLE INFO

Keywords:
Annealing
Phototransferred thermoluminescence
Thermal quenching
Competition effects
Synthetic quartz

ABSTRACT

Phototransferred thermoluminescence (PTTL) induced from annealed synthetic quartz using 470 nm blue light is reported. The quartz was annealed at 900 °C for 10, 30 and 60 min prior to use. A glow curve of conventional TL measured at 1 °C s^{-1} following irradiation to 200 Gy for the sample annealed for 10 min shows six peaks at 90, 122, 176, 210, 240 and 340 °C. The sample annealed for 30 min has peaks at 80, 110, 136, 196, 240 and 330 °C. Similarly, the sample annealed for 60 min also has six peaks at 80, 120, 134, 188, 235 and 340 °C. For ease of reference, these are labelled I-VI respectively. Peaks observed under PTTL are referred to as A1 onwards. Of the six peaks, only the first three are reproduced under phototransfer for the sample annealed for 60 min. When the duration of annealing is reduced to 10 min, PTTL is induced only at peaks A1 and A3. Interestingly, for the intermediate duration of annealing of 30 min, the only peak that appears under phototransfer is the first one, A1. For quartz annealed for 10 min, the PTTL appears as long as the preheating temperature does not exceed 560 °C. On the other hand, in the quartz annealed for 30 and 60 min, PTTL only appears for preheating to and below 450 °C. This shows that the occupancy of deep electron traps at temperatures beyond 450 or 560 °C is low in the said samples. The activation energy for peaks A1 and A3 was found to be about 0.68 eV. The PTTL peaks were studied for thermal quenching and peaks A1 and A3 were determined to be subject to this effect. The activation energy for thermal quenching was determined as 0.62 ± 0.04 eV in analysis using peak A1. In all cases, the PTTL intensity goes through a peak as a function of illumination time. The experimental dependence of PTTL intensity on illumination time is modelled using sets of coupled linear differential equations based on systems of donors and acceptors whose number is determined by preheating temperature. Competition effects involved in the PTTL have been discussed.

1. Introduction

Thermoluminescence is a widely discussed technique e.g. (Mckeever, 1985) whose aim is to thermally stimulate electrons from certain point defects in an irradiated material such that their passage to recombination centres through the conduction band produces light. The various electron traps in question are populated by ionization and their existence is evident as peaks in a temperature-resolved plot of intensity against temperature, a glow curve. If, after irradiation, the material is partially heated to empty only some of the filled electron traps, then no TL is observed when the material is reheated to the position of the removed peaks unless the electron traps are re-filled. When light is used to transpose electrons from filled electron traps to the empty ones, what results is phototransferred thermoluminescence (PTTL). This can be achieved in two ways. If the measurement is made at temperatures above ambient, then lower temperature peaks corresponding to lower activation energies are emptied first. As phrased before (Chithambo et al., 2017), the PTTL is induced by transferring electrons from deeper electron traps (or donor traps) to the empty shallower ones (acceptors). On the other hand, if the material is cooled to cryogenic temperatures after irradiation at room temperature, electrons can be phototransferred into electron traps that would ordinarily be unstable at room temperature.

PTTL has been used for various aims such study of TL mechanisms e.g (Chithambo et al., 2017), understanding annealing induced changes in the concentration of deep electron traps (Kalita and Chithambo, 2017, 2019) and for dosimetry e.g. (Bailiff et al., 1977). The enduring appeal of PTTL for dosimetry is exemplified in recent reports (Bossin et al., 2018; McKeever et al., 2017). Whereas the basis for dosimetry for irradiated samples is the link between irradiation dose and intensity, that under

* Corresponding author.
E-mail address: m.chithambo@ru.ac.za (M.L. Chithambo).

https://doi.org/10.1016/j.radmeas.2019.106236
Received 5 April 2019; Received in revised form 27 November 2019; Accepted 26 December 2019
Available online 30 December 2019
1350-4487/

PTTL is the dose due to optical transfer from a donor.

Mechanisms applicable to PTTL go back a long way e.g. (McKeever, 1991), have been explored (Morris and McKeever, 1994) and reviewed (McKeever and Chen, 1997). Alexander et al. (1997) discussed a mathematical method for PTTL for a simple system of two electron traps and one recombination centre. The concept was further developed to include an additional non-radiative recombination centre by Alexander and McKeever (1998). Their model assumes that there is retrapping into the electron traps. Inclusion of retrapping in the model makes the rate equations describing electron transport to be non-linear. Such equations do not have any analytical solution. To obtain an approximation to one, simplifying assumptions are made such as that retrapping is negligible. Alternatively, numerical simulations are used to arrive at a set of parameters that can generate plots of, say, intensity against duration of optical stimulation that resemble experimental results. If retrapping is omitted altogether, the equations become linear as appear in e.g. Wintle and Murray (1997).

Chithambo et al. (2017) formulated a mathematical method for analysing the PTTL of a system of any number of acceptors and donors. The method, also used here, describes charge transport in terms of coupled linear first order differential equations. The equations describe the transfer, by light, of a portion of electrons from a donor to an acceptor through the conduction band. The systems of coupled equations devised this way have analytical solutions which can be applied directly to experimental data.

The aim of this work is to study PTTL from synthetic quartz annealed at 900 °C. Heating quartz to elevated temperatures affects its phase (Gribble, 1988), its thermoluminescence and optically stimulated luminescence sensitivity (Bøtter-Jensen et al., 2003; Galloway, 2002), luminescence lifetimes (Galloway, 2002; Chithambo et al., 2011; Chithambo, 2018), and radioluminescence emission bands (Chithambo and Niyonzima, 2017; Pagonis et al., 2014). Indeed for the synthetic quartz of this report, investigations using radioluminescence (Chithambo and Niyonzima, 2017) showed that the amplitude of emission bands increases with annealing and that whichever emission band is dominant depends on annealing temperature. These changes are consistent with those in lifetimes caused by annealing as determined using time-resolved luminescence on the same quartz (Chithambo et al., 2011). Measurements using positron annihilation on the same material showed that no new defects are introduced by the annealing (Chithambo et al., 2011). PTTL for an unannealed version of the sample was reported by Chithambo et al. (2018) where it was seen that PTTL only ensued after removal of certain supposed donor traps. The question we address in this report is the nature of PTTL in annealed synthetic quartz, interpretation and analysis of its time response profiles as well as the influence of competition effects on phototransfer.

2. Experimental details

Samples consisted of commercially available synthetic quartz (Sawyer Research Products, Ohio, USA) ground into coarse grain. This is the same material studied by Chithambo et al. (2011, 2017, 2018). Samples were annealed at 900 °C for 10, 30 and 60 min. Measurements were made on three aliquots of similar mass using a RISØ TL/OSL DA-20 Luminescence Reader. The luminescence was detected by a photomultiplier tube (EMI 9635QA) through a 7 mm Hoya U-340 filter (transmission band 250–390 nm FWHM). Samples were irradiated *in-situ* at room temperature using a $^{90}Sr/^{90}Y$ beta source at a dose rate of 0.10 Gy s^{-1}. Unless otherwise stated, samples were heated at 1 °C s^{-1} after irradiation to 200 Gy. The procedure to measure PTTL was that following irradiation and, preheating to a specific temperature to remove a given peak(s), the sample was exposed to 470 nm blue LEDs (set at a power density of 72 mW cm^{-2} at sample position) for a specific time to transfer electrons from deeper to shallower electron traps. The sample was thereafter reheated to 500 °C to monitor the presence of any PTTL peaks induced at the position of the removed peak(s).

3. Glow curve features

Fig. 1 shows glow curves of synthetic quartz annealed at 900 °C for 10, 30 and 60 min. The high dose was used to facilitate measurement of PTTL. There are three discernible peaks at or near 90, 120 and 180 °C. The inset shows, on a semi-logarithmic scale, the glow curve for the sample annealed for 10 min. This shows that there are in fact more than just three peaks with additional ones apparent near 210, 240 and 340 °C. The presence of the six peaks was confirmed by thermal cleaning, a method for separating peaks described elsewhere (Mckeever, 1985).

4. General features of phototransferred thermoluminescence

PTTL test measurements were made by preheating an irradiated sample in turn to 120, 180, 250, 350 and 500 °C to remove peaks I, I-III, I–V and I-VI in succession. The proximity of peaks II and IV to their adjacent ones restricted the choice of preheating temperatures to remove one peak at a time. After each preheat, and cooling to room temperature, the sample was exposed to 470 nm blue light for a time and reheated to 500 °C to measure the complete glow curve. PTTL was monitored at this stage. Emission corresponding to preheating to 500 °C, that is, from any deep electron traps was studied only for the quartz annealed at 900 °C for 10 min. The signal in the samples annealed for 30 and 60 min was too low for reliable analysis. For reference in the presentations to follow, Table 1 lists the peaks, their positions, preheating temperatures and identity of PTTL peaks recorded.

When the sample annealed for 10 min was preheated to 120 °C to remove peak I, no PTTL was observed. There was also no PTTL following preheating to 180 °C to remove peaks I, II and III. However, after complete removal of peaks I-IV following preheating to 250 °C and indeed after preheating to 350 °C, two PTTL peaks were observed at 90 and 176 °C. We label these as A1 and A3. Further, when all the peaks (I–VI) were removed by preheating to 500 °C, still only two PTTL peaks, A1 and A3, were seen at 100 and 176 °C. Fig. 2 shows examples of PTTL peaks reproduced after preheating to 350 and 500 °C.

In the sample annealed for 30 min, only peak A1 was reproduced at 80 °C after preheating to either 250 or 350 °C. No distinct PTTL peak was observed after preheating to 500 °C. When the sample annealed for 60 min was preheated to 350 °C, PTTL peaks were observed at 80, 134 and 188 °C which we label as A1, A2 and A3. Features of peaks A1 and A3 after preheating to 250 °C are similar and will not be discussed. In summary, three PTTL peaks were reproduced in the sample annealed for

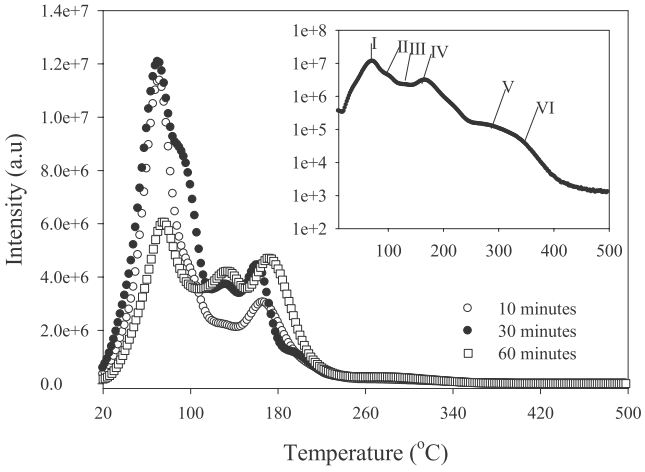

Fig. 1. Glow curves from samples annealed at 900 °C for 10, 30 and 60 min measured at 1 °C/s following beta irradiation to 200 Gy. The inset shows, on a semi-logarithmic scale, the glow curve of the quartz annealed at 900 °C for 10 min to better show the presence of other peaks. Unless otherwise stated, the intensity data here and throughout is in units of Counts/2 °C.

Table 1
Identity of peaks, their positions T_m and preheating temperatures T_{ph} for TL and PTTL corresponding to annealing time t_A (in minutes) as shown.

TL					PTTL						
t_A	10	30	60			10		30		60	
Peak label	Tm (°C)	Tm (°C)	Tm (°C)	Tph (°C)	Peak label						
I	90	80	80								
				120							
II	122	110	120								
III	176	136	134								
				180							
IV	210	196	188								
				250	A1		A3	A1			
V	240	240	235								
				350	A1		A3	A1	A1	A2	A3
VI	340	330	340								
				500	A1		A3				

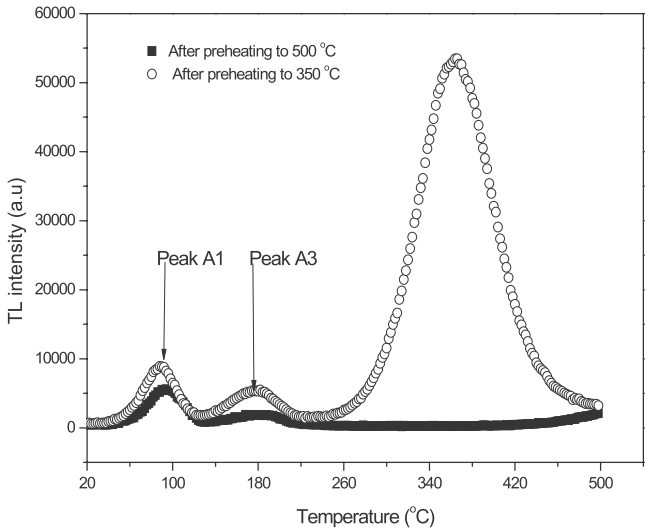

Fig. 2. Glow curves measured after preheating to 350 and 500 °C. The sample was exposed to 470 nm blue light for 20 s.

60 min, two in the sample annealed for 10 min and only one in the sample annealed for 30 min. Although PTTL was observed when the sample annealed for 10 min was preheated to 500 °C, this was not the case when the duration of annealing was increased to 30 or 60 min. The lack of proper PTTL in the latter reflects poor occupancy of any available deep traps or indeed their absence. These options will be examined.

5. Kinetic analysis

The conventional TL of the quartz used here has been studied before by Dawam and Chithambo (2018). PTTL peaks A1 and A3 were analysed for kinetic parameters to determine if they correspond to the conventional TL peaks. The PTTL was analysed using the whole glow peak and curve fitting methods (Pagonis et al., 2006) and phototransferred phosphorescence (Kombe-Atang and Chithambo, 2016).

5.1. Analysis using the whole glow peak method and phototransferred phosphorescence

The activation energy of peaks A1 and A3 were determined as 0.66 ± 0.01 eV and 0.68 ± 0.03 eV respectively using the whole glow peak method. The order of kinetics for the two peaks was found to be 1.2 indicating that the kinetics is approximately first order, within the accuracy of the data. That the order of kinetics for peak A1, the only one studied this way, is first order was verified using phototransferred phosphorescence in measurements between 40 and 60 °C.

5.2. Influence of heating rate on PTTL intensity – evidence of thermal quenching

Fig. 3 shows the influence of heating rate on PTTL intensity of peaks A1 and A3 for samples annealed for 10 and 60 min. Heating rates ranged from 0.2 to 5.0 °C s^{-1}, the latter being the reasonable upper limit of heating rate in TL experiments (Betts and Townsend, 1993; Betts et al., 1993). The intensity decreases with heating rate. This behaviour, for first order kinetics which applies to peaks A1 and A3, implies that the peaks are affected by thermal quenching.

If we assume that the PTTL intensity I_{uq} (in counts $^oC^{-1}$) at lower heating rates are less affected by thermal quenching and if I_q denotes an intensity corresponding to the highest heating rate where the quenching is most effective, then

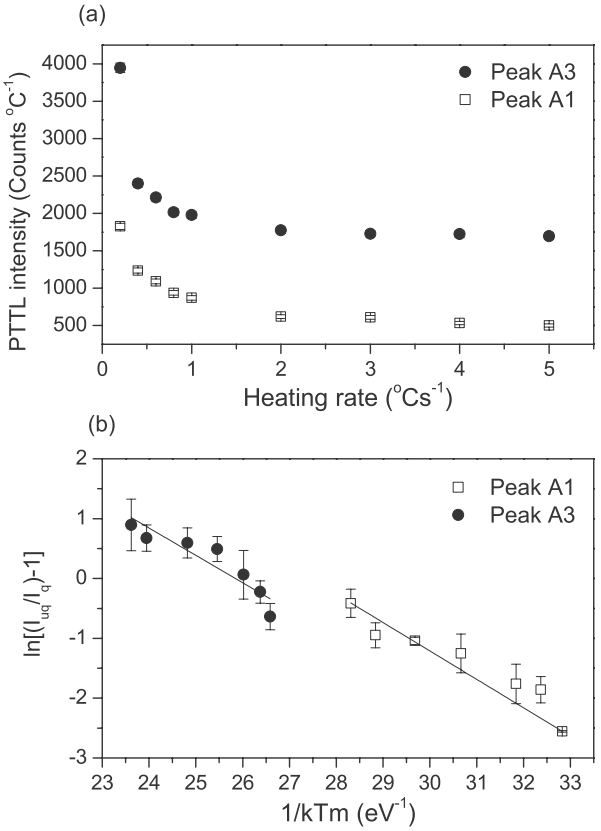

Fig. 3. PTTL intensity against heating rate for the sample preheated to 250 °C (a) a plot of $\ln[(I_{uq}/I_q)-1]$ against $1/kT_m$. used to quantify thermal quenching using peaks A1 and A3 (b).

$$\frac{I_q}{I_{uq}} = \frac{1}{1 + Cexp\ (-\Delta E/kT_m)} \quad (1)$$

where ΔE is the activation energy of thermal quenching, C is a constant and k is Boltzmann's constant (Pagonis et al., 2006). Fig. 3(b) shows plots of $\ln[(I_{uq}/I_q) - 1]$ against $1/kT_m$ for peaks A1 and A3 for measurements corresponding to preheating to 250 °C. The activation energy of thermal quenching was determined as 0.62 ± 0.04 eV using peak A1 and as 0.65 ± 0.05 eV using peak A3 in the sample annealed for 10 min. The values evaluated for samples annealed for 30 and 60 min are 0.63 ± 0.02 eV and 0.66 ± 0.03 eV. These are consistent with 0.65 ± 0.02 eV determined using peak 1 in the conventional TL (Dawam and Chithambo, 2018). The results show that the emission is from a common recombination centre. This is consistent with a previous study using radioluminescence (Chithambo and Niyonzima, 2017) which showed that changing the duration of annealing only alters the intensity not the position of the emission band.

Thermal quenching has been quantified using TL emission near 90 and 180 °C. Use of emission near ambient to study thermal quenching as before (Chithambo et al., 2017) requires comment. The emission of luminescence is subject to competing radiative and non-radiative transitions described as

$$\frac{1}{\tau} = \frac{1}{\tau_{rad}} + \frac{1}{\tau_{th}}\exp\left(\frac{-\Delta E}{kT}\right) \quad (2)$$

where $1/\tau_{\ rad}$ is the probability of radiative emission, $1/\tau_{\ th}$ is the probability of thermal excitation and ΔE is the activation energy of thermal quenching (Agullo-Lopez et al., 1988). The influence of these separate routes on the TL intensity can be distinguished even at temperatures near ambient. The reasoning is that if the number of electrons undergoing radiative transitions is drastically reduced, the luminescence intensity cannot be high enough to make up for any loss due to non-radiative transitions and thermal quenching becomes manifest.

The analysis provides a means to determine the frequency factor for the non-radiative process ν since $C = \nu\tau_{rad}$ where τ_{rad} is the luminescence lifetime (Chithambo, 2007). The value of C can be abstracted either by fitting as explained earlier or direct fit to data. The value of C in either case range from $5.0x10^5$ - $9.8x10^7$ for peak A1 and $1.3x10^5$ - $6.5x10^7$ for peak A3. Since τ_{rad} for this particular sample was measured as 54.5 μs (Chithambo et al., 2011), $\nu = 9.2x10^8 - 1.8x10^{11}$ s^{-1} using peak A1 and $\nu = 2.3x10^8 - 1.2x10^{11}$ s^{-1} using peak A3. The wide range in values of C and hence the frequency factor is due to imprecision in the corresponding data.

5.3. Curve fitting

The temperature dependence of the PTTL of peaks A1 and A3 obtained after preheating to either 350 or 500 °C for samples annealed for 10, 30 and 60 min were further analysed by curve fitting using the expression

$$I(T) = \left\{ I_m b^{\left(\frac{b}{b-1}\right)} exp\left(\frac{E}{kT}\frac{T-T_m}{T_m}\right)\left[(b-1)(1-\Delta)\frac{T^2}{T_m}\exp\left(\frac{E}{kT}\frac{T-T_m}{T_m}\right) + Z_m\right]^{-\frac{b}{b-1}} \right\}\eta(T) \quad (3)$$

where $\Delta = 2kT/E$, $\Delta_m = 2kT_m/E$, $Z_m = 1 + (b-1)\Delta_m$, I_m is the peak intensity, T_m is the peak position and $\eta(T)$ is the luminescence efficiency given by

$$\eta(T) = \frac{1}{1 + Cexp\ (-\Delta E/kT)} \quad (4)$$

The correction was necessary because thermal quenching causes the observed PTTL intensity to be less than that predicted by the Kitis et al. (1998) (within braces). The goodness of fit was checked by the 'figure of merit' (FOM) given by

$$FOM = \sum \frac{|y_{exp} - y_{fit}|}{y_{fit}} \quad (5)$$

where y_{exp} and y_{fit} denote experimental and fit-generated values respectively. The FOM for the samples annealed for 10, 30 and 60 min were all less than the Balian and Eddy (1977) limit of 3.5% and thus adjudged to be acceptable. Fig. 4 shows a glow curve for the sample annealed for 10 min obtained after preheating to 500 °C. The solid line through data is the best fit of Eq. (3) from which the activation energy for peaks A1 and A3 were found as 0.73 ± 0.02 eV and 0.68 ± 0.03 eV and the order of kinetics as 1.20 ± 0.04 and 1.10 ± 0.10 respectively.

The results of kinetic analysis are listed in Table 2. In particular, the value of the activation energy for peak A1 is consistent with that for the main peak under conventional TL, i.e. 0.67 ± 0.02 eV as reported by Dawam and Chithambo (2018). That study also showed that this peak is affected by thermal quenching with an activation energy of 0.65 ± 0.02 eV. These values are reproduced under phototransfer. Thus the main peak is properly reproduced under phototransfer.

6. Pulse annealing

The so called pulse annealing technique (Duller, 1994) was used to determine the role of electron traps as donors or acceptors during PTTL. An irradiated sample was preheated to a particular temperature to deplete specific electron traps. The sample was then exposed to 470 nm blue light for 20 s to transfer electrons from deeper traps to empty shallower ones and then heated again to 500 °C to monitor any PTTL. This procedure was repeated with the preheat temperature varied from 100 to 500 °C in steps of 10 °C. The most intense peak, that is, peak I, was studied in this experiment. The maximum intensity of reproduced peak A1 was noted for each preheating temperature.

Fig. 5 shows the dependence of intensity on preheating temperature for samples annealed for 10 and 60 min and in the inset, for 30 min. Fig. 5 shows intensity against preheating temperature. If the preheating temperature is below the position of a peak, the glow curve measures a conventional peak. If a preheating temperature exceeds the peak position and yet the peak re-appears then what is measured is a PTTL peak. Thus the same graph shows intensity of a conventional peak at first and that of a PTTL peak. The intensity is independent of preheating between 100 and 120 °C. This is because the amount of charge removed from any putative donor at these temperatures is negligible. When the sample was preheated between 120 and 190 °C, the intensity decreased sharply. The decrease occurs due to the continual removal of charge from donors, presumably electron traps corresponding to peaks II and III. For preheating to 200 °C and above, the intensity of A1 is apparently approximately independent of preheat temperature. However, as Fig. 5(b) clarifies, the intensity does continue to decrease with preheating up to 350 °C. This is evidence that electron traps associated with peaks IV to

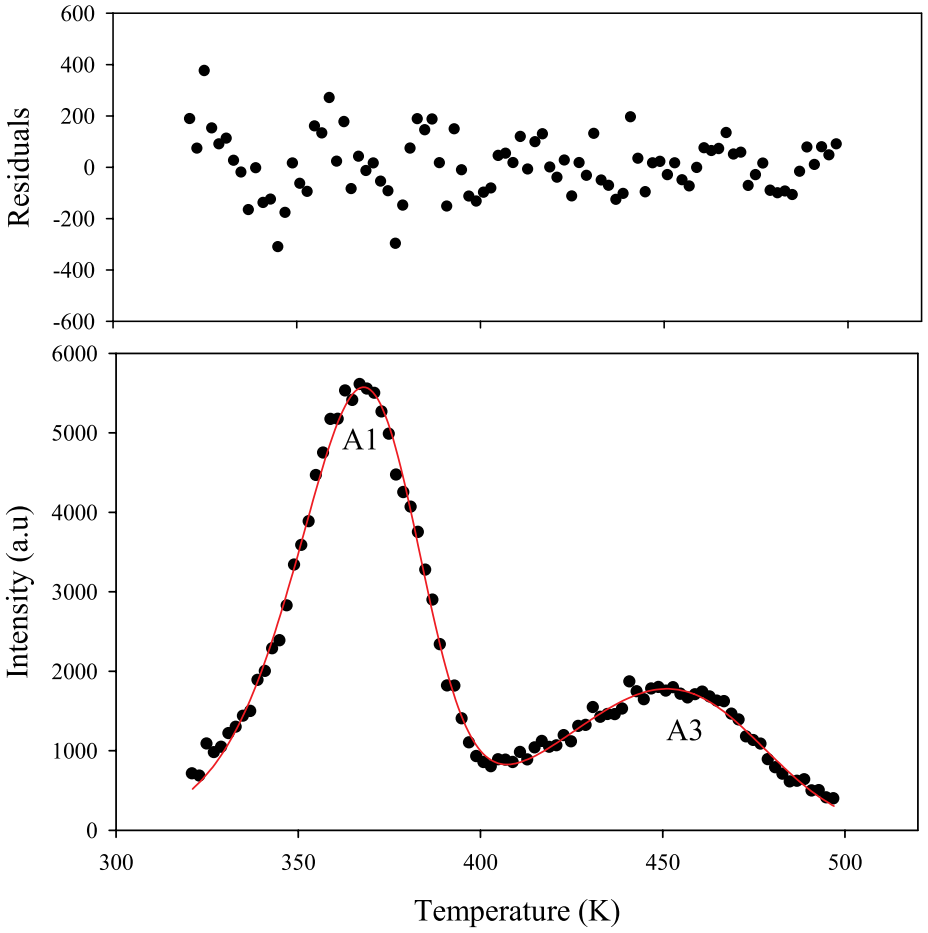

Fig. 4. A glow curve for the sample annealed for 10 min measured after preheating to 500 °C, The line is the best fit of Eq. (3).

VI also act as donors. The same outline applies to the inset to Fig. 5(a).

In order to examine the presence of donor traps above 500 °C, pulse annealing was carried out between 510 and 600 °C at 10 °C intervals. By removing all peaks in the glow curve, it would be expected that phototransfer would only ensue from source traps beyond 500 °C. The intensity of PTTL obtained this way was quite weak and cannot be represented as a function of preheating temperature. Instead, we only show selected glow curves so obtained. Fig. 6 shows glow curves exemplifying PTTL measured after preheating to 560, 570 and 600 °C for the sample annealed for 10 min. A weak PTTL peak is measured following preheating to 560 °C. When the preheating temperature is increased to 570 or 600 °C, PTTL is still observed but is ill defined. This indicates that deep electron traps beyond 570 °C make only a minimal contribution to the PTTL recorded from this sample.

7. Analysis of illumination-time dependence of PTTL intensity

The profile of PTTL intensity as a function of illumination time takes on various forms. The archetypal one is an increase followed by a decrease. Increase to saturation has also been observed as have extended growths through a peak (Chithambo et al., 2017). The range of experimental forms is considerable and cannot be accounted for by a single model.

Alexander and McKeever (1998) described the illumination-time dependent curves of PTTL intensity using sets of non-linear differential equations. Their method was based on a system of one acceptor and one donor. The family of non-linear differential equations such as arise in this approach do not have analytical solutions and approximations become necessary. Using a number of assumptions they predicted various dependences of PTTL intensity on illumination time. In comparison, Chithambo et al. (2017) developed a phenomenological model to explain the behaviour of PTTL intensity as a function of illumination time in a system with any number of acceptors and donors. The charge transport in this method is described by sets of coupled linear differential equations. These equations have analytical solutions which can be applied directly to experimental data. In this report, we will use the model of Chithambo et al. (2017). The analysis is based on the premise that when charge is stimulated from a donor only a portion is transferred to an acceptor and that any retrapping of stimulated electrons is negligible. The number of acceptors and donors and the extent of their contribution in the process is determined by experiment.

The PTTL will be explained with reference to the energy band diagram in Fig. 7. N_1 to N_7 are each the concentration of electrons at levels 1 to 7 whereas f_1 through f_7 are the corresponding probabilities of optical stimulation. Evaluating the latter provides a means to determine the photoionization cross-section σ since $f = \Phi\sigma$ where Φ is the intensity of stimulation light. The photoionization cross section is a measure of the ease with which an electron trap can be optically stimulated. The smaller the cross-section, the less stable the trap is.

For a system of n donors and one acceptor, the time-dependence of the concentration N_k of electrons at the k^{th} acceptor can be written as

$$N_k = e^{-\int \Gamma_j dt} \int \sum_{i=1}^{n} \Phi_i(t) e^{\int \Gamma_j dt}\, dt + c e^{-\int \Gamma_j dt} \tag{6}$$

where c is an integration constant and Γ_j is the coefficient of N_k in its rate equation and j is a label fo donor traps. The functions $\Phi_i(t)$ are for charge transport at each donor and are meant to be determined by experiment not formulated as general expressions and must be solved for each donor

Table 2
Kinetic parameters of PTTL peaks A1 and A3 determined using the whole glow peak method (WGP), curve fitting (CF) and phototransferred phosphorescence (PP).

Peak	Annealing time (minutes)	Preheat temp. (°C)	Method	E (eV)	b	ΔE (eV)	σ(cm^2) x10^{-18}	Reference
A1	10	250	WGP	0.66 ± 0.01	1.2			Sect. 5
	10	250					5.18	Fig. 8(a)
	30	250	WGP	0.67 ± 0.01	1.1			Sect. 5
	30	250					3.76	Fig. 8(b)
	60	250	WGP	0.66 ± 0.02	1.2			Sect 5
	10	350					4.82	Fig. 8(c)
	60	350					2.53	Inset Fig. 8(c)
	10	500					3.29	Inset Fig. 8(i)
	10	350	CF	0.73 ± 0.02	1.2			Sect. 5
	30	350	CF	0.75 ± 0.04	1.1			Sect. 5
	60	350	CF	0.57 ± 0.03				Sect. 5
	10	250	VHR			0.62 ± 0.04		Sect. 5
	30	250	VHR			0.63 ± 0.02		Sect. 5
	10	250	PP	0.60 ± 0.02	1			Sect. 5
	30	250	PP	0.62 ± 0.03	1			Sect. 5
	60	250	PP	0.52 ± 0.01	1			Sect. 5
A2	60	350					4.82	Fig. 8(d)
A3	10	250	WGP	0.68 ± 0.03	1.2			Sect. 5
	60	250	WGP	1.06 ± 0.04	1.2			Sect. 5
	60	350					4.34	Fig. 8(e)
	10	350					3.76	Inset Fig. 8(e)
	10	500					2.71	Fig. 8(i)
	10	500	CF	0.68 ± 0.03	1.1			Sect. 5
	60	350	CF	1.06 ± 0.05	1.3			Sect. 5
	10	250	VHR			0.65 ± 0.05		Sect. 5
	60	250	VHR			0.66 ± 0.03		Sect. 5

prior to integration in Eq. (5). For example if the term $f_k N_i(t)$ represents the amount of charge stimulated from the i^{th} donor then a portion $\alpha_i f_i N_i(t)$ is captured at an acceptor. The functions $\Phi_i(t)$ are not necessarily identical for each donor. Since the problem posed by the set of $(n+1)$ equations is an initial value one, the constant c can be determined. Equation (6) therefore represents particular solutions and will be used to describe the time-dependent evolution of PTTL intensity.

In what follows, the change of PTTL intensity with duration of illumination will be discussed with respect to the preheating temperature. This facilitates explaining the number of acceptors and donors involved in the PTTL at each stage.

7.1. PTTL following preheating to 250 °C - sample annealed for 10 min

When the sample annealed for 10 min was preheated to 250 °C to remove peaks I–V, only peaks I-IV were properly removed. Two PTTL peaks A1 and A3 were measured at 90 °C and at 176 °C. Peak V still remained although much reduced in intensity. Therefore the PTTL can be accounted for in terms of two separate systems of one acceptor and three donors comprising levels 5 to 7 in Fig. 7.

The dependence of electron concentration on stimulation time relevant for peaks A1 and A3 is

$$N_k = A_{1j}\left(e^{-f_5 t} - e^{-f_k t}\right) + A_{2j}\left(e^{-f_6 t} - e^{-f_k t}\right) + A_{3j}\left(e^{-f_7 t} - e^{-f_k t}\right) \quad (7)$$

where for the acceptor with label k (either 1 or 3), the scaling factors are $A_{lj} = \alpha_j f_j N_{ji}/(f_k - f_j)$ where N_{ji} are each the initial concentrations of electrons at electron traps $j = 5,\ 6$ or 7 at the start of illumination and α_j are constants of proportionality. In this case $l = 1,\ 2$ and 3.

7.2. PTTL following preheating to 350 °C - sample annealed for 10 min

When the sample was preheated to 350 °C to remove peak I-VI, only two peaks A1 and A3, were reproduced. This preheating left a low intensity remnant of peak VI. Thus levels 6 and 7 are considered donor traps. This constitutes two separate systems of one acceptor and two donors. The time dependence of electron concentration corresponding to peaks A1 and A3 are

$$N_k = B_{1j}\left(e^{-f_6 t} - e^{-f_k t}\right) + B_{2j}\left(e^{-f_7 t} - e^{-f_k t}\right) \quad (8)$$

where $k = 1$ or 3 and $B_{lj} = a_j f_j N_{ji}/(f_k - f_j)$ where all symbols retain their meanings.

7.3. PTTL following preheating to 350 °C – sample annealed for 60 min

When this sample was preheated to 350 °C to remove peak I-VI, three PTTL peaks A1, A2 and A3 were measured at 80, 134 and 188 °C. This preheating could not completely remove peak VI and so its associated electron trap is regarded as a donor. Thus, for each acceptor, there are two donors, levels 6 and 7. There are hence three systems of one acceptor and two donors. The time dependence of electron concentration at the acceptor electron traps will be described by equations similar (not identical) to Eq. (8).

7.4. PTTL following preheating to 500 °C – sampling deep electron traps

When the sample annealed for 10 min was preheated to 500 °C to remove all peaks in the glow curve, two PTTL peaks, A1 and A3, were reproduced at 100 and 176 °C. The supposed deep trap (level 7) is the donor. Thus we have two systems of one acceptor and one donor. The time dependence of electron concentration corresponding to acceptor level k (1 or 3) is

$$N_k = D_j\left(e^{-f_7 t} - e^{-f_k t}\right) \quad (9)$$

where $D_{lj} = \mu_j f_j N_{ji}/(f_k - f_j)$ where all symbols have meanings as before.

8. Analysis of illumination-time curves

Fig. 8 shows selected examples of the dependence of PTTL intensity

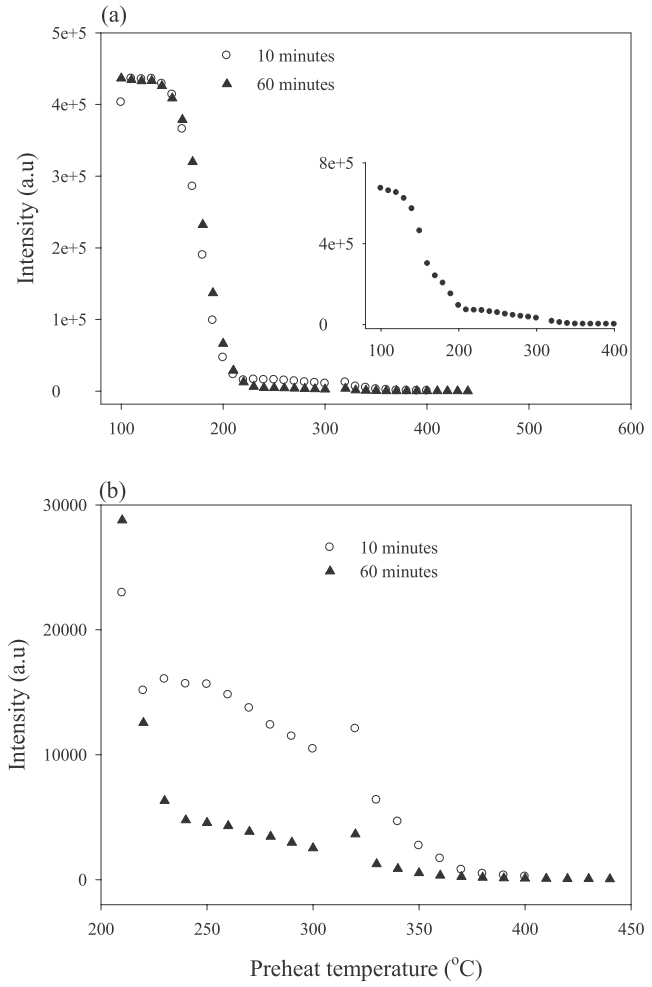

Fig. 5. The TL intensity for peak I against preheating (a) The same plot for preheating between 200 and 440 °C (b).

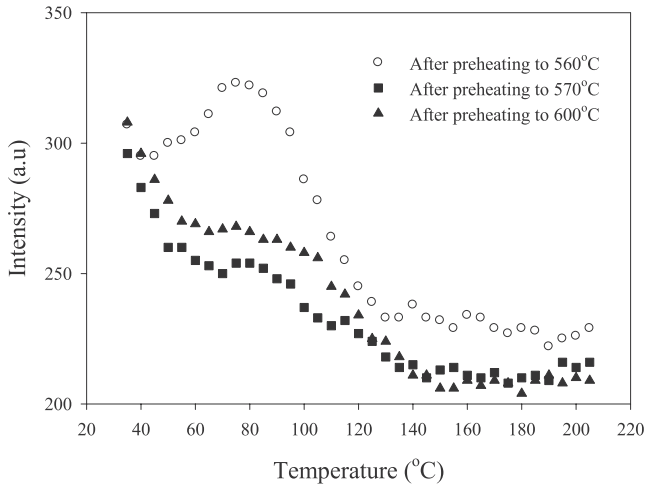

Fig. 6. Glow curves measured after preheating to 560, 570 and 600 °C.

on duration of illumination. All plots go through a peak with illumination time. The detailed behaviour differ and is affected by number and contribution of donor traps. The quartz studied each show at least six peaks I-VI. Thus qualitatively when say, peak I, is removed by preheating, it might be expected that phototransfer will reproduce it. This does not happen. Instead PTTL is only observed when a certain number of peaks have been removed and even so only certain peaks re-appear under phototransfer. The PTTL intensity is assumed to follow the concentration of charge at an acceptor as before e.g. (Chithambo et al., 2017, 2018; Wintle and Murray, 1997).

Profiles for systems of one acceptor and three donors are shown for peak A1 in Fig. 8(a) for the sample annealed for 10 min and in Fig. 8(b) for the one annealed for 30 min. The measurements are for preheating to 250 °C. The solid line through data in both cases is the best fit of Eq. (7). Plots for peaks A1 and A3 for the sample annealed for 60 min are similar to Fig. 8(a) and have been omitted. Here and throughout Fig. 8, the curve-fitting was based on the Marquardt–Levenberg minimization routine.

Fig. 8(c)–(e) show results for systems of one acceptor and two donors. These correspond to preheating to 350 °C. Comparing Fig. 8(a) and (c), the latter for peak A1 in the sample annealed for 10 min, it is apparent that we have a counter-intuitive result where the PTTL intensity has increased even though the number of donors has decreased. This points to the presence of a competitor for electrons released from deep traps influencing the PTTL. We deduce that this is level 6 (responsible for peak VI) since this is the only additional peak removed when the preheating temperature is changed from 250 to 350 °C. That a competition process may indeed be at play is evident in measurement of peak A1 for a system of one acceptor and one donor (inset to Fig. 8(f)). This will be explored later.

The intensity of peak A2, which only appears in the sample annealed for 60 min, is shown against illumination time in Fig. 8(d). The intensity goes through an extended growth to a maximum before decreasing. The result for peak A3 for the sample annealed for 60 min (inset to Fig. 8(e)) also goes through a peak but the subsequent decrease is slow and somewhat linear. These examples are shown fitted by Eq. (8). This characteristic is also observed when the preheating temperature is 500 °C (Fig. 8(f), main graph for peak A3 in the sample annealed for 10 min). The PTTL for samples annealed for 30 and 60 min was too weak for any systematic study.

The photoionization cross section for the electron trap corresponding to peak A1 in Fig. 8(a) was evaluated as 5.18×10^{-18} cm^2. For analysis using peak A3 in the same sample, the value was found as 2.53×10^{-18} cm^2. The full set of such values are listed in Table 2. All are of the order of 10^{-18} cm^2 and are comparable with literature values e.g. (Bøtter-Jensen et al., 2003; Kuhns et al., 2000).

9. Competition effects during phototransfer

9.1. Qualitative account

Phototransfered TL at peak A1 was only observed after the removal of peaks I-IV. There was no PTTL after removal of peaks I, I and II or I to III. These results go against the expectation that a PTTL peak ought to be reproduced when at least one shallow trap has been depleted and one or more supposed donors are intact. That the PTTL only appeared after some supposed donors were depleted suggests that some of these act as competitors for charge that would otherwise be captured at an acceptor. We discuss this with reference to peaks III to IV whose intensities are shown plotted against preheating temperature in Fig. 9.

If a preheating temperature is below the position of a particular peak, the latter is expected to contribute to the PTTL process as a donor and its intensity should remain unchanged if that contribution is negligible otherwise its intensity should decrease. The behaviour of peak IV in Fig. 9(a) fits this description. On the other hand, if an electron trap competes for phototransferred charge while also acting as a donor, the extent to which it also acts as an acceptor will be reflected in a plot of intensity against preheating temperature. As a case in point, the intensity of peak V, in Fig. 9(b), increases by nearly 60% when the preheating temperature is changed from 100 to 210 °C. Since the position of this peak is at 240 °C and the preheating temperatures are below this,

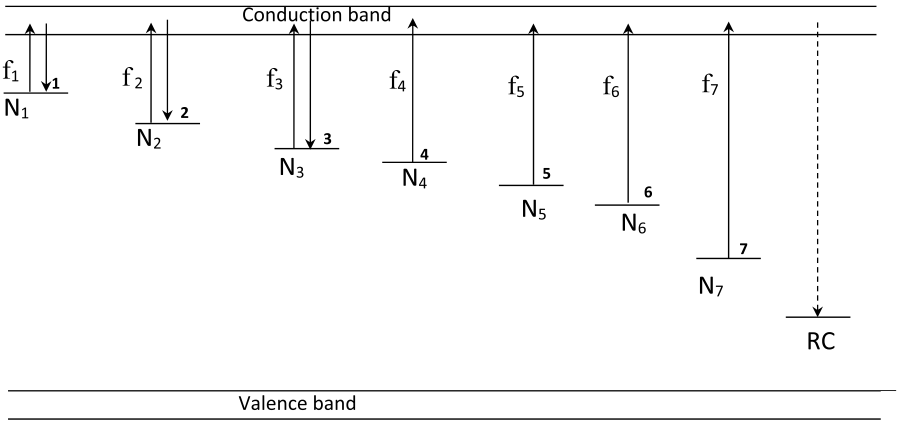

Fig. 7. An energy band scheme used to describe PTTL. Electron levels 1 through 7 are associated with electron concentration N_i as shown. The parameters f_i are each the probability of optical stimulation. The recombination centre, included for completeness, is shown as RC.

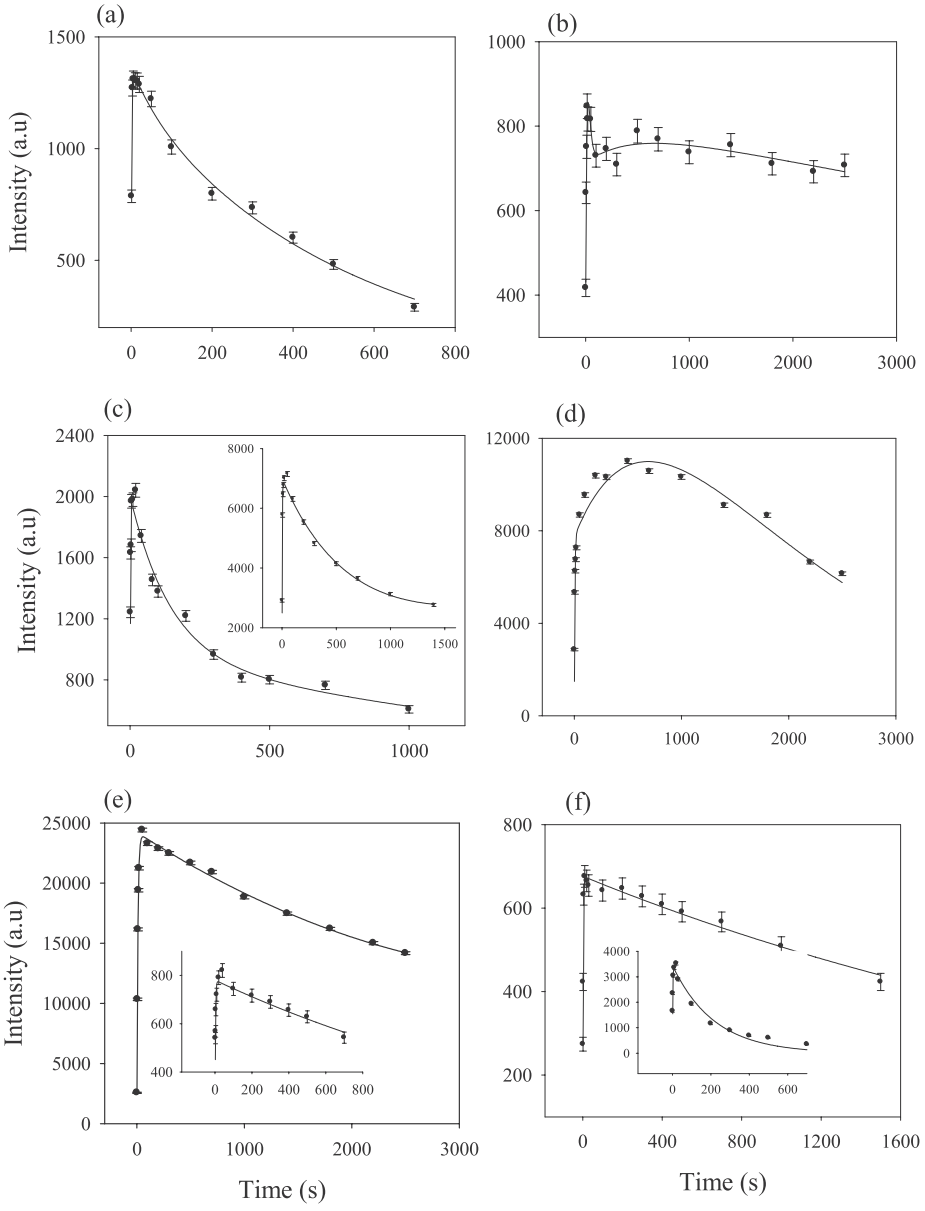

Fig. 8. The dependence of PTTL intensity on illumination time measured after preheating to 250 °C for peak A1 in the sample annealed for 10 min (a) for peak A1 in the sample annealed for 30 min (b). The data for preheating to 350 °C is shown for peak A1 for the sample annealed for 10 min (c) for peak A1 in the sample annealed for 60 min (inset to Fig. 9(c)), for peak A2 in the sample annealed for 60 min (d) and for peak A3 in the sample annealed for 10 and 60 min, (e) and inset to (e) respectively. The plots in (f) and the inset to (f) are for peak A3 in the sample annealed for 10 min (main graph) and peak A1 in the sample annealed for 10 min following preheating to 500 °C.

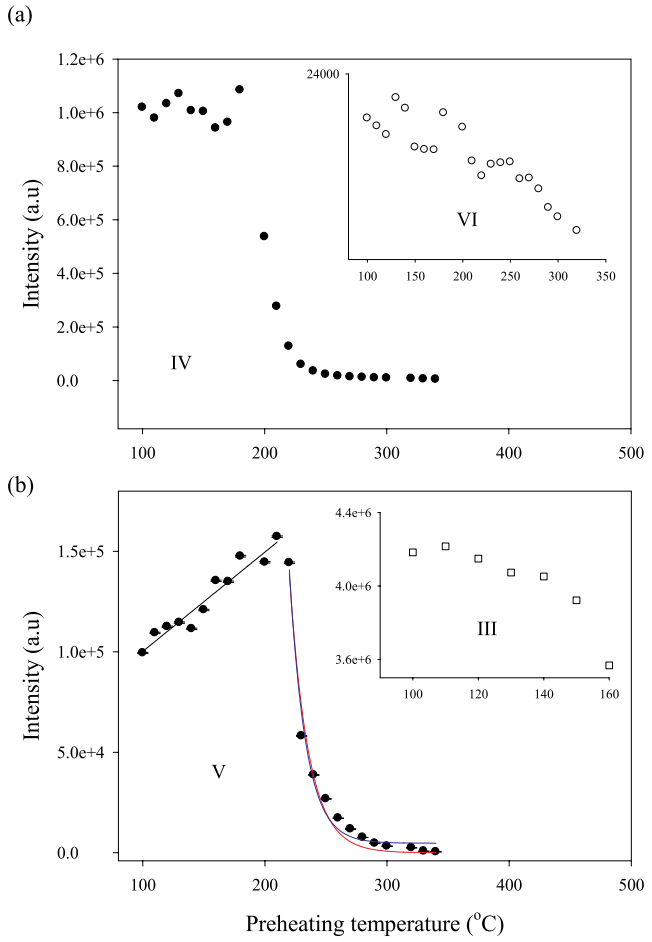

Fig. 9. The dependence of TL intensity on preheating for putative donors IV (a) VI (inset to (a) V (b) and III (inset to (b)). The solid red and blue lines in Fig. 9 (b) are fits of Eqs. (19) and (20).

the increase in intensity must be due to its electron trap acting as an acceptor. Beyond 210 °C, the intensity decreases. This is caused by depletion of trapped charge by preheating and somewhat by loss owing to optical stimulation.

The influence of possible competitors can also be examined in illumination-time profiles shown in Fig. 10. The maximum intensity of peak A1 in Fig. 10(a) increases with preheating temperature. This is unexpected because increasing the preheating temperature should cause a gradual depletion of donors. This would be reflected as a decrease in the intensity of PTTL from the acceptor. The results of Fig. 10(a) must mean that the effect of any competitor trap is reduced as the donor trap is depleted as was observed for peak V in Fig. 9(b). In contrast, the intensity of peak A3 in Fig. 10(b) decreases with preheating temperature. This can be ascribed to reduction of charge at donors with preheating. This is evident in the inset to Fig. 9(b). This behaviour is expected of a donor when retrapping is negligible. Since kinetic analysis showed that peak A3 follows first order kinetics, this change of intensity with preheating temperature is consistent with this conclusion.

9.2. Empirical model of competition effects

To model competition effects, we consider peak V in Fig. 9(b). The intensity of peak V is not independent of preheating temperature. This suggests that the concentration of electrons trapped at level 5 after each preheat is affected by competition effects. By this we mean processes that increase or depress the capture of electrons at electron traps during illumination and how this affects the signal output from acceptors or contribution of donors. The mechanisms involved are not obvious but an explanation can be forwarded. We assume that the concentration of electrons N_5 at level 5 depends on two independent parameters, a variable one N and a time-independent one N_A, that is, $N_5 = N + N_A$, where N is the number of electrons available in the conduction band after release from donors 6 and 7 and N_A is the number of electrons trapped at level 5 immediately after irradiation but before optical exposure of sample. Since the same dose of 200 Gy is used each time, N_A is constant. We further assume that electrons do not accumulate to any significant extent in the conduction band.

The concentration of electrons in the conduction band is affected either by optical exposure or irradiation. Since N_A is unchanged and the sample is exposed to light for 20 s each time, N changes due to competitive retrapping. When electrons are released to the conduction band from donors, some transit to recombination centres and others, to electron traps. However, unless a sample is preheated to at least 250 °C, there is no PTTL observed for peaks I to IV. This discounts their electron traps acting as competitors for charge released from levels 6 and 7. We presume then that there exists an as yet undetermined competitive route including the recombination one. If such competitive retrapping decreases with preheating, the remnant that can transfer to level 5 will increase each time the sample is exposed to light following each preheat.

9.2.1. Increase of signal with preheating (Fig. 9(b))

The number of electrons N available in the conduction band after stimulation from donor levels 6 and 7 at any time t can be written as

$$\frac{dN}{dt} = f_6 N_{6i} + f_7 N_{7i} - \lambda N \tag{11}$$

where N_{6i} and N_{7i} are the initial concentrations of electrons at levels 6 and 7 respectively and λ is the overall probability per unit time that a stimulated electron will transit the competitive route. The time-dependence of is N is therefore

$$N = \frac{(f_6 N_6 + f_7 N_7)}{\lambda}[1 - e^{-\lambda t}] \tag{10}$$

Fig. 9(b) shows that the signal for peak V initially increases with preheating although there are no new donors or new sources of electrons. Thus if indeed λ is negligible, we can use Taylor series to approximate Eq. (9) to

$$N \approx (f_6 N_6 + f_7 N_7)t \tag{12}$$

At each step where the sample is exposed to light after preheating, only a certain proportion of the ensuing electrons are captured at level 5. To use Fig. 9(b) as an illustration, between 100 and 210 °C, the preheating temperature is increased by 10 °C and so the sample is preheated consecutively 11 times. The first preheating to 100 °C is measurement 1, the one to 110 °C is measurement 2 and so on. If we replace t in Eq. (12) by a unitless dummy variable $t^{'}$ representing the number of measurement (1, 2, …as explained earlier) or 'preheat number', we can write that

$$N \approx (\alpha_6 f_6 N_6 + \alpha_7 f_7 N_7)t^{'} \tag{13}$$

where α_6 and α_7 are constants of proportionality. Further if the term λN in Eq. (10) decreases with each run, the bracketed term in Eq. (13) will increase and correspondingly N will increase linearly with $t^{'}$ or preheating. The solid line though data between 100 and 210 °C in Fig. 9(b) is the best fit of Eq. (13).

9.2.2. Decrease of signal with preheating (Fig. 10(b))

When the sample is preheated beyond 210 °C, the heating extends into the expanse of peak V. This depletes some charge trapped at level 5. Since peaks V and VI overlap, the preheating also reduces the remnant at level 6 due to ionization. The intensity of peak V therefore decreases in consecutive measurements due to these two effects. It is not possible to

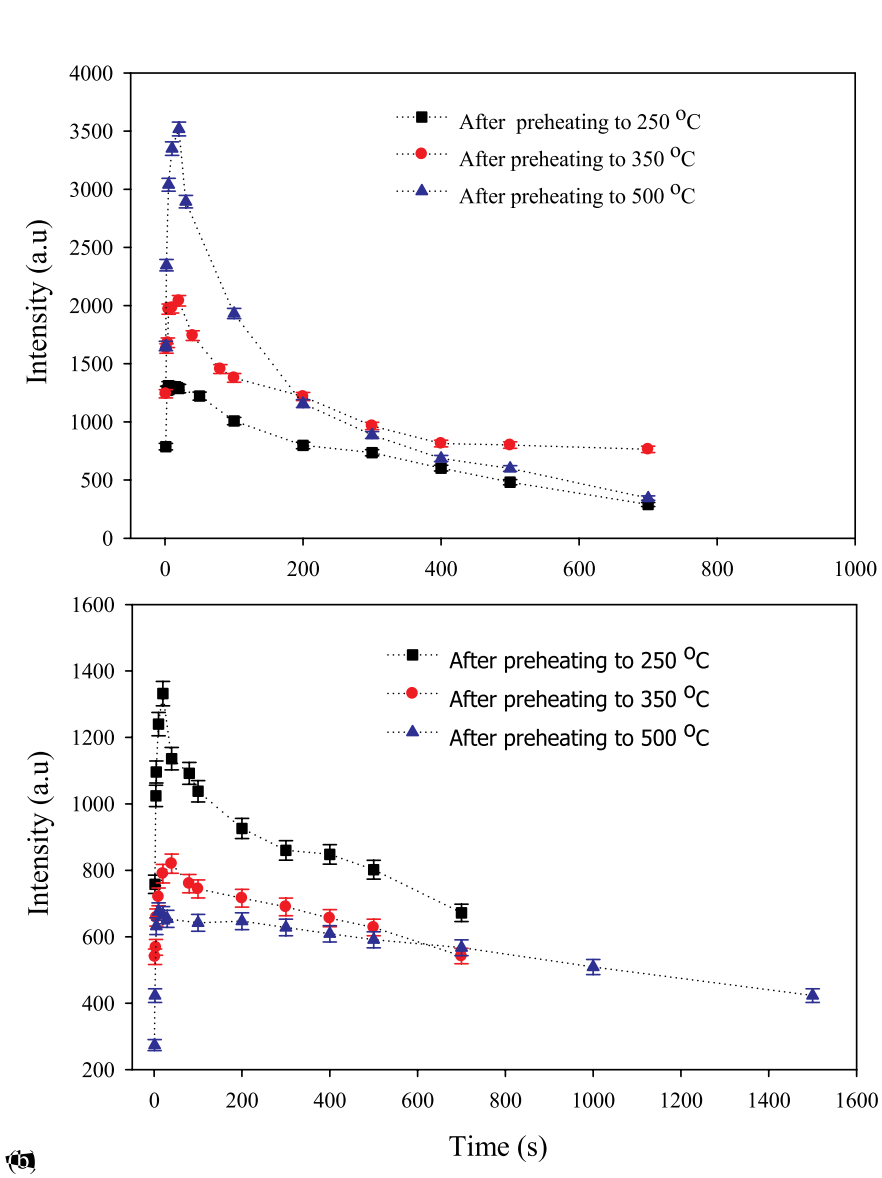

Fig. 10. Time-response profiles for peak A1 (a) and peak A3 (b) in the sample annealed at 900 °C for 10 min. The dotted lines are visual guides.

model accurately the dependence of charge reduction on preheating. However, the reduction due to optical stimulation can be addressed. We will do so in two ways, by approximation and by using an exact solution and then compare the results.

If we consider peak 5 as the acceptor, the rate of electron transfer during each illumination can be written as

$$\frac{dN_7}{dt} = -f_7 N_7 \tag{14}$$

$$\frac{dN_6}{dt} = -f_6 N_6 \tag{15}$$

$$\frac{dN_5}{dt} = -f_5 N_5 + \delta_6 f_6 N_6 + \delta_7 f_7 N_7 \tag{16}$$

where δ_6 and δ_7 are constants of proportionality. We can express the contribution from level 6, the one affected by preheating as some function, say, $g(t) = \delta_6 f_6 N_6$ to re-write Eq. (16) as

$$\frac{dN_5}{dt} = -f_5 N_5 + g(t) + \delta_7 f_7 N_7 \tag{17}$$

The solution of the coupled equations (14), (15) and (17) is

$$N_5 = \left(\frac{\delta_7 f_7 N_{7i}}{(f_5 - f_7)}\right) e^{-f_7 t} + \left[e^{-f_5 t}\left(g(t)\frac{e^{f_5 t}}{f_5} - \int g'(t)\frac{e^{f_5 t}}{f_5} dt\right)\right] + ce^{-f_5 t} \tag{18}$$

where c is a constant and all other parameters are as previously defined. Ignoring the exact form for $g(t)$ for now, we notice that the contribution within square brackets decreases each time the sample is preheated. The remaining terms, the first and third, are simple exponential decaying functions. Since the TL intensity is proportional to the concentration of trapped charge, its intensity will also decrease approximately exponentially with each run, in the form

$$N_5 = Ae^{-at'} + h(t') \tag{19}$$

where A and a are constants and $h(t')$ is some function subsuming terms within the square bracket and t' is a dummy variable denoting the run number or preheat number. In data fitting $h(t')$ would be a free fitting parameter left to vary.

If the case above is treated as a system of one acceptor and two donors, then by the solution of Eqs. (14)–(16), N_5 will depend on t' as

$$N_5\,\alpha\,B_1\left(e^{-f_6 t'}-e^{-f_5 t'}\right)+B_2\left(e^{-f_7 t'}-e^{-f_5 t'}\right) \quad (20)$$

where B_1 and B_2 are constants and other parameters are as defined before. The solid red line through data in Fig. 9(b) is the best fit of Eq. (19) while the blue line is the best fit of Eq. (20). Although the decrease due to preheating alone has been omitted in this discussion, both equations describe the data satisfactorily.

10. Conclusion

Phototransferred thermoluminescence of annealed synthetic quartz induced using 470 nm blue light has been studied. Samples were annealed at 900 °C for 10, 30 and 60 min. The glow curve measured at 1 °C s^{-1} after irradiation to 200 Gy shows six peaks for all samples. However, only three PTTL peaks were reproduced for the sample annealed for 60 min. When the duration of annealing was reduced to 10 min, only two PTTL peaks were induced. For an intermediate duration of 30 min only one PTTL peak was reproduced. Deep traps beyond 600 °C make a negligible contribution to the PTTL. All the PTTL peaks studied are affected by thermal quenching. The activation energy of thermal quenching for peaks A1 and A3 were evaluated as 0.62 ± 0.02 eV and 0.65 ± 0.02 eV respectively. The PTTL intensity goes through a peak as a function of illumination time. The change is modelled using sets of coupled linear differential equations based on systems of donors and acceptors whose number is determined by preheating temperature. Competition effects involved in the PTTL have been reported and modelled using an empirical model.

Declaration of competing interest

All authors have participated in (a) conception and design, or analysis and interpretation of the data; (b) drafting the article or revising it critically for important intellectual content; and (c) approval of the final version.

This manuscript has not been submitted to, nor is under review at, another journal or other publishing venue.

Acknowledgements

The authors gratefully acknowledge financial support from Rhodes University and National Research Foundation of South Africa.

References

Agullo-Lopez, F., Catlow, C.R.A., Townsend, P.D., 1988. Point Defects in Materials. Academic Press, London.
Alexander, C.S., McKeever, S.W.S., 1998. Phototransferred thermoluminescence. J. Phys. D Appl. Phys. 31, 2908–2920.
Alexander, C.S., Morris, M.F., McKeever, S.W.S., 1997. The time and wavelength response of phototransferred thermoluminescence in natural and synthetic quartz. Radiat. Meas. 27, 153–159.
Bailiff, I.K., Bowman, S.G.E., Mobbs, S.K., Aitken, M.J., 1977. The phototransfer technique and its use in thermoluminescence dating. J. Electrost. 3, 269–280.
Balian, H.G., Eddy, N.W., 1977. Figure-of-merit (FOM) an improved criterion over the normalized Chi-squared test for assessing goodness-of-fit of gamma-ray spectral peaks. Nucl. Instrum. Methods 145, 389.
Betts, D.S., Townsend, P.D., 1993. Temperature distribution in thermoluminescence experiments. I: some calculation models. Phys. D Appl. Phys. 26, 849–857.
Betts, D.S., Couturier, L., Khayrat, A.H., Luff, B.J., Townsend, P.D., 1993. Temperature distribution in thermoluminescence experiments. I: experimental results. J. Phys. D Appl. Phys. 26, 843–848.
Bossin, I., Bailiff, I.K., Terry, I., 2018. Phototransferred TL properties of alumina substrates. Radiat. Meas. 120, 41–46.
Bøtter-Jensen, L., Mckeever, S.W.S., Wintle, A.G., 2003. Optically Stimulated Luminescence Dosimetry. Elsevier, Amsterdam.
Chithambo, M.L., 2007. The analysis of time-resolved optically stimulated luminescence. II: computer Simulations and Experimental Results. J. Phys. D Appl. Phys. 40, 1880–1889.
Chithambo, M.L., 2018. An Introduction to Time-Resolved Optically Stimulated Luminescence. Morgan & Claypool Publishers, Bristol.
Chithambo, M.L., Niyonzima, P., Kalita, J.M., 2018. Phototransferred thermoluminescence of synthetic quartz: analysis of illumination-time response curves. J. Lumin. 198, 146–154.
Chithambo, M.L., Niyonzima, P., 2017. Radioluminescence of annealed synthetic quartz. Radiat. Meas. 106, 35–39.
Chithambo, M.L., Sane, P., Tuomisto, F., 2011. Positron and luminescence lifetimes in annealed synthetic quartz. Radiat. Meas. 46, 310–318.
Chithambo, M.L., Seneza, C., Kalita, J.M., 2017. Phototransferred thermoluminescence of Al_2O_3:C: experimental results and empirical models. Radiat. Meas. 105, 7–16.
Dawam, R.R., Chithambo, M.L., 2018. Thermoluminescence of annealed synthetic quartz: the influence of annealing on kinetic parameters and thermal quenching. Radiat. Meas. 120, 47–52.
Duller, G.A., 1994. A new method for the analysis of infrared stimulated luminescence data from potassium feldspars. Radiat. Meas. 23, 281–285.
Galloway, R.B., 2002. Luminescence lifetimes in quartz: dependence on annealing temperature prior to beta irradiation. Radiat. Meas. 35, 67–77.
Gribble, C.D., 1988. Rutley's Elements of Mineralogy. Unwin Hyman Ltd., London, UK.
Kalita, J., Chithambo, M.L., 2017. Phototransferred thermoluminescence in α-Al_2O_3:C, Mg under 470 nm blue light stimulation. J. Lumin. 188, 371–377.
Kalita, J., Chithambo, M.L., 2019. Phototransferred thermoluminescence and thermally-assisted optically stimulated luminescence dosimetry using α-Al_2O_3:C,Mg annealed at 1200 °C. J. Lumin. 205, 1–6.
Kitis, G., Gomez-Ros, J., Tuyn, J., 1998. Thermoluminescence glow-curve deconvolution functions for first, second and general orders of kinetics. J. Phys. D Appl. Phys. 31, 26–36.
Kombe-Atang, E.F.M., Chithambo, M.L., 2016. Phototransferred thermoluminescence and phosphorescence related to phototransfer in annealed synthetic quartz. In: Proceeding of the 60th Annual Conference of the South Africa Institute of Physics Conference, pp. 49–54.
Kuhns, C.K., Agersnap Larsen, N., Mckeever, S.W.S., 2000. Characteristics of LM-OSL from several different types of quartz. Radiat. Meas. 32, 413–418.
Mckeever, S.W.S., 1985. Thermoluminescence of Solids. Cambridge University Press, Cambridge.
McKeever, S.W.S., Chen, R., 1997. Luminescence models. Radiat. Meas. 27, 625–661.
McKeever, S.W.S., Minniti, R., Sholom, S., 2017. Phototransferred thermoluminescence (PTTL) dosimetry using Gorilla® glass from mobile phones. Radiat. Meas. 106, 423–430.
Morris, M.F., McKeever, S.W.S., 1994. Optical bleaching studies of quartz. Radiat. Meas. 106, 423–430.
McKeever, S.W.S., 1991. Mechanisms of thermoluminescence production: some problems and a few answers? Nucl. Tracks Radiat. Meas. 18, 5–12.
Pagonis, V., Chithambo, M.L., Chen, R., Chruścińska, A., Fasoli, M., Li, S.H., Martini, M., Ramseyer, K., 2014. J. Lumin. 145, 38–48.
Pagonis, V., Kitis, G., Furetta, C., 2006. Numerical and Practical Exercises Inthermoluminescence. Springer Science.
Wintle, A.G., Murray, A.S., 1997. The relationship between quartz thermoluminescence, phototransferred thermoluminescence, and optically stimulated luminescence. Radiat. Meas. 27, 611–624.